Combustion of large solid fuels in cement rotary kilns

Nielsen, Anders Rooma

Publication date:
2012

Document Version
Publisher's PDF, also known as Version of record

Combustion of large solid fuels in cement rotary kilns

Anders Rooma Nielsen

Ph.D. Thesis

March 2012

DTU Chemical Engineering
Department of Chemical and Biochemical Engineering

Combustion of large solid fuels in cement rotary kilns

Anders Rooma Nielsen
PhD Thesis
March 2012

FLSmidth A/S
Research & Development

DTU Chemical Engineering
Department of Chemical and Biochemical Engineering

Address: Centre of Combustion and Harmful Emission Control
Department of Chemical and
Biochemical Engineering
Technical University of Denmark
Søltofts Plads, Building 229
DK-2800 Kgs. Lyngby
Denmark
Phone: +45 4525 2800
Fax: +45 4525 4588
Web: www.chec.dtu.dk

Print: J&R Frydenberg A/S
København
March 2012

ISBN: 978-87-92481-66-5

Preface

This PhD project is part of an effort to strengthen the scientific based knowledge within alternative fuel combustion technology which is becoming a more integrated part of cement plants. The new knowledge obtained from the PhD project contributes to maintain FLSmidth's position as a technological leader in this field.

The project has been made in cooperation with the CHEC research group at the Department of Chemical and Biochemical Engineering at the Technical University of Denmark (DTU) and the Research and Development Department of FLSmidth A/S. The project has been partly sponsored by The Danish National Advanced Technology Foundation.

I would like to thank my supervisors Morten Boberg Larsen (FLSmidth), Kim Dam-Johansen (DTU) and Peter Glarborg (DTU) for all the time and patience they have invested in the supervision of this project. Also special thanks to the people at FLSmidth's research center Dania, the CHEC technicians group and the workshop at DTU for their support regarding the construction of a high-temperature rotary drum for combustion experiments as well as other matters. Thanks to all the other people at FLSmidth and CHEC, not mentioned here, who have also been involved in this project.

Finally, I would also like to thank the other PhD-students at CHEC, particularly those involved in the co-operation with FLSmidth, for providing a pleasant working atmosphere, for many fruitful discussions and for the social activities we have had.

Anders Rooma Nielsen

Valby, March 2012

Abstract

The cement industry has a significant interest in replacing fossil fuels with alternative fuels in order to minimize production costs and reduce CO_2 emissions. These new alternative fuels are in particular solid fuels such as refuse derived fuel (RDF), tire-derived fuel (TDF), meat and bone meal (MBM), waste wood, sewage sludge, paper and plastics. The alternative fuel share of the total energy varies significantly from region to region, but the general trend is towards increased alternative fuel utilization. Solid alternative fuels typically have physical and chemical properties that differ from traditional solid fossil fuels. This creates a need for new combustion equipment or modification of existing kiln systems, because alternative fuels may influence process stability and product quality. Process stability is mainly influenced by exposing the raw material bed in the rotary kiln to reducing conditions, which increases the tendency for deposit formations in the rotary kiln material inlet end, kiln riser duct and lower cyclone stages. Clinker quality may also be affected by minor compounds from the fuel ashes or from unburned carbon leaving the rotary kiln with the clinker.

This thesis provides an insight into the utilization of solid alternative fuels in the material inlet end of rotary kilns. This position is interesting because it allows utilization of large fuel particles, thereby eliminating the need for an expensive shredding of the fuels. The challenge, however, is that the solid fuels will be mixed into the cement raw materials, which is likely to affect process stability and clinker quality, as described above.

The mixing of fuels and raw materials was studied experimentally in a pilot-scale rotary drum and was found to be a fast process, reaching steady state within few drum revolutions. Thus, heat transfer by conduction from the cement raw materials to the fuel particles is a major heat transfer mechanism rather than convection or radiation from the freeboard gas above the material bed. Consequently, the temperature of the cement raw materials becomes a factor of great importance for heating the fuel particles. Combustion of different alternative fuels has been investigated experimentally in a pilot-scale rotary furnace under conditions similar to those in the material inlet end of cement rotary kilns. The main focus was on tire rubber and pine wood which are relevant fuels in this context. Heating, drying and devolatilization of alternative fuels are fast processes that primarily depend on heat transfer and fuel particle size. Devolatilization of a large wood or tire particle with a thickness of 20 mm at 900°C is for example around 2 minutes. By contrast, char oxidation is a slow process which may greatly reduce the amounts of solid fuels to be utilized in the material inlet end of rotary kilns due to the limited residence time. Several parameters control the rate of char oxidation: a) bulk oxygen concentration, b) mass transfer rate of oxygen to char particles, c) conversion pathway, d) bed material fill degree and e) char particle size and shape. Parameters such as temperature and rotational speed only have a minor influence on char oxidation subject to the conditions in cement rotary kilns. Models for devolatilization and char combustion of tire rubber and pine wood have been developed and compared with experimental results. The models may be modified to qualitatively predict conversion times in industrial rotary kilns. This will, however, require further model development and preferably validation against full-scale data.

Sulfur release from cement raw materials during alternative fuel combustion have been investigated both experimentally and with thermodynamical equilibrium calculations. Known effects of temperature and gas atmosphere on the decomposition of sulfates in the raw materials

were confirmed. In addition, new knowledge was obtained regarding the effects of alternative fuel types and fuel particle sizes on sulfur release: Particularly tire rubber led to a high sulfur release. For all tested alternative fuels, the sulfur release from raw materials was observed to primarily take place during fuel devolatilization where the rapid formation of reducing agents such as CO led to high sulfur release from the raw materials. It was found that the overall sulfur release could be reduced by using larger fuel particles due to a slower devolatilization rate and a reduced tendency for local reducing conditions.

Resume (in Danish)

Cementindustrien har en stor interesse i at erstatte fossile brændsler med alternative brændsler, med henblik på at minimere omkostninger og reducere CO_2-emissioner. Disse alternative brændsler er primært faste brændsler som affaldsbaserede brændsler (RDF), brugte dæk (TDF), kød- og benmel (MBM), træaffald, kloakslam, papir, pap og plastic. Alternativ brændsels andelen af den totale energi varierer meget fra region til region, men generelt er der en tendens til stigende anvendelse af alternative brændsler. Faste alternative brændsler har typisk anderledes fysiske og kemiske egenskaber end de traditionelle faste fossile brændsler. Dette skaber et behov for nyt forbrændingsudstyr eller modifikationer på eksisterende ovnsystemer fordi, at alternative brændsler kan påvirke processtabiliteten og produktkvaliteten. Processtabiliteten påvirkes hovedsageligt ved at eksponere råmaterialefyldningen i roterovnen for reducerende atmosfærer, hvilket forøger tendensen for aflejringer i materialeindløbet på roterovnen, stigrøret og i de nedre cyklontrin. Klinkerkvaliteten kan også påvirkes af grundstoffer i brændselsasken eller af uforbrændt kulstof, der transporteres ud af roterovnen med klinkerne.

Denne afhandling giver indsigt i anvendelsen af faste alternative brændsler i materialeindløbet på roterovne. Dette indfyringspunkt er interessant fordi, at det tillader anvendelse af store brændselspartikler, hvormed behovet for en omkostningstung neddeling af brændslerne kan undgås. Udfordringen er dog, at de faste brændsler vil blive blandet med cementråmaterialerne, hvilket kan påvirke processtabiliteten og klinkerkvaliteten, som beskrevet ovenfor.

Opblandingen af brændsler og råmaterialer er blevet undersøgt eksperimentelt i en pilotskala rotertromle, og viste sig at finde sted hurtigt, med opnåelse af fuld opblanding i løbet af få tromleomdrejninger. Dette medfører, at varmeovergang ved konduktion fra cementråmaterialerne til brændselspartiklerne må forventes at være en dominerende varmeovergangsmekanisme i forhold til konvektion eller stråling fra gassen over råmaterialefyldningen. Temperaturen af cementråmaterialerne bliver derfor af stor betydning for opvarmningen af brændselspartiklerne. Forbrænding af forskellige alternative brændsler er blevet undersøgt eksperimentelt i en pilotskala roterovn under procesforhold svarende til dem i materialeindløbet på industrielle roterovne. Fokus var på dækgummi og fyrretræ, som er relevante brændsler i denne kontekst. Opvarmning, tørring og devolatilisation af alternative brændsler er hurtige processer, som primært afhænger af opvarmningshastighed og partikelstørrelse. Devolatilisation af en stor fyrretræspartikel med en tykkelse på 20 mm ved 900°C tager for eksempel omkring to minutter. Koksoxidation er derimod en langsom proces, hvilket kan reducere mængderne af faste brændsler i materialeindløbet på roterovne betydeligt, på grund af den begrænsede opholdstid. Adskillige parametre påvirker hastigheden af koksoxidationen: a) iltkoncentrationen, b) masseovergang af ilt til kokspartiklen, c) omdannelsesvejen, d) fyldningsgraden i roterovnen og e) kokspartiklens størrelse og form. Parametre som temperatur og roterhastighed har kun en mindre indflydelse på koksoxidationen under de forhold, som er til stede i cement-roterovne. Modeller for devolatilisation og koksoxidation af dækgummi og fyrretræ er blevet udviklet og sammenlignet med eksperimentelle resultater. Modellerne er blevet modificeret til kvalitativt at kunne estimere

udbrændingstider i industrielle roterovne. Yderligere modeludvikling og eventuelt sammenligning med fuldskala-data er dog påkrævet.

Svovlfrigivelse fra cementråmaterialerne under forbrændingen af alternative brændsler er blevet studeret både eksperimentelt og med termodynamiske ligevægtsberegninger. Kendte effekter af temperatur og gas atmosfære på dekomponeringen af sulfater i råmaterialerne er blevet bekræftet. Derudover er der fremkommet ny viden om effekten af forskellige alternative brændsler og brændselspartikelstørrelsen på svovlfrigivelsen: Især forbrænding af dækgummi medfører høj svovlfrigivelse fra råmaterialerne. For alle testede brændsler fandt svovlfrigivelsen fra råmaterialerne primært sted under devolatilisationen, hvor hurtig frigivelse af reduktionsmidler som CO medførte høj svovlfrigivelse fra råmaterialerne. Svovlfrigivelsen kunne reduceres ved at benytte større brændselspartikler på grund af en langsommere devolatilisation og dermed en reduceret tendens til lokale reducerende forhold i fyldningen.

Table of Contents

1 Introduction

1.1 Background

Cement production is an energy-intensive process with an energy usage of approximately 3 MJ per kg cement clinker produced (VDZ, 2009). With an annual global cement production of 3 billion tonnes cement the cement industry is responsible for approximately 2% of the world's primary energy consumption[1] (Cembureau, 2009 and BP, 2010). This corresponds to approximately 10 times the total energy consumption of Denmark (the Danish Energy Agency, 2010).

Traditionally, cement production has mainly depended on the fossil fuels, such as coal, oil and natural gas. Due to competition in the cement market, increasing fossil fuel prices and environmental concerns, cement producers have increased the utilization of alternative fuels as a substitute for fossil fuels, in order to achieve the most economic fuel mix. In this context, "alternative fuels" cover all non-fossil fuels and waste from other industries. Secondary, waste or replacement fuels are also used as synonyms for alternative fuels.

The energy share covered by alternative fuels today is different from country to country, but is most prominent in Europe and USA, see also chapter 3 section 3.2.1. The reason is mainly that infrastructure for collecting the fuels is available and the existence of a clear legislation promotes utilization of alternative fuels in cement production (VDZ, 2009).
Besides these driving forces, the following major advantages are also achieved by utilizing alternative fuels in cement production:

1. Alternative fuels may be fully or partly CO_2-neutral.
2. Production costs are typically reduced due to fuel cost savings.
3. Waste from other industries may be recycled as valuable fuel.
4. Ash from the fuels is directly incorporated into the cement clinker.
5. Flame temperatures up to around 2000°C and high residence times provide good conditions for reduction of harmful organic compounds.

However, the following should be considered when alternative fuels are utilized:

1. How is the cement clinker quality affected?
2. How is the process stability and production capacity affected?
3. Is new technology required to combust specific alternative fuels?
4. What is the combustion kinetics for different alternative fuel types?
5. Are emissions of harmful species or other environmental aspects influenced? This could e.g. be the case by introducing a chlorine by-pass in gas exit from the rotary kiln, which is often installed in connection with alternative fuel utilization.
6. How are the alternative fuels transported, stored, handled and delivered?
7. Are the alternative fuels available in sufficiently large quantities to justify investments in required technology and equipment?

[1] The primary energy consumption covers energy from coal, oil, natural gas, nuclear and hydro electric power. Other energy sources such as wind power, solar energy, biomass or geothermal power are not included.

The main technical subject of this PhD project is to investigate how solid alternative fuels may be efficiently utilized in cement rotary kilns without negative impact on clinker quality or process stability. More specifically, the project is devoted to focus on combustion in the rotary kiln material inlet end (often called the kiln back-end). The strategy is to first provide a detailed analysis of current limitations and challenges associated with solid fuel combustion in cement rotary kilns. Then it is investigated how the inorganic chemistry in rotary kilns may be affected by utilizing alternative fuels in the material inlet end. Combustion of different alternative fuels in a pilot-scale rotary drum is conducted to obtain experimental data for validation of a combustion model. Based on the model, suggestions for modification of the process and technology will be described in order to optimize solid fuel combustion. Attention should also be given to the work of Larsen (2007) about alternative fuels in cement production. This work provides an overview of the most relevant alternative fuels, with particular focus on tire-derived fuels (TDF).

Detailed descriptions of stack emissions of harmful species will not be treated in this thesis. For the emissions of NO_x and SO_2 from cement production, attention should be given to the works of Jensen (1999), Hansen (2003) and Rasmussen (2011). Considerations in terms of economy, transport, storage, handling and delivery of alternative fuels are also beyond the scope of this thesis.

1.2 Structure

Chapter 2 of this thesis provides introductory information about cement chemistry and production. It contains process data for a typical, modern cement plant as well as a description of the main rotary kiln types.

Chapter 3 reviews the current status regarding utilization of alternative fuels in cement production: Types, amounts and technology. In addition, the chapter will introduce the reader to the main challenges associated with combustion of alternative fuels in the kiln system.

Chapter 4 provides a basic understanding of the mixing process of particles with different sizes and densities in rotary kilns. This is partly through a literature study and partly through mixing experiments in a steel/plexi glass rotary drum.

Chapter 5 describes heat-up, devolatilization and combustion of large solid fuel particles in rotary kilns. Combustion kinetics for tire-derived fuels and wood is reviewed. Combustion experiments in a rotary drum under conditions similar to those in the material inlet end of a rotary kiln are described. The results are examined using mathematical models for devolatilization and char combustion.

Chapter 6 focuses on inorganic chemistry in the rotary kiln material inlet end. The emphasis is on how the release of the inorganic volatile elements S, Cl, K and Na is affected by changes in gas atmosphere towards reducing conditions. Experiments with sulfur release from raw materials during solid fuel combustion are described.

Chapter 7 provides an analysis of industrial experience with alternative fuels. The analysis is divided into experience with wet and dry long kilns, suspension preheater (SP) kilns and modern calciner kilns. The chapter also describes a full-scale model to predict devolatilization and char combustion times for TDF and other alternative fuels in rotary kilns. Finally, the chapter provides

an analysis of different alternative fuels regarding their potential use in the material inlet of rotary kilns.

Chapter 8 contains the overall conclusions regarding alternative fuel combustion in the rotary kiln material inlet end. Suggestions for further work are provided.

1.3 Objective

The main objective with this thesis is to provide scientifically based knowledge regarding combustion of solid alternative fuels in cement production. This is achieved via a combination of theoretical and experimental investigations coupled with mathematical modeling.

The knowledge may be used to improve design basis, redesign existing technology or to develop new technology in order to achieve fuel flexible rotary kilns for optimal alternative fuel combustion. The knowledge may also be used to confirm (or refute) assumptions about fuel combustion issues in the material inlet end of rotary kilns – a location that is very complex to study experimentally due to the extreme process conditions.

1.4 References

BP Statistical Review of World Energy, 2010, http://www.bp.com.

Cembureau, Activity Report 2009, http://www.cembureau.be/

Energistyrelsen, Energistatistik (the Danish Energy Agency, Energy Statistics) 2010, http://www.ens.dk. (In Danish)

Hansen, J. P.; SO_2 Emissions from Cement Production. PhD Thesis, Technical University of Denmark, Department of Chemical Engineering, 2003. ISBN 87-90142-96-9.

Jensen, L. S.; NO_x from cement production – Reduction by primary measures. PhD Thesis, Technical University of Denmark, Department of Chemical Engineering, 1999.

Larsen, M. B.; Alternative Fuels in Cement Production. PhD Thesis, Technical University of Denmark, Department of Chemical Engineering, 2007. ISBN 978-87-91435-49-8.

Rasmussen, M. H.; Low SO2 emission preheaters for cement production. PhD Thesis, Department of Chemical and Biochemical Engineering, Technical University of Denmark, 2011.

VDZ, Activity Report 2007-2009, http://www.vdz.de

2 Cement Chemistry and Production

This chapter seeks to give the reader a fundamental understanding of cement chemistry and cement production, which is necessary to read and understand the succeeding chapters.

The section about cement chemistry and processing describes the most important chemical reactions that raw materials undergo during the formation of cement clinker in the cement plant.

The sections about cement production plants start with a basic overview of a modern cement production plant. Second, the development of kiln systems from the long wet and dry rotary kilns to modern calciner kilns is described. Typical process data for a modern calciner kiln are also described.

2.1 Cement Chemistry and Processing

2.1.1 History

Burnt limestone (mortar) has been used as a binder material for constructions for more than 2,000 years (Peray, 1986). It was early discovered that burning of limestone with certain impurities improved the quality. Through the years, much experience has been gathered, leading up to the modern cement production systems that exist in the early 21st Century. Cements can be defined as adhesive substances capable of uniting fragments or masses of solid matter to a compact whole (Hewlett, 1998). Cement sets and hardens by chemical interaction with water. Cements are widely used to produce adhesion between stones, bricks, etc. in the construction of buildings and engineering works. Today, the main type of cement that is used is *Portland cement* and it is primarily based on a mixture of burned limestone, sand and clay. Several other types of cement with different characteristics can be tailored for specific purposes, but this thesis will only describe the Portland cement.

2.1.2 Raw materials

The main raw materials used for the Portland cement is naturally occurring limestone, clay and sand. Limestone is the source of calcium ($CaCO_3$, $CaMg(CO_3)_2$), while clay and sand are the sources of silicon, aluminium and iron (Al_2O_3, SiO_2, Fe_2O_3) (Hewlett, 1998). In recent years, there has been an increasing tendency to use industrial wastes as alternative raw materials. Examples are coal fly ash from power plants, water treatment sludge or slags from alumina, phosphorus and steel production (Bhatty et al., 2004).

Solid fuels used for cement production – traditional or alternative - introduce a certain amount of ash components left after the combustion. The ash will also be incorporated in the final cement clinker. The total mixture of raw materials and ash should match the desired cement clinker chemistry. Thus, individual evaluations must be performed when either solid fuels or raw materials are changed.

2.1.3 Preparation of raw materials

The raw materials are crushed to particle sizes of approximately 25-100 mm and stored in separate raw material storages (Andersen, 1981), see Figure 2-1. These stores serve two purposes:

- As intermediate stores to allow cement production to continue even if no new raw materials are supplied.
- To even out the variations bound to exist in the chemical compositions of the raw materials.

After being reclaimed from their respective stores, the raw materials are mixed in the correct proportions and transported to the raw mill. The proportions will typically be 75-80 wt.-% limestone, 20-25 wt.-% clay and possibly smaller amounts of iron ore and/or sand to adjust the overall composition to meet the requirements for Portland cement (Andersen, 1981).

In the raw mill the mixed raw materials are ground to raw meal (almost as fine as wheat flour), with a particle size around 5-125 μm. The fineness of the particles is important to ensure good heating, calcining and burning capabilities of the raw materials (Bhatty et al., 2004).
In the raw mill, the raw meal is also dried by hot flue gases from the kiln system. The dried raw meal ready for production is then transferred to and stored in a silo. The silo serves two purposes:

- To further even out the variations in the chemical composition of the raw meal.
- Act as a buffer store to ensure continuous cement production in cases where no new raw materials are supplied.

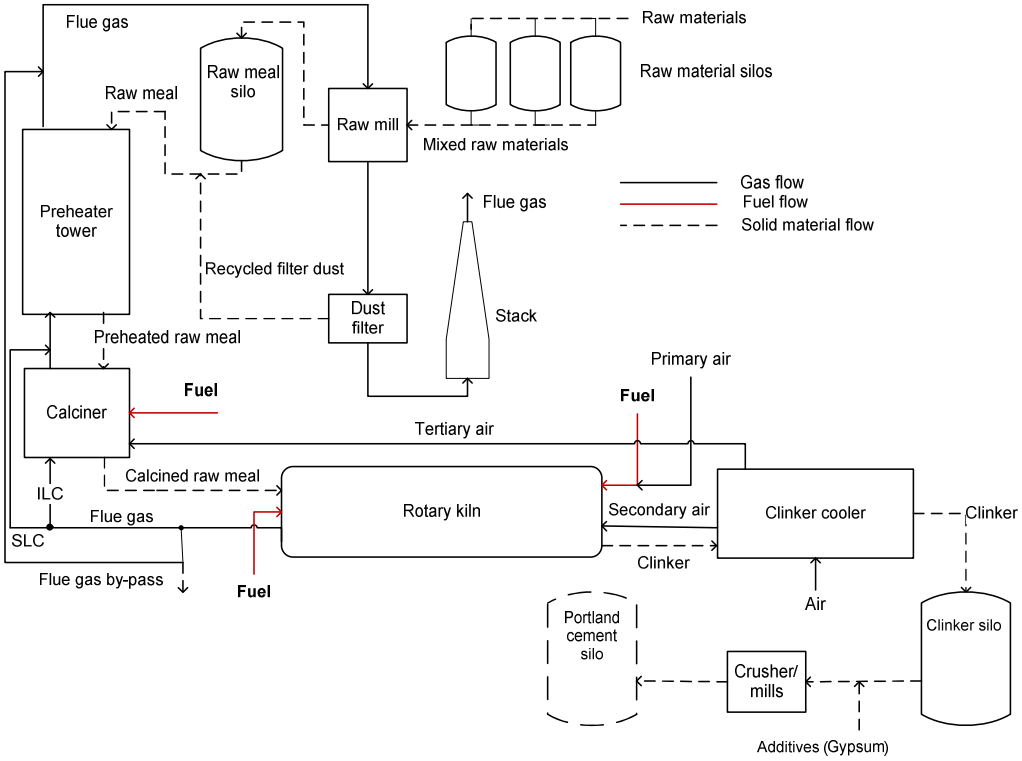

Figure 2-1: Typical process flow diagram of a modern cement production plant.

2.1.4 Preheating of raw meal

Raw meal from the silo is led to the top of the preheater tower and heated counter currently by direct contact with the hot flue gases from the rotary kiln and calciner, see Figure 2-1. Thus the preheater tower functions as a heat exchanger where the energy from the hot flue gases is transferred to the raw meal. After having passed the preheater cyclones, the raw meal will have reached a temperature of approximately 800ºC (Hewlett, 1998). The preheated raw meal is then admitted to the calciner where the first major chemical reaction takes place.
The hot flue gases from the rotary kiln may be passed through the calciner (In-Line Calciner, ILC) or bypassed (Separate-Line Calciner, SLC) before being directed into the preheater cyclones.

2.1.5 Calcination

In the calciner most of the calcium carbonate in the feed will be thermally decomposed to its oxide and carbon dioxide, see equation (2.1):

$$CaCO_3\ (s) \rightarrow CO_2\ (g) + CaO\ (s) \qquad \Delta H_{25°C,\ 1\ atm} = 1782\ kJ/kg\ CaCO_3 \qquad (2.1)$$

This very endothermic reaction consumes approximately 60% of the total energy required (Hewlett, 1998). Decomposition of $CaCO_3$ takes place when the temperature is higher than approximately 700ºC and continues until all CO_2 is expelled.

2.1.6 Clinker reactions

After having passed the calciner, the calcined raw meal is admitted to the rotary kiln where the remaining cement clinker reactions take place, see Figure 2-1. Calcined raw meal is also called hot meal in cement terminology in order to distinguish it from raw meal not yet calcined.

The names, chemical compositions and abbreviations used in cement nomenclature for the four main constituents of Portland cement clinker are shown in Table 2-1. Belite and alite are the strength-giving minerals. Alite reacts fast with water during hydration and accounts for the early strengths while belite reacts slower and gives the cement its late strengths (Hewlett, 1998). Ferrite and aluminate do not contribute to the strengths of the cement. But they possess important properties when burning clinker (Hewlett, 1998). These properties of ferrite and aluminate will be explained later in this section.

Name	Chemical composition	Nomenclature
Belite	$2CaO{\cdot}SiO_2$	C_2S
Alite	$3CaO{\cdot}SiO_2$	C_3S
Ferrite	$4CaO{\cdot}Al_2O_3{\cdot}Fe_2O_3$	C_4AF
Aluminate	$3CaO{\cdot}Al_2O_3$	C_3A

Table 2-1: Main constituents of Portland cement clinker.

Free lime (CaO), free periclase (MgO), earth alkali sulfates ($CaSO_4$, $MgSO_4$), Alkali sulfates (Na_2SO_4, K_2SO_4) and other minor components may also be found in the clinker (Theisen, 2007).

The requirements for the Portland cement clinker are (Hewlett, 1998):

a) > 67 wt.-% calcium silicates (C_2S and C_3S). The remainder must mainly be Fe_2O_3, Al_2O_3 and other oxides.
b) < 5 wt.-% MgO
c) The CaO/SiO_2 ratio by mass shall not be less than 2.0.

Clinker reactions occur at temperatures between 700-1450ºC, see Figure 2-2. The reactions forming the final clinker involve intermediate compounds, and the clinker reactions may be affected by minor compounds. The overall clinker reactions are described, while a detailed overview of the chemistry, phase relations etc. is provided by Hewlett (1998), Bye (1999) and Bhatty (2004).

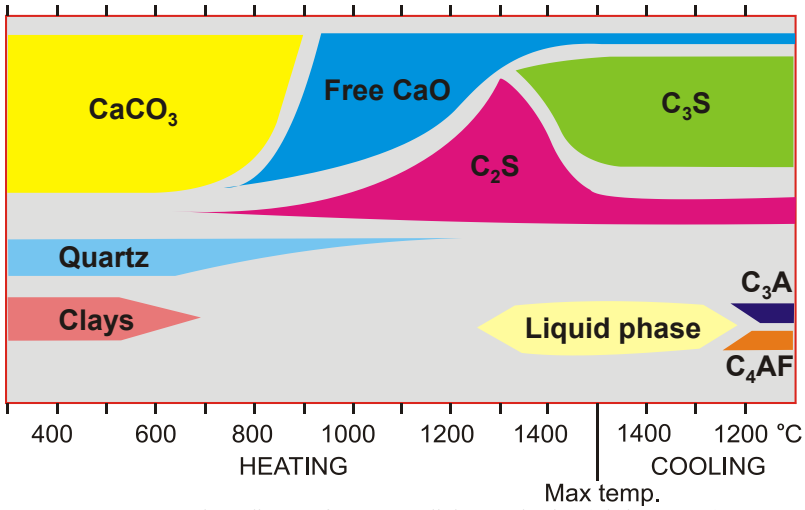

Figure 2-2 : Phase diagram for cement clinker production (Theisen, 2007).

The formation of belite from CaO and SiO_2 takes place at temperatures above 700ºC, see equation (2.2):

$$2\ CaO\ (s) + SiO_2\ (s) \rightarrow 2CaO{\cdot}SiO_2\ (s) \qquad (2.2)$$

This reaction is shown in Figure 2-2 where the silicate source quartz and the free CaO is being consumed while belite is created.

At temperatures above 1,300ºC, a liquid phase containing alumina (Al_2O_3) and iron oxide (Fe_2O_3) is formed. Alumina and iron oxide are not essential to the constitution of the final Portland cement product but, at this stage in the process, the liquid phase acts as a source of fluxes lowering the energy requirement thereby making the process economical (Hewlett, 1998). The liquid phase has a significant influence on the alite formation because it wets all the solid grains, forming an interpenetrating film. It has two functions (Hewlett, 1998):

- Its surface tension pulls the solid grains together, helping to form nodules known as "clinker".
- It facilitates material transport in the liquid phase.

The liquid phase acts as a media for increased diffusive transport, accelerating the formation of alite crystals from belite and free lime, see equation (2.3):

$$CaO\ (s) + 2CaO{\cdot}SiO_2\ (s) \rightarrow 3CaO{\cdot}SiO_2\ (s) \qquad (2.3)$$

Aluminate and ferrite will crystallize from the liquid phase when the temperature drops to approximately 1,230ºC according to (2.4) and (2.5):

$$3\ CaO\ (s) + Al_2O_3\ (l) \rightarrow 3CaO{\cdot}Al_2O_3\ (s) \qquad (2.4)$$

$$4\ CaO\ (s) + Al_2O_3\ (l) + Fe_2O_3\ (l) \rightarrow 4CaO{\cdot}Al_2O_3{\cdot}Fe_2O_3\ (s) \qquad (2.5)$$

The rotary movement of the rotary kiln also helps to create the clinker nodules, by creating a continuous rolling motion of the clinker material. This rolling motion is described in greater details in chapter 4. In addition, the inclination of the rotary kiln facilitates a continuous transport of the calcined raw materials from the rotary kiln material inlet towards the rotary kiln material outlet, where the clinker nodules are admitted to a clinker cooler.

2.1.7 Clinker Cooling

The Portland cement clinker has reached a temperature of up to 1,450ºC at the rotary kiln exit, see Figure 2-1. It is important to recover as much energy as possible and return it to the process. This is achieved by passing the hot clinker through a grate cooler where typically ambient air will pass the clinker, thereby cooling them by direct contact in cross current flow. The heated air is used for the combustion in the rotary kiln and in the calciner.
Experience has shown that it is important with a high rate of clinker cooling from 1,450ºC to 1,200ºC if the best strength-giving properties should be achieved. Microscopic investigations have revealed that a *slow* cooling from 1,450ºC to 1,200ºC often results in alite being partially transformed back into belite and free lime. This is undesirable since it may lead to setting problems with the final product (Hewlett, 1998).

2.1.8 Clinker grinding and storage

The clinker leaving the cooler has a variable particle size, typically of diameter 3-25 mm. Thus it is necessary to grind the clinker to a more uniform particle size. This can either be done directly after the cooler, or the clinker can be transferred to a silo until it is needed, see Figure 2-1. Cement clinker is, however, not a stable material: It reacts readily with water/water vapour and CO_2 from the air. This will result in pre-hydration and carbonation. Extended storage periods may therefore have an effect on the cement properties.

In connection with the clinker grinding, 3-6 wt-% gypsum ($CaSO_4 \cdot 2H_2O$) is added to the clinker. The gypsum has a marked effect on both the strength and the setting of cement (Theisen, 2007). Additives such as coal fly ash, sand or raw material may also be added at this point in order to contribute positively to the strength-giving properties of the cement (Hewlett, 1998). Some of these additives can replace a significant fraction of the clinker, thereby saving energy needed for calcination and clinker reactions. Thus the additives have a great potential to reduce energy consumption and CO_2-emissions per kg cement produced (WWF, 2008). For this reason, many cement companies seek to minimize their environmental impact by exploring the use of new Supplementary Cementitious Materials (SCM), examples being volcanic ashes or kaolinite clays (Ballan, 2011).
The grinding of clinker and additives can be performed with several different mill systems. When a sufficient fineness is reached, the final Portland cement product is transferred to a cement silo. It is stored in this silo until it is being packed and shipped to the end users.

2.2 The kiln system

The production of cement may be divided into three parts: 1) Preparation of raw materials, 2) pyro-processing and 3) clinker processing, storage and shipment. Pyro-processing covers the thermal treatment of the raw materials necessary to obtain the cement clinker. Pyro-processing takes place in the preheater, calciner, rotary kiln and cooler. These sections are commonly referred to as the *kiln system*. This section will aim to describe the modern kiln system since alternative fuels are fired in the calciner or the rotary kiln part of the kiln system.

2.2.1 Rotary kiln

The rotary kiln is often referred to as the heart of every cement plant. This is where the chemical clinker formation reactions take place. The rotary kiln is simply a long, cylindrical tube consisting of an outer steel shell and an inner refractory lining, see Figure 2-3. Typical lengths and diameters for modern rotary kilns are between 40-100 m, and 3-6 m, respectively. Rotary kilns are inclined 1-3° and rotate 1-5 rpm in order to facilitate mass transport and ensure clinker forming processes such as nodulization. Production capacity is typically 2,000-4,000 tonnes of clinker per day (tpd), but may be as high as 12,000 tpd (FLSmidth, 2009).

In the material outlet, the rotary kiln is equipped with a burner. The burner's main function is to form a flame to provide energy for the clinker reactions to take place. The flame of the rotary kiln burner should be short, narrow and strongly radiant in order to achieve a good heat transfer from the flame to the materials in the bed (Vaccaro, 2006). Figure 2-3 illustrates the kiln burner and flame. The hot material bed is seen below the burner.
Modern rotary kiln burners are often designed to burn a variety of fuels. This is today achieved by using multi-channel burners with separate channels for fuels and primary air which make it possible to adjust primary air amounts, injection velocities and momentum independently of the fuel flows (Vaccaro, 2006, FLSmidth, 2011). Swirl may be used to enhance mixing and stabilize the flame. The recent trend in multiple fuel burners is to use a single common fuel channel which allows more flexibility towards fuel particle size and type (FLSmidth, 2009).

Figure 2-3: Left: Outer view of a rotary kiln seen from above. Dimensions (LxD) = 40 m x 4 m. The tertiary air duct is seen next to the rotary kiln, see also section 2.2.4. Right: Inner view of a rotary kiln seen from the burner end.

In early cement plants, the kiln system consisted only of a rotary kiln: Raw materials were dried, preheated, calcined and burned to clinker on their way through the rotary kiln. This process required very long rotary kilns, often significantly longer than 100 m. The raw materials were either introduced as dry raw meal or as water/raw material slurry, and this type of plants were therefore commonly referred to as dry long kilns or wet long kilns, respectively. Due to a low energy efficiency, this type of cement plants is very expensive to operate, and are rarely constructed today. However, many wet and dry long kilns still exist, especially in North America (Bhatty, 2004).

The rotary kiln consists of an outer steel shell and an inner refractory lining for thermal insulation, in order to maintain and resist the high process temperatures. In a rotary kiln, the refractory usually consists of bricks of special composition and sizes, able to withstand high temperatures. However, the refractory may also be a cast lining of concrete. The refractory lining is subject to a wide range of destructive influences through the mechanical dynamics of the rotary kiln, the chemistry of the cement clinker process and the type of fuels used. The intensity of these stresses varies according to the operating conditions and kiln sections (Bartha, 2004). The rotary kiln is therefore equipped with a range of refractory bricks with different properties to ensure appropriate kiln zone lining.

The burning zone refractory lining usually suffers the greatest wear due to the higher temperatures in the burning zone. However, the burning zone lining is protected by a coating layer which prolong the lifetime of the refractory lining. The coating is a mass of clinker or dust particles that adheres to the wall of the kiln, having changed from a liquid or semiliquid to a solidified state (Peray, 1986). Generally, the burning zone refractory lifetime is 9 to 12 months depending on the specific kiln type and operating conditions. The refractory lifetime of the colder rotary kiln material inlet zone is typically 12 to 48 months. Thus, these different rotary kiln zones do not have to be replaced quite as frequently (Bartha, 2004).

The most used brick types today are chromium-free magnesia-alumina-spinel bricks with MgO content of 80-95 wt.-% and Al_2O_3 content of 3-18 wt.-%. Minor compounds are typically Fe_2O_3, Mn_2O_3, SiO_2, CaO and ZrO_2 (Bartha, 2004 and Harder, 2008). These brick types are regarded as having the longest service life and the best price/performance ratio (Harder, 2008).

The increased use of alternative fuels in the cement industry may lead to higher levels of recirculating alkali metals and sulfur within the kiln system, see chapter 3, section 3.4.4. Recirculating alkali metals and sulfur cause large quantities of salts to condense in and on the refractory lining, predominantly in the temperature window 750°C to 1,100°C (Harder, 2008). Salt compounds enter into reactions with refractory bricks that contain alumina and the bricks can be destroyed by salt crystallization and alkali spalling. Sulfur oxides make the reactions even worse, by formation of alkali sulfate salts (Klischat et al., 2002).
Various strategies are used by the refractories industry to counteract these wear processes. These include use of additives that produce low gas permeability and reduce the infiltration tendency of alkalis. Other solutions are sealing or impregnating the refractory material to form a protective zone (Harder, 2008). One of the most successful and widespread solutions is addition of 3-6 wt.-% silicon carbide, SiC, which leads to an appreciable resistance to alkali attack (Klischat et al., 2002, Bartha, 2004 and Harder, 2008). The addition of SiC leads in situ to formation of liquid phases, which seal the refractory surface and protect against alkali infiltration (Bartha, 2004).

Increased circulation of inorganic volatiles such as sulfur and chlorine in the kiln system, due to increased alternative fuel utilization also entails a higher risk of kiln shell corrosion (Jøns and

Østergaard, 2001). Efforts have been made to identify suitable refractory steels for cement rotary kilns, with characteristics that are a compromise between good creep resistance, high corrosion resistance in the presence of chlorine and sulfur, and strong resistance to abrasion when hot (Corcuera, 2004).

2.2.2 Design of modern rotary kilns for ILC systems

This section will outline important design criteria for modern rotary kilns. Since these design criteria may differ between different kiln systems, focus will be on the In-Line Calciner (ILC) type which is described in greater detail in section 2.2.4. Cement plants of the ILC type are among the most commonly built cement plants in recent years, and this trend seems to continue.

The rotary kiln dimensions depend on the required production capacity and of the thermal load. The production capacity is related to the mass and energy balances through the rotary kiln because the production capacity is a function of the hot flue gas volume passing through the rotary kiln per time unit. The thermal load can be expressed by the two terms a) volumetric load and b) burning zone load.
The volumetric load is a measure of the production in tpd clinker per m^3 kiln volume inside lining, and has the unit tpd/m^3. The volumetric load decreases when the kiln dimensions increases. Typical volumetric loads for ILC type rotary kilns are between 3.6 and 5.3 tpd/m^3. However, the volumetric load can be higher if the burnability of the raw materials is good.
The burning zone load is defined as energy quantity per time per area of burning zone, and has the units W/m^2. If the kiln dimensions are increased, the burning zone load will decrease because the energy quantity per time unit will be distributed over a larger area. Typical burning zone loads for ILC rotary kilns are 2.9 to 6.2 MW/m^2. The burning zone load must be kept between these specific limits in order to ensure a sufficient refractory lining lifetime.

Modern rotary kilns may be supported by either two or three supports. The 3-support rotary kilns typically have a length-diameter (L/D) ratio of 16 to 18 whereas 2-support rotary kilns typically have L/D ratio of 10-14 (FLSmidth, 2005). A 2-support rotary kiln is shown in Figure 2-4. The material inlet end is shown to the right and the grate cooler is shown to the left.
Each support has two rollers which support the rotary kiln and facilitates its rotary movement. Only one pair of supporting rollers is connected to a kiln drive which rotates the entire rotary kiln. The other pair of rollers acts simply as supports for the rotary kiln. To ensure optimal contact between the rollers and the rotary kiln, self-adjusting supports have been developed which can equalize the load between the rollers, also under varying operating conditions (FLSmidth, 2005).
Both ends of the rotary kiln are equipped with lamella seals to prevent hot gas and solid materials from escaping from the kiln system. Lamella seals are a relatively new invention which has successfully replaced traditional pneumatic and spring seals. Lamella seals are practically maintenance-free (FLSmidth, 2005).

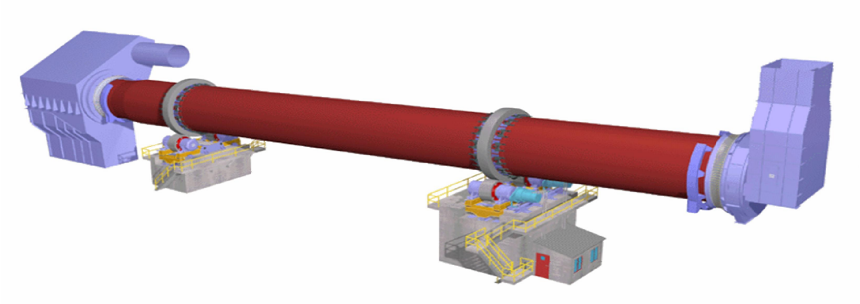

Figure 2-4: 2-support rotary kiln. Each support has two rollers, one of them with kiln drives (FLSmidth, 2005).

2-support rotary kilns have several advantages compared to 3-support rotary kilns: Eliminating one kiln support reduces the total initial installation cost, and fewer components need to be maintained. The shorter rotary kiln dimensions also lead to a lower heat loss from the kiln surface.
It is well-known that kiln shells may suffer deformation, e.g. due to short kiln shutdowns or other situations that involves temporary cooling-heating cycles. For a 3-support rotary kiln such deformation may cause loss of contact with one or two of the supporting rollers and increased loads on the other rollers. In comparison, the 2-support rotary kiln will always maintain contact with all four supporting rollers.
2-support rotary kilns usually have a larger diameter than 3-support rotary kilns of the same production rate and volumetric load, resulting in a lower burning zone load. The lower burning zone load results in improved burning zone refractory lifetime (FLSmidth, 2005).

One drawback with the shorter L/D ratio of a 2-support rotary kiln is that it may lead to higher temperatures of the flue gases leaving the rotary kiln, depending on calcining degree of the partially calcined raw meal fed to the rotary kiln, raw meal burnability and other process conditions. In order to avoid deposit build-ups in the kiln riser duct caused by high temperatures, it may be necessary to control temperatures by feeding raw meal from the second-lowest preheater cyclone to the kiln riser duct (FLSmidth, 2005).
Regarding alternative fuel combustion in the rotary kiln, it may be necessary to increase the length of the rotary kiln in order to ensure sufficient time for fuel burnout and ash sintering.

2.2.3 Preheater and calciner systems

In modern cement plants, raw meal is preheated to calcination temperature in a multi-stage cyclone preheater, see Figure 2-5. The raw material feed is fed to the system between the 1st and 2nd cyclone preheater. Heat exchange with the gas takes place followed by a gas/solid separation in the 1st stage cyclone (the top cyclone). The gas that leaves the 1st stage is transferred to the raw mill, dust filter and finally to the stack. In this way, as much heat as possible is recycled. The solids are conveyed to the gas between the 2nd and 3rd stage where they experience a similar heat exchange and gas/solid separation. The solid residence time through a 5-stage cyclone preheater is in the range of 50 seconds (Strauß et al., 1987).
Most of the calcination process takes place in a separately fired calciner. The calciner is not only designed to decompose $CaCO_3$ to CaO, but also to convert the fuel sufficiently and to reduce emissions to a minimum.

There are different kinds of calciner systems, but the two main types are:

1) In-line calciner (ILC)
2) Separate line calciner - Downdraft (SLC-D)

The ILC system may also be connected to separate equipment for combustion of solid alternative fuels, such as the HOTDISC. This will be described in greater detail in chapter 3, section 3.3. In the following, a representative description of an ILC system will be given.

2.2.4 In-Line Calciner (ILC) system

The ILC system shown in Figure 2-5 is characterized in that the flue gas from the rotary kiln is led directly through the calciner. The degree of calcination in the ILC system is very high, often in the range of 90-95%. The production capacity is in the range of 1,500-12,000 tpd and the ratio of firing in the calciner is typically 55-65%.

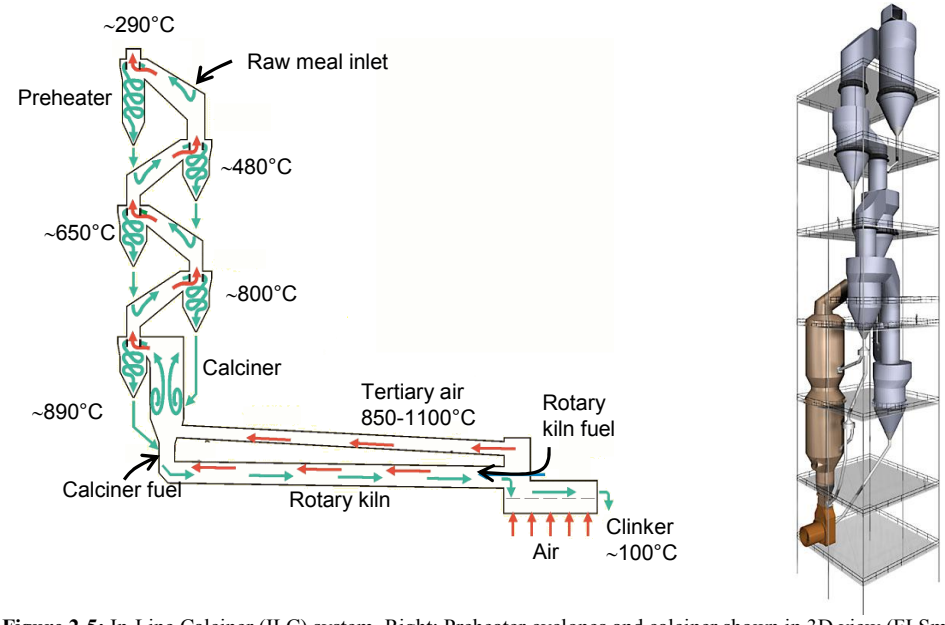

Figure 2-5: In-Line Calciner (ILC) system. Right: Preheater cyclones and calciner shown in 3D view (FLSmidth, 2011).

A part of the combustion air in the calciner is drawn directly from the cooler through a separate tertiary air duct between the cooler and the calciner. Thus, the gas volume through the rotary kiln is reduced and the size of the rotary kiln can be smaller. In addition, the ILC system provides good conditions for reduction of NO_x formed in the rotary kiln due to reducing conditions in the region between the calciner fuel injection and the tertiary air admission (Jensen, 1999). The reducing zone is illustrated in Figure 2-6, which also shows the tertiary air duct above the reducing zone. Above the fuel inlet and tertiary air duct is an oxidizing zone where the fuel is combusted, leading to an increase in temperature. This temperature increase is controlled by addition of raw meal to the lower calciner part, which uses the heat for the calcination reaction. Above the restriction is the

calcining zone where most of the endothermic calcination reaction takes place, facilitated by an efficient heat transfer from gas to solids. Gas and solid particles leaves the calciner through a loop duct, which provides good conditions for CO oxidation by improving the gas mixing.

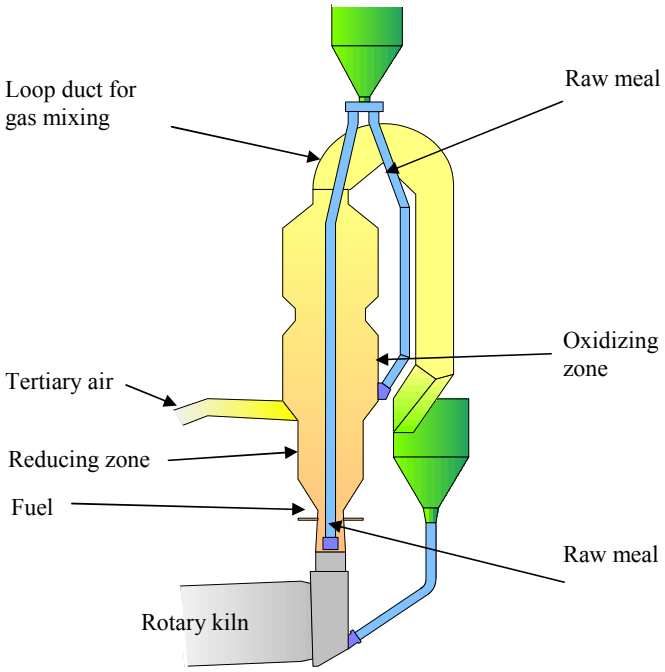

Figure 2-6: The In-Line-Calciner. Notice the NO_x-reducing zone in the lower calciner part (Sønderborg, 2007).

The ILC system is also well suited for alternative fuels in solids forms, because they burn in suspension imaging single particle behavior. The suspension type burning ensures good external mass and heat transfer (Larsen, 2007).
The temperature in the ILC system reflects the equilibrium temperature of calcination and is typically 850-900°C. In the lower part, the oxygen level is low because fuel is admitted without its combustion air. In the region of the tertiary air duct, preheated air increases the oxygen content to typically 11-12% O_2. The oxygen level decreases from this point and up to the lowermost cyclone due to the combustion process and due to a dilution with formed CO_2. In modern FLSmidth calciners the gas velocity through the calciner is normally kept at 8 m/s and the gas retention time is about 3-4 seconds before the loop duct starts (Sønderborg, 2007).

2.3 Overview of process data

This section provides an overview of important process data for a modern calciner kiln. The given process data are representative of an ILC system.

Temperatures and retention times for both gas and solids are shown in Table 2-2. From this table it is observed that the solid material is heated from approximately 100°C in the preheater to 1,450°C in the rotary kiln burning zone, and then finally cooled to approximately 100°C in the clinker cooler. The gas being transported in the opposite direction is observed to enter the system at ambient temperature in the clinker cooler (or as primary air through the kiln burner). The gas then reaches temperatures of up to around 2,000°C in the rotary kiln burning zone whereafter the gas temperature gradually decreases through the rotary kiln, calciner and preheater before it leaves the kiln system at temperatures around 350°C. The gas is then used to preheat the cement raw materials in the raw mill, and will finally leave through the stack at temperatures around 100°C. It should be noted that gas and material retention times are typical values, but will depend on the specific cement plant layout.

Equipment	Preheater	Calciner	Rotary kiln	Cooler
Gas temperature (°C)	350-880	880-1100	1100-2000	1100-ambient
Gas retention time	≈ 5-10 s	≈ 3-4	≈ 5-10 s	≈ 1 s
Material temperature (°C)	100-780	780-900	900-1450	1400-100
Material retention time	≈ 50 s	≈ 5 s	15-30 min	≈ 30 min

Table 2-2: Typical temperatures and residence times in a modern calciner kiln (Cembureau, 1999).

Oxygen concentrations in a modern calciner kiln

Clinker cooler and rotary kiln
The combustion air enters the kiln system through either the clinker cooler or kiln burner as ambient air with oxygen concentration around 21 vol.-%. In the rotary kiln the oxygen concentration decreases as the combustion proceeds to approximately 2-7 vol.-% in the rotary kiln gas outlet. However, a fraction of the combustion air is bypassed via the tertiary air duct and will be transported directly from the clinker cooler to the calciner as approximately 1,000°C hot, atmospheric air.

Calciner
In the lower part of the calciner, the oxygen level is low because fuel is admitted without its combustion air, see Figure 2-6. In the region of the tertiary air duct, preheated air increases the oxygen content to typically 11-12 vol.-% O_2. The oxygen level decreases from this point and up to the lowermost cyclone due to the combustion process and due to a dilution with formed CO_2.

Preheater
In the preheater section, the oxygen concentration is only slightly affected by oxidation reactions of minor components in the raw meal, e.g.:

1. Formation of SO_2 from pyrite (FeS_2) which is the main reason for SO_2 emissions from cement plants (Hansen, 2003).
2. Recarbonation of CaO forming $CaCO_3$.
3. Combustion of organic bound carbon.

In addition, small amounts of atmospheric air (false air) are often introduced into the preheater section due to the slightly negative pressure.

Stack
Oxygen levels in the stack flue gas are typically around 5-10 vol.-%.

2.4 Conclusions for chapter 2

Production of Portland cement requires that the raw materials limestone, clay and sand are heated up to approximately 1,450°C in order to first calcine limestone and, secondly, facilitate the clinker reactions between lime and silicates. The main strength giving components in Portland cement are belite (C_2S) and alite (C_3S).

The production of cement may be divided into three parts: 1) Preparation of raw materials, 2) pyro-processing and 3) Clinker processing, storage and shipment. Pyro-processing covers the thermal treatment of the raw materials necessary to obtain the cement clinker. Pyro-processing in a modern cement plant takes place in the preheater, calciner, rotary kiln and cooler. These sections are commonly referred to as the *kiln system*.

Since the calcination is a very endothermic process, 50-60% of the total energy is usually fired into the calciner, whereas the remaining 40-50% is fired through the kiln burner. However, some cement plants do also fire a part of the energy into the rotary kiln material inlet end or through separate combustion devices coupled to the kiln system. This will be described in greater detail in chapters 3 and 7.

Temperatures in the kiln system range from ambient temperatures up to 2,000°C, and oxygen levels range from 2 vol.-% to 21 vol.-% dependent on position in the kiln system.
Solid and gas retention times vary in the different sections of the kiln system. In the rotary kiln, gas retention times may be in the order of 5-10 seconds, while solid retention times may be as long as 15-30 minutes.

2.5 References

Andersen, P. S.; The Cement Factory; FLSmidth & Co. A/S, Valby, Denmark, 1981.

Ballan, J.; Refining pozzolan – the greener alternative. Highlights, FLSmidth, 32-33, May 2011.

Bartha, P.; The cement rotary kiln and its refractory lining. Interceram, Refractories Manual, 14-17, 2004.

Bhatty, J. I., Miller, F. McG. and Kosmatka, S. H. (Editors); Innovations in Portland Cement Manufacturing, Portland Cement Association (PCA), Illinois, USA, 2004. ISBN: 0-89312-234-3.

Bye, G. C.; Portland Cement; 2nd edition, Thomas Telford, London, 1999. ISBN 0-7277-2766-4.

Cembureau; Best Available Techniques for the Cement Industry, Belgium, 1999. Available from: http://cembureau.be/.

Corcuera, A.; Refractory steels: AFs and corrosion problems. World Cement, 99-102, November, 2004.

FLSmidth; Burning bright, World Cement, 101-102, December 2009.

FLSmidth; Preheater calciner systems, Brochure, FLSmidth, Valby, Denmark, 2011. Available from: http://flsmidth.com.

FLSmidth; ROTAX-2 Kiln components, Brochure, FLSmidth, Valby, Denmark, 2005. Available from: http://flsmidth.com.

FLSmidth; Fast payback burner upgrades. International Cement Review, 121-122, May 2011.

Hansen, J. P.; SO_2 Emissions from Cement Production. PhD Thesis, Technical University of Denmark, Department of Chemical Engineering, 2003. ISBN 87-90142-96-9.

Harder, J.; Trends in refractory materials for the cement industry. ZKG International, Vol. 61, No. 5, 36-45, 2008.

Hewlett, P. C. (Editor); Chemistry of Cement and Concrete; 4th edition, John Wiley & Sons Inc., New York, 1998. ISBN 0-340-56589-6.

Jensen, L. S.; NO_x from cement production – Reduction by primary measures. PhD Thesis, Technical University of Denmark, Department of Chemical Engineering, 1999.

Jøns, E. S. and Østergaard, M. J.; Kiln Shell Corrosion, IEEE-IAS/PCA Cement Industry Technical Conference, Vancouver, British Columbia, Canada, 343-359, 2001.

Klischat, H.-J., Liever, H. and Wirsing, H.; Alkali-resistant linings for the security and preheating zones in rotary cement and lime kilns subject to chemical attack. ZKG International, No. 6, 66-75, 2002.

Larsen, M. B.; Alternative Fuels in Cement Production; PhD Thesis, Department of Chemical Engineering, Technical University of Denmark, 2007. ISBN 978-87-91435-49-8.

Peray, K. E.; The Rotary Cement Kiln; 2nd edition, Edward Arnold Ltd., Victoria, Australia, 1986. ISBN 0-7131-3609X.

Strauß, F., Steinbiß, E. and Wolter, A.; Measurement of retention times in cement burning systems with the aid of radionuclides. ZKG-International, 9, 441-446, 1987.

Sønderborg, H. R.; The International Cement Production Seminar 2007, Volume IA, Lecture 05-01; FLSmidth A/S, Valby, Denmark, 2007.

Theisen, K.; The International Cement Production Seminar 2007, Volume II, Lecture 06-02/03; FLSmidth A/S, Valby, Denmark, 2007.

Vaccaro, M.; Burning alternative fuels in rotary cement kilns, IEEE Conference Paper, 127-136, 2006.

WWF, A blueprint for a climate friendly cement industry. WWF International, Gland, Switzerland, 2008.

3 Alternative fuels in cement production

This chapter provides an overall insight into the use of alternative fuels in cement production. Section 3.1 describes the general requirements for alternative fuels to be used, and section 3.2 reviews current trends in the cement industry. Section 3.3 describes technology for combustion of alternative fuels, advantages as well as disadvantages. Finally, section 3.4 provides an overview of challenges related to the substitution of fossil fuels with alternative fuels.

3.1 Requirements for alternative fuels in cement production

The global cement production in 2009 was estimated to be 3 billion tonnes (Cembureau, 2009). The fuel energy consumption is about 3 MJ/kg cement (Schneider, 2009), corresponding to a total global energy consumption of approximately $9 \cdot 10^{12}$ MJ/year. It is estimated that the cement industry is responsible for approximately 2% of the world's primary energy consumption, corresponding to approximately 10 times the total energy consumption of Denmark (BP, 2010 and ENS, 2010). It is also estimated that cement production accounts for 5% of the global CO_2-emissions, arising partly from fuel combustion, thermal calcination of limestone, electricity use and transport (CSI, 2005; PBL, 2007).

Fuel consumption accounts for a significant fraction of the total cement clinker production costs, which makes it attractive for cement producers to consider cheaper substitute fuels. In addition, increasing concerns about CO_2-emissions put pressure on the cement industry to reduce emissions, e.g. by substituting fossil fuels with CO_2-neutral fuels. However, the cement industry has certain requirements with respect to alternative fuels, the most important ones being:

1. Overall clinker production costs.
2. Availability (must be available in sufficiently large amounts).
3. Legislation (a clear legislation and permission from local authorities is often mandatory before specific alternative fuels can be used).
4. Technical possibility for transport, handling and combustion of the specific alternative fuel.

In addition to these general requirements for alternative fuels, there are some fuel specific requirements as well:

1. The content of water (as low as possible).
2. Content of minor components must be within acceptable limits.
3. Emissions, process stability and product quality must not be affected negatively.
4. Alternative fuel size and shape.
5. Energy density.

Re 1: An increase in water content compared to traditional fuels can increase the flue gas volume. This may decrease the production capacity of the cement kiln if ID-fan capacity is insufficient (Krennbauer, 2006). The change in production capacity depends mainly on the water content of the fuel. Pre-drying of the fuel can help to reduce this problem, or the cement plant can be equipped with an ID-fan with a sufficiently large capacity to compensate for an increase in exhaust gas

volume. Too high moisture contents of the alternative fuel may also slow the drying and combustion process and potentially move the combustion zone in e.g. the calciner.

Re 2: Most chemical elements from the fuel ash are incorporated into the cement clinker. However, volatile elements such as chlorine, sodium, potassium, sulfur, mercury and thallium will partly evaporate in the hotter regions of the kiln system. These volatile elements may condense from the gas phase again in e.g. the preheater, being captured in the bag filter, or being removed through a bypass or escape with the stack gases. In order to ensure the cement quality and process stability, it is therefore necessary to control the levels of all chemical inputs via the fuel. This will be further explained in section 3.4.

Re 3: Substitution to a specific alternative fuel must not have any negative effect on the emission level, process stability or product quality. Such considerations will be described further in section 3.4.

Re 4: The combustion behavior of solid fuel particles depends on the particle size and shape. If there are large variations in fuel particle size and shape, it becomes challenging to control the cement production. For this reason, there are often requirements to the maximum allowable fuel particle size, and sometimes also shape, to be used in a specific kiln system. Please note here that the virgin fuel shape may change considerably upon combustion, see also section 5.1.1.

Re 5: It is generally desirable to have as high an energy density as possible, in order to reduce transportation costs. Some alternative fuels have relatively low energy densities. Consequently, larger fractions must be fed to the kiln system to give the same energy as fuels with a higher energy density. These low energy density fuels may still be attractive to use, if the price is low enough to balance the additional costs associated with transport, handling, etc.

Many of the alternative fuels that are available for the cement industry in large amounts consist of mixtures of waste with fluctuations in composition. Thus, alternative fuels are often relatively in-homogenous fuels. Since modern cement kiln systems are always designed to operate with a continuous clinker production, fluctuations in fuel quality may occur, necessitating a stringent process control.

3.2 Types and quantities of alternative fuels

A study of the various types of alternative fuels has been provided by Larsen (2007) and Schneider (2009). It is evident from these studies that the amounts of alternative fuels are increasing for each year. The substitution rate is particularly high in Europe, Japan and in North America. This is mainly due to the fact that these regions have developed the necessary infrastructure and handling facilities as well as having established clear legislations with respect to landfills, waste incineration, emission levels, etc. (CSI, 2005; Sutou and Yukio, 2000).

3.2.1 Energy share by alternative fuels

The thermal energy share covered by alternative fuels in cement production varies from region to region. One of the leading regions is Germany which had a thermal share covered by alternative fuels of 54% in 2008 (Schneider, 2009). This is an average thermal share for 50 German cement plants. A few individual cement plants are reported to have alternative fuels energy shares in the range 90-100% (Scheuer, 2003). Chinese cement producers, which were responsible for 54% of the global cement production in 2009 utilizes practically no alternative fuels as yet, but interest in alternative fuel utilization is on the rise (Cembureau, 2009 and Chang-Ming, 2007).

Table 3-1 shows the thermal energy share from alternative fuels reported by a number of cement producers, responsible for approximately 20% of the global cement production. The thermal energy share is observed to be in the range of 0.7% to 22% with typical values around 12%. All of these cement producers have a common goal to increase their use of alternative fuels in the future. ICR Research has also recently estimated the global average alternative fuel share to be around 12%, which corresponds well with the figures reported here (ICR Research, 2011).

Cement producer	% Thermal energy share covered by alternative fuels	Global share of cement production in % (million tonnes)	Year	Reference
Lafarge	12	4.5 (136)	2010	Lafarge, 2010
Holcim	12	4.4 (132)	2009	Holcim, 2009
CEMEX	20	3.2 (96)[1]	2010	CEMEX, 2010
Heidelberg Cement	22	2.6 (78)	2010	Heidelberg, 2010
Taiheiyo Cement	12	1.4 (43)	2010	Tayheiyo, 2010
Grasim	0.8	1.1 (33)	2008	Grasim, 2008
SCG	14	1.0 (32)	2010	SCG, 2010
ACC	0.7[2]	0.7 (21)	2010	ACC, 2010
Siam City Cement	5	0.5 (15)	2009	Siam City, 2010
CRH	14[2]	0.4 (13)	2009	CRH, 2009
Cementir	6	0.3 (10)	2009	Cementir, 2009

Table 3-1: Thermal energy share covered by alternative fuels by cement producer (average values for all the cement producer's cement plants). [1]This figure is the annual production *capacity* and not the *actual* annual production. [2]This figure includes used oil as alternative fuel.

3.2.2 Types and quantities of alternative fuels

Many types of alternative fuels are applied in the cement industry. Figure 3-1 shows the alternative fuel types and amounts in the German cement industry in 2010. This figure gives an indication of the diversity with respect to physical and chemical properties between the different fuels. The majority of the alternative fuels are in solid form, while liquids are less common.

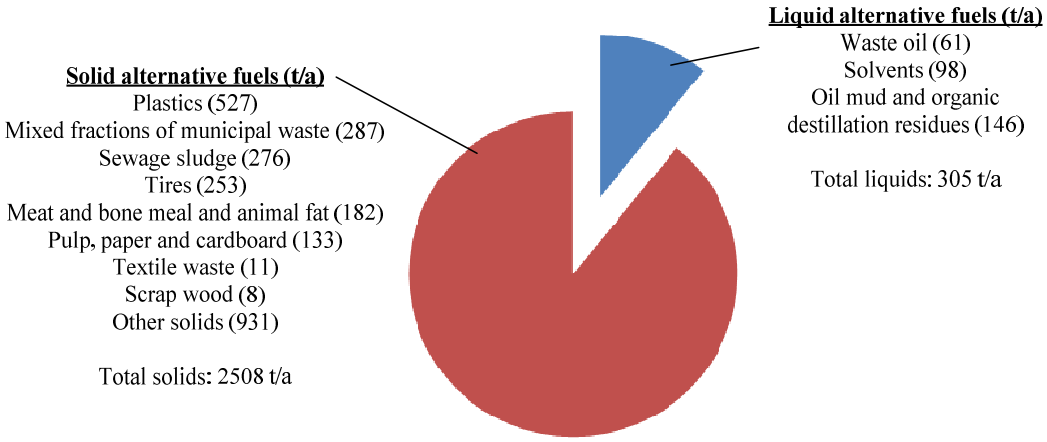

Figure 3-1: Alternative fuels used in German cement production in 2010 (VDZ, 2010).

Combustion in cement kiln systems provides society with a useful waste management option that can be an economically viable and environmentally sound alternative to land disposal, treatment or incineration. In recent years, the "mad cow" disease has created vast amounts of meat and bone meal which have successfully been destroyed in a number of cement kilns. In some countries, e.g. Norway, national policy makes cement kilns the preferred solution for hazardous waste management (CSI, 2005).

The type of alternative fuel deployed depends on local conditions and may differ substantially from country to country. In Germany for example, there is a tendency to increased use of processed commercial and industrial waste due to the EC directive 1999/31/EC which bans the landfill of unprocessed waste (Schneider, 2009). This type of waste is often referred to as Refuse Derived Fuel, RDF. Other important alternative fuels in German cement industry are meat and bone meal, tire-derived fuels, waste oil and processed municipal waste.

Another example is in Switzerland, where the Swiss pharmaceutical industry produces large amounts of organic waste solvents every year. These waste solvents are popular alternative fuels in the cement industry due to their usually high energy content and because they are easy to handle. In 2002, 30,600 tonnes of waste solvents were used by the Swiss cement industry, representing a share of approximately 14% of the total energy consumption (Seyler et al., 2005).

3.2.3 Fuel analysis

In this section, fuel analysis for some commonly used alternative fuels are presented, see Table 3-2. The values are approximate, and may deviate depending on source, age, pre-treatment, etc. However, the values give an impression of heating values and elemental compositions in the

different fuels. In addition, the fraction of volatile matter and fixed carbon are important for the combustion characteristics.

The volatile content of the most commonly deployed alternative fuels is observed to be in the range 54-100 wt. %. This is significantly higher than for coals or petcoke used in cement production, being 6-38 wt. %. Consequently, the char content is generally quite low, 0-30 wt. % for alternative fuels whereas the char content in coal and petcoke is in the range 50-90 wt. % (Jensen, 1999).

The ash content of some alternative fuels, e.g. refuse derived fuels (RDF), meat and bone meal (MBM) or tire-derived fuel (TDF), may be as high as one-third of the total mass. The high ash content may be problematic if the ash contains a large fraction of elements which may affect the cement quality adversely. This could for example be phosphorus in MBM or zinc in TDF. However, the ash may also contain elements that can contribute positively to the process: Calcium, silicon, alumina or iron from the ash will reduce the need of raw materials, making the cement production more economic.

Biomass, here presented in the form of pine wood, wheat straw and rice husks, are seen to have quite similar elemental composition and lower heating value of around 15-20 MJ/kg. However, both lower heating value and content of ash, water as well as elements such as sulfur, potassium, sodium and chlorine may differ significantly depending on the specific biomass type.

RDF is an inhomogeneous mixture of processed commercial and industrial waste. Lower heating value and elemental composition may vary significantly depending on location, but lower heating values are often in the range of 14 MJ/kg (Tokheim, 2005). The content of particularly chlorine is often relatively high. The high chlorine content needs to be considered if RDF is to be used as alternative fuel, see section 3.4.

TDF is a widely used alternative fuel in cement production and is one of those alternative fuels that are most similar to coals: The lower heating value is around 31-33 MJ/kg and coals are around 30-35 MJ/kg (Jensen, 1999). The similarity exists also with respect to content of volatile matter, char and sulfur.

MBM has lower heating values in the range of 16-20 MJ/kg. The sulfur and chlorine contents of MBM may be up to 1 wt.-% and 0.6 wt.-%, respectively.

Plastics, here presented as poly ethylene, PE, have the highest lower heating values of 40-44 MJ/kg. They consist of almost 100 wt. % volatile matter, making them similar to oils. For this reason, plastics are generally considered as excellent alternative fuels. An exception, however, is poly-vinyl chloride, PVC, which contains approximately 57 wt. % chlorine. Due to the high chlorine content, the heating value is around 19 MJ/kg, less than half the value of other common plastics. The high chlorine content is also undesirable for process reasons, which will be described in section 3.4.

Sewage sludge consists mainly of volatiles and ash, with fixed carbon contents typically less than 6 wt.-%. The lower heating value is around 14-19 MJ/kg which is quite low. Sewage sludge may also contain relatively high amounts of sulfur and chlorine, up to 0.8-1 wt.-%.

Table 3-2: Fuel analyses and heating values of alternative fuels commonly used in the cement production. Units are dry wt.% and MJ/kg dry basis. Notes are: a) Volatile matter, b) Fixed carbon (char), c) Pine wood, d) Refuse Derived fuel, e) Tire-derived Fuel, f) Meat and Bone Meal, g) Poly-Ethylene, h) Poly-Vinyl-Chloride, i) by difference, j) lower heating value calculated from the higher heating value, k) Sewage Sludge.

	Proximate analysis			Ultimate analysis								Lower heating value	Reference
	VM[a]	FC[b]	Ash	C	H	N	S	Cl	O[i]	Na	K		
Wood[c]	79-83	15-17	0.3-0.5	49-51	5.8-6.0	0.06-0.07	0.01-0.03	-	36-44	-	-	19.7-19.8[j]	Hassan et al., 2009 Gaur and Reed, 1998
Wheat straw	74.5	12.9	6.8	45.9	5.96	1.1	0.2	0.63	39.4	0.02	1.81	18.1[j]	Stenseng, 2001
Rice husks	61-69	16-17	15-20	38-42	3.0-4.8	0.4-0.6	0.1-0.2	-	36-54	0.11	2.18	15.4[j]	Chen et al., 2011 Várgehyi et al., 2011 Karmaka et al., 2011
RDF[d]	60-84	2-16	8-32	42-72	5-11	0.8-2.4	0.1-0.6	0.1-3.9	3-36	0.1-0.2	0-0.1	14	Tokheim, 2005 and Kobyashi et al., 2005
TDF[e]	54-66	23-30	7-23	64-81	5.6-7.2	0.3-0.5	1.4-1.6	0.15	2.0-5.6	~ 0	~ 0	31.0-32.8	Chen et al., 2001 Larsen, 2007 Chinyama et al., 2007
MBM[f]	65-72	7.2-9.7	17.5-28.3	42.1-45.9	5.8-6.4	7.5-11.2	0.38-0.97	0.35-0.58	15.3-38.4	0.31	0.07	16.2-19.9	Aho, M. et al., 2005 Ayllon, M. et al., 2006 Käänte, U. et al, 2004
PE[g]	100	~ 0	~ 0	86	14	~ 0	~ 0	~ 0	~ 0	~ 0	~ 0	40.2-44.2[j]	Panagiotou, T., 1994 Wang, Z. et al, 2004
PVC[h]	91	9	1	38	5	~ 0	~ 0	57	~ 0	~ 0	~ 0	19.2[j]	Panagiotou, T., 1994 Wang, Z. et al, 2004
SS[k]	48-64	0-6	17-50	28-39	3.8-4.1	3.8-4.3	~ 1	0.1-0.8	29-36	0.24	0.63	14.0-19.1	Measured

3.3 Technologies for alternative fuels combustion

The traditional firing points in a cement plant are the calciner and kiln burner, see chapter 2. With the introduction of alternative fuels these two units have been subject to modifications in order to optimize the combustion. However, is it still required to use relatively small fuel particles to ensure a) the desired flame profile in the kiln burner and b) sufficient fuel burnout in the calciner.
Since many alternative fuels are costly to downsize, it is often desirable to utilize coarse alternative fuels directly, thereby minimizing the shredding expense. This has led to the development of various forms of extensional equipment for combustion of lumpy alternative fuels. Selected types of extensional equipment will be described in this section.

3.3.1 HOTDISC

The HOTDISC from FLSmidth is a combustion chamber designed for combustion of large solid fuels, such as whole tires, automobile dashboards and upholstery, wood waste and RDF (Keefe, 2003, FLSmidth, 2008, 2009 and 2011). It is a large, rotating hearth furnace, integrated with the preheater and calciner. Figure 3-2 shows the HOTDISC and its typical position in a calciner kiln. The combustion air is hot tertiary air from the cooler. Raw meal from the lower cyclone stages of the preheater is added to control temperatures inside the HOTDISC. It is possible to add cold raw meal in order to control the temperature in the HOTDISC.

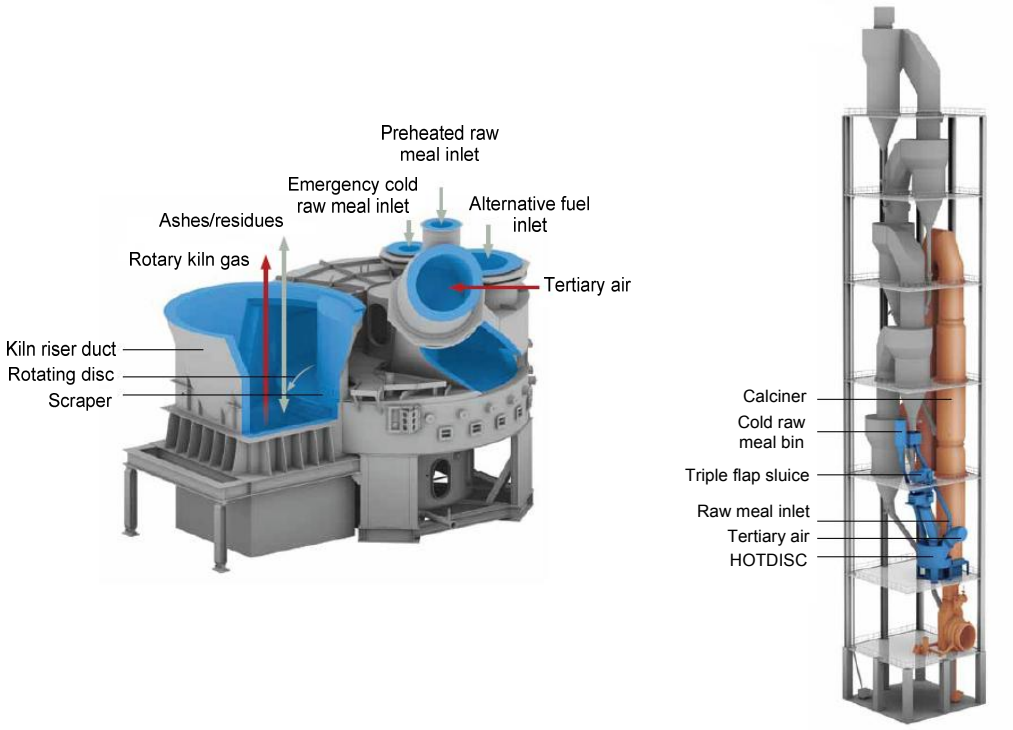

Figure 3-2: Left: A cross-sectional view of the HOTDISC. Right: The position of the HOTDISC in a calciner kiln (FLSmidth, 2011).

In the HOTDISC, it is possible to adjust the disc rotational speed to ensure sufficient residence time for fuel burnout. The fuel is transported approximately 270 degrees on the disc before it reaches the scraper, where ash, partially calcined raw meal and possible unburned fuel will be discharged into the lower calciner or riser duct.

Five HOTDISC units are in operation as of early 2011 and three new HOTDISC units are under installation. In 2008, the HOTDISC technology was awarded the Global Fuels Award in the category: Most innovative technology for alternative fuel use.

3.3.2 The Pre-Combustion Chamber (PCC)

According to Schmidthals (2003) the Pre-Combustion Chamber (PCC) is designed for large fuel particles of wood and TDF. The PCC is shown in Figure 3-3 next to the calciner. In the PCC, thermal conversion of large fuels take place under strongly sub-stoichiometric conditions ($\lambda \approx 0.2$) producing a lean gas that is used as gaseous fuel in the calciner. The remaining solids are conveyed by a discharge system into the kiln inlet via a rectangular discharge channel. Entrainable fractions of char and ash are lifted into the calciner, while larger solid fractions, e.g. steel wires from tires, drop into the kiln inlet (Schmidthals, 2003).

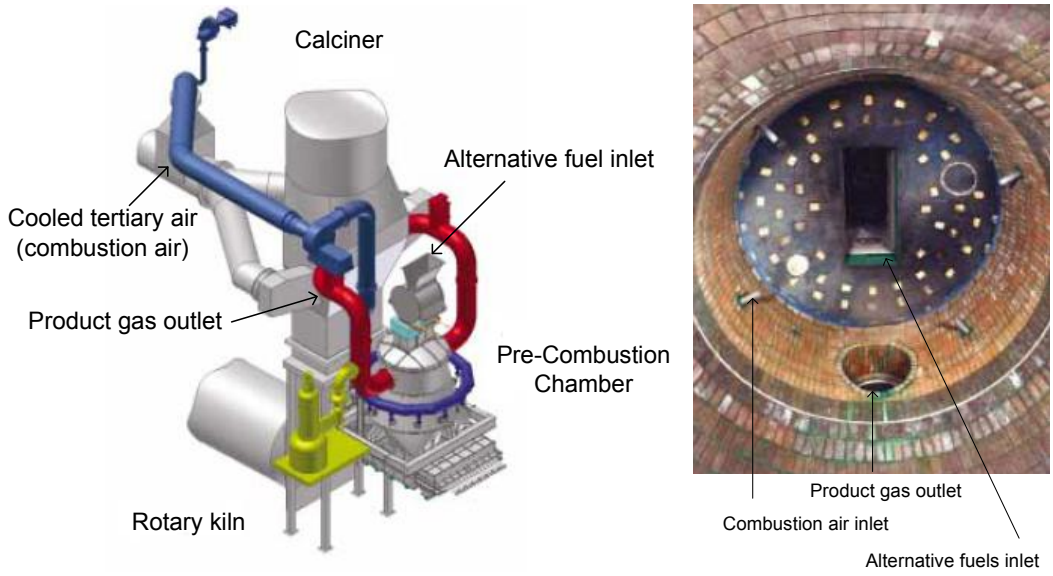

Figure 3-3: Left: PCC shown next to the calciner. Right: Bottom-to-top view inside the PCC (ThyssenKrupp, 2002).

3.3.3 Gasifiers

Gasifiers for gasification of alternative fuels are in use at some cement plants (Wirthwein et al., 2002 and Saito et al., 1987). The gasifiers produce a gaseous fuel that is used in the calciner while the solid residues are used as raw materials for cement production.

A circulating fluidized bed gasifier is installed at a German cement plant and use waste from the paper industry as well as packing and plastic waste as alternative fuels. It has a capacity of up to 20-25 t/h of alternative fuels, producing about 50,000 Nm^3/h of gas with a heating value around 3,000-5,000 kJ/Nm^3. This is sufficient to cover approximately 40% of the total energy consumption (Wirthwein et al., 2002).

So-called refuse energy gasifiers (REGs) utilize whole tires. The energy recovery from the gasifiers is reported to be as high as 95%. To the author's knowledge, two REGs are in operation today at Japanese cement plants. The tire capacities are 300-400 kg/h and 500-800 kg/h, respectively. This corresponds to overall fuel substitution rates of 5-7% and 11-18%, respectively (Saito et al., 1987).

3.3.4 Kiln material inlet firing and mid-kiln firing

Several cement plants have experience with combustion of lumpy alternative fuels in either the material inlet end of rotary kilns or through the kiln shell (mid-kiln firing). Firing directly into the rotary kiln is attractive given that it requires no additional combustion devices. But as will be explained in further details in subsequent sections, as well as in chapters 6 and 7, there are challenges associated with combustion processes in the rotary kiln, where solid fuels and cement raw materials are in physical contact. Still, some cement plants do utilize up to 20% of the total thermal energy by either kiln material inlet or mid-kiln firing. Full-scale experience with lumpy alternative fuel combustion in rotary kilns is the subject of chapter 7.

There are a number of technologies for alternative fuel combustion in the rotary kiln material inlet end and/or mid-kiln. Some solutions are illustrated in Figure 3-4: To the left is shown a feed shelf system which allows tires to be fired into the kiln material inlet. Above the feed shelf is seen a "fork" which holds the tire in the calciner, while the tire-devolatilizes/combusts. The tire is then released, whereby solid residues in the form of steel wires or unburned char are dropped into the rotary kiln. On the right of Figure 3-4 is shown an example of mid-kiln firing: Every time the rotary kiln has rotated one revolution, a tire is dropped through a flap damper and into the rotary kiln. Mid-kiln firing is predominantly used in long wet and long dry rotary kilns.

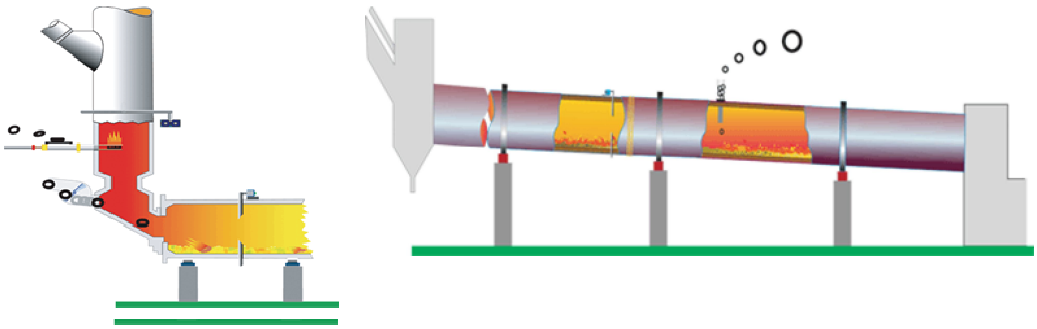

Figure 3-4: Solutions for back-end firing (left) and mid-kiln firing (right) (Cadence Recycling, 2009).

3.4 Effect of alternative fuels on process stability and product quality

The utilization of alternative fuels in cement production may alter the input of minor elements introduced to the kiln system, since some alternative fuels have a different chemical composition than traditional fossil fuels. It is important to be aware of the effect of these minor elements as they may affect the stability of the kiln system or clinker quality. This section will describe the influence of minor elements on the kiln system and clinker quality.

3.4.1 Cement chemistry

A number of elements may be introduced with the alternative fuels, and could affect the clinker production. Such components are typically:

1. Alkali metals (potassium and sodium).
2. Sulfur
3. Chlorine
4. Zinc
5. Phosphorous
6. Iron
7. Unburned carbon in the material charge.
8. Quartz (Silicon)

Re 1-2. Alkali metals (sodium and potassium) and sulfur can affect the cement chemistry as well as the kiln system stability. High alkali levels in the final cement can react with moisture and produce a gel which expands and gives rise to cracking in concretes (Hewlett, 1998). The alkali content of the cement can be controlled through careful selection of the raw materials or by extracting high-alkali dust from the kiln system.
When sufficient sulfur is present in the clinker, the alkalis are normally present as sulfates such as K_2SO_4, Na_2SO_4, $Na_2SO_4{\cdot}3K_2SO_4$ (aphthitalite), $(CaO{\cdot}SiO_2)_2{\cdot}CaSO_4$ (sulfate-spurrite) and/or $2CaSO_4{\cdot}K_2SO_4$ (langbeinite). In the absence of sufficient sulfate in the clinker, Na_2O can enter the C_3A and increase the reactivity, potentially leading to setting problems. K_2O will normally enter the C_2S where it enhances the reactivity to water and may inhibit its conversion to C_3S. A reducing atmosphere in the kiln is reported to facilitate the transfer of alkalis from the sulfate forms to the C_3A and C_2S (Hewlett, 1998).
When the alkalis are present as sulfates in the burning zone of the kiln system, the viscosity of liquid phase is decreased, thus promoting the formation of C_3S (Hewlett, 1998).

The term alkali equivalent, Na_2O_e, is normally used to describe the amount of alkali present in the clinker product:

$$Na_2O_e = \frac{MW_{Na_2O}}{MW_{K_2O}} wt\%K_2O + wt\%Na_2O = 0.66 \cdot \text{wt\%}K_2O + \text{wt\%}Na_2O \qquad (3.1)$$

Higher alkali levels in cement (> 0.8wt% Na_2O_e) have the effect of increasing the early strength of the cement at the expense of the late strength (Hewlett, 1998).

Excess amounts of sulfur tend to form $CaSO_4$. The amount of sulfur available for forming $CaSO_4$ is termed excess SO_3 and may be calculated by the empirical formula:

$$\text{Excess } SO_3 = \text{Total } SO_3 - \frac{M_W(SO_3)}{M_W((K_2O)} \cdot K_2O - \frac{1}{2} \cdot \frac{M_W(SO_3)}{M_W(Na_2O)} \cdot Na_2O$$
$$= \text{Total } SO_3 - 0.85 \cdot K_2O - 0.65 \cdot Na_2O \quad (3.2)$$

Where total SO_3, K_2O and Na_2O are the clinker concentrations in g/kg clinker, and are determined by a chemical analysis. Analyses of different clinker compositions have revealed that nearly the entire amount of potassium and half the amount of sodium forms sulfate (Hansen, 2003).

It is highly desirable for as much as possible of the alkalis and sulfur to be discharged from the kiln system with the clinker. Otherwise, some of the alkalis and sulfur are volatilized in the high temperature zones of the rotary kiln and condense as sticky, low-melting point solids in the colder parts. This can cause blockage problems known as coating and ring formation. Condensation of sticky solids also serves to attract dust and bind it, which gives further rise to blockage problems (Hewlett, 1998). This is explained in further details in section 3.4.4.

Re 3. Chlorides readily volatilize in the burning zone and condense in the cooler parts to combine with alkalis and sulfates to form low melting point mixtures. Their effect upon the operation of kiln systems is so severe that it has often been necessary to either set an upper limit for the chlorine content of the raw materials/fuel, or to introduce a chlorine bypass in the kiln/preheater system. A bypass can be very effective to remove chlorides from the kiln system. Operation with a chlorine bypass is described in greater detail in chapter 6. The chlorine content in Portland cements is typically restricted to 0.1 wt% in order to avoid serious problems of reinforcement corrosion in concrete (Hewlett, 1998). Some cement manufacturers also produce low chlorine cements.

Re 4. Small amounts of zinc (0.01-0.2 wt.-%) have been reported to increase the reactivity of C_3A and may give rise to time-setting problems (Hewlett, 1998). This may reduce the use of tire-derived fuels (TDF) in cement production, since TDF contains a variable amount of zinc (1.00-1.25 wt.-%). If the total energy share covered by TDF approaches 30%, the quantities of zinc in the clinker reaches the acceptable limit (Pipilikaki, P. et al., 2005).

Re 5. Phosphorus is normally present in the clinker as P_2O_5 in a range of 0.03 to 0.22 wt%. Amounts of P_2O_5 higher than 0.5-1.0 wt% stabilize C_2S to an extent where conversion to C_3S is inhibited. The addition of small amounts of fluorine-containing compounds prevents this effect (Hewlett, 1998). P_2O_5 is particularly present in meat and bone meal (MBM), but may also be present in household waste.

Re 6. Tire-derived fuels (TDF) contain a relatively large amount of steel (up to 25 wt% for truck tires) (Norcini et al., 1998). During the combustion process, TDF will thus contribute as an iron source, thereby lowering the demand for iron sources in the raw material mixture.

Re 7. Incomplete burnout of the fuel may cause reducing conditions in the material charge in the kiln. These reducing conditions may increase the emissions of SO_2 as well as damage the refractory lining in the kiln. This will be explained in further details in section 3.4.4. Reducing conditions may also produce so-called brown clinker which differs in color from traditional Portland cement.

Re 8. Sewage sludge contains silicates (quartz sand) with coarser grains than normally seen in cement raw meal. Coarser silicate particles may react with already formed alite to produce belite, thereby resulting in lower cement strength. Use of large quantities of sewage sludge may therefore be harmful to cement quality.

Trace elements such as As, Cd, Cr, Cu, Ni and V from the alternative fuels will be incorporated into the clinker. Due to their small quantities, these trace elements normally do not affect the clinker quality in any measurable degree. The hazardous risk from these elements can also be considered to be of minor importance because the trace elements are firmly incorporated into the crystal phases during cement hydration (Wanzura, 2003).

3.4.2 Emissions

Generally, assuming a correct equipment design, the use of alternative fuels will not lead to increased emissions, compared to fossil fuels (Karstensen, 2008, Lee et al., 2007, Lemarchand, 2000, Prisciandaro et al., 2003, Realff et al., 2005 and Wurst, 2003). However, emissions from by-pass should be considered because a bypass is most often needed when using alternative fuels. The application of alternative fuels may interact with the process conditions in the bypass extraction area with attendant risk of bypass emissions. This section will briefly review how stack emissions are affected when alternative fuels are used in cement production.

3.4.2.1 Legislation

Cement plants located in the European Union which use alternative fuels are subject to Directive 2010/75/EU about industrial emissions (Directive 2010/75/EU). Important emission limits are summarized in Table 3-3.

Pollutant	Emission limit	Unit
Dust	30	mg/Nm^3 @ 10 vol-% dry
SO_2	50[1]	mg/Nm^3 @ 10 vol-% dry
NO_x	500	mg/Nm^3 @ 10 vol-% dry
HCl	10	mg/Nm^3 @ 10 vol-% dry
HF	1	mg/Nm^3 @ 10 vol-% dry
Hg and Tl	0.05	mg/Nm^3 @ 10 vol-% dry
Dioxins and furans	0.1[1]	TE^a/Nm^3 @ 10 vol-% dry
TOC	10	mg/Nm^3 @ 10 vol-% dry
CO	Set by local authorities	

Table 3-3: Emission limits for co-incineration of alternative fuels in cement kilns. a: TE = Toxic Equivalents (Directive 2010/75/EU). [1] Exemptions may be authorized by the competent authority in cases where SO_2 and TOC arises from others sources than the fuel, e.g. from the raw materials.

Older cement plants in the EU may be allowed to have higher NO_x emissions than 500 mg/Nm^3, but only if they fulfil the requirements mentioned in a BAT (Best Available Technique) reference document for the lime, cement and magnesium oxide manufacturing industries written by the European Parliament (European Commission, 2010).

Each pollutant, except dust, presented in Table 3-3 will be briefly described in the following sections.

Emissions may differentiate significantly between individual cement plants. For this reason, emission data from European cement plants have since 2001 been registered in the European Pollutant Release and Transfer Register (E-PRTR). Emission data will be evaluated for each cement plant with a production capacity above 500 tpd, and regularly published on the internet (European Commission, 2011).

3.4.2.2 SO_2

SO_2 emissions from modern cement plants originate mainly from oxidation of pyrite, Fe_2S, or organically bound sulfur in the upper preheater stages. SO_2 originating from the fuel is to a great extent absorbed by limestone in the calciner or lower preheater stages (Hansen, 2003). An exception is, however, cement plants operating with a bypass: The flue gas purged through this bypass is normally a) released to the atmosphere through a separate stack or the main stack, thereby giving rise to SO_2 emissions, or b) recirculated to the preheater, calciner or clinker cooler (Heidelberg Cement, 2010). SO_2 emissions from cement plants have attracted much attention in recent years, and reference is made for the works of Hansen (2003) and Rasmussen (2011).

3.4.2.3 NOx

NO_x emissions from cement plants may arise from either thermal NO_x or from nitrogen in fuels. A detailed description of NO_x formation and reduction is given by Jensen (1999). In addition, Larsen (2007) reviewed the effect of co-firing alternative fuels on NO_x-emissions. He found that NO_x emissions generally decreased when alternative fuels were used.
The emission limits of NO_x of 500 mg/Nm^3 have made it necessary for new cement plants to use NO_x reduction measures such as staged combustion, described in chapter 2, section 2.2.4, or the SNCR technique (VDZ, 2005).

3.4.2.4 HCl and HF

Emissions of acidic gases such as HCl and HF are generally very low due to the alkaline conditions in the kiln system: Chlorine and fluorine are predominantly bound as salts rather than HCl and HF (VDZ, 2005). However, cement plants operating with a chlorine bypass have been reported to emit HCl and HF (Heidelberg Cement, 2010).

3.4.2.5 Hg and Tl

Mercury and thallium are highly volatile heavy metals that are able to escape through the stack as opposed to other heavy metals, which are primarily incorporated into the clinker (Hewlett, 1998). Stack emissions of particularly mercury from cement plants as well as power plants and waste incineration plants, have attracted much attention in recent years. For detailed information about mercury release and capture, reference is made to the works of Paone (2008) and Zheng (2011).

3.4.2.6 Dioxins and furans

Dioxins and furans cover a wide range of poly-chlorinated organic compounds, of which many are toxic. Since the toxicity of individual dioxins and furans fluctuates, the toxicity is defined in the unit Toxic Equivalents per Nm^3, TEQ/Nm^3. 1 TEQ/Nm^3 is defined as the toxicity for the dioxin

2,3,7,8-tetrachlorodibenzodioxin (TCDD), and the toxicity of all other dioxins and furans are evaluated relative to TCDD (Directive 2010/75/EU).
A review article about formation, release and control of dioxins and furans from cement kilns are provided by Karstensen (2008). Dioxin and furan emissions from cement kilns are generally very low, because oxygen concentrations, temperatures and residence time are sufficient to ensure full conversion of organic species to their ultimate combustion products CO_2 and H_2O.
Formation of dioxins and furans are typically caused by improper mixing of fuel and combustion air in the calciner, where residence time and temperature are lower than in the rotary kiln (Karstensen, 2008). For cement plants operating with a bypass, it is important to keep the bypass filter temperature below 250°C since higher temperatures may generate dioxins and furans (Wirthwein, 2007).

3.4.2.7 CO and TOC – Total Organic Carbon

Alternative fuels have different combustion characteristics than fossil fuels, which may influence the CO formation mechanism. CO oxidation rates drop drastically with temperature in the temperature window 650°C to 950°C – and almost no CO oxidation takes place below 650°C (Larsen, 2011). It is therefore important that the calciner is designed to oxidize CO before it escapes to the preheater.

Overall, CO and TOC emissions from the kiln system may be caused by four main factors (Larsen, 2011):

1) Incomplete mixing of fuel and oxidizer in the calciner system.
2) Fluctuations in fuel feed rate.
3) Incomplete fuel burnout in the calciner system.
4) Organic carbon in the raw materials.

Regarding the first three bullet points, CO emissions may be minimized by a proper equipment design and operation to match the specific fuels. The fourth bullet point is not connected with alternative fuels but depends on the organic carbon content of the raw materials.

3.4.3 Local reducing conditions

It is widely accepted in the cement industry that cement clinker should be burned in an oxidizing atmosphere. Sub-stoichiometric oxygen concentrations in the kiln system cause deterioration of clinker quality and affect kiln process stability negatively (Hewlett, 1998). This section will describe how alternative fuels may cause local reducing conditions in the kiln system, and why local reducing conditions have a negative impact on clinker quality and process stability.

3.4.3.1 Local reducing conditions caused by incomplete fuel combustion

Incomplete combustion of solid fuels may lead to unburned fuel dropping into the material charge in the rotary kiln. This is illustrated in Figure 3-5 where unburned fuel can reach the material charge in four different ways:

1) Coarse solid fuels fired into the calciner may drop through the riser duct and into the rotary kiln.
2) Coarse solid fuels fired through the kiln burner may not be completely combusted in the flame, and will consequently fall into the material charge.
3) Solid fuels fired into the calciner may be light enough to be carried upwards through the calciner and into the lower cyclone stage. But if the combustion is incomplete, unburned carbon may be transported with calcined raw meal from the lower cyclone stage and into the rotary kiln material inlet end.
4) Direct firing of, typically large, solid fuels into the rotary kiln material inlet end.

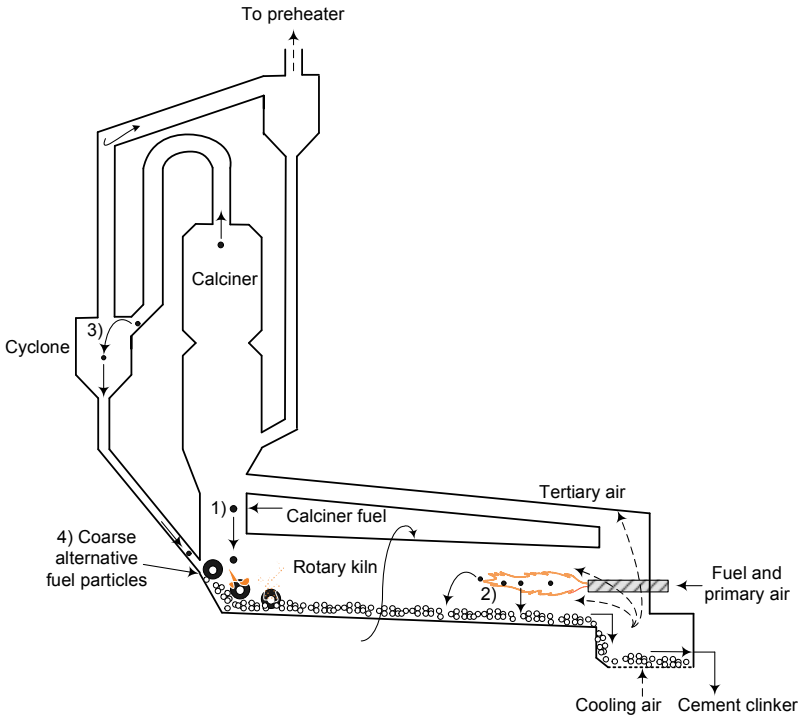

Figure 3-5: Solid fuels dropping into the material charge in the rotary kiln.

Partially burned or unburned alternative fuels in the material inlet end of the rotary kiln can consume oxygen and thereby cause reducing conditions. Reducing conditions in the material charge do not necessarily mean reducing conditions in the gas phase.
Reducing conditions in the material charge may also occur if the kiln burner flame shape or direction is such that the flame impinges on the material charge and consumes all oxygen near the material charge.

3.4.3.2 Effects of local reducing conditions on the clinker quality

It is widely accepted that Portland cement should be burned under oxidizing combustion conditions in order to ensure a good product quality (Klauss, 2000). The main effect of clinker burning under reducing conditions is mainly due to the raw material component Fe_2O_3 (Fe(III)) being reduced to

FeO (Fe(II)) or, in the case of strong reducing conditions, elemental Fe (Fe(0)). Reduction of Fe(III) under reducing conditions take place at temperatures above 450°C. Fe(II) affects the clinker quality for the following reasons (Klauss, 2000):

- Fe(II) catalyzes alite decomposition ($3CaO{\cdot}SiO_2 \rightarrow 2CaO{\cdot}SiO_2 + CaO$), the main strength-giving component in cement.
- Less ferrite ($4CaO{\cdot}Al_2O_3{\cdot}Fe_2O_3$) is formed. Instead, more aluminate ($3CaO{\cdot}Al_2O_3$) is formed, which may lead to altered setting during the hydration of cement mortar.

In addition to these effects on cement quality, the color of the cement may also change. This is commonly known as “brown clinker”.

3.4.3.3 Effects of local reducing conditions on process stability

Local reducing conditions in the material charge in either the rotary kiln material inlet end or in the kiln burning zone have an effect on the process stability of the entire kiln system. The process stability is mainly affected by increased release of sulfur from the raw meal to the gas phase, which may be summarized by the overall reaction:

$$CaSO_4\,(s) + CO\,(g) \leftrightarrow CaO\,(s) + CO_2\,(g) + SO_2\,(g) \qquad (3.3)$$

Similar reactions with alkali sulfates are possible, releasing both sulfur and alkali metals to the gas phase. Chapter 6 describes the reductive decomposition of sulfates in greater detail.

3.4.4 Alkali, sulfur and chlorine: Circulation in the kiln system

This section provides overall insight into the volatilization of Cl, S, K and Na from the raw materials and fuel during the combustion process and clinker reactions in the kiln system.

A cycle of volatiles that evaporate in the hot part of the rotary kiln and condense in the cold part of the rotary kiln, calciner and preheater, trap the volatiles in the kiln system, causing accumulation of volatiles within the circulation loop. This phenomenon is well-known in the cement industry.

Circulation of chlorine in the kiln system is mainly related to high temperatures in the rotary kiln and is hardly affected by the kiln atmosphere (Locher and Klein, 2009). Circulation of alkali metals and sulfur is related to both high temperatures and the kiln atmosphere: Alkali metals and sulfur present in the partially calcined raw meal as sulfates are sensitive to reducing conditions which favors release to the gas phase. Particularly sulfur bound as $CaSO_4$ (commonly referred to as excess sulfur) is sensitive to reducing conditions (Nievoll et al., 2009). The reactions leading to sulfur and alkali release is described in further details in chapter 6.

Circulation of large amounts of the volatile elements Cl, Na, K and S are problematic because these elements may a) condense and form eutectic salt mixtures of alkali sulfates and alkali chlorides, and/or b) react with clinker minerals and form complex compounds. Both options can lead to sticky deposit build-ups in the rotary kiln, riser duct and lower cyclone stages. The melting point of the eutectic salt mixtures depends on the composition, but can be well below 900°C (Palmer, 1990). Deposit build-ups inside the rotary kiln are often called kiln rings. Kiln rings are more severe build-ups than the coating layer that normally adhere to the internal walls in the rotary kiln. While the

coating layer consisting of cement raw materials is desirable because it protect the refractory bricks from erosion and reduces heat loss to the surrounding atmosphere. Kiln rings induce operational instability and restrict gas and material flow to a point where production must be stopped (Palmer, 1990). Kiln rings in the material inlet end can be formed for several reasons besides circulation of volatiles. These other reasons may be frequent changes in chemical composition and fineness of raw meal, excessive dust generation within the rotary kiln, frequent variations in temperatures in the freeboard gas through the kiln length, etc. Peray (1986) gives a detailed description of the reasons and mechanisms behind ring formation.

The chemical composition of the kiln ring depends on the location along the rotary kiln length due to variations in temperature and kiln atmosphere (Palmer, 1990). Investigations of kiln rings from several industrial rotary kilns have confirmed that sulphospurrite ($2C_2S{\cdot}CaSO_4$) is a main ring-building mineral phase, with typical concentrations in the range of 25-30% (Nievoll et al., 2009). Sylla (1974) found that besides sulphospurrite was also spurrite ($2C_2S{\cdot}CaCO_3$) and calcium sulphoaluminate ($C_3A_3{\cdot}CaSO_4$) frequently found in kiln rings. Sylla reported that spurrite was primarily formed in CO_2-rich atmospheres at temperatures between 700-900°C. Spurrite formation was observed to be favored by the presence of chlorides and alkalies. Sulphospurrite and calcium sulphoaluminate was stable at the temperature intervals 900-1,150°C and 950-1,300°C, respectively. The stability range of sulphospurrite and calcium sulphoaluminate was observed to increase if the SO_2 concentration in the kiln gas increased.

Potgieter and Wirth (1996) reported that the mechanism of kiln ring formation was related to the presence of either a low melting $CaO\text{-}Al_2O_3\text{-}SiO_2$ liquid phase or a $(Na, K)_2O$ containing liquid phase. The liquid phase acts as a binding agent for building up the ring on the refractory lining. In particular the high concentration of alkali liquid phase increases the stickiness and thus enhances adhesion of dust and raw meal which becomes incorporated into the kiln ring.

Katsioti et al. (1995) studied the formation of coatings in the lowest cyclone stage and in the rotary kiln inlet. The coatings in the lowest cyclone stage were found to contain high levels of spurrite and chlorides, mainly KCl. The coatings in the kiln inlet contained only high levels of spurrite, MgO and CaO. The coatings in both positions were explained to be caused by circulation of alkali metals and chlorine in the kiln system. A maximum limit of 500 ppm chlorine in the raw meal entering the rotary kiln was recommended in order to reduce coating formation in the lowest cyclone stage.

Sutou et al. (1999) reported that coating formation in the lower cyclone stages and kiln riser duct was caused by the interaction of CaO and SiO_2 with chlorine and sulfur circulating in the kiln system. Particularly the low-melting point minerals sulphospurrite ($2C_2S{\cdot}CaSO_4$) and chloroellestadite ($3C_2S{\cdot}3CaSO_4{\cdot}CaCl_2$) were reported to be problematic.

Circulation of volatiles in the kiln system may also lead to corrosion of rotary kiln shells. Jøns and Østergaard (2001) studied kiln shell corrosion in 12 suspension calciner kilns. They found that corrosion was particularly severe when the kiln gas contained high levels of both sulfur and chlorine. In addition, increased sulfur circulation may lead to increased calciner corrosion. This may be caused by condensation of sulfuric acid on the inner steel shell.

3.5 Conclusion

The use of alternative fuels in the cement industry has increased significantly during the last 20 years, and this tendency will continue in the future due to strong drivers such as economic and environmental concerns. Some of the most important alternative fuels are solid fuels such as tire-derived fuels, refuse derived fuels, meat and bone meal and waste wood. These fuels have physical and chemical characteristics different from traditional, fossil fuels, which create a need for modified or new combustion equipment.

Since many of the solid, alternative fuels are expensive to down-size, it is attractive to be able to feed these fuels as relatively coarse fuel particles. This may be problematic in the traditional firing points in the kiln main burner or calciner, which have led to the development of extensional equipment that is specially designed for large solid fuel particles. The HOTDISC is an example of such specially designed equipment. Another firing point which may be attractive for firing of coarse alternative fuels is the material inlet end of rotary kilns. It is relatively straightforward to feed fuels into this location, and high temperatures and long retention time in the rotary kiln provide good conditions for fuel burn out. A challenge, however, may be that direct, physical contact between fuels and raw meal can affect the overall process stability of the kiln system – or maybe the product quality.

Some types of alternative fuels contain relatively high levels of volatile inorganic elements such as chlorine, sulfur and alkali metals, and may potentially increase the amount of these volatile elements that circulates in the kiln system. In addition, local reducing conditions in the material charge caused by insufficient fuel-air mixing can lead to increased release of sulfur and alkali metals from the raw materials. And finally, the fuel combustion may increase local temperatures in the rotary kiln which also lead to increased release of sulfur, alkali metals and chlorine from raw materials.
All in all, solid fuels fired into the material end of rotary kilns have the potential of increasing the circulation of inorganic volatiles in the kiln system. Increased circulation of inorganic volatiles is problematic because it accelerates deposit formation in the rotary kiln, riser duct and lower cyclone stages.

3.6 References

ACC; Sustainable Development Report 2010 – Web Update. ACC Limited, Mumbai, India, 2010.

Aho, M. and Ferrer, E.; Importance of coal ash composition in protecting the boiler against chlorine deposition during combustion of chlorine-rich biomass, Fuel, 84, 201-212, 2005.

Ayllón, M., Aznar, M., Sánchez, J. L., Gea, G. and Arauzo, J.; Influence of temperature and heating rate on the fixed bed pyrolysis of meat and bone meal, Chem. Eng. Journal, 121, 85-96, 2006.

BP Statistical Review of World Energy, 2010, http://www.bp.com.

Cadence Recycling, 2009. http://www.cadencerecycling.com.

Cembureau, Activity Report 2009, Belgium.

Cementir, Environmental Report 2009, Cementir Holding, Rome, Italy, 2009.

Cemex, CEMEX Annual Report 2010, Mexico, 2010.

Chang-Ming, G. Domestic cement industry production profit function between waste and gaps (report translated from Chinese language). China Cement Association. China, 2007.

Chen, L. H., Chen, K. S. and Tong, L. Y.; On the pyrolysis kinetics of scrap automotive tires. Journal of Hazardous Materials B84, 43-55, 2001.

Chen, T., Wu, C., Liu, R., Fei, W. and Liu, S.; Effect of hot vapor filtration on the characterization of bio-oil from rice husks with fast pyrolysis in a fluidized-bed reactor. Bioresource Technology, 102, 6178-6185, 2011.

Chinyama, M. P. M. and Lockwood, F. C.; Devolatilisation behaviour of shredded tyre chips in combusting environment. Journal of the Energy Institute, Vol. 80, No. 3, 162-167, 2007.

CRH, Corporate Social Responsibility Report 2009, Ireland, 2009.

CSI (Cement Sustainability Initiative), Guidelines for alternative fuels selection and use, World Business Council for Sustainable Development, Switzerland, 2005.

Directive 2010/75/EU. Available from: http://www.europa.eu.

ENS; Energistatistik, Energistyrelsen (Energy Statistics, the Energy Agency), Copenhagen, Denmark, 2010. http://www.ens.dk.

European Commission; Reference Document on Best Available Techniques in the cement, lime and magnesium oxide manufacturing industries. Seville, Spain, 2010. Available from http://eippcb.jrc.es/reference.

European Commision; European Pollutant Release and Transfer Register, 2011. Available online: http://ec.europa.eu/environment/air/pollutants/stationary/eper/index.htm

FLSmidth, HOTDISC three years after. Highlights, April, 16-17, 2008.

FLSmidth, Latest generation HOTDISC successfully installed in Slovenia. Highlights, December, 26-27, 2009.

FLSmidth, HOTDISC Combustion Device. Brochure, FLSmidth, Valby, Denmark, 2011.

Gaur. S. and Reed, T. B.; Thermal Data for Natural and Synthetic Fuels, Marcel Dekker, Inc. New York, USA, 1998. ISBN: 0-8247-0070-8.

Grasim, Sustainability Report 07-08. Grasim Industries Limited. Mumbai, India, 2008.

Hansen, J. P.; SO_2 Emissions from Cement Production. PhD Thesis, Technical University of Denmark, Department of Chemical Engineering, 2003. ISBN 87-90142-96-9.

Hassan, E.-B. M., Steele, P. H. and Ingram, L.; Characterization of fast pyrolysis bio-oils produced from pretreated pine wood, Appl. Biochem. Biotechnol., 154:182-192, 2009.

Heidelberg Cement; Annual Report 2010, Heidelberg, Germany, 2010.

Heidelberg Cement; Innovations in kiln gas bypass systems. Cement International, No. 2, Vol. 8, 61-66, 2010.

Hewlett, P. C. (Editor); Chemistry of Cement and Concrete; 4th edition, John Wiley & Sons Inc., New York, 1998. ISBN 0-340-56589-6.

Holcim, Corporate Sustainable Development Report 2009, Switzerland, 2009.

ICR Research; Sustained Efforts. International Cement Review, 74-78, August 2011.

Jensen, L. S.; NO_x from cement production – Reduction by primary measures. PhD Thesis, Technical University of Denmark, Department of Chemical Engineering, 1999.

Jøns, E. S. and Østergaard, M. J. L.; Kiln shell corrosion. IEEE-IAS/PCA Cement Industry Technical Conference, Vancouver, Canada, 343-359, April, 2001.

Karmaka, D. T. and Datta, A. B.; Generation of hydrogen rich gas through fluidized bed gasification of biomass. Bioresource Technology, 102, 1907-1913, 2011.

Karstensen, K. H.; Formation, release and control of dioxins in cement kilns, Chemosphere, 70, 543-560, 2008.

Katsioti, M., Kasselouri, V., Ftikos, Ch. and Parissakis, G.; Control of chloride content and gas temperature to prevent coating formation in a suspension preheater kiln. World Cement, 67-70, October, 1995.

Keefe, B. P. and Shenk, R. E.; An innovative solution for waste utilization, IEEE, 197-206, 2003.

Klauss, J. Burning cement clinker under reducing conditions in a rotary kiln, ZKG International, 132-144, Vol. 53, No. 3, 2000.

Kobyashi, N., Itaya, Y., Piao, G., Mori, S., Kondo, M., Hamai, M. and Yamaguchi, M; The behaviour of flue gas from RDF combustion in a fluidized bed, Powder Technology, 151, 87-95, 2005.

Krennbauer, F.; Secondary fuels and their influence on the cement burning process; ZKG-International, 5, 63-71, 2006.

Kääntee, U., Zevenhoven, R., Backman, R. and Hupa, M.; Cement manufacturing using alternative fuels and the advantages of process modelling, Fuel Processing Technology, 85, 293-301, 2004.

Lafarge, Annual Report 2010, Paris, France, 2010.

Larsen, M. B.; Alternative Fuels in Cement Production; PhD Thesis, Department of Chemical Engineering, Technical University of Denmark, 2007. ISBN 978-87-91435-49-8.

Larsen, M. B.; Alternative fuels in cement production – a new opportunity. Paper from FLSmidth. Valby, Denmark, 2011.

Lee, V. K. C., Kwok, K. C. M., Cheung, W. H. and McKay, G.; Operation of a municipal solid waste co-combustion pilot plant, Asia-Pac. J. Chem. Eng., 2, 631-639, 2007.

Lemarchand, D; Burning Issues, International Cement Review, 65-67, February 2000.

Locher, G. and Klein, H.; Modelling circulating sulfur, chlorine and alkali systems in the clinker burning process; Part 2: Theory and discussion. Cement International, Vol. 7, 4, 64-75, 2009.

Nievoll, J., Jörg, S., Dösinger, K. and Corpus, J.; Studying ring formation. World Cement, 78-83, December, 2009.

Norcini, M., Tassistro, N., Quaresima, R., Scoccia, G. and Volpe, R.; Use of chopped tyres as auxiliary fuel in clinker kilns: Industrial experience at the Cagnano Amiterno cement works. Proceedings of the 6th NCB international seminar on cement and building materials, 3, 1998.

Palmer, G.; Ring formation in cement kilns. World Cement, 538-543, December, 1990.

Panagiotou, T. and Levendis, Y.; A study on the combustion characteristics of PVC, Poly(stirene), Poly(ethylene), and Poly(propylene) particles under high heating rates, Combustion and Flame, 99, 53-74, 1994.

Paone, P.; Heavy metals in the cement industry: A look at volatile cycles and simple mitigation techniques. IEEE Cement Industry Technical Conference, 65-75, Miami, Florida, USA, 2008.

PBL (The Netherlands Environmental Assessment Agency); "Global CO2 emissions: increase continued in 2007", Available from: http://www.pbl.nl/en/publications/2008/GlobalCO2emissionsthrough2007.html, May 2011.

Peray, K. E.; The Rotary Cement Kiln; 2nd edition, Edward Arnold Ltd., Victoria, Australia, 1986. ISBN 0 7131 3609X.

Pipilikaki, P., Katsiosi, M., Papageorgiou. D., Fragoulis, D. and Chaniotakis, E.; Use of tire-derived fuel in clinker burning, Cement & Concrete Composites, 27, 843-847, 2005.

Potgieter, J. H. and Wirth, W.; An investigation into ash-ring formation in a rotary lime kiln. ZKG, 3, 166-171, 1996.

Prisciandaro, M, Mazziotti, G. and Veglió, F.; Effect of burning supplementary waste fuels on the pollutant emissions by cement plants: A statistical analysis of process data, Resources, Conservation and Recycling, 39, 161-184, 2003.

Rasmussen, M. H.; Low SO2 emission preheaters for cement production. PhD Thesis, Department of Chemical and Biochemical Engineering, Technical University of Denmark, 2011.

Realff, M. J., Lemieux, P., Lucero, S., Mulholland, J. and Smith, P. B.; Characterization of transient puff emissions from the burning of carpet waste charges in a rotary kiln combustor, IEEE Conference, 212-228, 2005.

Saito, I., Sakae, K. Ogiri, T. and Ueda, Y.; Effective use of waste tyres by gasification in cement plant, World Cement, 18, 264-269, 1987.

SCG; Sustainability Report 2010, Siam Cement Corporation. Bangkok, Thailand, 2010.

Scheuer, A.; Utilization of alternative fuels and raw materials in the cement industry, Cement International, 1, 48-66, 2006.

Schmidthals, H.; The Pre-Combustion Chamber for secondary fuels – development status of a new technology, IEEE Conference, 207-218, 2003.

Schneider, M; Activity Report 2007-2009, Verein Deutscher Zementwerke, 2009, http://www.vdz.de.

Seyler, C., Hellweg, S., Monteil, M and Hungerbühler, K.; Life cycle inventory for use of waste solvent as fuel substitute in the cement industry, Int J LCA, 10 (2), 120-130, 2005.

Siam City Cement; Sustainable Development Report. Siam City Cement Public Co. Ltd., Bangkok, Thailand, 2010.

Stenseng, M.; Pyrolysis and combustion of biomass; PhD Thesis, Department of Chemical Engineering, Technical University of Denmark, 2001.

Sutou, K., Harada, H. and Ueno, N.; Concentration is the key, International Cement Review, 36-41, June 1999.

Sutou, K. and Yukio, K.; Using waste responsibly, International Cement Review, 2000.

Sylla, H.-M.; Investigations on the formation of rings in rotary cement kilns, ZKG, 499-508, 10, 1974.

Taiheiyo Cement Corporation; Corporate Social Responsibility Report 2010. Tokyo, Japan, 2010.

Tokheim, L.-A.; An alternative solution, World Cement, November 2005.

ThyssenKrupp, Forum – Technische Mitteilungen, English version, Dec. 2002. Available from: http://www.thyssenkrupp.com/documents/Publikationen/Techforum/Forum_12_02_eng.pdf.

Várhegyi, G., Bobály, B.; Jakab, E. and Chen, H.; Thermogravimetric study of biomass pyrolysis kinetics. A distributed activation energy model with prediction tests. Energy & Fuels, 25, 24-32, 2011.

VDZ, Environmental Data of the Cement Industry 2005. Available from: http://www.vdz-online.de.

VDZ, Environmental data of the German Cement Industry 2010. Available from: http://www.vdz-online.de.

Wang, Z., Richter, H., Howard, J. B., Jordan, J., Carlson, J. And Levendis, Y.; Laboratory investigation of the products of the incomplete combustion of waste plastics and techniques for their minimization, Ind. Chem. Eng. Res., 43, 2873-2886, 2004.

Wanzura, F., Wendt, B.; Influence of the use of secondary materials on the levels of heavy metals in Portland cement clinkers and cement. ZKG-International, 10, 53-60, 2003.

Wirthwein, R., Scharf, K.-F., Scur, P. and Drebelhoff, S.; Operating experience with a fluidized bed gasifier using waste materials for lean gas making, ZKG International, 55, No. 1, 61-69, 2002.

Wirthwein, R.; Experiences in operating bypass systems at CEMEX Germany. ECRA Seminar, Germany, September 2007.

Wurst, F. and Prey, T.; Dioxin emissions when using alternative fuels in the cement industry, ZKG International, 56, No. 4, 74-77, 2003.

Zheng, Y.; Mercury removal from cement plants by sorbent injection upstream of pulse jet fabric filter. PhD Thesis, Department of Chemical and Biochemical Engineering, Technical University of Denmark, 2011.

4 Mixing of large and small particles in rotary kilns

This chapter seeks to provide a basic understanding of the mixing process of particles with different sizes and densities in the material bed of rotary kilns. Through a literature study, the present knowledge is described. Subsequently, sections about experimental work, results and discussion will present the results obtained from raw material/ fuel particle mixing experiments in a pilot-scale rotary kiln at ambient conditions. The chapter ends with a conclusion and description of practical implications.

4.1 Introduction

Solid fuel particles entering a rotary kiln may be rapidly distributed into the raw material bed. Depending on fuel and raw material particle characteristics as well as kiln operational parameters, the solid fuels may be partly or fully buried in the raw material bed. The exact position of the fuel particles has importance for the heat and mass transfer mechanism to the fuel particles. For this reason it is important to obtain a basic understanding of the mixing process.

As a rotary kiln turns on its axis the solids bed inside is subjected to transverse motion. The bed motion can take many forms, depending on variables such as rotational speed, kiln diameter, fill degree, bed/wall friction and bed particle characteristics. The different bed motions - slipping, slumping, rolling, cascading, cataracting and centrifuging, are illustrated in Figure 4-1. These six characteristic flow patterns have great influence on the radial mixing, surface renewal, heat transfer, dust generation and axial transport - for the continuous operation. For example, it is widely recognized that the slipping mode, in which the bed slides against the inner kiln walls, drastically reduces mixing of the solids and heat transfer. For conditions relevant for clinker nodulization in cement rotary kilns, the characteristic bed motion is the rolling mode (Boateng, 2008). The main focus is therefore on the rolling mode. It should be noted however, that other bed motions are possible, particularly in the material inlet end of the rotary kiln where the partially calcined raw material particles enter with particle sizes typically in the order of 5-90 μm with diameter based average sizes around 20 μm.

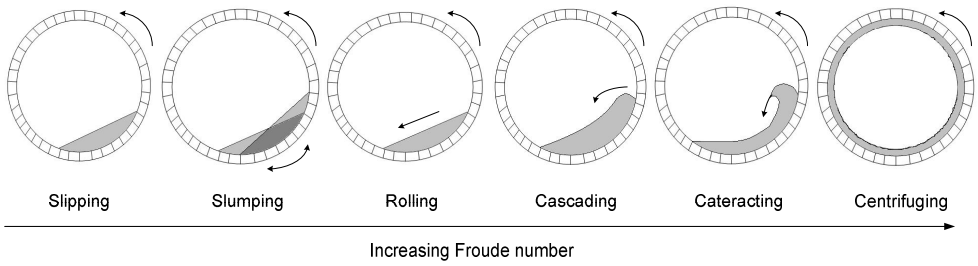

Figure 4-1: Bed behavior with Froude number tendency.

The surface of the rolling bed is approximately flat and inclined at an angle commonly described as the dynamic angle of repose, β. The angle of repose increases with increasing rotational speed (Yang et al., 2003) and is reduced with increasing particle size (Rao et al., 1991). For cement raw

materials the angle of repose is typically between 30-50° (Henein et al., 1983). The structure of the bed comprises two layers, the active layer (surface) and the passive layer (sub-surface). This is illustrated in Figure 4-2. In the passive layer the bed is closely packed and the particles rotate with the kiln at fixed radius. Under these circumstances the possibility of particle mixing is quite small (Ingram et al., 2005). When the particles reach the surface, they roll downwards and rejoin the passive layer. In the active layer the particles are in motion and this is where mixing occurs. The active layer thickness increases with increasing rotational speed and bed depth, because more material is transported through the active layer as well as the passive layer per unit time. The number of particles passing through the active layer increases also with increasing rotational speed and decreasing particle size (Henein et al. 1983).

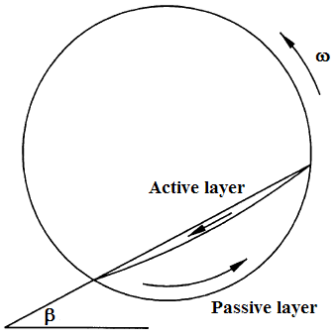

Figure 4-2: End view of rotary kiln showing active and passive layers as well as the angle of repose.

Henein et al. (1983) have performed extensive work to establish bed behavior diagrams for a number of compounds. This type of bed behavior diagrams is useful to predict mode of bed motion based on bed depth and Froude number (rotational speed). The Froude number is here defined as:

$$Fr = \frac{\omega^2 R}{g} = \frac{\left(\frac{2\pi n}{60}\right)^2 R}{g} \qquad (4.1)$$

where ω has the unit rad/s and n has the unit min^{-1}. R is the drum radius and g is the gravitational acceleration in m/s^2. Mellmann (2001) investigated different operating regimes based on the Froude number. He found that rolling beds typically occur for Froude numbers between $10^{-4} < Fr < 10^{-2}$ for fill degrees higher than 10%. This result is in good correlation with Froude numbers reported by Henein et al. (1983) from experiments in a rotary drum with limestone and sand. Henein et al. found useful correlations for scaling-up. The bed behavior is not only characterized by bed fill degree and Froude number for a given material. Particle size and shape must also be considered. For particles with same shape and for kilns with the same diameter (D) and fill degree (and same bed/wall and particle/particle friction), the bed motion from one particle size (d_p) to another can be described as (Henein et al., 1983):

$$Fr_1\left(\frac{D}{d_p}\right)_1^{1/2} = Fr_2\left(\frac{D}{d_p}\right)_2^{1/2} \tag{4.2}$$

This correlation is also valid for scaling of bed behavior from one diameter to another, for the same particle shape and size.

Cement rotary kilns are slightly inclined with the raw materials entering in the upper end and flowing by gravity and kiln rotation to the lower end. A large fuel particle will spend some of its time in the active layer, on the bed surface, and the remainder of the time in the passive layer below the bed surface. The time that the fuel particle will be present in the active layer relative to the time in the passive layer, depends on a number of parameters, such as bed fill degree, rotational speed, raw material characteristics, fuel particle size, shape and density.
Although mixing occurs in both the axial and transverse direction, mixing in the transverse direction is much more rapid (Sherrit et al., 2003). This is true for mixing in both industrial rotary kilns as well as in horizontal, rotary drums.

The theoretical probability, P, of a large fuel particle to be visible in top of the bed rather than being buried in the bed may be described as proportional to the volume occupied by the fuel particle relative to the total available volume:

$$P \propto \frac{\frac{V_{fuel}}{\theta}}{V_{total}} \propto \frac{\frac{V_{fuel}}{\theta}}{\frac{V_{fuel}}{\theta} + V_{raw\ material}} \propto \frac{\frac{V_{fuel}}{\theta}}{\frac{V_{fuel}}{\theta} + \frac{\pi}{4} \cdot L \cdot D^2 \cdot F} \cdot 100\% \tag{4.3}$$

where L and D is the kiln length and diameter, respectively, and F is the bed fill degree. θ is the sphericity which is a measure for the non-sphericity of the fuel particle, defined as:

$$\theta = \left(\frac{\text{Surface of sphere}}{\text{Surface of particle}}\right)_{\text{of same volume}} \tag{4.4}$$

With this definition, θ = 1 for spherical particles and 0 < θ < 1 for all other particle shapes. The sphericity is included because the shape of the particles is likely to affect the degree of visibility, because for particles of the same volume, the external particle surface area increases when the sphericity decreases. This may be illustrated with the three particle shapes shown in Figure 4-3. All three particles have a volume of 1 cubic unit, but their external surface areas are quite different depending on their shape. The surface area increases with decreasing sphericity and thus the particle is more likely to be fully or partly visible in the bed.

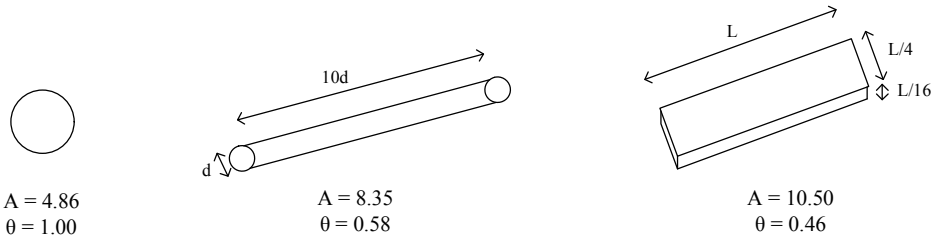

Figure 4-3: External surface areas and sphericities for three particles with the same volume.

Equation (4.3) includes the kiln dimensions, bed fill degree, volume and sphericity of the fuel particle. The probability increases as the fuel volume increases. However, parameters such as rotational speed, fuel density and raw material density are not included, even though they are likely to have an effect. Attempts have been made to correlate experimental values for mixing with the operating parameters and properties of granular material. Sherrit et al. (2003) provide a review of such correlations. However, these correlations are based on mixing of particles with the same or similar particle sizes. A similar correlation can be derived from experiments to yield a correlation of the form:

$$P = \frac{\frac{V_{fuel}}{\theta^a}}{\frac{V_{fuel}}{\theta^a} + \frac{\pi}{4} D^2 L F^b} \cdot Fr^c \cdot \left(\frac{\rho_{raw\ material}}{\rho_{fuel}} \right)^d \cdot 100\% \qquad (4.5)$$

where a, b, c and d are experimentally determined fitting parameters. Fr is the Froude number which includes the rotational speed. $\rho_{raw\ material}$ and ρ_{fuel} is the density of raw material and fuel particles, respectively.
Equations (4.3) and (4.5) are only valid for $d_{p,\ fuel} << $ bed depth since fuel particles with all dimensions exceeding the bed depth cannot be fully covered by the bed.

4.2 Literature study on mixing and segregation in rotary kilns and drums

Much research has been done to describe mixing of uniform particles in rotary kilns or rotary drums (e.g. Woodle et al., 1993, Santomaso et al., 2005, Puyvelde, 2006 and Kwapinska et al., 2006). Less information is available about the mixing of particles with different size, shape and density. This is relevant when large alternative fuel particles are mixed with raw material particles of much smaller particle size. The degree of mixing of these fuel particles is important since their burnout behavior depends on mass and heat transfer. As it will be described in this section, most of the current research about mixing of particles with different sizes has been made with spheres of different materials, and typically with size ratios of less than 5.

When particles of different sizes and densities are mixed in the presence of a gravitational field, segregation usually occurs. In theory, large low-density particles will drift towards the top of the layer, followed lower down by smaller low-density and large high-density particles. The smallest

high-density particles will collect in the bottom. The reason is that dense particles can push lighter neighbour particles away and move downwards (Tanaka, 1971). Regarding particle size, an explanation has been provided by Savage and Lun (1988): During mixing of several layers of particles in a bed, void spaces between the particles are undergoing continual random changes. If a void space is large enough, then a particle from the above layer can fall into it as the layers move relative to each other. The probability of finding a void space that a small particle can fall into is larger than the probability of finding a void space that a large particle can fall into. Thus, this gravity-induced size-dependent void filling mechanism creates a tendency for small particles to end at the bottom and large particles to end at the top.

Tallon and Davies (2008) have developed a method for in-situ measurement of mixing of materials with different particle density or packing density. The principle is that a small cup is mounted to the inner drum wall and is filled with material during rotation. The mass of material in the cup is then measured by a load cell when the cup is above the free surface of the bed particles. This gives a good indication of the mixing process.

Orpe and Khakhar (2001) studied the flow and segregation of 2 mm spheres of sand, glass and steel in rotating cylinders. They found that particle surface roughness only had a very small effect on the flow and segregation. However, similar experiments with 1-3 mm spheres of stainless steel, mild steel and brass in rotating cylinders have shown that surface roughness *can* affect segregation (Hajra and Khakhar 2004). Hajra and Khakhar furthermore reported that segregation of large 2 or 3 mm spheres in smaller 1 or 1.5 mm spheres were independent of the size of the larger spheres, but depended strongly on the size of the smaller spheres.
Clément et al. (1995) studied mixing of 3 mm steel spheres in 1.5 mm steel spheres in a rotating cylinder and found that the smaller particles had a tendency to stay in the centre, while the larger particles dwelled on the edges. This finding was confirmed by Cantelaube et al. (1995 and 1997) who made experiments with glass particles of diameters from 6 to 20 mm. Cantelaube et al. (1995) also reported that segregation of large particles appeared very quickly after the start of drum rotation, typically in less than one drum revolution. Alonso et al. (1991) found that 1-4 mm diameter spheres of different materials had a tendency to segregate with the smallest particles in the core, but that particle size and density could mutually compensate to reduce segregation.
Thomas (2000) studied segregation of spherical glass spheres of variable diameter between 45 µm and 7.5 mm. She found that there was a segregation of large particles at the bed surface *only if the size ratio between large and small particles were below 5*. For size ratios above 5, the large particles could be located anywhere in the bed depending on their size and mass. This was explained by segregation being a result between various effects, counteracting each other. For example, the geometrical void effect will push the large particles to the bed surface and the mass effect will push it to the bottom of the bed by pushing away smaller particles.

For fuel particles in an industrial rotary kiln, the fuel particles will release volatiles during the devolatilization and CO/CO_2 during the char oxidation, see chapter 5. The fuel particles may also break into smaller particles during the combustion process. Thus, fuel particle density, shape and size may change over time and this is likely to affect the mixing process.

4.3 Experimental

An experimental study was carried out to investigate mixing of large solid fuel particles in a rolling bed of cement raw materials. Key parameters such as fuel particle size and density were studied as well as the parameters rotational speed and raw material fill degree.

4.3.1 Experimental set-up

A pilot-scale rotary kiln with inner diameter and length of 50 cm was constructed and used for the experiments, see Figure 4-4. The kiln walls were made of a deck plate with a thickness of 5 mm, and a rough inner surface. The two end walls consisted of 600 mm diameter plexi glass plates with a thickness of 5 mm, which were mounted with butterfly screws for easy removal during loading and unloading of the pilot-scale rotary kiln. The pilot-scale rotary kiln was placed horizontally on rollers connected to a motor with variable speed.

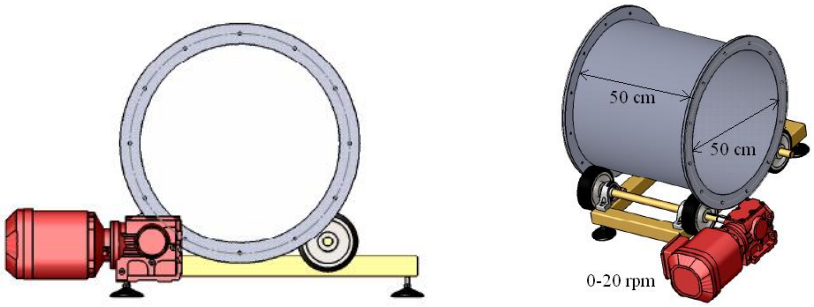

Figure 4-4: Sketch of pilot-scale rotary kiln used in the experiments.

4.3.2 Bed materials and fuel characteristics

The experiments were all made with cement raw materials with physical and chemical properties as shown in Table 4-1. The raw material has a particle size that is significantly smaller than that of the fuel particles.

Chemical composition	
$CaCO_3$	78.4 wt.-%
SiO_2	13.5 wt.-%
Fe_2O_3	2.3 wt.-%
Al_2O_3	3.3 wt.-%
Minor components	2.6 wt.-%
Bulk density	1,200 kg/m^3
Mean particle size	18 µm
Sieve interval, µm	
0-5	21.4 wt.-%
5-10	13.3 wt.-%
10-20	19.0 wt.-%
20-30	12.5 wt.-%
30-60	18.9 wt.-%
60-90	8.2 wt.-%
90-400	6.6 wt.-%

Table 4-1: Composition and physical properties of cement raw material used in the experiments.

The 15 different fuel particles used in the experiments are presented in Table 4-2. These fuel particles all have different shapes, sphericities, sizes, volumes, weights and solid densities, given in the table per particle. These fuel particles were chosen because they are representative for the fuel types that may be relevant to use in industrial rotary kilns. The sphericity is defined in equation (4.4). As indicated by Table 4-2 some of the fuel particles have significantly larger dimensions than the raw material, and the size ratio may be as high as 10^4. The size ratio is, however, realistic, since solid fuels used in industrial cement rotary kilns may also have dimensions up to 1-2 m, whereas the cement raw material particle sizes generally are below 100 µm.

Sample No.	Particle type	Shape / Sphericity	Size [cm]	Volume [cm^3]	Weight [g]	Density [kg/m^3]
1	Charcoal	Oval / 0.95	5.5x5.5x3.0	56.8	45	792
2	Charcoal	Oval /0.95	5.5x2.8x3.0	29.0	23	792
3	Charcoal	Irregular / 0.89	2.8x2.8x3.0	10.1	8	792
4	Ceramic	Spherical / 1.0	D=0.6	0.11	0.32	2829
5	Wood	Cubic / 0.81	2x2x2	8.0	3.3	470
6	Wood	Cylindric / 0.87	D=2.2, L=2	7.6	5.1	665
7	Wood	Cylindric / 0.84	D=2.2, L=4	15.2	10	665
8	Wood	Rectangular / 0.67	1.8x4.5x8.1	66.0	31	470
9	Wood	Rectangular / 0.56	1.8x4.5x16.5	134.0	78	470
10	Tire rubber	Rectangular / 0.78	2.5x2.0x4.0	20.0	22	1100
11	Tire rubber	Rectangular / 0.75	2.5x5.0x6.0	75.0	82.5	1100
12	Tire rubber	Rectangular / 0.59	2.5x8.0x17.0	340.0	374	1100
13	Plastic	Cylindric / 0.73	D=1.3, L=5.3	7.0	2.4	341
14	Plastic	Cylindric / 0.73	D=1.3, L=5.3	7.0	4.0	569
15	Plastic	Cylindric / 0.73	D=1.3, L=5.3	7.0	7.7	1095

Table 4-2: Fuel particles used in the experiments. Size, volume and weight are per particle. The density is the solid density.

4.3.3 Experimental procedure

The desired fill degree is obtained by filling the pilot-scale rotary kiln with the desired volume of raw material. The fill degree is here defined as the percentage of the kiln cross sectional area that is covered by raw material. A fixed number of fuel particles are placed on top of the raw material, along the center line: 20 fuel particles were used in each experiment, except for the experiments with the largest fuel particles, sample no. 9 and no. 12 in Table 4-2. For these experiments with the two largest fuel particles, only 10 fuel particles were used. The rotation is started with the desired rotational speed. The rotational speed used in the experiments is varied between 3 and 16 rpm. It should here be noted that a rotational speed of 13 rpm in the experimental set-up corresponds to approximately 5 rpm in an industrial rotary kiln with a 4 m diameter, if the scaling correlations found by Henein et al. (1983) are used.

A video camera was used to record the mixing in order to document the experiments. At time intervals of 30 seconds the rotation is stopped and the number of fuel particles visible on top of the bed are counted. Then the rotation is started again. This start-stop cycle is repeated until uniform mixing is achieved, or for at least 180 seconds. All fuel particles visible on the top of the bed are included, even if a significant fraction of the fuel particle is buried in the bed.

4.3.4 Assumptions and uncertainties

This section discusses the main differences between the pilot-scale rotary kiln and industrial rotary kilns. The discussion presents assumptions that have to be made in order to account for uncertainties when results may be transferred from the pilot-scale rotary kiln and to industrial scale conditions.

1. The experiments are made at ambient temperature. It is a foregone conclusion that the fuel particle/raw material mixing at ambient temperature is the same as at high-temperature conditions. An uncertainty, however, is the surface properties of the particles which may be quite different at ambient and high-temperature conditions. At high temperatures the raw materials may stick to the fuel particles and e.g. affect sphericity and flowability of the fuel particles.

2. The pilot-scale rotary kiln is not inclined. It is a foregone conclusion that the lack of material transport in the axial direction has no significant effect on the overall mixing process since mixing in the transverse plane is dominating (Sherrit, 2003).

3. It is a foregone conclusion that the dimensions of the pilot-scale rotary kiln are sufficiently large to allow up-scale to industrial rotary kilns without introducing too much uncertainty. This assumption is based on the fact that several researchers have used similar rotary drums to simulate industrial conditions, and in many cases experimental results have been successfully validated against published full-scale data (Henein et al., 1983, and Mellmann, 2001).

4. It is a foregone conclusion that Henein et al.'s (1983) scaling principles of rotational speed for rolling beds can be applied for the conditions used in these experiments. This assumption is confirmed by visual observations of bed motion prior to the experiments, where the rolling motion is seen to be dominant.

5. It is a foregone conclusion that the bed-wall friction coefficient in the pilot-scale rotary kiln is of comparable size to industrial kilns: The steel wall used in the pilot-scale rotary kiln has a rough surface. In addition, the kiln walls are covered by a thin layer of raw material that adheres to the surface. This is assumed to be comparable to an industrial kiln where the wall is typically covered by a coating layer consisting of raw materials.

6. Under industrial conditions the fuel particles will release volatiles, CO and CO_2 during the devolatilization and char oxidation. The fuel particles may also break into smaller fragments. This induces a high degree of uncertainty on the mixing experiments made in this study and the actual mixing process in industrial rotary kilns. It is, however, assumed that the mixing experiments in this study will provide a fundamental understanding of the mixing process under industrial conditions.

4.4 Results and discussions

4.4.1 General observations

The mixing was generally observed to be a fast process that was completed in less than 30 seconds, or after a few kiln rotations. After this initial mixing, a steady state was reached were the percentage of visible particles did not change significantly. This observation is in correspondence with Cantelaube et al. (1995) who also reported that the mixing process appeared very quickly after the start of drum rotation.

The rotational velocity is varied from 3 rpm to 16 rpm, corresponding to approximately 1 to 6 rpm in an industrial, 4 m diameter rotary kiln according to the scaling correlations found by Henein et al. (1983). The bed behavior should be in the rolling regime under these conditions. The rolling bed behavior was also observed to be dominant.

Henein et al. (1983) reported that the dynamic angle of repose should be between 30° and 50° for cement raw materials in the rolling motion. He also reported that the angle of repose is independent of fill degree and rotational speed when the rolling motion dominates. In the experiments the angle of repose were generally measured to be between 30° and 40°, and thus in good correspondence with the findings of Henein et al. (1983).
All experiments have been repeated three times. The repeatability is generally good with standard deviations of the experiments generally within 4-8%.

Based on the experimental data, optimal values for the fitting parameters a, b, c and d used in equation (4.5) were determined. The fitting parameters were found by comparing equation (4.5) with all experimental values and then modifying the equation until the best fit was found. The fitting parameters are shown in Table 4-3 with uncertainties in parenthesis. The visibility predicted by the correlation will be shown graphically in Figures 4-6 to 4-9. From the table it is seen that the correlation actually only contains three fitting parameters since b = 1. In addition, it should be noticed that the correlation may be further simplified by using c = 0. This will only have a slight effect on the values predicted by the correlation and will reduce the number of fitting parameters to two.

a	b	c	d
1.5 ± 0.2	1 ± 0.2	-0.1 ± 0.01	0.5 ± 0.2

Table 4-3: Fitting parameters used in the correlation between percent visible particles and experimental data.

4.4.2 Effect of fuel particle size and shape

The effect of particle size and shape on the mixing efficiency has been investigated for fill degrees between 5% and 30% and rotational speeds between 3 rpm and 16 rpm. 12 samples with different sizes and shapes were used in the experiments, see Table 4-2 for details. An example for a fill degree of 10% and a rotational speed of 13 rpm is shown in Figure 4-5. It is observed that particles, regardless of size and shape, decreases rapidly from 100% percent visibility to significantly lower values. The mixing takes place within the first 30 seconds, corresponding to 1-8 kiln rotations. Subsequently, the particles are to a large degree covered by raw material and only appear on top of the bed randomly.

It is noted that the large, rectangular samples number 9 and 12 are significantly more visible on top of the bed: After 30 seconds approximately 47% and 58% of these particles are still visible, respectively. And these percentages are more or less constant with time. By contrast, the smallest particles which are the spherical ceramic particles denoted sample 4, drop from 100% to 0% during the first 30 seconds. Subsequently, the small particles are not observed anymore on top of the bed, during the 180 seconds that the experiment runs. The largest and most visible fuel particles number 9 and 12 are also the least spherical particles, whereas the smallest and least visible fuel particles are also the only truly spherical particles used in the experiments. These results indicate that not only the fuel particle dimensions but also the fuel particle shape, expressed as sphericity, are important for the visibility above the bed. This effect of sphericity is further confirmed by comparing sample number 1 and 8 which have similar volumes of 57 cm^3 and 66 cm^3, respectively, but quite different sphericities of 0.95 and 0.67. It is observed that the least spherical particle is the most visible. However, the density of the two samples is not identical and this may affect the visibility as well. In order to determine the effect of shape with greater accuracy, it is necessary to conduct more experiments with fuel particles of similar volumes and densities but different shapes.

The experiments have been repeated for different fill degrees and rotational speeds and the tendency is the same under all conditions: Fuel particles with large dimensions have a higher probability of being visible on top of the bed compared to smaller particles that are to a higher degree buried in the bed. This geometric effect on the degree of visibility was also predicted by equation (4.3) and (4.5).

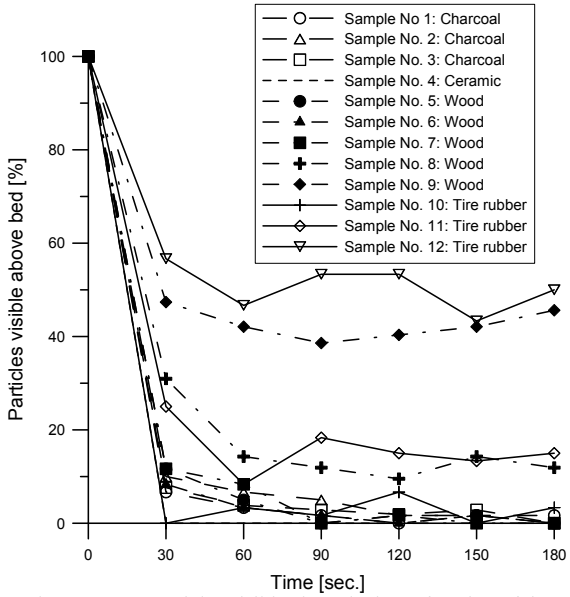

Figure 4-5: Example of raw data: Percent particles visible above bed as a function of time. 10% fill degree and 13 rpm.

Figure 4-6 shows the visibility of all the different fuel particles at steady state, sample no. 1 to sample no. 12, as a function of the fuel particle volume. Steady state is here defined as the time interval between 30 seconds and 180 seconds, where the percent visibility is relatively constant. The small ceramic spheres, sample no. 4, had the smallest volume of 0.11 cm^3 per particle, and had a steady state visibility of close to 0%. Several of the tested fuel particles had volumes around 10 to 60 cm^3, but different sphericities and densities. The steady state visibility is still low, around 3-7%. For fuel particles with volumes larger than 100 cm^3 the percent visibility increases significantly, up to 50% for the largest particle with a volume of 340 cm^3. The standard deviation varied from 0% to 8% during the experiments, and was observed to be greatest for the largest fuel particles.

Figure 4-6 also shows the estimated probability for the particles to be visible based on equations (4.3) and (4.5). Even though equation (4.3) does not take the effect of density and rotational speed into account, a fairly good consistency is seen between the theoretical and experimental values, for volumes up to around 100 cm^3. But for the largest particles, equation (4.3) under-estimate the probability: This is particularly observed for the particle with a volume of 134 cm^3, where the observed visibility is 43% but the theoretical probability is only 21%. The reason why equation (4.3) fails to give a good estimation of the theoretical visibility for the largest particles may be that it becomes increasingly difficult for the largest particles to be fully buried in the bed, as their dimensions increases. Thus the degree of visibility will deviate more and more from the theoretical predictions as the particle dimensions are increased.

Equation (4.5) which includes correlations for rotational speed and density gives a good consistency between theoretical and experimental values for most of the particles. Fitting parameters used are shown in Table 4-3. The greatest deviation is for the particles with volumes of 57, 66 and 75 cm^3 which deviates 12%, 18% and 6% from the experimental values,

respectively. One reason could be that these three particles have quite different volumes of 792 kg/m^3, 470 kg/m^3 and 1100 kg/m^3, respectively. It may be difficult to fit the model to give good predictions of all combinations of densities, shapes, volumes and operational parameters.

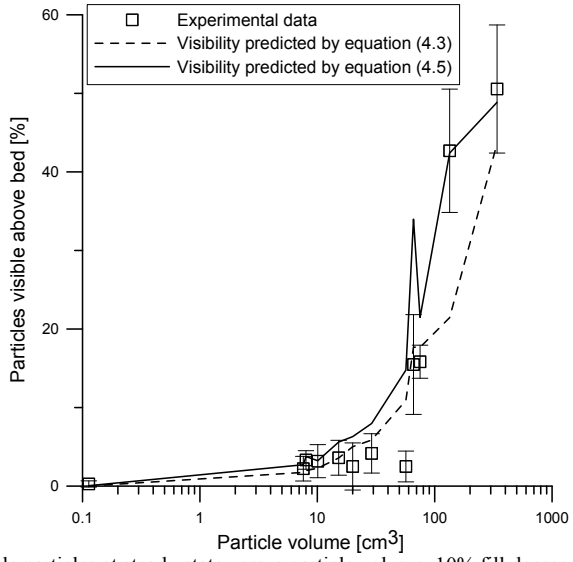

Figure 4-6: Percent visible particles at steady state versus particle volume. 10% fill degree, 13 rpm.

The observations regarding fuel particle size and the degree of visibility above the bed is in good correspondence with the theory about void filling presented by Savage and Lun (1988), which also predicts that it becomes increasingly more difficult for a large particle to sink to the bottom as the particle size increases. The observations may also be considered as a pure geometric effect where increasing dimensions of the fuel particles imply a decreasing probability that the fuel particles will be fully covered by the raw material bed.

4.4.3 Effect of bed fill degree

The raw material bed fill degree has been varied for all samples in the following range: 5%, 10%, 15% and 20%. This range of fill degrees covers the situation in industrial cement rotary kilns, where fill degrees typically are 8-15%. Figure 4-7 shows the effect of fill degree for tire rubber particles of three different sizes and thus with three different volumes, as specified in Table 4-2. For all three particle sizes, the percent visibility is observed to decrease with increasing fill degrees. The large particles are around 80% visible at the 5% fill degree. At 10% fill degree and 15% fill degree is the percentages around 50% and 40%, respectively.

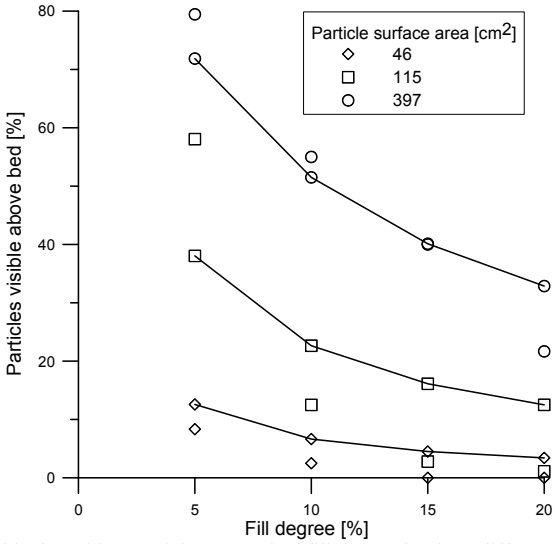

Figure 4-7: Percent visible tire rubber particles versus bed fill degree for three different particle sizes. Predicted values are shown with solid lines and experimental values are shown with symbols. 10 rpm.

It was found that the fill degree is an important parameter for the percentage of fuel particles that is present on top of the bed. Especially small particles will, regardless of shape, rapidly be buried in the bed. Larger particles will, due to their proportions, only be partly buried in the bed whereas part of the particles will be sticking out in the freeboard above the bed.
The degree of visibility predicted by equation (4.5), and with the fitting parameters shown in Table 4-3, is shown with solid lines for each of the three particle sizes. The correlation provides the right tendencies and generally fits the experimental data reasonably well. However, relatively large deviations between model and experimental values of up to 20% are observed for the medium sized tire rubber particles.

4.4.4 Effect of bed rotational speed

Figure 4-8 shows the effect of rotational speed on the mixing of tire rubber particles, samples no. 10, 11 and 12 in Table 4-2. The rotational speed is expressed in terms of the dimensionless Froude number. It is observed that the percentage of visible particles decreases when the Froude number increases: Approximately 28% of the medium-sized particles are visible at the lowest Froude number of 0.0024 (3 rpm), whereas only 9% are visible at the highest Froude number of 0.0702 (16 rpm). For the largest particles, 68% of the particles are visible at the lowest Froude number and 48% are visible at the highest Froude number. The smallest particles, however, does not show any particular dependence of Froude number. The same tendencies were also observed for other fill degrees and other particles.
The degree of visibility predicted by equation (4.5) and with the fitting parameters from Table 4-3 is shown with solid lines for each of the three particle sizes. The correlation fits the experimental data reasonably well with deviations generally less than 10%.

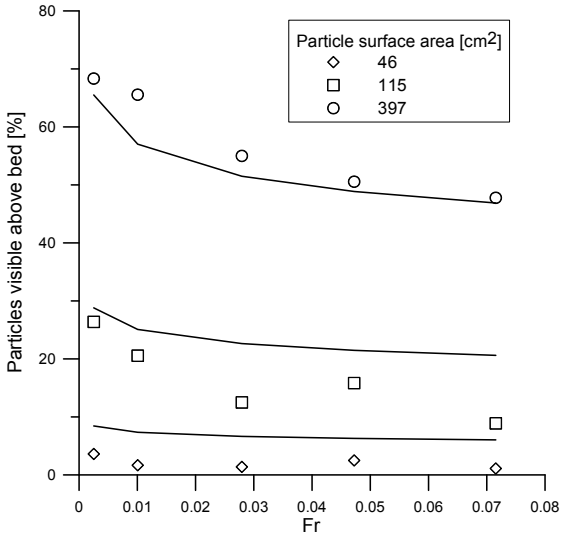

Figure 4-8: Percent visible tire rubber particles versus Froude number for three different particle sizes. 10% fill degree. Predicted values are shown with solid lines and experimental values are shown with symbols.

The effect of the rotational speed on percentage of visible particles can be explained by the fact that a high rotational speed is equal to more bed revolutions and thus a more efficient mixing process relative to a lower rotational speed. It should, however, be noted that the percent visibility of particles seems to stabilize at a certain percentage for each rotational speed. Thomas (2000) and Cantelaube et al. (1997) also studied the effect of rotational speed on the segregation of particles up to 3 mm and 20 mm in diameter, respectively. They found no effect of the rotational speed for these particle sizes, which are in correspondence with the observations in this study, for the smallest particles.

4.4.5 Effect of fuel density

The effect of particle density was studied by filling plastic containers with materials of different weight. Thus, the outer dimensions of the particles were identical, but the densities were varied from low, medium and high, see Table 4-2 for details. Figure 4-9 shows the percentage of visible particles versus the raw material/fuel particle density ratio for fill degrees of 5%, 10% and 15%, and rotational speed of 10 rpm. Standard deviations on the results presented in Figure 4-9 were between 2% and 6%. It is observed that the greatest effect of particle density appears with the 5% fill degree: The low-density particles stabilize at a level around 18% visible particles, the medium-density particles stabilizes at level around 11% visible particles, whereas the high-density particles is only 4% visible. The same effect of particle density is also observed at 10% and 15% fill degree.

Figure 4-9 also shows the values predicted from equation (4.5) and fitting parameters from Table 4-3, with solid lines and symbols. Equation (4.5) predicts the visibility excellent for the fill degrees of 10% and 15%. But for the lowest fill degree of 5% there is a quite high deviation between correlation and experimental values: The low-density fuel particles are around twice as visible as predicted by equation (4.5). There is thus a poor relationship between the fitting parameter for density, and some combinations of operational parameters.

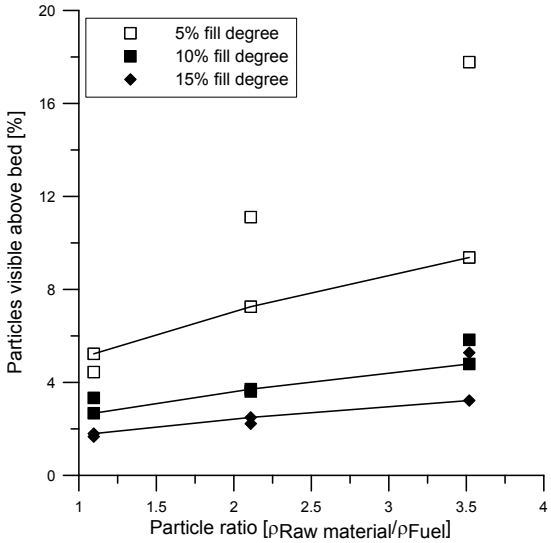

Figure 4-9: Percent particles visible above bed at steady state versus particle density. Estimated values are shown with solid lines and symbols while experimental values are shown with symbols only. 10 rpm.

The effect of particle density on the percent visibility is in good correspondence with the "push-away" theory presented by Tanaka (1971), which states that dense particles are more likely to push away other particles and sink to the bottom.

4.4.6 Effect of tumblers

The pilot-scale rotary kiln was equipped with four tumblers in order to study the effect on the mixing process. The tumblers had a height of 80 mm and were placed symmetrically in the kiln, see Figure 4-10. The tumblers are expected to improve the mixing process by lifting particles from the passive layer up to 180° along the inner kiln wall before the particles falls down on the active layer. The bed material fill degree will consequently be lowered, since some of the bed material is lifted away from the bed. This is expected to expose more solid fuel particles to the freeboard above the bed.

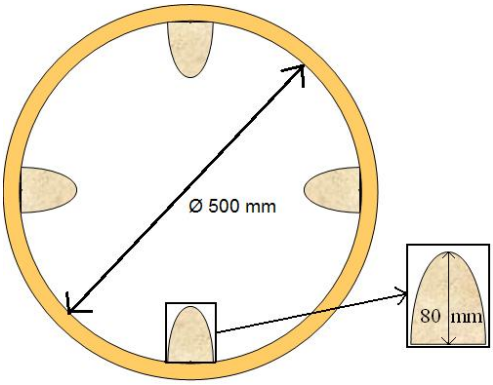

Figure 4-10: Four tumblers placed symmetrically in the pilot-scale rotary kiln.

A comparison of the percentage of visible tire rubber particles at 5%, 10% and 15% fill degrees and 10 rpm *with* and *without* tumblers are shown in Figure 4-11. It is seen that the fuel particles are generally more visible with the tumblers installed, typically with an improvement of 10-20%. An exception is the medium-sized fuel particles at 5% fill degree: Here the visibility of the particles is 58% without tumblers, which is higher than with tumblers, where the visibility was 50%. The standard deviations on the results with tumblers were generally higher than for the results without tumblers, and were up to 17% in one case.
The degree of improved mixing with tumblers installed was found to increase with increasing rotational speed.

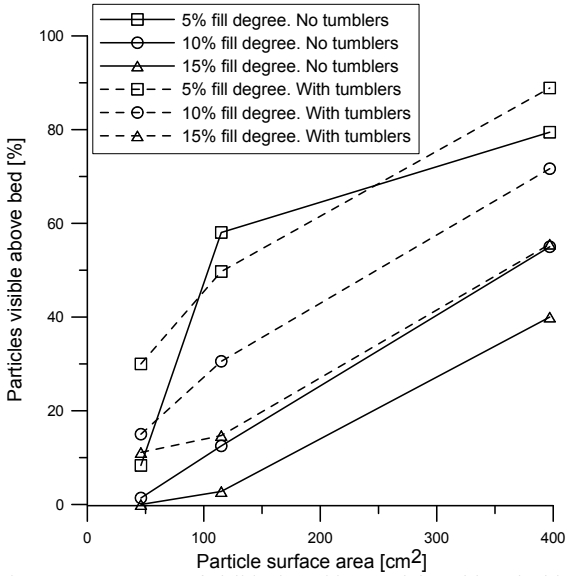

Figure 4-11: Comparison between percentage of visible tire rubber particles with and without tumblers at steady state. 10 rpm.

Based on the experiments with tumblers it was found that tumblers generally improve the mixing process. This is also in good correspondence with the fact that standard deviations on the results with tumblers were generally higher than for the results without tumblers, because improved mixing results in a more random distribution of the particles. Thus it becomes more difficult to repeat the results of individual experiments, leading to a higher standard deviation.
During the experiments with the tumblers, it was clear that the bed behavior changed from rolling to a more cataracting character: Raw materials and fuel particles were lifted up and fell down again on top of the bed. The improved mixing caused by this new bed behavior is likely to improve heat and oxygen transfer from the freeboard gas to the fuel particles in an industrial rotary kiln. However, the tumblers will also result in a dustier atmosphere in the rotary kiln, which may lead to more dust entrained in the flue gas leaving the rotary kiln.

4.5 Practical implications

Equation (4.5) is applied to conditions of an industrial rotary kiln in order to estimate the effect of fuel particle volume and sphericity on the percent visibility above the raw material bed. Typical values for a cement rotary kiln are shown in Table 4-4.

Rotary kiln	
Inner diameter, m	4.35
Total rotary kiln length, m	51
Material inlet section length, m	10
Rotational speed, min^{-1}	4
Angle of tilt, °	3
Raw material flow, tpd (kg clinker/s)	3500 (40.51)
Mean raw material residence time, min	11
Mean raw material fill degree, %	11
Raw material bulk density, kg/m^3	1200

Table 4-4: Typical data for a modern cement rotary kiln (FLSmidth ROTAX 2 kiln).

Two selected fuels, tire rubber and wood are studied. The fuel densities will decrease rapidly during the heating and devolatilization process in the material inlet where raw material temperatures and gas temperatures are typically 900°C and 1100°C, respectively. It is a foregone conclusion that the fuel char densities are representative during the mixing process. The char density of tire rubber is assumed to be 340 kg/m^3 and the char density of wood is assumed to be 160 kg/m^3.

Figure 4-12 shows the percent visibility of tire rubber char and wood char particles as a function of the fuel particle volume and for three different fuel particle sphericities of 0.5, 0.75 and 1.0, respectively. The volume of fuel particles is assumed to be distributed over the first 10 meters of the material inlet end of the rotary kiln, where the combustion is assumed to take place. The percent visibility is observed to increase linearly with the fuel particle volume. It is interesting to note that the sphericity of the fuel particles have a great effect on the percent visibility: A pure spherical fuel particle ($\theta = 1.0$) is least visible due to its compact shape which leads to a high degree of fuel coverage by raw materials. As the fuel particle sphericity decreases, the percent visibility increases due to the larger dimensions of the fuel particles. The increasing dimensions of fuel particles of the same volume but decreasing sphericity are illustrated in Figure 4-3. The tendency with sphericity and visibility is the same for tire rubber char and wood char but it is observed that the wood char is considerably more visible than tire rubber char due to its lower density.

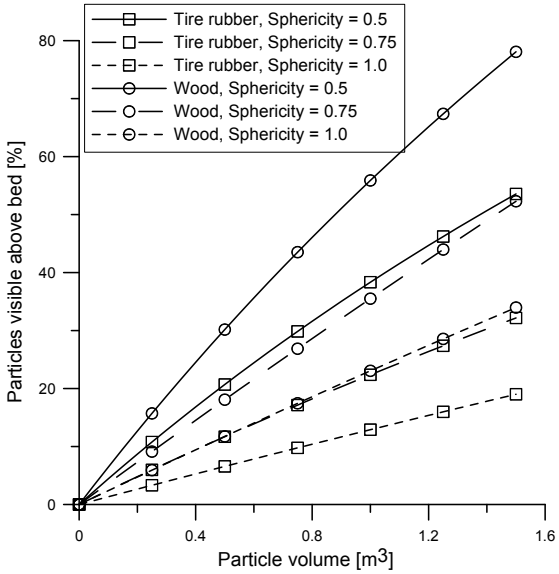

Figure 4-12: Estimated degree of visibility of tire rubber char and wood char particles as a function of fuel particle volume and sphericity. Estimated by equation (4.5).

An important practical implication for combustion processes in industrial rotary kilns can be concluded to be the shape of the fuel particles, because low-sphericity fuel particles are expected to be in better contact with the gas phase, which may improve the combustion process. Also the fuel particle density will have an effect on the gas-fuel contact.

4.6 Conclusions for Chapter 4

During experiments in a pilot-scale rotary kiln distribution of large solid fuel particles in cement raw materials were studied. The results were evaluated as the percentage of fuel particles visible above the bed at specific time intervals.

The fuel particles were to a large degree buried in the cement raw materials within less than 30 seconds. Subsequently, the percentage of visible fuel particles stabilized at a specific level, depending on fuel particle size. There was a clear tendency that large fuel particles were more visible than smaller fuel particles. Fuel particle dimensions and sphericity are important parameters for the degree of visibility: Large dimensions and low sphericity increases the degree of visibility.

Low-density fuel particles were more present above the bed than high-density fuel particles which were to a higher degree buried in the bed. The influence of density was particularly pronounced at low fill degrees.

The bed fill degree is of major importance for the percentage of visible fuel particles in the bed. Small bed fill degrees favor the number of fuel particles visible above the bed.

There is a tendency that an increase in rotational speed reduces the number of fuel particles visible above the bed. However, the effect of rotational speed was not as significant as the effect of bed fill degree.

Installation of tumblers in the pilot-scale rotary kiln increased the percentage of fuel particles visible above the bed, typically with a 10-20% improvement. However, the tumblers also led to a more cataracting bed behavior which generates more dust entrained in the freeboard gas.

A correlation for the percentage of visible fuel particles and the operating parameters was presented and compared with the experimental results. The correlation generally predicted the degree of visibility reasonably well. However, the correlation failed to give good predictions in some cases with low-density fuel particles.

The results indicate that large, solid fuel particles entering an industrial cement rotary kiln will rapidly be fully or partly covered by cement raw materials. Thus, heat transfer by conduction from the cement raw materials to the fuel particles must be expected to be a major heat transfer mechanism rather than convection or radiation from the freeboard gas above the material bed. Consequently, the temperature of the cement raw materials becomes of great importance for the heating of the fuel particles. In addition, it must be expected that mass transfer of oxygen from the freeboard gas to the fuel particles will be hindered by the cement raw materials covering the fuel particles.
It was found that large fuel particles were in better contact with the freeboard than smaller fuel particles of the same thickness. Thus, shredding of fuels to smaller particles is not necessarily expected to improve the combustion process in the material inlet end of cement rotary kilns. Since shredding is typically relatively energy-intensive and results in high wear on the shredding equipment, there is reason to believe that it will be advantageous that solid fuels, e.g. whole tires, undergo combustion in the material inlet end of cement rotary kiln as large particles rather than small particles.
The results also indicated that the bed fill degree is of major importance for the gas-fuel contact, whereas the rotational speed only showed a minor importance. Finally, installation of tumblers in the material inlet end of cement rotary kilns may be useful to improve gas-fuel contact, thereby improving the combustion process.

4.7 References

Alonso, M., Satoh, M. and Miyanami, K.; Optimum combination of size ratio, density ratio and concentration to minimize free surface segregation. Powder Technology, 68, 145-152, 1991.

Boateng, A. A.; Rotary kilns. Elsevier Inc., USA, 2008. ISBN: 978-0-7506-7877-3.

Cantelaube, F. and Bideau, D.; Radial segregation in a 2d drum: An experimental analysis. Europhys. Lett., 30 (3), 133-138, 1995.

Cantelaube, F., Bideau, D. and Roux, S.; Kinetics of segregation of granular media in a two-dimensional rotating drum. Powder Technology, 93, 1-11, 1997.

Clément, E., Rajchenbach, J. and Duran, J.; Mixing of a granular material in a bidimensional rotating drum. Europhys. Lett., 30 (1), 7-12, 1995.

Hajra, S. K. and Khakhar, D. V.; Sensitivity of granular segregation of mixtures in quasi-two-dimensional fluidized layers. Phys. Rev. E, 031304, 1-4, 2004.

Henein, H., Brimacombe, J. K. and Watkinson, A. P.; Experimental study of transverse bed motion in rotary kilns, Metallurgical Transactions B, 14B, 191-205, 1983.

Ingram, A., Seville, J. P. K., Parker, D. J., Fan, X. and Forster, R. G.; Axial and radial dispersion in rolling mode rotating drums, Powder Technology, 158, 76-91, 2005.

Kwapinska, M., Saage, G. and Tsotsas, E.; Mixing of particles in rotary drums - A comparison of discrete element simulations with experimental results and penetration models for thermal processes. Powder Technology, 161, 69-78, 2006.

Mellmann, J.; The transverse motion of solids in rotating cylinders - forms of motion and transition behaviour, Powder Technology, 118, 251-270, 2001.

Orpe, A. V. and Khakhar, D. V.; Scaling relations for granular flow in quasi-two-dimensional rotating cylinders. Phys. Rev. E, 64, 031302, 1-13, 2001.

Puyvelde, D. R. van; Comparison of discrete elemental modelling to experimental data regarding mixing of solids in the transverse direction of a rotating kiln. Chem. Eng. Sci., 61, 4462-4465, 2006.

Rao, S. J, Khakhar, D. V. and Bhatia, S. K.; Axial transport of granular solids in horizontal rotating cylinders: Part 2. Experiments in a non-flow system, Powder Technol. 67, 153–162, 1991.

Santomaso, A., Olivi, M. and Canu, P.; Mixing kinetics of granular materials in drums operated in rolling and cataracting regime. Powder Technology, 152, 41-51, 2005.

Savage, S. B. and Lun, C. K. K.; Particle size segregation in inclined chute flow of dry cohesionless granular solids. J. Fluid. Mech., 189, 311-335, 1988.

Sherritt, R. G., Chaouki, J., Mehrotra, A. K. and Behie, L. A.; Axial dispersion in the three-dimensional mixing of particles, Chemical Engineering Science, 58, 401-415, 2003.

Tallon, S. and Davies, C. E.; In-situ monitoring of axial particle mixing in a rotating drum using bulk density measurements. Powder Technology, 186, 22-30, 2008.

Tanaka, T.; Segregation models of solid mixtures composed of different densities and particle sizes. Ind. Eng. Chem. Process Des. Develop., 10 (3), 332-340, 1971.

Thomas, N.; Reverse and intermediate segregation of large beads in dry granular media. Phys. Rev. E, 62 (1), 961-974, 2000.

Woodle, G.R. and Munro, J. M.; Particle motion and mixing in a rotary kiln. Powder Technology, 76, 241-245, 1993.

Yang, R. Y., Zou, R. P. and Yu, A. B.; Microdynamic analysis of particle flow in a horizontal rotating drum, Powder Technol. 130, 138–146, 2003.

5 *Heat-up, devolatilization and combustion of large solid fuel particles*

This chapter seeks to provide insight into the heat-up, devolatilization and char combustion of large solid fuel particles fired into the material inlet end of cement rotary kilns. Limited knowledge is available about combustion of these large fuel particles, since focus has mainly been on suspension firing of small coal or petcoke particles in the rotary kiln main burner or in the calciner.

In chapter 3 it was shown that solid alternative fuels in the cement industry comprises a long list of different fuel types. The main emphasis in this chapter will be on tire-derived fuels (TDF) and wood because TDF and wood is expensive to shred to smaller particle sizes, thereby making TDF and wood attractive to utilize as coarse fuels fired into the material inlet of rotary kilns.

The experimental results are obtained from a pilot-scale, high-temperature rotary drum specifically designed to simulate the process conditions in the material inlet end of industrial rotary kilns.

The chapter includes an introduction to solid fuel combustion and a literature study on devolatilization and char combustion kinetics for large TDF and wood particles. The remaining part of the chapter contains experimental investigations of large fuel particles and model analysis of obtained results.

5.1 Introduction to solid fuel combustion

In this section a brief introduction to solid fuel combustion is presented. It is followed by a description of heating, drying and devolatilization of solid fuel particles and finally a description of the combustion of solid fuel char particles.

The combustion of a solid fuel may be divided into four stages: Heating, drying, pyrolysis/devolatilization, gas and char combustion. These stages are illustrated in Figure 5-1. After initial heating to around 100°C, water evaporates and is transported away from the particle. The next step is pyrolysis or devolatilization which is the release of volatiles without or with an oxidizing atmosphere, respectively. In the following, the term devolatilization will be used, unless reference is specifically made to a situation without oxygen being present. If sufficient oxygen is available, the released volatiles will burn in a flame front at the surface of the fuel particle. The final step is char combustion where the remaining fuel particle consisting almost exclusively of carbon and ash inorganic minerals is converted into the ultimate residue, ash.

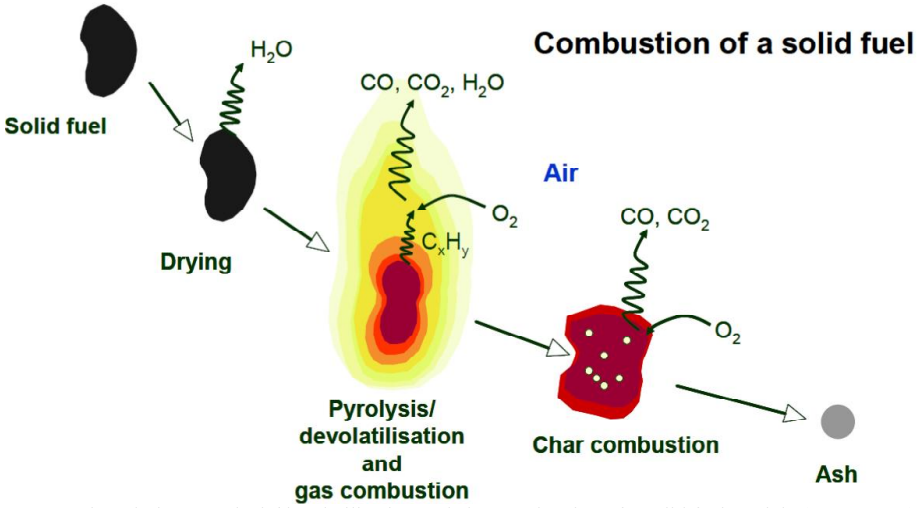

Figure 5-1: Heating, drying, pyrolysis/devolatilization and char combustion of a solid fuel particle (Hupa, 2008).

When a solid fuel particle is fired into the rotary kiln material inlet, heating mainly takes place by conduction from the cement raw materials. In addition, convection and radiation from the gas phase and kiln walls may contribute, depending on the actual position of the fuel particle in the rotary kiln. This is illustrated in Figure 5-2 where fuel particles are shown under three different situations:

1) Fully covered by raw materials where heat transfer is by conduction from the hot raw materials and where mass transfer of oxygen to the fuel particle is hindered by the raw materials. Mass transfer of devolatilization and combustion products away from the fuel particles may also be hindered by the raw materials in the bed.
2) Partly covered by raw materials where heat transfer is by all three mechanisms radiation, convection and conduction. Mass transfer to and from the fuel particle may be partly hindered by the raw materials in this position.
3) On top of the raw materials bed, where heat transfer is predominantly by radiation and convection. However, even in this position a fraction of the heat transfer will be by conduction from the raw materials since the fuel particle is always in physical contact with the raw materials. Mass transfer between the fuel particle and freeboard gas is optimal in this position.

The fraction of the particle surface that is covered by raw materials may be described as Y, where Y = 1 corresponds to the situation where the fuel particle is completely covered by raw materials and where Y = 0 corresponds to a situation where the entire fuel particle surface area is exposed to the freeboard gas. Please refer to chapter 4 for a thorough discussion on parameters affecting the Y-value. In chapter 4 was also presented the probability P, for fuel particles to be visible above the bed, see equations (4.3) and (4.5). The relationship between Y and P cannot be correlated by any simple expression because it is two fundamentally different ways to describe the distribution of solid fuel particles in the bed.

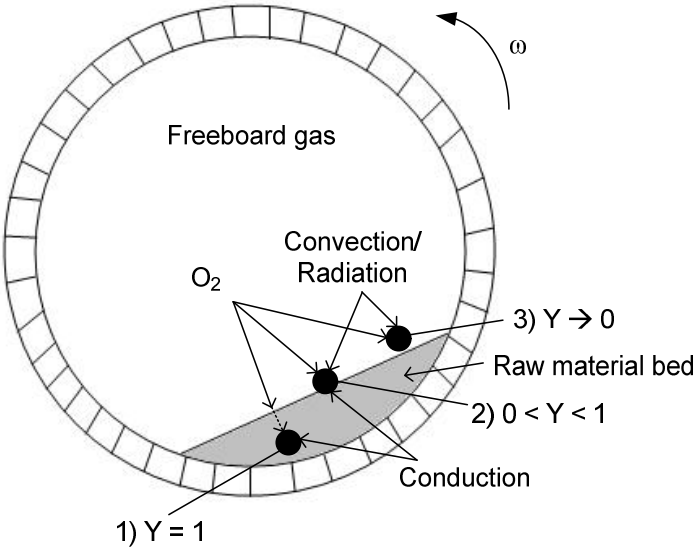

Figure 5-2: Fuel particle at three different locations in the rotary kiln: Covered by raw materials, partly covered and above the raw material bed.

5.1.1 Solid fuel conversion pathways

During devolatilization and char oxidation, a solid fuel particle can follow various conversion pathways. The overall combustion kinetics of different solid fuels may be significantly affected by the type of conversion pathway. Figure 5-3 shows examples of typical solid fuel conversion pathways. Reaction path K illustrates the reshaping of virgin fuel particles which may occur during heating. Reaction path A illustrates the direct devolatilization of gases from the solid fuel. Paths B and C show formation of intermediate liquid and tar products, respectively, before being evaporated to gas by path D. For devolatilization through reaction path I, the solid fuel particle shrinks during devolatilization with or without simultaneous formation of smaller char particles. If sufficient oxidizer is present, the gas produced through the devolatilization will be combusted in the gas phase to the ultimate gaseous combustion products.

The char combustion may also follow different pathways. In pathway F the char fragments into smaller char particles. In pathway G the char is converted as a shrinking particle and in pathway H, the char is converted as a particle with constant size. Pathway H may be described by either an unreacted shrinking core, H1, or a progressive conversion model, H2 (Levenspiel, 1999). In pathway J, the agglomeration of char may create larger char particles that are subsequently converted via pathway F, G or H.

It is important to understand which pathway a specific fuel particle follows during conversion, because it can greatly influence the conversion time. Fuels that follows pathway I are for example expected to reach full conversion much faster than fuel that follow pathway E. And if the char cracks into smaller fragments, pathway F, the smaller particle sizes are expected to result in a faster conversion relative to a larger char particle by pathway G, H and J.

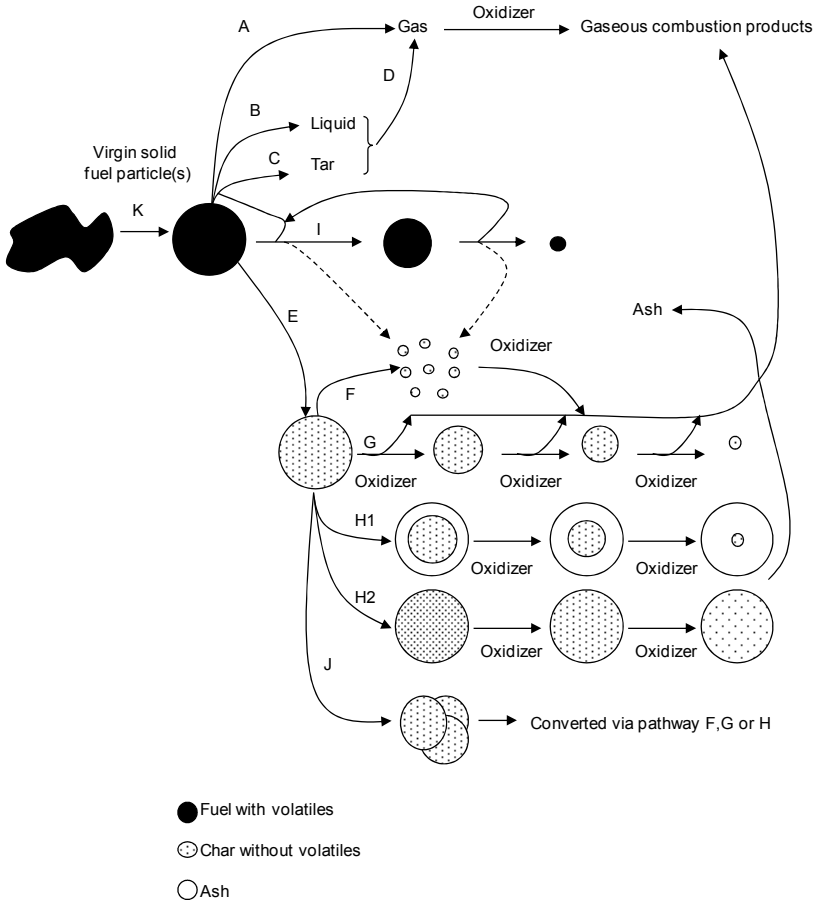

Figure 5-3: Typical conversion pathways involved in the combustion process of a solid fuel particle (Larsen, 2007).

5.1.2 Heating of solid fuel particles

Upon heating to approximately 100°C, moisture is evaporated and transported through the outer particle volume and away from the particle surface. Thus the particle is dried. The heating of the particle depends on the particle size: For small particles with diameters in the order of 10-100 μm, temperature during heat up can be assumed to be uniform throughout the particle. For larger particles, however, internal temperature gradients may exist, and these need to be taken into consideration (Agarwal et al., 1986).
An approximate definition of when the particle is isothermal and when it is non-isothermal is given by the dimensionless Biot number, Bi:

$$Bi = \frac{hd_p}{2k_p} \qquad (5.1)$$

The Biot number expresses the heat transfer to the particle relative to the rate at which heat is transported into the particle. h is the heat transfer coefficient, d_p is the particle diameter and k_p is the thermal conductivity of the particle. When Bi < 1, the particles may be considered to be isothermal, while it is more complex for Bi > 1 where non-uniform temperatures inside the particle must be taken into consideration.

5.1.3 Devolatilization of large fuel particles

Devolatilization of solid alternative fuels is important because alternative fuels typically contain a relatively high amount of volatiles, see fuel analyses in chapter 3 section 3.2.3. As a consequence, a high proportion of the heating value is released during the devolatilization.

For solid fuel particles where the char layer is retained during devolatilization, several physical and chemical processes influence the devolatilization process, see Figure 5-4. The devolatilization process is initiated by external heating when the particle surface temperature reaches the lower devolatilization temperature, T_{Vol1}. Heat is transported into the material by conduction through the char, reacting and virgin layers. Radiative heat transfer may play a role in the char and reacting layers. In the reacting layer, volatiles are released, leading to an outward mass transport through the char and reacting layer. The gaseous devolatilization products typically consist of CO, hydrocarbons (C_xH_y) and tar. The outward mass-flow may cool the hotter solid when the cooler mass flows from the inner particle. Pyrolysis reactions may be either endothermic or exothermic, and the latter may increase the intra-particle temperature locally and consequently conduct heat both inwards and outwards. In an oxidizing atmosphere, the devolatilization products may ignite in a flame front above the outer surface, enhancing the external heat transfer to the surface. This may accelerate the overall devolatilization process depending on particle size. The ultimate devolatilization products in an oxidizing atmosphere are CO_2 and H_2O. The devolatilization can be assumed to be finished when the centre of the fuel particle reaches the upper devolatilization temperature, T_{Vol2}.

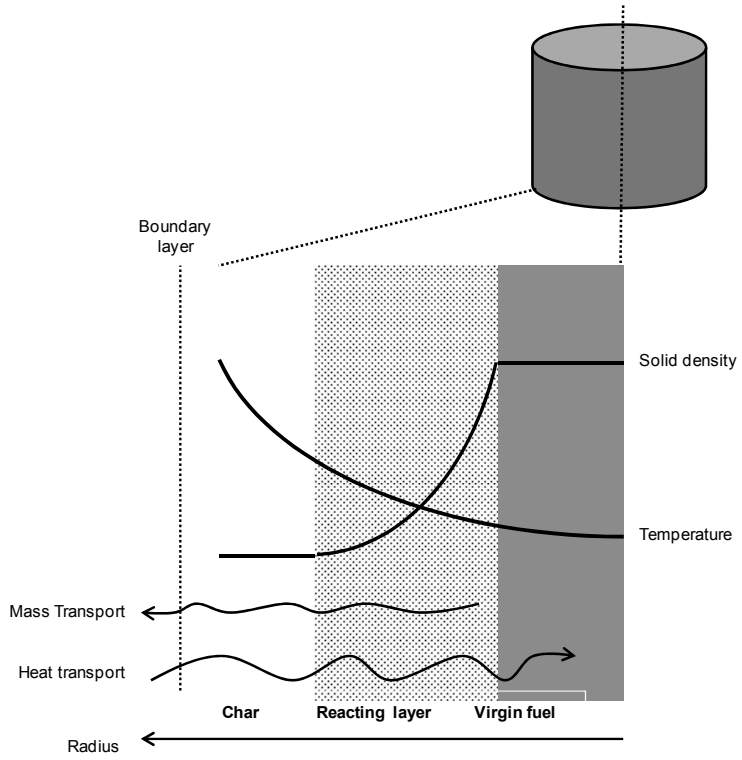

Figure 5-4: Radial cross section of partially devolatilized solid, cylindrical fuel particle (Larsen, 2007).

5.1.4 Char oxidation

After the devolatilization the remaining char is a product rich in carbon. Char oxidation may be assumed to start when the devolatilization is finished, because the flame formed during the combustion of the volatiles may effectively prevent oxygen transport to the surface of the char. During the char conversion, oxygen is transported from the surrounding gas to the solid fuel outer surface, and eventually also further into the particle matrix by pore diffusion. Oxygen is adsorbed to the surface of the solid matrix, where it reacts with solid carbon and desorbs as gaseous combustion products, CO and/or CO_2. The products are transported to the surface and further away through the boundary layer.

Large char particles often burn under diffusion limitations which means that the oxygen concentration near the char particles is not constant. Thus the mass transfer rate of oxygen to the char may become the dominant rate limiting parameter.

5.2 Literature study on devolatilization and char combustion kinetics of large particles

This section will provide an overview of devolatilization and char combustion of tire-derived fuels and wood described in the literature. The focus is on large fuel particles, being of most relevance in the material inlet end of cement rotary kilns.

5.2.1 Tire-derived fuels (TDF)

Devolatilization of large TDF particles have been studied by Bouvier et al. (1987), Yang et al. (1995), Schmidthals (2001), Giddings et al. (2002), Larsen et al. (2006), Chinyama and Lockwood (2007). In addition, several studies have been made with micro-TGA on small TDF samples to determine reaction kinetics and composition of oil, gas and char (Conesa et al. (1998), Leung et al. (1998) and Kyari et al. (2005)). Bouvier et al. (1987) studied the pyrolysis of cubic tire chips with sizes from 5 to 20 mm at temperatures from 433°C to 590°C and under inert conditions. The conversion times were approximately 100 s for a 5 mm cubic tire particle at 590°C, while it was around 400 s for a 20 mm cubic tire particle at 590°C. Yang et al. (1995) studied the pyrolysis time for a tire rubber cylinder with a diameter of 40 mm and a length of 60 mm under vacuum and at 510°C. The pyrolysis time was approximately 50 minutes. Schmidthals (2001) found that TDF particles in the sizes 10-20 mm x 50-70 mm pyrolysed within 10 minutes in air and within 20 minutes in nitrogen, both at 650°C. Giddings et al. (2002) made a visual study of tire chip devolatilization in a laboratory tube furnace at 900°C. The tire chips had dimensions from 12 mm to 152 mm and masses from 2 to 30 g, which are not particularly well-defined particle sizes. But the devolatilization time of a 7 g tire chip (no exact dimensions given) took approximately 120 s at 900°C. The devolatilization time was reported to depend on the tire chip thickness. Larsen et al. (2006) studied the devolatilization of cylindrical tire rubber particles with diameters from 7 to 22 mm and heights of 35 mm at temperatures up to 840°C in an inert atmosphere. The reported devolatilization times at 840°C were 75 to 300 s when increasing the particle diameter from 7.5 to 22 mm. Chinyama and Lockwood (2007) studied the devolatilization times of tire rubber particles with thicknesses in the range 6-12 mm and in the temperature interval from 700-1,000°C. The devolatilization times were found to be 30-100 seconds depending on thickness and temperature. These results reported in literature about devolatilization of large TDF particles show clear tendencies for devolatilization time to increase with increasing particle size and decrease with increasing temperature and/or oxygen concentration.

Previous work on tire char combustion has been made with few mg of tire char particles in the 100-500 µm size in TGA reactors and drop tube reactors (Atal and Levendis, 1995, Masi et al., 1997, Leung and Wang, 1998, Conesa et al., 1998, Larsen et al., 2007). Atal and Levendis (1995) studied the combustion of tire char with particle size of around 500 µm in air and at 1,200°C. The char conversion time was well below 1 s. Atal and Levendis also reported that tire char burned 2-4 times faster than bituminous coal char. Masi et al. (1997) found that a TDF char particle with a diameter of 100 µm reached full conversion after 6 s at 5 vol.-% O_2 and 850°C. According to Masi et al. (1997), a medium rank coal char would require 100 s to reach full conversion under the same conditions. Masi et al. (1997) also compared intrinsic TDF char reactivity with the intrinsic char reactivity of RDF and biomass (Robinia Pseudoacacia) and found that the TDF char was most reactive. Larsen et al. (2007) studied the combustion of tire char with particle size between 102 and 212 µm at 10 vol.-% O_2. The observed conversion times were from 9 s at 750°C to 4 s at 850°C. Larsen et al. (2007) concluded that the TDF chars were very reactive at temperatures of 850°C and higher. As a consequence, intra-particle kinetics was concluded to be less important because the

reaction would take place at the outer particle surface. In addition, the ash layer formed on the particle surface was observed to be very porous, and could easily be removed by slight mechanical interaction. In the rotary kiln, the rotational movement of the kiln is assumed to remove the ash layer rapidly, leaving an unconverted char particle.

5.2.2 Wood

Devolatilization of large wood particles has been studied by Winter et al. (1997), Di Blasi (2000), de Diego et al. (2002), Di Blasi and Branca (2003) and Jand and Foscolo (2005). Winter et al. (1997) measured temperature profiles in spherical 3-20 mm diameter beech wood particles at oxygen partial pressures from 0 to 21 kPa and temperatures from 700°C to 950°C. The experiments were made in a fluidized bed with silica sand as bed material. The devolatilization time of a 10 mm diameter beech wood particle at 800°C and oxygen partial pressure of 10 kPa was approximately 55 s. Di Blasi (2000) compared model predictions with measured values for beech wood particles in the particle sizes 0.2-2 mm under fast pyrolysis conditions in a fluidized bed reactor. Conversion times were reported to be 2-50 s at 527°C. Devolatilization of non-spherical pine wood particles with equivalent diameters, d_{eff}, in the range 10 to 45 mm and in the temperature interval 650 to 850°C has been investigated by de Diego et al. (2002). The reported devolatilization times for 10 to 30 mm diameter particles were for example from 30 s to 150 s at 850°C. The devolatilization was reported to be only slightly affected by a change in atmosphere from air to nitrogen. Di Blasi and Branca (2003) studied temperature profiles in cylindrical beech wood particles with lengths of 20 mm and diameters from 2 to 10 mm. The experimental set-up was a fluidized bed with sand as bed material and an inert atmosphere of nitrogen. Bed temperatures were from 439°C to 834°C. An empirical correlation was suggested for the devolatilization time, and the devolatilization time for a 10 mm diameter beech wood particle at 834°C was for example found to be approximately 40 s. Jand and Foscolo (2005) studied the pyrolysis of spherical beech wood particles with diameters from 5 to 20 mm and in the temperature interval 560-740°C, in a fluidized bed gasifier with sand as bed material. The devolatilization times at 740°C were from 40 s to 140 s, depending on the particle diameter.
The results reported in literature about devolatilization of large wood particles are as indicated above typically based on experiments in fluidized bed reactors with sand as bed material and at temperatures in the interval 400°C-1,000°C. The wood types are either beech wood or pine wood. The general tendencies are that devolatilization times will increase with increasing particle size and decrease with increasing temperatures. The effect of atmosphere seems to be of minor importance.

Most studies with wood char combustion are made with wood chars with particle sizes in the µm range. Examples from the literature are Janse et al. (1998), Senneca (2007) and Shen et al. (2009). These studies typically use TGA experiments to obtain information about char intrinsic kinetics. Jand and Foscolo (2005) studied the char combustion of large spherical beech wood char particles with diameters from 5 to 20 mm at 740°C and in air in a fluidized bed reactor. The char oxidation times were found to be approximately 150 s for a 5 mm diameter char particle and 500 s for a 20 mm diameter char particle. Mermoud et al. (2006) studied the steam gasification of large spherical beech wood particles with initial diameters of 10 to 30 mm in a macro-TG apparatus. The temperatures were 830-1,030°C and the steam partial pressures were 0.1-0.4 atm H_2O. The char conversion time was found to depend strongly on particle size, steam partial pressure and temperature. From this study it also appears that steam gasification of wood char is relatively slow compared to char oxidation in an oxidative atmosphere: For example, the conversion time for a 20 mm diameter particle at 930°C and 0.2 atm H_2O was 2,500 s whereas the char oxidation time for a

20 mm diameter particle at 740°C and 21 vol.-% O_2 was 500 s, according to Jand and Foscolo (2005). However, the results reported in literature do indicate that carbon conversion from fuel chars in rotary kilns may not only depend on oxygen concentration, temperature and particle size but also on H_2O concentration in the bulk gas.

5.3 Experimental

In order to study the combustion of solid fuel particles under conditions similar to those in the material inlet end of an industrial rotary kiln, a new experimental set-up has been designed and constructed. This section will describe the requirements to this experimental set-up as well as the practical considerations and assumptions that have been made.

5.3.1 Pre-experimental considerations

It is of interest to be able to investigate parameters such as rotational speed and bed fill degree. A systematic investigation of these parameters coupled with gas composition, gas velocity, temperature, characteristics of the fuels and raw materials may provide new knowledge. Two specific topics should be investigated with the experimental set-up:

1. Systematic investigation to predict sensitivity of sulfur chemistry towards solid alternative fuels: This is the subject of chapter 6.
2. Systematic investigation to predict combustion behavior for selected alternative fuels as a function of key process parameters.

The information gained through these systematic investigations may help to identify critical operational limitations regarding use of alternative fuels in the material inlet end, e.g. optimal fuel types and amounts, conversion times and extent of sulfur release from the raw materials.

The experimental set-up must be able to simulate the process conditions in the material inlet end of an industrial rotary kiln. The flue gas temperature in the material inlet end of cement rotary kilns is typically 1,000-1,200°C and the temperature of the fully or partly calcined raw materials from the bottom stage cyclone is typically 850-890°C. The solid fuels have not been heated prior to being fired into the rotary kiln. It is thus required to be able to feed solid fuel at ambient temperature into raw materials which have been preheated to 800-900°C. The raw materials must be continuously rotated in order to have the raw material bed in a predominantly rolling motion.
In an industrial rotary kiln, there is a constant heat transfer from the hot flue gas to the raw material bed and rotary kiln walls due to the temperature gradients. Temperature profiles at specific positions along the axial rotary kiln length can be maintained due to the continuous flow of gases and raw materials. In a pilot-scale experimental set-up made for batch experiments with addition of one batch of fuels to preheated raw materials, a stable temperature profile cannot be maintained if gas of one specific temperature passes a bed of raw materials of another temperature: The temperature gradient will gradually reduce until both gas and raw material bed reach the same temperature. If gas and bed temperatures change during the experiment, it becomes uncertain what the actual average temperature was during the experiment. In order to eliminate this uncertainty it was decided to make the experiments under conditions where gas and raw material bed had the same temperature. This approach also has the advantage that no heat transfer takes place between gas, walls and bed, if there are uniform temperatures at all positions. Thus it is possible to neglect

considerations about whether heat transfer should be by radiation and convection from the gas to the bed or by radiation and conduction from the walls to the bed.

5.3.2 Experimental set-up

After careful consideration it was decided to construct a high-temperature rotary drum based on a commercially available chamber furnace. The chamber furnace was supplied by Nabertherm and can reach a maximum operating temperature of 1,300°C. It is electrically heated by heating elements embedded in two side walls and the floor. The chamber furnace was modified by drilling holes in the rear wall and door for positioning of a steel drum, as seen in Figure 5-5. The steel drum is made of the steel type Sandvik MA253 which can be used for temperatures up to 1,150°C. The drum is supported by a steel tube on rollers which passes through the rear wall hole in the chamber furnace. This steel tube is connected to a motor by means of a roller chain, in order to rotate the drum. The part of the steel tube that is outside the chamber furnace is water cooled in order to protect the rollers, roller chain and gas seals against the high temperatures.

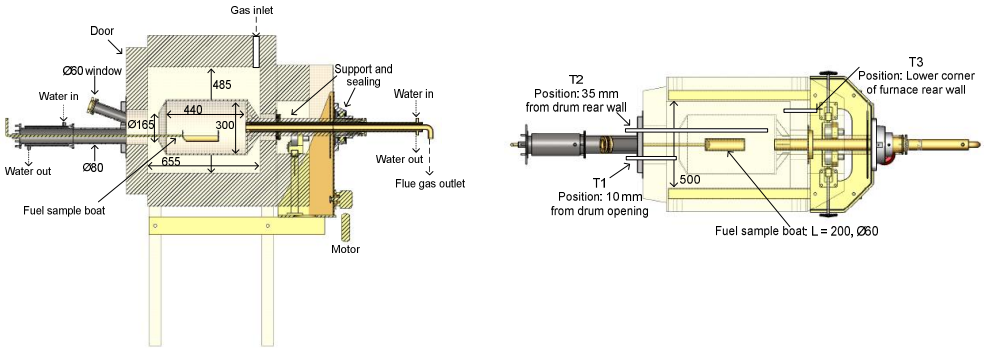

Figure 5-5: High-temperature rotary drum. Left: Side view. Right: Top view.

Gas can be transported to the chamber furnace through a hole in the roof. The furnace has been designed to achieve sufficient heating of reactant gas before entering the rotary drum, which was also verified by temperature measurements. The gas is transported into the rotating steel drum due to an externally placed gas pump that pumps the gas through the rotating drum and steel tube whereafter the gas exits the reactor for subsequent cooling and analysis.
The chamber furnace door is equipped with a window for visual inspection, two holes for thermocouples and a centrally placed water-cooled tube for solid fuel addition. The solid fuels are placed in a sample container which can be pushed into the hot rotary drum or pulled out to the water-cooled tube.
The experimental set-up is shown in Figure 5-6. The gas supply can be up to 500 NL/min of air and nitrogen. The gas is transported to the rotary drum reactor during the experiments, but may also be bypassed during calibration of flow controllers, leakage tests, etc.
The temperature is measured at three different locations in the rotary drum reactor: At the rear wall in the chamber furnace (T1), in the center of the rotary drum (T2) and at the door just in front of the rotary drum (T3). A pump transports the flue gas out of the rotary drum reactor. Before passing the pump, the flue gas is cooled in a heat exchanger and soot particles are captured in a filter. After having passed the pump, the flue gas is either sent directly to the stack, or to the gas analyzers for measurement of O_2, CO, CO_2, SO_2 and NO. The fraction of the flue gas that are transported to the

analyzers will pass another two filters, a gas cooler for condensation of water and a sample gas pump before reaching the gas analyzers.

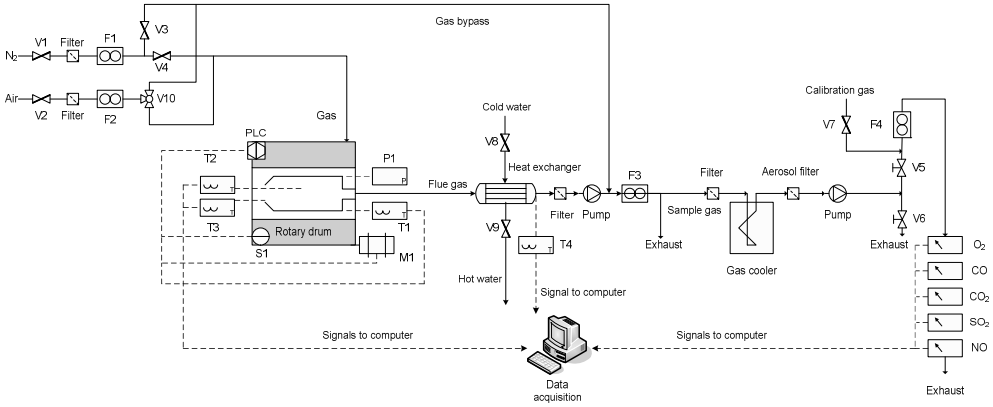

Figure 5-6: Sketch of the high-temperature rotary drum experimental set-up.

The key specifications for the experimental set-up are presented in Table 5-1. The maximum operating temperature should not exceed 1,000°C, because the drum steel strength decreases drastically at high temperatures. The volumetric raw material fill degree may be up to 17%. For practical reasons, however, the fill degree should be lower, because some of the raw materials will drop out of the rotary drum if the rotary drum is filled to the edge.

Parameter	Value
Operating temperature	≤ 1,000°C
Rotational speed	0-20 min^{-1}
Pressure	Atmospheric, ± 25 mbar
Gas flow	≤ 500 NL/min
Oxygen concentration	≤ 21% O_2
Load capacity	≤ 6 L
Fill degree	≤ 17%

Table 5-1: Key specifications for high-temperature drum experimental set-up.

The amount of solid fuels per experiment depends strongly of the type of fuel: The fuel amount increases as the volatile content in the fuel decreases. For a fuel consisting of pure volatiles, the fuel amount is limited to the order of 5 g per experiment due to the rapid devolatilization which increases the pressure in the experimental set-up and heavy soot deposition in the filters due to incomplete fuel oxidation in the furnace. The solid fuel volume can be increased as the content of volatiles decreases. For a fuel consisting of pure char, the fuel amount per experiment may be significantly higher, e.g. in the order of 50 g, since the fuel char oxidation is controlled by a relatively slow mass transfer of oxygen to the fuel particle.

5.3.3 Fuel samples

Proximate and ultimate analyses as well as lower heating values for the tested fuel samples are shown in Table 5-2. Tire rubber and pine wood are cut into cylindrical and rectangular shapes, respectively. The main focus has been on single particles of tire rubber and pine wood, but experiments have also been conducted with polypropylene and petcoke. Polypropylene and petcoke has been chosen as additional reference fuels due to their contents of volatiles and char representing limiting cases for solid fuels. The experiments with polypropylene and petcoke were *not* with single particles but instead with a batch of several small particles. The polypropylene was in the form of rectangular flakes with a thickness of 1 mm. The petcoke particles were approximately spherical with average diameters ≈ 1 mm.

	Proximate analysis			**Ultimate analysis**				**LHV**
	VM	FC	Ash	C	H	N	S	MJ/kg
Tire rubber	64.6	32.6	2.8	87.4	7.1	0.3	1.2	36.9
Pine wood	75.3	24.5	0.2	38.9	5.2	0.1	-	16.2
Polypropylene	97.5	0.0	2.5	83.0	14.0	0.0	-	44.5
Petcoke	13.4	85.1	1.5	87.3	3.7	1.5	4.7	34.0

Table 5-2: Fuel analyses and lower heating values (LHV) for solid fuels used in the experiments. Units are in wt.-% as received and MJ/kg.

5.3.4 Experimental method

Raw materials are placed in the drum to obtain the desired volumetric fill degree. The reactor door is closed, and the reactor is heated to the desired temperature. The drum always rotates when the reactor is heated, and keeps the raw materials in a rolling motion, with an angle of repose of approximately 30-40°. It is the thermocouple T2 in the center of the rotary drum that is used to determine the temperature prior to and during the experiments. The fuel sample is placed in the sample boat, and the sample boat is then positioned in the water-cooled tube. The water-cooled tube is closed in the end, in order to obtain a controlled atmosphere inside the rotary drum reactor. The gas to the reactor is adjusted to the desired flow and oxygen concentration. The temperature at T2 and oxygen concentration at the O_2 analyzer is monitored. When a stable temperature and oxygen concentration are reached, the fuel sample boat is pushed into the rotary drum, turned 180° and pulled out in the water-cooled tube again. The fuel sample will thus drop into the preheated raw materials and immediately be heated, followed by devolatilization and char oxidation. Temperatures and flue gas compositions are continuously logged during the experiments with 1 s intervals.

An example from a typical experiment with combustion of one tire rubber cylinder is shown in Figure 5-7. The oxygen concentration is observed to decrease from 10 towards 7 vol.-% when the devolatilization starts. At the same time, the CO concentration increases from 0 ppm to approximately 450 ppm, and the CO_2 concentration increases from 0 to 2.5 vol.-% during devolatilization. The char oxidation is assumed to be finished when the CO_2-concentration becomes lower than 0.04 vol.-%. This assumption is in good agreement with the visual observations during the experiment where red-glowing char particles can be observed in the bed until the CO_2-concentration reaches values below around 0.04 vol.-% CO_2.

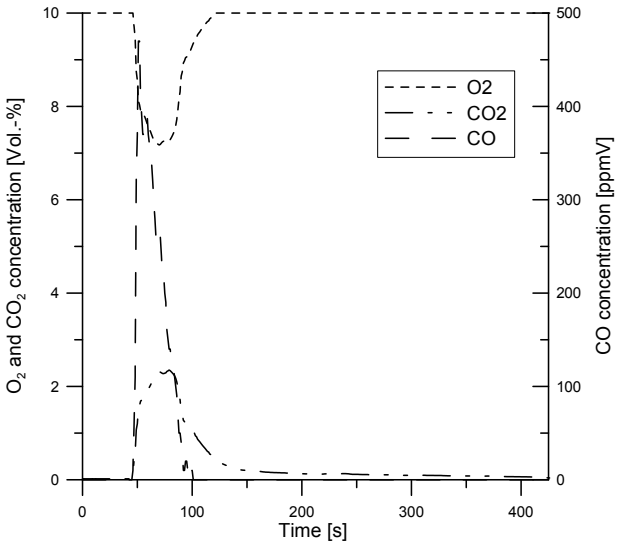

Figure 5-7: Example of experiment with combustion of a tire rubber cylinder. 900ºC and 10 vol.-% O_2. 5% volumetric fill, coarse sand, 6 rpm, 100 NL/min. Particle dimensions: D = 9 mm and L = 25 mm.

The degree of fuel conversion against time is derived, assuming that the fuel conversion is proportional to the carbon conversion, by integration of the concentration profiles of CO_2 and CO:

$$X(t) = \frac{\int_0^t y_{CO} + y_{CO_2} dt}{\int_0^\infty y_{CO} + y_{CO_2} dt} \qquad (5.2)$$

5.3.5 Repeatability and uncertainties

The repeatability of the experiments is generally found to be acceptable. Nearly all experiments were repeated at least three times to ensure the repeatability. However, individual experiments have only been made once or twice if they were not part of the initial plan for experiments. The filters in the experimental set-up have been cleaned regularly in order to avoid increases in pressure drop over the system, which were observed to affect the repeatability of individual experiments. Carbon mass balances were also performed regularly to test if all released carbon could be detected as CO or CO_2.

A sensitivity analysis was conducted to estimate the uncertainty on the degree of fuel conversion, see Appendix A. The sensitivity analysis indicates an overall relative uncertainty on the estimated degree of fuel conversion in the order of ± 6%.

5.4 Results and discussion

In this section, the experimental results are presented and analyzed. The main focus with the analysis is to identify the main rate limiting parameters for the devolatilization as well as char oxidation.

5.4.1 General observations

During the experiments it was possible to monitor the devolatilization and char oxidation process visually through the window. This gave a good impression of the main reaction pathways for the different fuels. For all the fuels, a flame front surrounding the fuel particles was observed almost immediately after insertion into the rotary drum, indicating the start of the devolatilization process. This is shown in Figure 5-8, left, which shows a tire rubber particle shortly after insertion into the rotary drum.

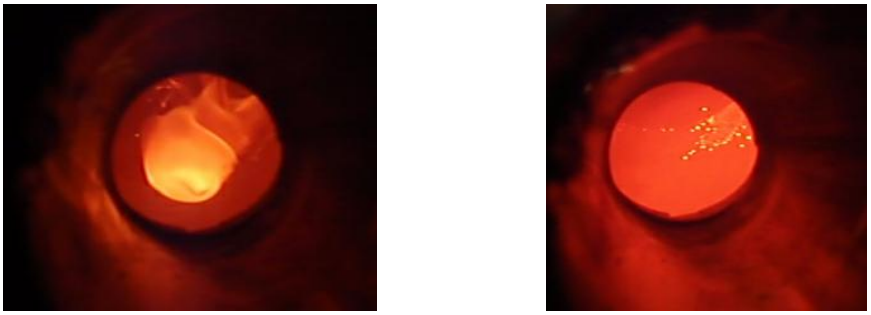

Figure 5-8: Left: Tire rubber particle during devolatilization. Right: Tire rubber char fragments during char oxidation.

The tire rubber particles were observed to predominantly keep the particle shape under the devolatilization but with some degree of fragmentation. After the devolatilization, the tire char fragmented into several smaller char particles, as shown in Figure 5-8, right. This observation indicates that a model for tire char oxidation should not be based on initial fuel particle size; it may be based on the initial fuel mass and fixed carbon content instead. In this way, uncertainties about actual particle sizes during the char combustion are avoided.

The pine wood and petcoke particles kept their shape during the devolatilization process and, to a large extent, also during the char oxidation process. This observation indicates that an unreacted shrinking core model could be suitable to describe the pine wood char and petcoke char oxidations, see the conversion pathways in Figure 5-3.

The polypropylene plastic particles melted and behaved like a boiling liquid during the devolatilization process.

Most of the experiments have been made with coarse sand as the raw material. This raw material was chosen because 1) it is largely inert and 2) gives the desired rolling motion of the bed. It was attempted to use real cement raw material, but without success due to the sticky nature of the raw material which partly resulted in a thick coating layer on the inner drum wall and partly in clinker nodulization.

5.4.2 Effect of fuel sample mass

The effect of fuel sample mass has been investigated with tire rubber, pine wood and petcoke. Figure 5-9 left shows the conversion time versus mass for tire rubber cylinders with dimensions D = 9 mm and L = 25 mm and roughly spherical tire rubber granulate particles with D = 2 mm. The masses are in the interval 1.8 g to 15 g and the results shown are made at 900°C, 10 vol.-% O_2 and in an empty rotary drum. It is observed that the conversion time increases linearly with mass for the tire cylinders as well as for the tire granulate. It is furthermore observed that there are no particular differences in conversion time for the tire cylinders and tire granulates when the mass is the same. Thus the initial fuel particle size of the tire rubber does not have any particular effect on the conversion time. This result is in good correspondence with the visual observation that the tire rubber rapidly cracks into several small fragments after the devolatilization so conversion time will be a function of overall tire rubber mass rather than tire rubber particle size.
The results are quite different with pine wood and petcoke where the conversion time was observed to be a function of both particle size and sample mass, indicating that these fuels follow another conversion pathway than tire rubber, as illustrated in Figure 5-3.

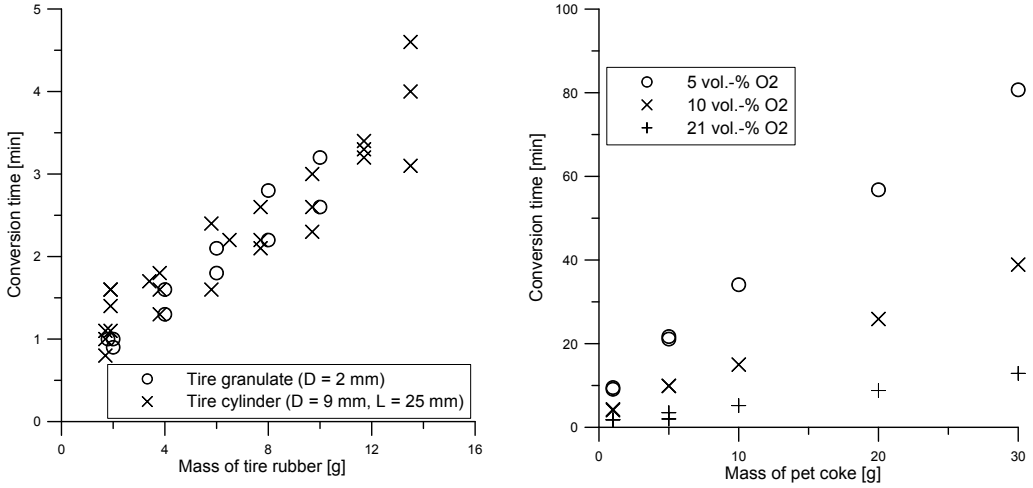

Figure 5-9: Left: Conversion time versus mass for tire rubber granulate and cylinders. 10 vol.-% O_2. Right: Conversion time versus mass for petcoke at different oxygen concentrations. Petcoke particle size = 2-4 mm. Empty rotary drum, 900°C, 6 rpm, 100 NL/min. Conversion times evaluated at 80% carbon conversion.

Figure 5-9 right shows the conversion time for petcoke particles in the size interval 2-4 mm, and at masses from 1 g to 30 g. The conversion time is observed to increase linearly with sample mass and is observed to be significantly longer than for tire rubber. It is also observed that the conversion time is roughly halved when the oxygen concentration increases from 5 vol.-% to 10 vol.-% and from 10 vol.-% to 21 vol.-%. This illustrates the strong dependency of the bulk oxidizer concentration for petcoke which predominantly consists of char. The effect of oxygen concentration for pine wood and tire rubber will be shown in section 5.4.6.

It should be noted that some of the experimental data for tire rubber and petcoke combustion shown in Figure 5-9 has been obtained by project students Yu Jiang and Dawid Jan Bialas, respectively.

5.4.3 Effect of fuel particle size and shape

The effect of fuel particle size has been studied with cylindrical tire rubber particles and rectangular wood particles. The rectangular wood particles are also used to study the effect of fuel particle shape. Figure 5-10 left shows the conversion curves for three tire rubber cylinders of different diameters (and different masses) at 900°C and 10 vol.-% oxygen. The overall conversion time is observed to increase when the particle diameter (and mass) increases. It should be noted that the devolatilization time also increases when the particle diameter increases. However, based on the study of fuel sample mass shown in Figure 5-9 it must be concluded that the increase in overall tire rubber conversion time is due to the increase in mass rather than the increase in particle diameter, since the tire char rapidly fragment into several smaller char particles.

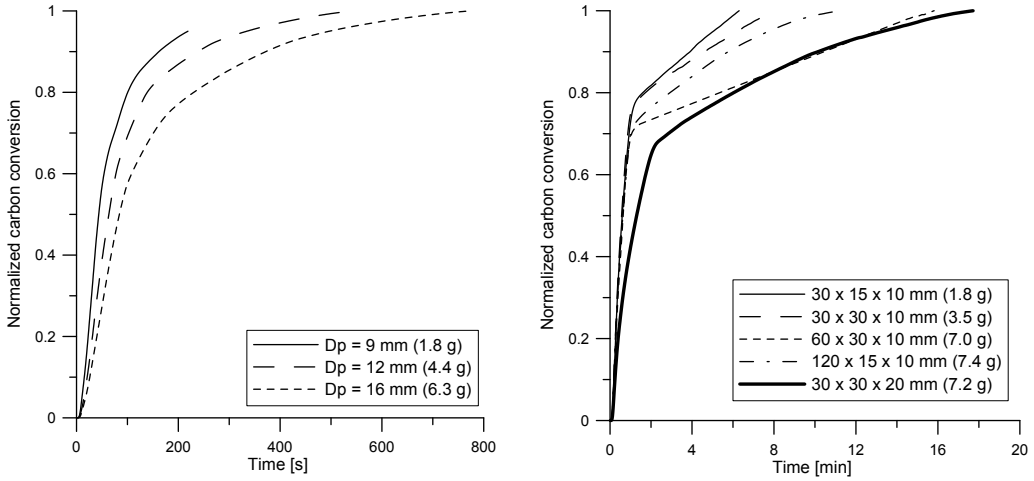

Figure 5-10: Left: Carbon conversion for three different tire rubber cylinders. $L_{Cylinder}$ = 25 mm. Right: Carbon conversion for pine wood particles of different sizes. T = 900°C, 5% fill, coarse sand, 10 vol.-% O_2, 6 rpm, 100 NL/min.

Figure 5-10 right shows the carbon conversion versus time for five pine wood particles with different masses, sizes and shapes. Four of the particles have a thickness of 10 mm while the fifth particle has a thickness of 20 mm. It is observed that the devolatilization time is approximately 1 minute for the four 10 mm thick particles whereas the devolatilization time is around 2 minutes for the 20 mm particle – the exact devolatilization times are shown in the model analysis, section 5.5.2. The char oxidation times are generally observed to increase when the mass of char increases, but it is also observed that the shape influences the char oxidation time. Three of the particles have approximately the same mass of 7 g, but different char oxidation times: The longest of the 10 mm thick particles, with dimensions 120 x 15 x 10 mm, is fully combusted after approximately 11 minutes while the shorter, more compact particles with dimensions 60 x 30 x 10 mm and 30 x 30 x 20 requires approximately 16 and 18 minutes for full conversion, respectively. Regarding particles with similar mass but different shapes, the reason for the difference in conversion times may be explained by the external surface area of the particles, which is largest for the particle that reaches full conversion first.

Overall, the results indicate that particle thickness and external surface area have an effect on both the devolatilization time and the char combustion time.

5.4.4 Effect of raw material particle size

Four different raw material types have been tested, see Table 5-3. The first raw material type was authentic "raw meal" from a cement plant. However, this raw material could not be used for the experiments because of its sticky characteristics during heating: The raw meal adhered to a high degree to the rotary drum inner walls and formed nodules during the experiments. In addition, the raw meal did not roll in the drum but was instead in a slumping motion, see Figure 4-1.
The fine sand did only to a small degree adhere to the inner rotary drum walls, but it was also predominantly in a slumping motion rather than in the desired rolling motion.
The medium and coarse sand did not adhere to the rotary drum inner walls and were in the desired rolling motion, making these two raw material types suitable for the experiments.

Raw material type	Particle size distribution	Average particle size (d50%)
Raw meal	2-140 μm	18 μm
Fine sand	2-140 μm	31 μm
Medium sand	90-500 μm	250 μm
Coarse sand	400-800 μm	600 μm

Table 5-3: Raw materials tested in the experiments.

Figure 5-11 shows the conversion versus time as a function of the raw material type for one pine wood particle with dimensions 60 x 30 x 10 mm and 10 g of small petcoke particles with average diameters of 1 mm. It is observed that the time for pine wood devolatilization is identical regardless of the raw material. The char oxidation time for the medium sand and the coarse sand are practically the same, approximately 17 minutes for pine wood and 40 minutes for petcoke. But the time for char oxidation is significantly longer for the fine sand than for the medium and coarse sand, approximately 35 minutes for pine wood and 100 minutes for petcoke. The reason is believed to be that the fine sand follows a slumping bed motion whereas the medium and coarse sand follows a rolling bed motion. In the slumping motion, mixing is less efficient than in the rolling motion, which means that covered fuel particles will be in poor contact with oxygen from the freeboard gas. Another reason may be that diffusion of oxygen through the bed to the fuel particle is slower when the bed material is fine sand relative to coarse sand.
The results for tire rubber conversion are not shown, but the tendency was the same: The conversion time were significantly longer with the fine sand as bed material relative to tire conversion times in the medium and coarse sand.

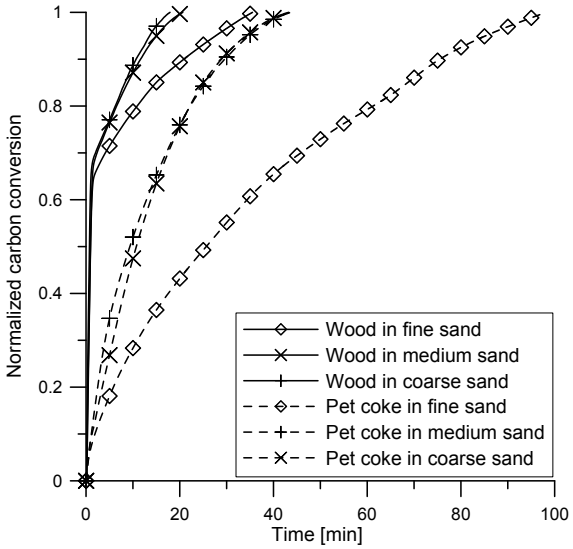

Figure 5-11: Carbon conversion for pine wood and 10 g petcoke particles in different raw materials. Wood particle dimensions: 60 x 30 x 10 mm. Petcoke average particle diameter: 1 mm T = 900°C, 5% fill, 10% O_2, 6 rpm, 100 NL/min.

5.4.5 Effect of raw material bed fill degree

The effect of the raw material bed fill degree on the conversion time has been investigated for tire rubber, wood, petcoke and polypropylene. Figure 5-12 left shows the conversion time for cylindrical tire rubber particles at volumetric fill degrees of 0% (empty rotary drum), 5% and 10% at 900°C and 10 vol.-% oxygen. The overall carbon conversion times are observed to be highly influenced by the fill degree: In an empty rotary drum, the conversion time is around 100 s while it is around 200 s at 5% fill degree. For the highest fill degree of 10%, the conversion time is 600 s, significantly longer than for the other two cases. It is also interesting to note that the shape of the curves are quite different, indicating that the fraction of volatile carbon and char carbon are different depending on the drum fill degree. The reason may be differences in the heating mechanism, depending on whether the tire cylinder is buried in the bed or only exposed to the wall and freeboard gas. It has previously been reported that the heating rate of tire rubber has a significant effect on the volatile/char ratio (Leung and Wang, 1998).

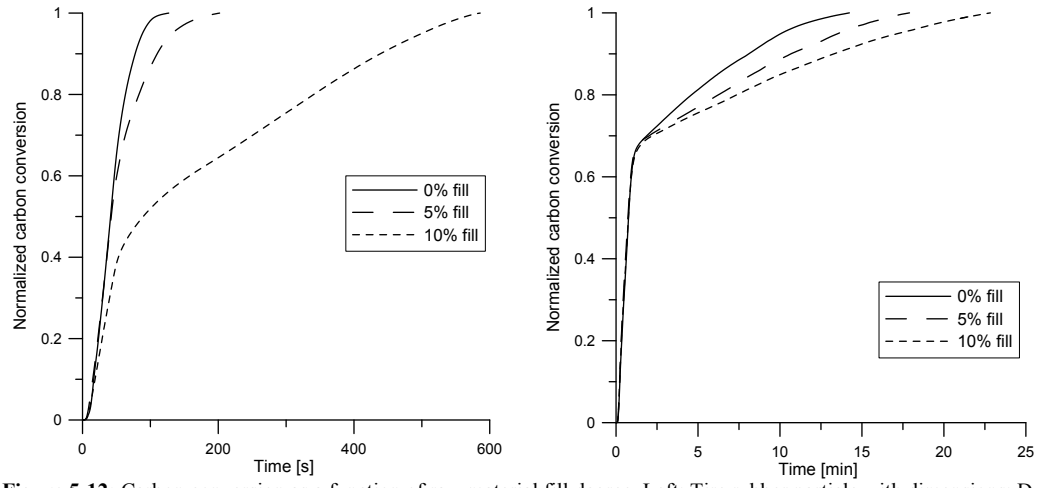

Figure 5-12: Carbon conversion as a function of raw material fill degree. Left: Tire rubber particle with dimensions: D = 9 mm, L = 25 mm. Right: Pine wood particle with dimensions: 60x30x10 mm. Coarse sand. T = 900°C, 10% O_2, 6 rpm, 100 NL/min.

Figure 5-12 right shows the conversion time for a pine wood particle at fill degrees of 0% (empty rotary drum), 5% and 10%. The devolatilization time is observed to be identical for the three cases while the char oxidation time increases with increasing fill degree. Thus the raw material fill degree is of importance for the char oxidation time, which is likely to be due to diffusion limitations of oxygen to the char particle when fully or partly covered with raw materials.

Similar experiments conducted with 2-4 mm petcoke particles, containing almost exclusively char, showed a tendency for increasing conversion time when the bed fill degree increased from 0% to 5%. However, it was observed that the petcoke conversion time only changed slightly when the fill degree increased from 5% to 10%. This observation was seen regardless of the oxygen concentration. Experiments with polypropylene, containing exclusively volatiles, showed no or little difference in conversion time when the bed fill degree increased. Thus the overall tendencies regarding the raw material fill degree indicate that the effect on conversion time strongly depends on the fuel type. The reason why devolatilization rate is independent of fill degree may be due to the fact that the fuel is swiftly buried in raw material, see chapter 4, and that the heat transfer rate therefore is independent of fill degree.

5.4.6 Effect of oxygen concentration

The effect of the oxygen concentration on the conversion time for the fuels tire rubber, wood and petcoke has been investigated in the interval 5 vol.-% to 21 vol.-%.
Figure 5-13 left shows the conversion time for cylindrical tire rubber particles as a function of the oxygen concentration. It is seen that the conversion time increases when the oxygen concentration decreases. The increase is approximately linear with conversion times of 140, 170, 200 and 380 s at 21, 15, 10 and 5 vol.-% O_2.

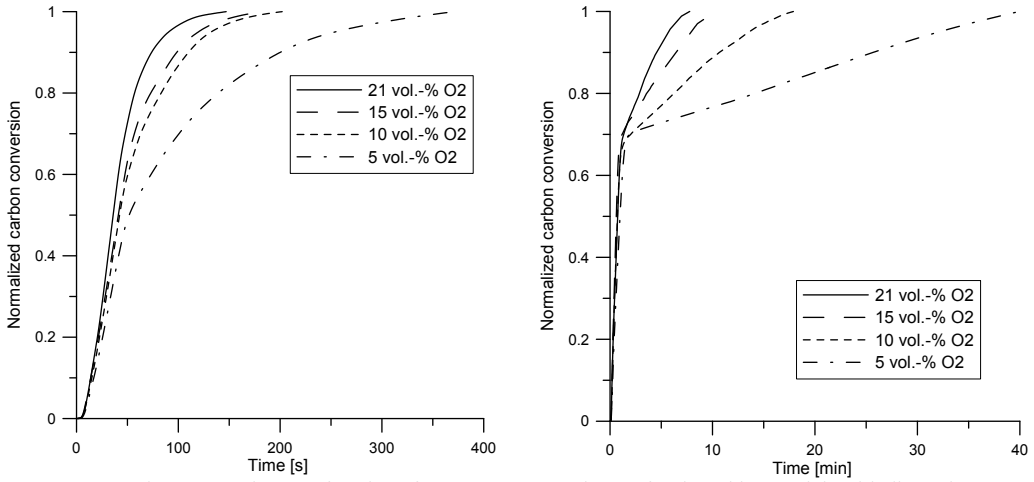

Figure 5-13: Carbon conversion as a function of oxygen concentration. Left: Tire rubber particle with dimensions: D = 9 mm, L = 25 mm. Right: Pine wood particle with dimensions: 60x30x10 mm. Coarse sand, 5% fill. T = 900°C, 6 rpm, 100 NL/min.

Figure 5-13 right shows the conversion time for pine wood particles as a function of the oxygen concentration. It is observed that the oxygen concentration has practically no effect on the devolatilization time, but a significant effect on the char oxidation time. Full conversion is reached in less than 10 minutes at the highest oxygen concentrations of 21% and 15% O_2, respectively. At 10% O_2 the conversion time is 18 minutes and at 5% O_2 is the conversion time 40 minutes. Thus the oxygen concentration clearly has a significant effect on the conversion time of pine wood char, and the conversion time increases approximately linear as the oxygen concentration decreases.

The effect of oxygen concentration was also studied for petcoke, where a linear relationship between conversion time and oxygen concentration was also found, as is the case with pine wood and tire char.
Overall, it can be concluded that the oxygen concentration is an important parameter for the conversion time of the char because the char oxidation is dependent on oxygen diffusion to the char.

5.4.7 Effect of rotational speed

The effect of drum rotational speed on the conversion time has been studied for tire rubber, wood and petcoke. Figure 5-14 left shows the conversion time for cylindrical tire rubber particles as a function of rotational speed in a bed with 5% fill degree at 900°C and 10 vol.-% O_2. It is observed that the conversion time increases when the rotational speed decreases. The conversion time is e.g. 100 s at 20 rpm and 200 s at 6 rpm, a factor 2 in difference. The conversion time increases dramatically to 440 s at the lowest rotational speed of 3 rpm. The reason is likely to be a change in bed behavior, which could also be observed visually: The bed motion is slumping at 3 rpm while it is rolling at 6 rpm and higher rotational speeds. The difference between slumping and rolling bed motions was illustrated in Figure 4-1. This difference in bed motion affects the mixing process and thus the conversion time of the fuel particles. It is also possible that the fuel particle break-down is more significant at higher rotational speeds due to stronger forces acting on the fuel particles.

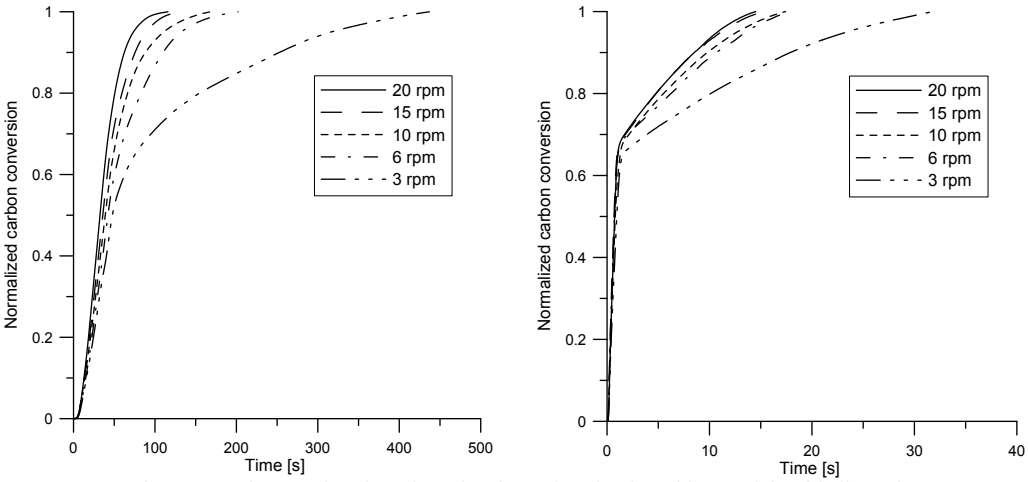

Figure 5-14: Carbon conversion as a function of rotational speed. Left: Tire rubber particle with dimensions: D = 9 mm, L = 25 mm. Right: Pine wood particle with dimensions: 60x30x10 mm. Coarse sand, 5% fill. T = 900°C, 10% O_2, 100 NL/min.

Figure 5-14 right shows the conversion time for pine wood particles as a function of rotational speed in a bed with 5% fill degree at 900°C and 10 vol.-% O_2. It is observed that there is no difference for the devolatilization time. For the char oxidation, the conversion time increases slightly when the rotational speed is decreased in the interval 20 rpm to 6 rpm. But when the rotational speed is lowered to 3 rpm, then the conversion time is increased significantly (33 minutes relative to 17 minutes at 6 rpm). This large effect at the lowest rotational speed is due to a change in bed behavior, from rolling to slumping.

Experiments with petcoke in the interval 3 rpm to 20 rpm also showed that the conversion time increases as the rotational speed decreases. This tendency is observed for all tested rotational speeds with differences in conversion times of up to 2 minutes between one rotational speed and the next tested rotational speed.
Overall the results indicate that the rotational speed has an effect on the conversion time, particularly if there is a shift in the dominant bed motion when going from one to another rotational speed.

5.4.8 Effect of temperature

The effect of temperature on the conversion time has been investigated for the fuels tire rubber and pine wood for the temperatures 700°C, 800°C, 900°C and 1,000°C.

Figure 5-15 left shows the conversion time of tire rubber as a function of temperature. It is observed that both the devolatilization time and the char oxidation time decreases when the temperature increases. The conversion time at 1,000°C is observed to be around 160 s, while it is 490 s at 700°C.

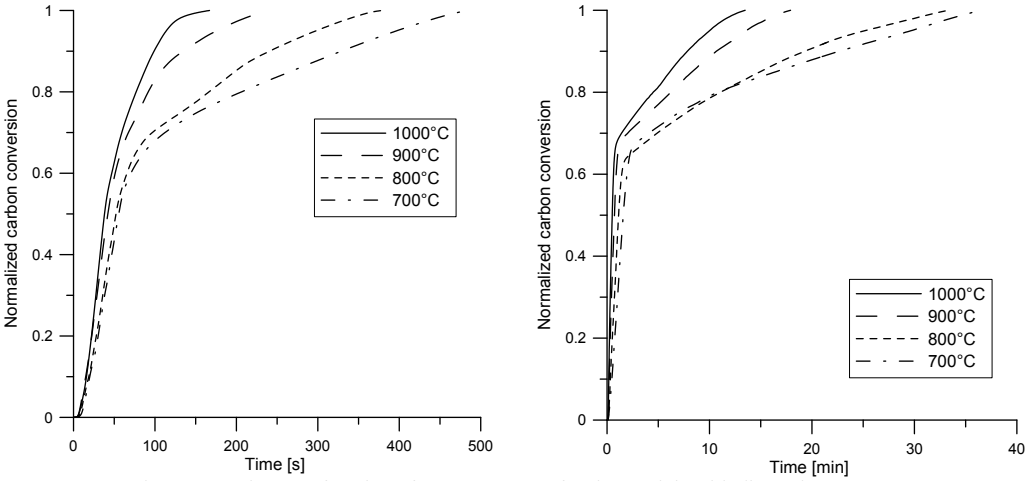

Figure 5-15: Carbon conversion as a function of temperature. Left: Tire particle with dimensions: D = 9 mm, L = 25 mm. Right: Pine wood particle with dimensions: 60x30x10 mm. Coarse sand, 5% fill. 6 rpm, 10% O_2, 100 NL/min.

Figure 5-15 right shows the conversion time for pine wood particles as a function of temperature in the temperature interval 700°C to 1,000°C. Both the devolatilization time and the char oxidation time increases when the temperature decreases. However, the time difference for the char oxidation at 700°C and 800°C is quite small, 0 to 1 minute, whereas the time is significantly shorter at 900°C and 1,000°C.

The effect of temperature on the conversion time of polypropylene flakes has also been studied. The result was that the conversion time decreased as the temperature increased, similarly as for tire rubber and pine wood.

5.4.9 Conclusions for experimental parameter study

A parameter study has been conducted for four selected fuels; tire rubber, polypropylene, petcoke and pine wood.

Fuel particle size and shape were investigated for tire rubber and pine wood. The result was that the fuel particle thickness and external surface area is important for the conversion time, both in terms of devolatilization and char oxidation.

For polypropylene (and the devolatilization part of the other fuels) temperature is the rate determining parameter.

For the char oxidation part of tire rubber, wood and petcoke, the parameters char mass, oxygen concentration, temperature, raw material fill degree and raw material characteristics are all important parameters, but the rotational speed was also observed to have an effect on the conversion time.

5.5 Model analyses

This section seeks to develop and verify mathematical models for devolatilization and char oxidation of selected alternative fuels. The models are to be used under conditions similar to those in the material inlet end of cement rotary kilns and may be modified to predict fuel conversion times in cement rotary kilns. This industrial modelling will be described in greater detail in chapter 7.

5.5.1 Model for devolatilization

The heat up of a large, spherical particle may be derived by solving the unsteady heat transfer differential equation:

$$\frac{\partial T_p}{\partial t} = \frac{1}{r^2}\frac{\partial}{\partial r}\left(r^2 \frac{k_p}{\rho_p C_p}\frac{\partial T_p}{\partial r} \right) \qquad (5.3)$$

with the following boundary and initial conditions:

$$k_p \frac{\partial T_p}{\partial r} = Y h_{Cond}\left(T_b - T_p\right) + \left(1-Y\right)\left(h_{Conv}\left(T_g - T_p\right) + \sigma\varepsilon_p\left(\varepsilon_g T_g^4 - \alpha_g T_p^4\right) + \sigma\varepsilon_p\left(\varepsilon_w T_w^4 - \alpha_w T_p^4\right)\right) \quad \text{for r = R} \qquad (5.4)$$

$$\frac{\partial T_p}{\partial r} = 0 \quad \text{for r = 0} \qquad (5.5)$$

where R is the initial radius of the particle, k_p is the thermal conductivity of the particle, ρ_p is the virgin fuel density and C_p is the specific solid heat capacity. h_{Cond} and h_{conv} are the heat transfer coefficients for conduction and convection, respectively. T_p, T_b, T_g and T_w are temperatures of particle, bed, bulk gas and inner kiln walls, respectively. Y is the dimensionless distribution of fuels in the bed, as illustrated in Figure 5-2. Linjewile et al. (1993) studied the heat transfer to large 6-10 mm diameter petcoke particles from a fluidized bed of sand of particle sizes ≤ 1 mm. The conductive heat transfer coefficients were in the range of 200-500 W/m^{2}K. Convective heat transfer under different kiln operating parameters in pilot plant scale has been studied by Tscheng and Watkinson (1979). Based on their experimental results with sand and limestone, correlations have been proposed for convective heat transfer coefficients, h_{Conv}.

Equation (5.4) expresses that all heat transferred to the surface of the particle is conducted into the particle, and equation (5.5) expresses that the gradient at the particle center is zero due to symmetry. In equation (5.4) it should be realized that the existence of a flame front around the fuel particle may increase T_g and T_p locally. Wildegger-Gaissmaier et al. (1990) have suggested a correlation for the temperature increase due to a flame front during volatile combustion around large coal particles. However, when implementing this correlation in the devolatilization model in the present study, significantly faster devolatilization times were found, which corresponded poorly with the experimentally found devolatilization times. The correlation for the flame front is therefore not included in equation (5.4).

Equation (5.3) must be solved numerically. However, an analytical solution has been suggested by Agarwal et al. (1986):

$$\frac{T_a - T_p}{T_a - T_{p,0}} = 2\sum_{i=1}^{\infty} \frac{\sin\beta_i - \beta_i \cos\beta_i}{\beta_i - \sin\beta_i \cos\beta_i} \left[\frac{\sin\left[\beta_i \frac{r_p}{r_{p,0}}\right]}{\left[\beta_i \frac{r_p}{r_{p,0}}\right]} \right] e^{-\left(\beta_i^2 \alpha t / r_{p,0}^2\right)} \qquad (5.6)$$

where T_a is the mean average temperature surrounding the particle. T_a may be estimated as $T_a = Y \cdot T_b + (1\text{-}Y) \cdot T_g$. α is the thermal diffusivity, $\alpha = k_p/(\rho_p C_p)$.

The β_i's are the positive solutions to the equation:

$$\beta \cdot \cos\beta = (1\text{-}Bi) \cdot \sin\beta \qquad (5.7)$$

where Bi is the Biot number. An efficient heat transfer coefficient, h_{eff}, is used to calculate Bi, where $h_{eff} = Y \cdot h_{Cond} + (1\text{-}Y) \cdot (h_{Conv} + h_{rad})$, and $h_{rad} = \varepsilon_g \sigma \cdot (T_g^2 + T_p^2) \cdot (T_g + T_p)$ (Szekely et al., 1976).

The time, τ_{devol}, required for complete devolatilization corresponds to the time needed for the fuel particle centre to reach the upper devolatilization temperature, T_{Vol2}, as described in section 5.1.3. This time is determined from equation (5.6) by using $T_p(0, t) = T_{Vol2}$ (Agarwal et al., 1984). However, equation (5.6) should only be used to determine the devolatilization time for an initially dry particle, since the equation does not take the particle moisture content into consideration. The moisture content of a fuel particle may influence the devolatilization time considerably (Agarwal et al., 1984 and 1986, and de Diego et al., 2002). Agarwal et al. (1984) studied the drying of wet coals during fluidized bed combustion and proposed a correlation for the total drying time:

$$\tau_{Drying} = \frac{0.14}{\alpha_{eff}} \left[C_0 \left(\frac{Bi + 4}{Bi} \right)^{1.1} \left(\frac{\lambda}{C_P (T_b - T_e)} \right)^{1.09} \right] r_p^2 \qquad (5.8)$$

where α_{eff} is the effective thermal diffusitivity, C_0 is the moisture content, C_p is the fuel heat capacity, λ is the latent heat of vaporization, r_p is the particle radius, T_b and T_e are the bed temperature and temperature at the wet/dry interface, respectively. This correlation fitted the drying time within ±15% for $0.3 \leq C_0 \leq 1.8$ g water/g dry fuel, $1 \leq Bi \leq 20$, $400 \leq T_b \leq 1400$ K.

If drying and devolatilization is considered to be sequential processes, then equations (5.8) and (5.6) may be used to calculate the drying time and the devolatilization time. This approach is suitable for low Biot numbers because the tendency of the particle to be isothermal is greater. But for higher Biot numbers, the devolatilization may start before the drying is completed, and a combined approach is thus required (Agarwal et al., 1986). Several analytical and numerical procedures have been suggested in the literature, as summarized by Agarwal et al. (1986) and de Diego et al. (2002). de Diego et al. (2002) studied devolatilization of wet pine wood particles and found a useful correlation, based on a modified power-law relationship, which included both moisture content, temperature and particle size:

$$\tau_{devol} = a_0(T)\left(d_{sph}\theta\right)^{1.6\pm0.1}\left(1+1.7\cdot y_{H_2O}\right) \qquad (5.9)$$

where d_{sph} is the equivalent spherical diameter of the fuel particle in mm and θ is the sphericity of the fuel particle, see section 5.5.2 for definitions of d_{sph} and θ. y_{H2O} is the weight fraction of water in the fuel particle. a_0 is a temperature dependent constant which was found to decrease approximately linearly with temperature: a_0 = 1.89, 1.38, 1.03 and 0.89 at 650°C, 750°C, 850°C and 950°C, respectively. This correlation gave excellent fits with experimentally found devolatilization times for cubic and rectangular pine wood particles of thicknesses from 4 to 15 mm. The moisture content was up to 50 wt.-%.

5.5.2 Validation of devolatilization model

In section 5.5.1 an analytical expression for the heating of large fuel particles was given, see equation (5.6). If the temperature required for complete devolatilization, T_{Vol2}, is known, e.g. from TGA-measurements reported in literature, the analytical expression may be used to determine the time required for full devolatilization. Table 5-4 shows the temperatures for initial and final devolatilization temperatures for the fuels tire rubber and pine wood.

Fuel	T_{Vol1} [K]	T_{Vol2} [K]	Reference
Tire rubber	523	773	Chinyama et al. (2007)
Pine wood	473	773	Kim et al. (2010)

Table 5-4: Temperatures for initial and final devolatilization of tire rubber and pine wood.

Experiments with non-spherical tire rubber and pine wood particles of different size and shapes have been conducted to study the devolatilization time. Since the model assumes that the fuel particles are spherical, it is necessary to represent the non-spherical fuel particles as spherical particles of diameter, d_{eff}, characterized by the non-spherical and spherical particles having the same total surface area (Kunii and Levenspiel, 1991):

$$d_{eff} = \theta \cdot d_{sph} \qquad (5.10)$$

where d_{sph} is the equivalent spherical diameter, defined as the diameter of a sphere with the same volume as the particle. θ is the sphericity defined as:

$$\theta = \left(\frac{\text{Surface of sphere}}{\text{Surface of particle}}\right)_{\text{of same volume}} \qquad (5.11)$$

The experimentally found devolatilization times are determined by means of the normalized carbon conversion curves for the fuels. Figure 5-16 shows an example with pine wood, where the devolatilization time is observed to begin at time 0 s and end at time 80 s. The devolatilization ends when the slope of the conversion curve is observed to decrease significantly, indicating the start of the slower char oxidation. It is relatively straight-forward to determine devolatilization times for pine wood but more complex for tire rubber: Tire rubber shows no clear end point for devolatilization, see e.g. Figure 5-10 left. For tire rubber the end of devolatilization has been defined when the normalized carbon conversion is 0.7.

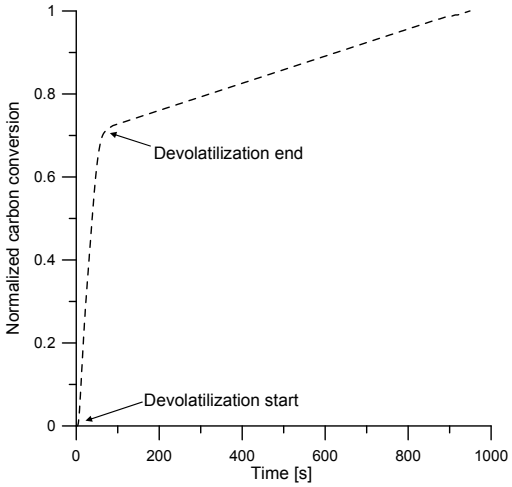

Figure 5-16: Determination of devolatilization time for a pine wood particle at 900ºC and 10 vol.-% O_2. 5% volumetric fill, coarse sand, 100 NL/min, 6 rpm. Particle dimensions: 60 x 30 x 10 mm (7.0 g).

Devolatilization of tire rubber

A comparison between experimental values and values predicted by the model for tire rubber is shown in Figure 5-17. Values used in the model can be found in Appendix B. In the model the fraction of the fuel particle surface that is covered by raw materials, Y, is 0.2. This fraction was chosen based on visual observations during the experiments, where the cylindrical tire rubber particle was observed to be free of the raw material bed during most of the devolatilization. The experimental values were obtained for four different tire rubber particle diameters from 10 mm to 18.5 mm and at 900°C. The two smallest tire rubber particles were also studied at 700°C, 800°C and 1,000°C. The model is in acceptable agreement with the experimental values, which were found to have devolatilization times from approximately 40 to 120 seconds, depending on temperature and tire rubber particle size. The model generally overestimates the effect of temperature compared to the experimental findings: For the two smallest fuel particles, the difference in experimentally found devolatilization times was smaller than predicted by the model.

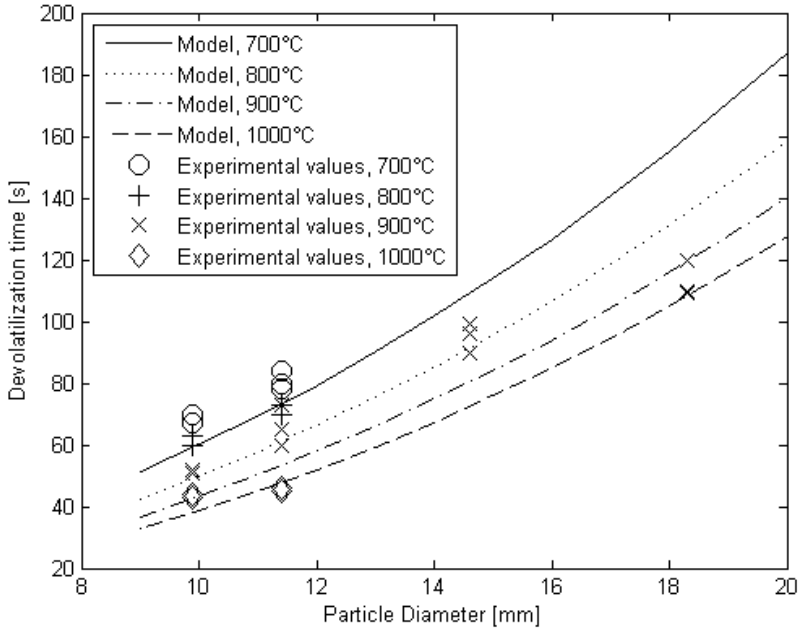

Figure 5-17: Comparison of tire rubber devolatilization time predicted by model and by experimentally found values. 10% O_2. 5% volumetric fill degree in rotary drum. Y = 0.2. $\alpha = 1.25 \cdot 10^{-7}$ m^2/s.

Chinyama and Lockwood (2007) studied the devolatilization times of tire rubber particles with thicknesses in the range 6-12 mm and in the temperature interval from 700-1,000°C. The devolatilization times were found to be 30-100 seconds depending on thickness and temperature, which were typically 20 seconds longer than the values found in this study for the same particle sizes and temperatures. This difference in times may be due to different heat transfer mechanisms at the two experimental conditions: In the experiments conducted by Chinyama and Lockwood (2007), heat transfer to the tire rubber particles were exclusively by convection and radiation, whereas heat transfer in this study were also partly by conduction from the raw materials and drum wall. Another reason may be the mechanical influence from the rotary drum in this study, which is likely to increase fragmentation of the fuel particle during devolatilization – in fact, the tire rubber particles were observed to fragment a little during the experiments, thereby leading to smaller fuel particle sizes.
Larsen et al. (2006) also studied the devolatilization of cylindrical tire rubber particles with diameters from 7 to 22 mm and heights of 35 mm at temperatures up to 840°C in an inert atmosphere. The reported devolatilization times at 840°C were 75 to 300 s when increasing the particle diameter from 7.5 to 22 mm. These devolatilization times are approximately twice as long as indicated by the results from this study. The reason for the deviations may again be differences in the heat transfer mechanisms due to different experimental conditions as well as the mechanical influence in this study. In addition, the experiments conducted by Larsen et al. (2006) were made under an inert atmosphere while the present study was made under oxidizing conditions which are likely to have accelerated the devolatilization rate.

Devolatilization of pine wood

A comparison between experimentally found values and values predicted by the model for pine wood is shown in Figure 5-18. Values used in the model can be found in Appendix B. The experimental values were obtained for five different pine wood particle diameters from 12 mm to 26 mm and at 900°C. The pine wood particles of diameters 15 and 20 mm were also studied at 700°C, 800°C and 1,000°C. The model is observed to be in acceptable agreement with the experimental values, which were found to have devolatilization times from approximately 40 to 170 seconds, depending on temperature and particle size. However, the experiments conducted at 700°C and 800°C are generally 20-30 seconds longer than the devolatilization times predicted by the model and in one case, with a particle diameter of 20 mm and at 700°C is the deviation 50 seconds.

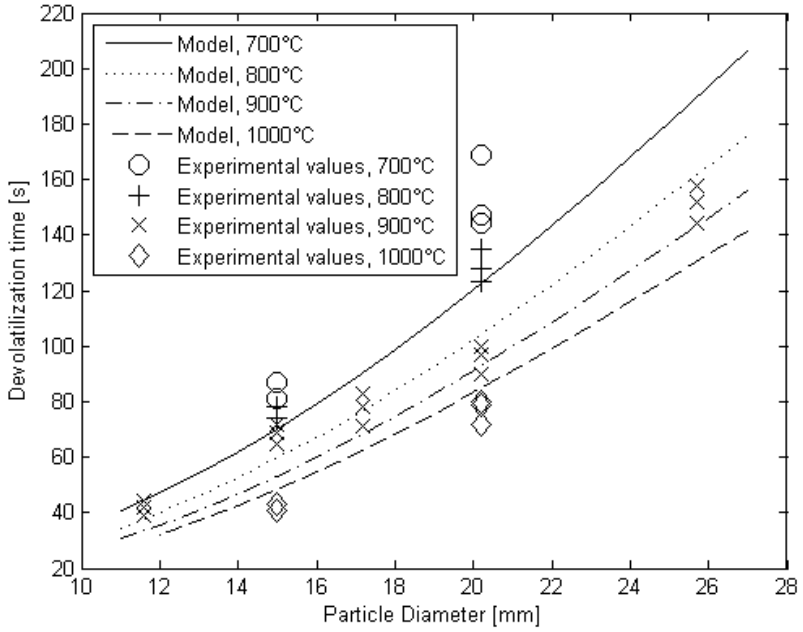

Figure 5-18: Comparison of pine wood devolatilization time predicted by model and by experimentally found values. 10% O_2, 5% volumetric fill degree in drum. Y = 0.2. $\alpha = 1.9 \cdot 10^{-7}$ m^2/s.

Devolatilization of non-spherical pine wood particles with equivalent diameters, d_{eff}, in the range 10 to 45 mm and in the temperature interval 650 to 850°C has been investigated by de Diego et al. (2002). The reported devolatilization times were in good correspondence with the values found in the present study. For example, at 850°C the devolatilization times for 10 to 30 mm diameter particle were reported to be from 30 s to 150 s, whereas the results from this study indicate devolatilization times from 25 s to 180 s at 850°C. These minor differences in devolatilization times may be due to different characteristics of the pine wood used in the experiments. The correlation for pine wood devolatilization suggested by de Diego et al. (2002) and described in section 5.5.1, equation (5.9), also fits the experimental results from this study nicely, and may be used as a simplified model to predict pine wood devolatilization times.

The found devolatilization times for pine wood are also in relatively good consistency with devolatilization times for beech wood particles of similar size as reported by Di Blasi and Branca (2003) and Jand and Foscolo (2005), see the literature study in section 5.2.2.

5.5.3 Model for char combustion

The aims of this section are to derive a model for char conversion in the rotary drum, including the main rate limiting parameters for char conversion. In section 5.5.4 the char combustion model will be validated against experimental results, and in chapter 7 the model will be modified into a realistic char conversion model for the material inlet end of industrial rotary kilns. The char conversion model may be used in combination with models for drying and devolatilization of virgin fuel particles, or it may stand alone to simulate the fate of char particles dropping from calciners through the kiln riser duct and into the material inlet end of rotary kilns.
Figure 5-19 shows a rotary kiln where char particles are buried in the raw material bed. The bulk oxygen volume fraction is denoted $y_{O2,\infty}$, and the oxygen volume fraction at the bed surface is called $y_{O2,surf}$. The oxygen volume fraction at the char particle surface is called $y_{O2,part}$. The mixing of large particles into a bed of smaller particles was shown in chapter 4 to be a fast process, typically taking only a few bed revolutions.

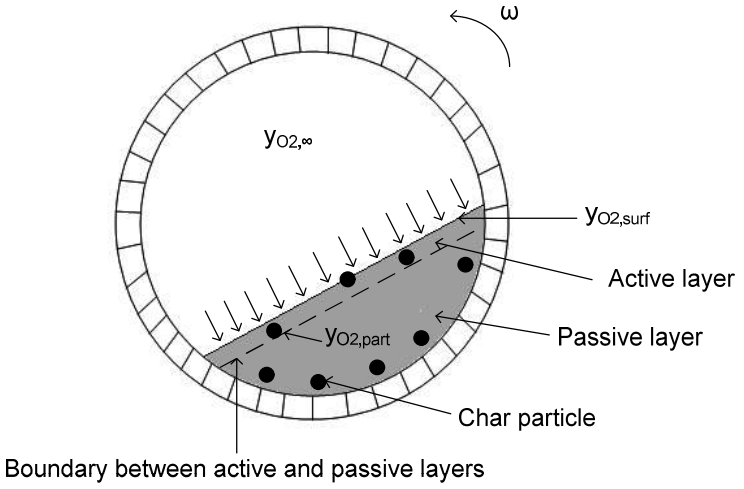

Figure 5-19: Oxygen mass transfer to char particles in a bed of cement raw materials in a rotary kiln.

In a cement rotary kiln it may be assumed that mass transfer of oxygen into the active layer is fast while oxygen mass transfer into the passive layer takes place by a relatively slow diffusion, see Figure 5-19. Since the char particles will continuously be transported through the active and passive layers, respectively, it may be assumed that char oxidation primarily takes place when the char particles are present in the active layer.

With the above mentioned considerations in mind, a model for char oxidation applicable for the conditions in the material inlet end of a rotary kiln should include the following:

1. External mass transfer of oxygen to bed surface.
2. Mass transfer of oxygen through the active layer.
3. Diffusion of oxygen into the char particle.
4. Chemical reaction of char and oxygen.

The external mass transfer of oxygen to the bed surface can be written as the mass transfer coefficient k_g multiplied by the driving force:

$$r = k_g \cdot \frac{P}{RT_g} \cdot \left(y_{O_2,\infty} - y_{O_2,surf} \right) \qquad \left[\frac{\text{mol O}_2}{\text{m}^2 \cdot \text{s}} \right] \qquad (5.12)$$

where k_g is found from a Sherwood correlation. For the rotary drum, where the gas flow is in the laminar regime, the following correlation is used (Green and Perry, 2008):

$$Sh = \frac{k_g L}{D_{O_2}} = 0.646 \,\text{Re}^{1/2}\, Sc^{1/3} \qquad (5.13)$$

where Re is calculated from the rotary drum length, L. This correlation is valid for laminar flow over a flat plate, which is roughly similar to the situation with gas flow above the bed surface.

For an industrial rotary kiln where the gas flow is in the turbulent regime, this correlation is used (Green and Perry, 2008):

$$Sh = \frac{k_g D_i}{D_{O_2}} = 0.023 \,\text{Re}^{0.83}\, Sc^{0.44} \qquad (5.14)$$

Re is calculated from the rotary kiln diameter, D_i. This correlation is valid for turbulent flow in pipes.

In case of a rotary kiln/drum without raw materials and few fuel particles, the mass transfer coefficient may be found from a Sherwood correlation for flow past single spheres (Green and Perry, 2008):

$$Sh = \frac{k_g \cdot d_p}{D_{O_2}} = 2 + 0.6 \cdot \text{Re}_{d_p}^{1/2} \cdot Sc^{1/3} \qquad 2 \le \text{Re}_{d_p} \le 800,\ 0.6 \le \text{Sc} \le 2.5 \qquad (5.15)$$

The mass transfer of oxygen from the bed surface into the active layer can be written as the mass transfer coefficient in the active layer, k_{AL}, multiplied by the driving force and the probability that the char particles are in the active layer, P_{AL}, at any given time:

$$r = P_{AL} \cdot k_{AL} \cdot \frac{P}{RT_b} \cdot \left(y_{O_2,surf} - y_{O_2,\text{part surf}} \right) \left[\frac{\text{mol O}_2}{\text{m}^2 \cdot \text{s}} \right] \qquad (5.16)$$

The probability for the char particles to be in the active layer may be estimated by the experimentally determined correlation suggestion by equation (4.5) in chapter 4, which gave a correlation for the percentage of visible fuel particles at the bed surface. This correlation may be used since the active layer thickness is quite small and therefore it may be assumed that the number of fuel particles in the active layer is practically the same as the number of fuel particles that are visible above the bed surface. The mass transfer coefficient in the active layer, k_{AL}, has been determined by Heydenrych (2001):

$$k_{AL} = \sqrt{D_{O_2,eff}\frac{6(1-\varepsilon)\cdot Sh\cdot D_{O_2}}{d_p^2}} \quad , Sh = 3.8 \qquad (5.17)$$

where $D_{O2,\,eff}$ is the effective diffusion coefficient of oxygen:

$$D_{O_2,eff} = \frac{\varepsilon}{\tau} D_{O_2} \qquad (5.18)$$

D_{O2} is the diffusion coefficient for oxygen in air, τ is the bed tortuosity and ε is the bed porosity or void fraction available for gas flow. Dias et al. (2006) found that the tortuosity, τ, of a mixed bed of granular particles could be described as $\tau = 1/\varepsilon^n$, where n depends on the particle packing but is usually in the range of 0.4-0.5.

The rate of oxygen diffusion into the char particle may be estimated by the expression:

$$r = \frac{D_{O_2,part}}{r_p(t)}\cdot\frac{P}{RT_p}\cdot\left(y_{O_2,\text{part surf}} - y_{O_2,\text{part core}}\right)\left[\frac{\text{mol O}_2}{\text{m}^2\cdot\text{s}}\right] \qquad (5.19)$$

where $D_{O2,\,part}$ is the intra-particle oxygen diffusion coefficient, r_p is the particle radius, $y_{O2,\,part\,surf}$ and $y_{O2,\,part\,core}$ are the oxygen volume fractions at the particle surface and at the intra-particle ash/char interface, respectively. $D_{O2,\,part}$ may be calculated from:

$$D_{O_2,part} \approx \frac{\varepsilon_{part}}{\tau_{part}} D_{O_2} \approx \frac{1-\frac{\rho}{\rho_0}}{\tau_{part}} D_{O_2} \approx \frac{1-\frac{\rho_0\cdot(1-y_{Vol}-y_{ash})}{\rho_0}}{\tau_{part}} D_{O_2} \approx \frac{y_{Vol}+y_{ash}}{\tau_{part}} D_{O_2} \qquad (5.20)$$

where the char particle porosity, ε_{part}, is calculated by subtraction of the weight fractions of volatiles and ash, y_{Vol} and y_{ash}. The char particle tortuosity for chars is typically around 3 to 5 (Johnsson and Jensen, 2000).

The rate of reaction at the unreacted char outer surface between char and oxygen is found from the intrinsic rate expression multiplied with the total moles and divided by the char surface area and product distribution ratio between CO and CO_2:

$$r = \frac{n_C}{A_{char}\cdot\zeta}\cdot k_0\cdot\exp\left(-\frac{E_a}{RT_p}\right)\cdot y_{O_2,\text{part core}}^{n}\cdot(1-X)^m \quad \left[\frac{\text{mol O}_2}{\text{m}^2\cdot\text{s}}\right] \qquad (5.21)$$

where ζ is the product distribution ratio between CO and CO_2, X is the char fractional conversion degree and A_{char} is the char surface area. A correlation between temperature and the CO/CO_2 ratio, ζ, during combustion of different coal chars has been reported by Arthur (1951):

$$\zeta = \frac{CO}{CO_2} = 10^{3.4} \cdot \exp\left(-\frac{51916 J/mol}{R \cdot T}\right) \tag{5.22}$$

This correlation may be used to estimate ζ at different temperatures under the assumption that it is representative for other chars than coal chars.
At pseudo steady state, the O_2 flux balances the consumption at the char particle surface and the char conversion may be expressed as:

$$\frac{dn_C}{dt} = \zeta \cdot A_{surf} \cdot r \quad \left[\frac{\text{mol C}}{s}\right] \tag{5.23}$$

The conversion may also be expressed in terms of fractional conversion, X, instead of moles, n_C, by inserting:

$$X = 1 - \frac{n_C}{n_{C,0}} \tag{5.24}$$

and

$$dX = \frac{1}{n_{C,0}} dn_C \tag{5.25}$$

The following expression is then obtained:

$$\frac{dX}{dt} = \frac{\zeta \cdot A_{surf} \cdot r}{n_{C,0}} \tag{5.26}$$

The unknown oxygen concentrations $y_{O2,surf}$, $y_{O2,part\ surf}$ and $y_{O2,part\ core}$ may be found by solving the four equations (5.12), (5.16), (5.19) and (5.21) for the four unknowns r, $y_{O2,surf}$, $y_{O2,part\ surf}$ and $y_{O2,partcore}$. This is easily done for n = 1 in equation (5.21), whereas a numerical solution procedure is required for n ≠ 1. For n = 1, the following expression for char conversion is derived:

$$\frac{dX}{dt} = \frac{A_{surf} \cdot \zeta}{n_{C,0}} \cdot \frac{y_{O_2,\infty}}{\frac{R \cdot T_g}{k_g \cdot P} + \frac{R \cdot T_b}{P_{AL} \cdot k_{AL} \cdot P} + \frac{r_{p,0} \cdot (1-X)^{1/3} \cdot R \cdot T_p}{D_{O_2,part} \cdot P} + \frac{\zeta \cdot A_{char}}{n_{C,0} \cdot (1-X)^{m+1} \cdot k_0 \cdot \exp\left(-\frac{E_a}{R \cdot T_p}\right)}} \tag{5.27}$$

This expression includes the "resistances" external oxygen transport, oxygen transport into the bed, diffusion into the char particle and chemical reaction between char and oxygen. The intra-particle

diffusion term may be omitted for small char particles, or for char particles that rapidly fragments into many smaller char particles. It may also be shown that the term for char oxidation kinetics becomes negligible at high temperatures above 900°C. Fuel specific, kinetic data and densities used in the model are summarized in Appendix B. Appendix C includes calculations on char density, oxygen concentration and the diffusion coefficient.

5.5.4 Analysis and comparison of char combustion model

This section analyzes the char combustion model under the experimental conditions in the rotary drum and compares the model predictions with experimental results. The purpose is to study effects of mass, oxygen concentration, bed fill degree and temperature on the char conversion time.

Figure 5-20 left shows the char conversion times for three different pine wood char particles of masses of 0.12 g, 0.24 g and 0.88 g, respectively. The initial fuel particle dimensions are 30 x 10 x 8 mm, 30 x 10 x 15 mm and 60 x 30 x 10 mm, respectively. The oxygen concentration is 5, 10 or 21 vol.-% O_2. It is observed that the model, shown with solid lines, predicts a linear relationship between conversion time, char mass and oxygen concentration. The experimental data also confirm this linear relationship: The conversion time for the 0.88 g char particle is for example around 300 s, 600 s and 1300 s at oxygen concentrations of 21 vol.-%, 10 vol.-% and 5 vol.-% O_2. As shown in Figure 5-20, left the model is generally observed to give a good fit to the experimental data in the experiments with different char masses and oxygen concentrations.

.

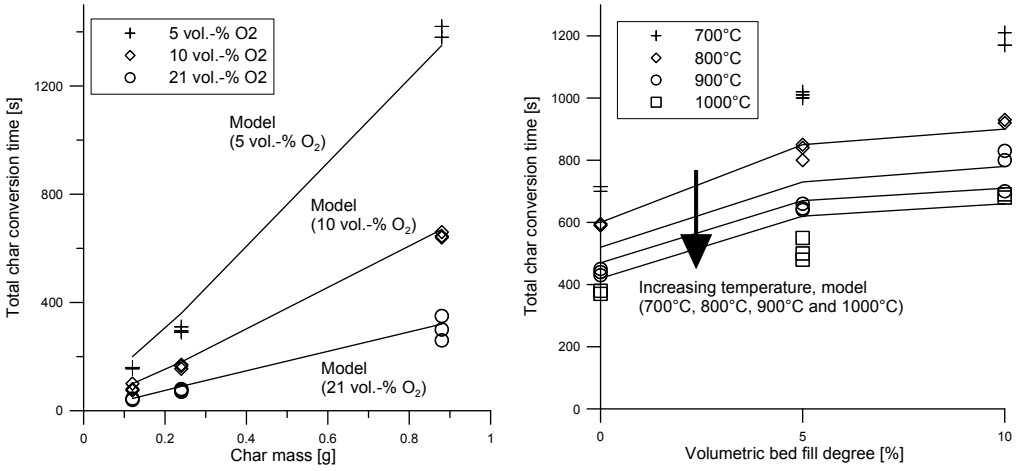

Figure 5-20: Comparison of experimental data with model predictions for pine wood. Left: Effect of char mass and oxygen concentration on the char conversion time. 900°C, 5% fill degree, 100 NL/min. Initial particle dimensions: 30 x 10 x 8 mm, 30 x 10 x15 mm and 60 x 30 x 10 mm. Right: Effect of raw material fill degree and temperature on model predicted char conversion time for a pine wood char particle with initial dimensions of 60 x 30 x 10 mm. Char mass = 0.88 g. 10 vol.-% O_2, 100 NL/min. Char conversion evaluated at 80% conversion degree.

Figure 5-20 right shows the char conversion time as a function of volumetric bed fill degree and temperature. The fill degrees are 0% (only char in the reactor), 5% or 10%, and the temperatures are 700°C. 800°C, 900°C or 1000°C. It is observed that the char conversion time increases when the

bed fill degree increases. The model shows the same tendencies in temperature dependence as the experimental results. However the experimental data show greater differences in conversion time as a function of temperature than the model, particularly at 700°C where the deviation is up to 350 s at 10% fill degree corresponding to a deviation of around 30%.

Figure 5-21 left shows the char conversion time for three different tire rubber char cylinders with masses of approximately 0.6 g, 1.4 g and 2.0 g, respectively. The oxygen concentration is 5, 10 or 21 vol.-% O_2. The model, shown with solid lines, predicts a linear increase in conversion time with char mass and a linear decrease with oxygen concentration. For example, the predicted conversion time for 2 g of char is observed to be halved from 570 s to 280 s when the oxygen concentration is doubled from 5 vol.-% to 10 vol.-%. Thus the model predicts that external mass transfer of oxygen is a main rate limiting parameter. The model gives the best agreement with the experimental values at 10 vol.-% and 21 vol.-% O_2, where the deviation is generally within ± 50 s. But the model fails to give good agreement with the experiments at 5 vol.-% O_2 and char masses of 1.4 g and 2.0 g. In these cases, the deviations are up to nearly 30%.

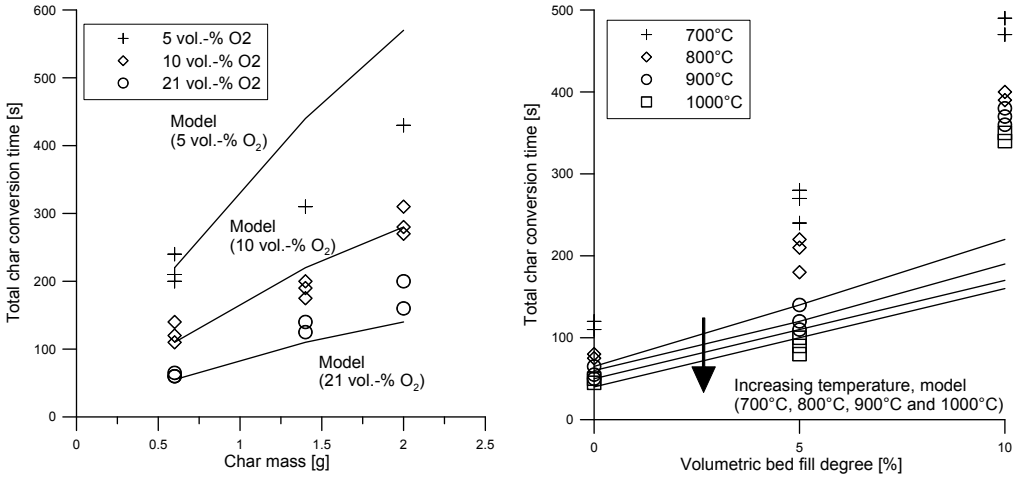

Figure 5-21: Left: Comparison between model predictions and experimental data for char conversion time of three different tire rubber char cylinders with lengths of 25 mm and initial diameters of 9, 12 and 16 mm, respectively. 900°C, 5% raw material fill, 100 NL/min. Char masses and oxygen concentrations indicated in figure. Right: Effect of raw material fill degree and temperature on model predicted char conversion time for tire char cylinder with a length of 25 mm and initial diameter of 9 mm. Char mass = 0.6 g. 10 vol.-% O_2, 100 NL/min. Char conversion evaluated at 80% conversion degree.

Figure 5-21 right shows the predicted effect of raw material fill degree in the interval 0-10% and in the temperature interval 700°C to 1000°C for a cylindrical tire rubber char particle. Experimental values are also compared with the model. Both experimental values and the model indicate that the char conversion time increases with volumetric bed fill degree and decreases when the temperature increases. The model only fits the experimental values in the case with a fill degree of 0%, corresponding to a situation with only char in the rotary drum and no cement raw materials. However, the experimental values at 700°C and 0% fill show longer conversion times than predicted by the model: 120-130 s relative to 65 s, respectively. At 5% fill degree, the model only

fits the experimental values at 900°C and 1000°C, but under-estimates the conversion times at 700°C and 800°C by a factor of 2. And at a fill degree of 10%, the model under-estimate the effect of fill degree and temperature by a factor of 2.5 to 3, depending on temperature. The effect of fill degree seems to increase more with fill degree for tire rubber than for pine wood. The reason for these differences may be related to the chemical and physical properties of the different chars: Tire char fragments into several small particles while the wood char to a high degree retains its size and shape.

Conclusions for char conversion model
A model for char conversion has been suggested and compared with experimental data for tire char and pine wood char. The model includes the four resistances external oxygen diffusion to raw material bed, oxygen transport into the bed, intra-particle oxygen diffusion and chemical reaction at the char surface. By analysis of the char conversion model, equation (5.27), it was found that most resistance was due to external oxygen diffusion and oxygen transport into the bed. Intra-particle oxygen diffusion and chemical reaction kinetics were found to be minor resistances to char oxidation.
The model is in good correspondence with the observed conversion times for pine wood char. However, it under-estimates the effect of bed fill degree for tire char. The model also under-estimates the effect of the lowest temperatures of 700°C and 800°C on the conversion time for both pine wood char and tire char. Regarding the effect of material fill degree on the char conversion time, it is necessary to carry out further experiments with different fuel chars and particle sizes/shapes to obtain a better basis for model validation. Regarding the effect of temperature, it is possible that the model does not give a realistic prediction for the reaction kinetics. It is also possible that the set-point temperature used in the model is different from the actual surface temperature of the char particles during char oxidation.

5.6 Conclusions for chapter 5

Combustion of a solid fuel particle consists of the following steps: heating, drying, devolatilization and char oxidation. Ash is the ultimate product left after complete combustion. In a cement rotary kiln where gas and solid temperatures are typically higher than 900°C, heating, drying and devolatilization are typically rapid processes, whereas char oxidation may be a significantly slower process. The reason is that char oxidation is dependent on oxygen transport to the char particle before the oxidation can take place.

Experiments with different solid fuels in a high-temperature rotary drum have been conducted in order to quantify the effect of key process parameters such as bed fill degree, drum rotational speed, temperature, etc. on the fuel conversion time. The process conditions have been chosen to simulate the process conditions in the material inlet end of an ILC rotary kiln. The main focus has been on tire rubber and pine wood.

The results showed that devolatilization of tire rubber and pine wood was mainly influenced by the temperature and fuel particle size. The char oxidation was influenced by all investigated parameters, i.e. fuel sample mass, particle size, temperature, oxygen concentration, bed fill degree and rotational speed. Rotational speed, however, was only of importance if there was a shift in bed motion, e.g. from slumping to rolling. For changes in rotational speed where the dominant bed motion was maintained as the rolling motion, the effect of rotational speed was of minor importance.

The tire char was observed to fragment into smaller particles during the char oxidation, leading to shorter conversion times than for pine wood char which predominantly behaved as one shrinking particle during the char oxidation.

Devolatilization and char oxidation models have been developed and compared with experimental results and published data. The devolatilization models fits well to the experimental data for pine wood and tire rubber. The char oxidation model for pine wood char also fits well with experimental data. However, there is a tendency that the effect of temperature is under-estimated by the char model for pine wood char. For tire char, the char oxidation model does not give good predictions, particularly regarding temperature and bed fill degree.

5.7 References

Agarwal, P. K., Genetti, W. E., Lee, Y. Y. and Prasad, S. N.; Model for drying during fluidized-bed combustion of wet low-rank coals, Fuel, 63, 1020-1027, 1984.

Agarwal, P. K., Genetti, W. E. and Lee, Y. Y.; Devolatilization of large coal particles in fluidized beds, Fuel, 63, 1748-1752, 1984.

Agarwal, P. K., Genetti, W. E. and Lee, Y. Y.; Coupled drying and devolatilization of wet coal in fluidized beds. Chem. Eng. Sci., 41 (9), 2373-2383, 1986.

Arthur, J. R.; Reactions between carbon and oxygen. Transactions of the Faraday Society, Vol. 47, Is. 2, 164-178, 1951.

Atal, A. and Levendis, Y. A.; Comparison of the combustion behavior of pulverized waste tyres and coal. Fuel, Vol. 74, No. 11, 1570-1581, 1995.

Bouvier, J. M., Charbel, F. and Gelus, M.; Gas-solid pyrolysis of tire wastes – kinetics and material balances of batch pyrolysis of used tires. Resources and Conservation, 15, 205-214, 1987.

Chinyama, M. P. M. and Lockwood, F. C.; Devolatilisation behaviour of shredded tyre chips in combusting environment. J. Energy Institute, 80, 3, 162-167, 2007.

Conesa, J. A., Font, R., Fullana, A. and Caballero, J. A.; Kinetic model for the combustion of tyre wastes. Fuel, 77, 13, 1469-1475, 1998.

Dias, R., Teixeira, J. A., Mota, M. and Yelshin, A.; Tortuosity variation in a low density binary particulate bed. Separation and Purification Technology, 51, 180-184, 2006.

Di Blasi, C.; Modelling the fast pyrolysis of cellulosic particles in fluid-bed reactors. Chem. Eng. Sci., 55, 5999-6013, 2000.

Di Blasi, C. and Branca, C.; Temperatures of wood particles in a hot sand bed fluidized by nitrogen. Energy & Fuels, 17, 247-254, 2003.

De Diego, L. F., García-Labiano, F., Gayán, P, Abad, A. and Adánez, J.; Coupled drying and devolatilisation of non-spherical wet pine wood particles in fluidized beds. J. Analytical and Applied Pyrolysis, 65, 173-184, 2002.

De Diego, L. F., García-Labiano, F., Gayán, P, Abad, A. and Adánez, J.; Modeling of the devolatilization of nonspherical wet pine wood particles in fluidized beds. Ind. Eng. Chem. Res., 41, 3642-3650, 2002.

Giddings, D., Pickering, S. J., Simmons, K. and Eastwick, C. N.; Combustion and aerodynamic behavior of car tyre chips in a cement works precalciner. J. of the Inst. of Energy, September, 75, 91-99, 2002.

Green, D. W. and Perry, R. H.; Perry's Chemical Engineers' Handbook, p. 5-63 to p. 5-70, McGraw-Hill, 8th ed., 2008. ISBN: 978-0-07-142294-9.

Heydenrych, M. D.; Modelling of rotary kilns. PhD Thesis, University of Twente, The Netherlands, 2001. ISBN: 90-36515440.

Hupa, M.; Lecture notes from "Chemistry in Combustion Processes", Åbo Akademi, Finland, 2008.

Jand, N. and Foscolo, P. U.; Decomposition of wood particles in fludized beds. Ind. Eng. Chem. Res., 44, 5079-5089, 2005.

Janse, A. M. C., de Jonge, H. G., Prins, W. and van Swaaij, W. P. M.; Combustion kinetics of char obtained by flash pyrolysis of pine wood. Ind. Eng. Chem. Res., 37, 3909-3918, 1998.

Johnsson, J. E. and Jensen, A.; Effective diffusion coefficients in coal chars. Proceedings of the Combustion Institute, Vol. 28, 2353-2359, 2000.

Kim, S.-S., Kim, J., Park, Y.-H. and Park, Y.-K.; Pyrolysis kinetics and decomposition characteristics of pine trees. Bioresource Technology, 101, 9797-9802, 2010.

Kunii, D. and Levenspiel, O.; Fluidization Engineering. Butterworths, Boston, MA, USA. 2nd ed., 1991. ISBN: 0-409-90233-0.

Kyari, M., Cuncliffe, A. and Williams, P. T.; Characterization of oils, gases, and char in relation to the pyrolysis of different brands of scrap automobile tires. Energy & Fuels, 19, 1165-1173, 2005.

Larsen, M. B., Schultz, L., Glarborg, P., Skaarup-Jensen, L., Dam-Johansen, K., Frandsen, F. and Henriksen, U.; Devolatilization characteristics of large particles of tyre rubber under combustion conditions. Fuel, vol. 85, 1335-1345, 2006.

Larsen, M. B.; Alternative Fuels in Cement Production. PhD Thesis, Technical University of Denmark, Department of Chemical Engineering, 2007. ISBN 978-87-91435-49-8.

Larsen, M. B., Hansen, M. L., Glarborg, P., Skaarup-Jensen, L., Dam-Johansen, K. and Frandsen, F.; Kinetics of tyre char oxidation under combustion conditions. Fuel, vol. 86, 2343-2350, 2007.

Laurendeau, N. M.; Heterogeneous kinetics of coal char gasification and combustion. Prog. Energy Combust. Sci., Vol. 4, 221-270, 1978.

Leung, D. Y. C. and Wang, C. L.; Kinetic study of scrap tyre pyrolysis and combustion. J. Anal. & Appl. Pyrolysis, 45, 153-169, 1998.

Levenspiel, O.; Chemical reaction engineering. John Wiley & Sons, Inc. 3rd edition, 1999.

Linjewile, T. M., Hull, A. S. and Agarwal, P. K.; Heat transfer to a large mobile particle in gas-fluidized beds of smaller particles. Chem. Eng. Sci., 48, 21, 3671-3675, 1993.

Masi, S., Salatino, S. and Senneca, O.; Combustion rates of chars from high-volatile fuels for FBC application. Fluidised Bed Combustion, Vol. 1, 135-143, 1997.

Mermoud, F., Golfier, F., Salvador, S., Van de Steene, L. and Dirion, J. L.; Experimental and numerical study of steam gasification of a single charcoal particle. Combustion and Flame, 145, 59-79, 2006.

Perry Chemical Engineers Handbook, 7th edition, Mc-Graw Hill, 1999.

Schmidthals, H.; Luftvergasung von Altreifen zur integrierten stofflichen und energetischen Nutzung im Klinkerbrennprozess. Doktor-Ingenieur Dissertation, Fakultät für Maschinenbau, Ruhr-Universität Bochum, Germany, 2001.

Shen, D. K., Gu. S., Luo, K. H., Bridgwater, A. V. and Fang, M. X.; Kinetic study on thermal decomposition of woods in oxidative environment. Fuel, 88, 1024-1030, 2009.

Senneca, O.; Kinetics of pyrolysis, combustion and gasification of three biomass fuels. Fuel Processing Technology, 88, 87-97, 2007.

Szekely, J., Ewans, J. W. and Sohn, H. Y.; Gas-solid reactions. New York, Academic Press, 51, 1976.

Tscheng, S. H. and Watkinson, A. P.; Convective heat transfer in a rotary kiln. Can. J. Chem. Eng., Vol. 57, 433-443, August 1979.

Wildegger-Gaissmaier, A. E. and Agarwal, P, K.; Drying and devolatilization of large coal particles. Fuel, 69, 44-52, 1990.

Winter, F., Prah, M. E.and Hofbauer, H.; Temperatures in a fuel particle burning in a fluidized bed: The effect of drying, devolatilization and char combustion. Combustion and Flame, 108, 302-314, 1997.

Yang, J., Tanguy, P. A. and Roy, C.; Numerical model for the vacuum pyrolysis of scrap tires in batch reactors. AIChE Journal, Vol. 41, No. 6, 1500-1512, June 1995.

Yang, J., Tanguy, P. A. and Roy, C.; Heat transfer, mass transfer and kinetics study of the vacuum pyrolysis of a large used tire particle. Chem. Eng. Sci., Vol. 50, No. 12, 1909-1922, 1995.

6 *Inorganic chemistry in the kiln system*

As described in chapter 3, local reducing conditions caused by alternative fuel combustion in the material inlet end of rotary kilns have the potential of increasing the internal circulation of sulfur, chlorine and alkali metal species. In addition, alternative fuels may introduce increased amounts of sulfur, alkali metals or chlorine to the system which will also affect the internal circulation involving these elements and may subsequently affect process stability of the kiln system. This chapter seeks to provide insight into the inorganic chemistry of the elements sulfur (S), chlorine (Cl) and alkali metals (Na and K) in the kiln system, when alternative fuels are utilized. Main emphasis is on sulfur, because this element is mostly affected by combustion conditions.

The chapter starts with a literature study about release and capture of inorganic volatile elements. Then a section describes thermodynamic equilibrium calculations to theoretically investigate the inorganic chemistry in the kiln system under different atmospheres.
The experimental part presents the results from experiments with sulfur release from calcined raw materials in a laboratory scale experimental set-up under oxidizing and reducing atmospheres. And finally, sulfur release from raw materials under the influence of different solid fuels is described. The experiments with solid fuels are made in the specially designed high-temperature rotary drum that was described in chapter 5.

6.1 Introduction

6.1.1 S, Cl, Na and K species in the rotary kiln, calciner and lower preheater cyclones

This section will briefly review the forms of the elements S, Cl, Na and K at different positions in the kiln system.

Figure 6-1 shows the chemical bonding of main S-, Na-, K- and Cl-containing species at different locations in the lower preheater cyclones, calciner, rotary kiln and clinker cooler. Multiple other species are possible, but are omitted for clarity. The preheated raw material from the upper preheater cyclones (not shown) enters the lower cyclone stages. Because the raw material have been preheated to around 650°C, only inorganic bound sulfur is present in the raw materials, mainly in the form of alkali or calcium sulfates (Hansen, 2003). The alkali metals may be bound as sulfates, chlorides or carbonates.

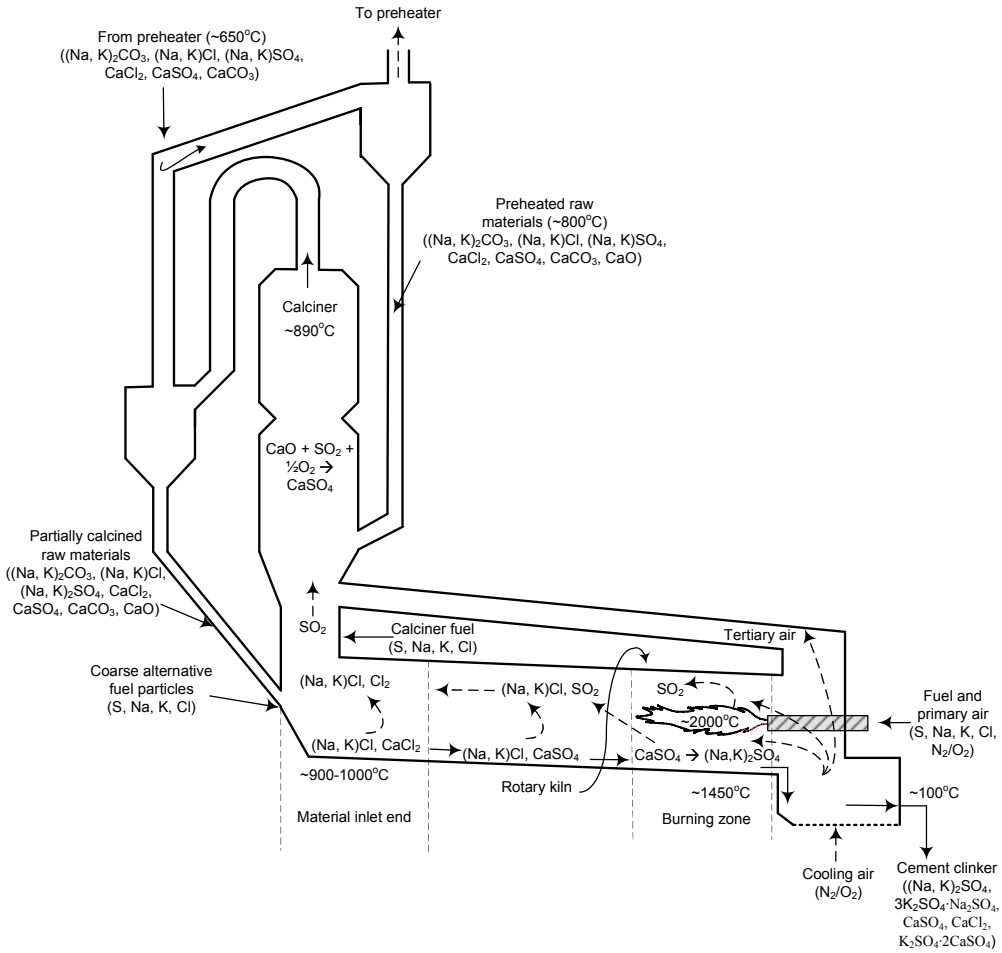

Figure 6-1: The identity of main S-, Na-, K- and Cl-containing species in the kiln system. Solid flows shown with solid arrows and gas flows shown with dotted arrows.

S, Cl, Na and K may also be introduced to the kiln system with the fuels, depending on fuel type (see also table 3-2 in chapter 3 with chemical compositions of relevant fuels):
TDF will break the C-S bonds in the original tire during pyrolysis at temperatures above 200°C, and the sulfur will be released to the gas phase as either H_2S or SO_2 (Díez et al., 2004).
RDF consists of a variety of organic and inorganic compounds, and as a consequence, the inorganic volatile input from RDF may fluctuate. S, Cl, Na and K in RDF tend to be released as HCl, alkali chlorides, alkali sulfates, H_2S and SO_2 (Kobyashi et al., 2005).
PVC decomposes in the temperature interval 200-400°C to HCl and a coke-like residue (Zevenhoven et al., 2002).
Meat and bone meal (MBM) devolatilizes at temperatures above 300°C. Chlorine from MBM may be partly devolatilized into the gas phase as HCl or alkali chlorides (Aho and Ferrer, 2005). The sulfur from the MBM may be released to the gas phase as either SO_2 or H_2S (Ayllón et al., 2006). It

is possible that the formed alkali chlorides and the gaseous SO_2 react to form alkali sulfates (Aho and Ferrer, 2005).
The release of inorganic volatiles from straw, wood and annual biomass has been studied (Jensen et al., 2000, Davidsson et al., 2002 and Knudsen et al., 2004). The general trend is that the release of K, Cl and S is strongly dependent on both the temperature and the inorganic composition of the fuel. In the temperature interval 200-400°C the organic matrix is destroyed and Cl and K are released from their original binding sites and transferred to a liquid tar phase. Chlorine may further be released to the gas phase as HCl while potassium is bound as KCl, K_2CO_3 or to char-matrix functional groups such as carboxylics and phenoxides (Jensen et al., 2000). At temperatures above 500-700°C, a large fraction of potassium in the form of KCl is released. The fuel sulfur is also released from the organic S-compounds at these temperatures. At temperatures above 800°C, K_2CO_3 decomposes whereas potassium is released as free K atoms or as KOH. At temperatures above 1000°C potassium may be released to the gas phase from the char matrix and from potassium silicates (Jensen et al., 2000). Inorganic bound sulfur will also be released as SO_2 at these high temperatures (Knudsen and Lin et al., 2004).

The calciner acts as a fast fluidized-bed reactor where good contact between hot gas from the rotary kiln or tertiary air duct and raw materials from the preheater provide excellent conditions for gas-to-solid heat transfer that drives the endothermic calcination of limestone. Besides calcination of limestone, the conditions in the calciner with temperatures in the range of 800-900°C, good gas-solid mixing and excessive amounts of CaO also favor the SO_2 capture reaction (Lyngfelt and Leckner, 1989):

$$CaO\ (s) + SO_2\ (g) + ½O_2\ (s) \leftrightarrow CaSO_4\ (s) \qquad (6.1)$$

The relative amounts of alkali sulfates in the partially calcined raw material leaving the calciner are small compared to the amount of $CaSO_4$ due to the excessive amounts of calcium (Jøns, 2010). The partially calcined raw material also contains a high concentration of chlorine in the form of either alkali or calcium chlorides. This is due to the condensation of chlorine species from the kiln gases when the gas is transported through the calciner and lower cyclone stages. Chlorides, which are very sensitive to high temperatures, will to a high degree evaporate as alkali chlorides in the rotary kiln, the evaporation factor typically being close to 1 (Locher et al., 2009).

Alkali metals may evaporate as chlorides, sulfates or elemental alkali metals. Complex vapour equilibria exists in the rotary kiln, where alkali, sulfur and chlorine species may dissociate to species that strongly interacts with combustion products such as CO_2, CO, H_2O, H_2 or O_2 (Bhatty et al., 2004). As a result, the gas phase contains several other species than indicated in Figure 6-1, for example SO_3, HCl, NaOH and KOH.

During the gradual heating of the calcined raw material, a sulfate melt is formed which facilitates formation of alkali sulfates, Na_2SO_4 and K_2SO_4, which are more thermodynamically stable than $CaSO_4$ (Choi et al., 1988). $CaSO_4$ will decompose at the high temperatures present in the burning zone and predominantly form SO_2:

$$CaSO_4\ (s) \leftrightarrow SO_2\ (g) + ½O_2\ (g) + CaO\ (s) \qquad (6.2)$$

SO_2 formed in the rotary kiln is transported with the kiln gases to the calciner, where the previously described sulfur capture on CaO takes place. Thus, an internal sulfur cycle in the rotary kiln and

calciner is established. The fraction of sulfur released as SO_2 depends on the sulfur-to-alkali ratio in the rotary kiln: High levels of alkali metals will favor formation of alkali sulfates rather than formation of free SO_2 (Rosholm et al., 1998).
After the rotary kiln, the cement clinker is quench-cooled by ambient air as cooling air. The relatively low chlorine content may be distributed in the major clinker phases or be present as chlorides. Sulfur and alkali metals in the cement clinker are mainly bound as Na_2SO_4, K_2SO_4, $3K_2SO_4{\cdot}Na_2SO_4$ (aphthitalite), $CaSO_4$, $K_2SO_4{\cdot}2CaSO_4$ (calcium langbeinite) or as substituents in the major clinker phases, mainly alite and belite (Miller and Tang, 1996, Taylor, 1999, Twomey et al., 2004).
The reason why $CaSO_4$ is sometimes found in clinker despite its thermodynamic instability at the high temperatures that prevail in the burning zone, may be related to the nodulization environment: The dense interior of large clinker nodules have been reported to contain elevated levels of both alkali metals and sulfur, indicating that these inorganic volatiles may be trapped in the inner core of clinker nodules (Masaki et al., 2002).
Experiments with raw materials mixed with gypsum have shown that an effective grinding to small particle sizes will help to stabilize $CaSO_4$ (Tsoumeleas et al., 2000). This is achieved by the formation of complex compounds such as $2CaSO_4{\cdot}K_2SO_4$ and $Na_2Ca(SO_4)_2$ which can withstand temperatures up to 1520°C. This important stabilization may be explained by the fact that small particles will be in better contact with each other in the molten phase of the clinker, and thereby alkali and sulfur-containing species may easier form stable compounds.

6.2 Literature study on release and capture of inorganic volatile elements

6.2.1 High-temperature reactions between SO_2 and limestone

Absorption of SO_2 on limestone under fluidized bed and entrained flow conditions have been studied extensively during the last decades (Lyngfelt and Leckner, 1989/1999, Dam-Johansen et al., 1991 Hansen et al., 1991/1993, Hansen, 2003, Tarelho et al., 2005, Rasmussen, 2011). Even though these investigations are not directly applicable to describe the conditions in the material inlet end of cement rotary kilns, they do include relevant descriptions of mechanisms for sulfur release and capture by limestone at temperatures up to 1200°C and under oxidizing as well as reducing atmospheres. An important point to note, however, is that these investigations only include reactions between limestone and sulfur species, whereas a full investigation of the reactions taking place in cement rotary kilns should also include other major components present in the cement raw materials as they may affect the sulfur chemistry. In addition, the Ca/S molar ratio studied under fluidized bed conditions were typically in the range of 1:1 to 4:1 which differs from the conditions in cement rotary kilns where there is a massive excess of Ca relative to S: The Ca/S molar ratio in the raw material that enters the rotary kiln is typically higher than 10:1 (Hewlett, 1998).

6.2.1.1 Mechanisms for sulfur capture and release from limestone

The following reaction mechanism for reductive decomposition of $CaSO_4$ in fluidized beds has been proposed (Hansen et al., 1993):

$$CaSO_4\,(s) + CO\,(g) \leftrightarrow CaSO_3\,(s) + CO_2\,(g) \qquad (6.3)$$

$CaSO_3$ (s) ↔ CaO (s) + SO_2 (g) (6.4)

CO is believed to react directly on $CaSO_4$, giving $CaSO_3$ and CO_2. CO_2 is rapidly desorbed, while $CaSO_3$ disproportionates and forms CaO and SO_2. $CaSO_3$ is believed to be an important reaction intermediate. The formed CaO is subsequently sulphidized to CaS according to:

CaO (s) + SO_2 (g) + 3CO (g) ↔ CaS (s) + 3CO_2 (g) (6.5)

Returning to oxidizing conditions, CaS is oxidized to CaO by the reaction:

CaS (s) + 1.5O_2 (g) ↔ CaO (s) + SO_2 (g) (6.6)

The CaS oxidation is a rapid and very exothermal reaction which may lead to a temperature increase (Tian and Guo, 2009). The final step is the formation of $CaSO_4$ by reaction of CaO, SO_2 and O_2, which is also an exothermal reaction (Tian and Guo, 2009):

CaO (s) + SO_2 (g) + ½O_2 (g) ↔ $CaSO_4$ (s) (6.7)

Hansen et al. (1991 and 1993) studied phase equilibria for the SO_2-CaO-$CaSO_4$-CaS-CO-CO_2 system. They performed experiments in an electrically heated laboratory scale fixed bed reactor developed to simulate the changing oxidizing and reducing conditions similar to the conditions particles will experience in a fluidized bed reactor. They found that any transformation between $CaSO_4$ and CaS takes place via CaO. This transformation cycle is shown in Figure 6-2, which also illustrates the competition between sulfur capture and sulfur release. This competition depends on parameters such as partial pressures of SO_2, CO and CO_2, see the phase diagram in Figure 6-3. Temperature is a very important parameter: An increase in temperature in the interval 800-1200°C will shift the equilibrium towards CaO and release more SO_2 (Hansen et al., 1991).

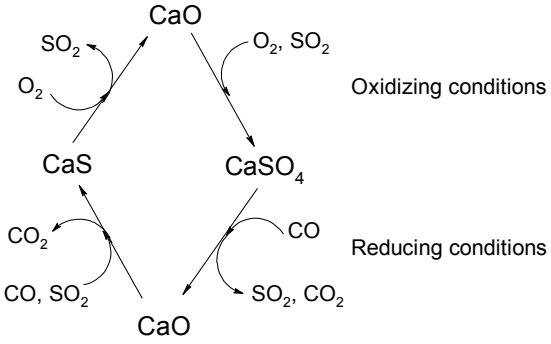

Figure 6-2: Sulfur transformation during periodically changing oxidizing and reducing conditions (Hansen et al., 1993).

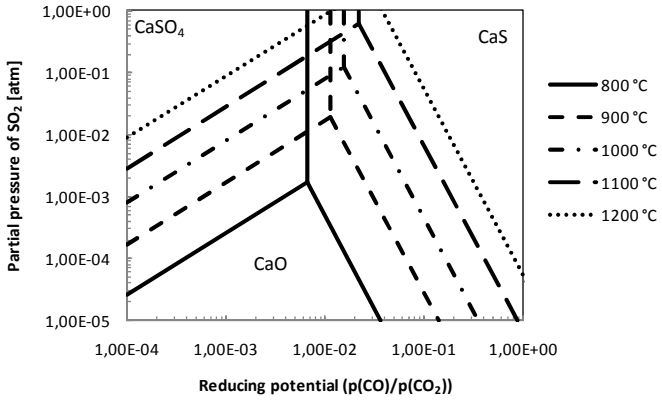

Figure 6-3: Phase diagram for the SO_2-CaO-$CaSO_4$-CaS-CO-CO_2 system (Based on thermochemical data from Barin, 1995).

Hansen et al. (1993) found that the competition between sulfur capture and sulfur release under alternating oxidizing and reducing conditions were shifted towards more sulfur release when the temperature increased.
Lyngfelt and Leckner (1989) reported a decrease in the sulfur capture ability of limestone at temperatures above 880°C and reducing conditions, due to reductive decomposition of $CaSO_4$.
Tarelho et al. (2005) found a maximum sulfur capture efficiency of limestone at around 825°C. Higher temperatures reduced the sulfur capture efficiency, particularly under reducing conditions.

6.2.1.2 Effect of reducing agent on the sulfur release

During devolatilization and combustion of alternative fuels in an oxygen-lean environment several reducing agents may be formed; CO, H_2, CH_4 as well as other hydrocarbons. It is well documented that reducing agents such as CO and H_2 can promote reductive decomposition of $CaSO_4$ (Hansen et al., 1991 and 1993). The rate of reductive decomposition depends on the specific reducing agent. Hansen et al. (1993) studied the rate of reductive decomposition with all three reducing agents CO, H_2 and CH_4. It was observed that the rate of decomposition was fastest with H_2 as reducing agent. This is in agreement with earlier findings by Wheelock and Boylan (1960) who reported that the rate was increased by a factor two or three when the reducing agent was H_2 instead of CO. Also Diaz-Bossio et al. (1985) reported that the rate of reductive decomposition was fastest with H_2 relative to CO. Hansen et al. (1993) did not detect any reductive decomposition of $CaSO_4$ with CH_4 as a reducing agent even though the reaction is thermodynamically feasible. It was assumed to be because reductive decomposition of $CaSO_4$ with CH_4 is a very slow process that did not have sufficient time to proceed during the 30-second intervals used in the experiments.
Turkdogan and Vinters (1976) also showed that elemental carbon could be used as a reducing agent. The conversion rate of $CaSO_4$ to SO_2 and/or CaS was reported to be determined by the rate of oxidation of carbon to CO which then rapidly reduced $CaSO_4$.

6.2.2 Removal of chlorine from the kiln system

Increased input from fuels or raw materials of chlorine in the kiln system has made it necessary for many cement plants to install a so-called bypass system. The purpose of the bypass system is to remove a fraction of the chlorine from the kiln gas stream, the primary aim being to avoid blockages predominantly in the lower preheater cyclone stages, and to reduce kiln shell corrosion and refractory degradation.

The bypass typically starts at a gas extraction point located immediately after the kiln gas outlet from the rotary kiln. This position is usually chosen because the chlorine concentration in the flue gas is high. A small bypass at this point is sufficient to remove a large amount of chlorine from the kiln system (FLSmidth, 2008). The removal efficiency of chlorine depends on the chlorine concentration in the kiln gas. It is usually sufficient to extract less than 10% of the kiln gas. Sutou et al. (1999) reported that 90% of the chlorine can be removed by extracting 5% of the kiln exhaust gas when the chlorine concentration in the calcined raw materials entering the rotary kiln is in the range from 5000 ppm to 7500 ppm.

The extracted kiln gases containing chlorine and kiln dust are quench cooled by air to condense the chlorides from the gas. The condensed chlorides are then separated from the gas in an electrostatic precipitator (ESP) or a bag filter (BF). In some installations, a conditioning tower is positioned between the quenching section and the ESP/BF in order to reduce the volume of gases and thereby the size and cost of the ESP/BF. The gases from the ESP/BF are often drawn by their own fan to a common stack. The separated dust has high chlorine content and may be reused in the cement plant, used in other industries or disposed of (FLSmidth, 2008).

Besides achieving the above-mentioned advantages, the bypass reduces the flue gas flow through the preheater and thereby reduces the load on the ID fan. The overall heat consumption generally increases by 6-8 kJ/kg clinker per percentage point of bypass gas. Gaseous emissions of CO, HCl and SO_2 may be emitted with the bypass gases unless the process is appropriately designed (FLSmidth, 2008), see also section 3.4.2.

6.3 Equilibrium calculations on influence of reducing conditions

To provide the basis for a better understanding of the inorganic chemistry in the rotary kiln material inlet, thermodynamic equilibrium calculations were performed using the commercially available software FactSage 6.0. This program uses the principle of minimization of the total Gibbs free energy to calculate the equilibrium composition of a chemical system with known total elemental composition, temperature and pressure.

6.3.1 Input data

The equilibrium calculations are based on the composition of calcined cement raw material and of the flue gas leaving the rotary kiln. These compositions are shown in Table 6-1 and 6-2. It should be noted that the calcined raw material used in the calculations contains a relatively high amount of chlorine and sulfur, relative to the guidelines for a stable kiln operation.

Calcined raw material	Weight-%	Moles/kg clinker
SiO_2	18.00	3.000
Al_2O_3	4.76	0.467
Fe_2O_3	2.30	0.144
CaO	56.80	10.128
K_2O	2.50	0.266
Na_2O	0.20	0.032
S total	2.66	0.829
Cl	1.17	0.330

Table 6-1: Calcined raw material composition used in the equilibrium calculations.

Oxidizing conditions, $\lambda = 1.3$	Vol.-%	Moles/kg clinker	Reducing conditions, $\lambda = 0.9$	Vol.-%	Moles/kg clinker
CO_2	25.00	5.580	CO_2	25.00	5.580
H_2O	5.00	1.116	H_2O	5.00	1.116
O_2	5.00	1.116	O_2	0.00	0.000
CO	0.10	0.022	CO	2.00	0.446
SO_2	0.05	0.011	SO_2	0.05	0.011
N_2	64.85	14.475	N_2	67.95	15.167
Total	100.00	-	Total	100.00	-

Table 6-2: Flue gas compositions used in the equilibrium calculations.

The following input data were used:

- Chemical compositions of calcined raw material and flue gas as specified in Table 6-1 and 6-2. All elements inserted as moles/kg clinker.
- It is a foregone conclusion that there is one kg calcined raw material and 0.5 Nm^3 flue gas for each kg clinker produced.
- The following elements were included: C, H, N, O, S, Cl, K, Na, Ca, Si, Fe, Al.
- The flue gas is either oxidizing ($\lambda = 1.3$) or reducing ($\lambda = 0.9$).
- Temperature: 800-1500°C, step size: 25°C.

- Pressure: 1 atm.

For the equilibrium calculations, ideal gas phase compounds, solid phase compounds and liquid phase compounds were included from the FactSage 6.0 compound database. A list of all compounds included in the equilibrium calculations are enclosed in Appendix D.

6.3.2 Limitations

The equilibrium model has the following limitations, which should be considered when comparing the results to actual conditions:

- The model does not consider mass transfer and kinetic limitations. In an industrial rotary kiln, the residence time may be too short for the species to come into contact with each other and for reactions to take place. Furthermore, the residence time may be too short for the transformation or decomposition of some compounds to take place. Therefore, the predicted formation of compounds may exceed that occurring in reality.
- The model does not take into account in which form the elements are initially present in the calcined raw material and flue gas. In reality, the elements may be bound in different minerals and be released at different temperatures. This may affect the distribution of the element between the solid, liquid and gas phase. It may also affect the compounds formed and the phase distribution of other elements.

Because of these limitations, the results of the equilibrium calculations cannot be used for a quantitative comparison to experimental data, but only to determine which species are thermodynamically favored under different gas atmospheres.

6.3.3 Influence of reducing conditions

In order to investigate the effect of changing the atmosphere from oxidizing to reducing, the calcined raw material is exposed to a) an atmosphere with 5 vol.-% oxygen and b) an atmosphere with 0 vol.-% oxygen and 2 vol.-% CO. The exact composition of calcined raw material and flue gas is given in Table 6-1 and Table 6-2.

The equilibria for oxidizing and reducing conditions are shown in Figure 6-4. Only the main sulfur-containing compounds are included for clarity. The figure shows the sulfur distribution between $CaSO_4$, CaS and SO_2 at various temperatures and under either oxidizing or reducing atmosphere. It is noted that no alkali sulfates are formed in the studied case, because formation of alkali chlorides is thermodynamically favored.
The most important observation from Figure 6-4 is that the decomposition of $CaSO_4$ to CaO and SO_2 takes place at lower temperatures when reducing conditions are prevailing: Under oxidizing conditions, $CaSO_4$ is stable until approximately 1100°C. At temperatures between 1100°C and 1350°C, $CaSO_4$ is gradually decomposed forming CaO and SO_2. Above 1350°C, $CaSO_4$ is not thermodynamically stable and all sulfur is released as SO_2. The situation is very different under reducing conditions, where $CaSO_4$ is observed to be partly reductively decomposed already at temperatures below 800°C. The reductive decomposition continues until approximately 1300°C. At higher temperatures, all sulfur is present as SO_2. The reductive decomposition of $CaSO_4$ takes place

because sulfates can be used as an oxygen donor under reducing conditions. It should also be noted that a fraction of the sulfur is present as CaS under reducing conditions. However, CaS is only stable at temperatures below 850°C, and the sulfur is released as SO_2 at higher temperatures. This is in correspondence with the $CaSO_4$-CaS-CaO-SO_2-O_2-CO phase diagram in Figure 6-3.

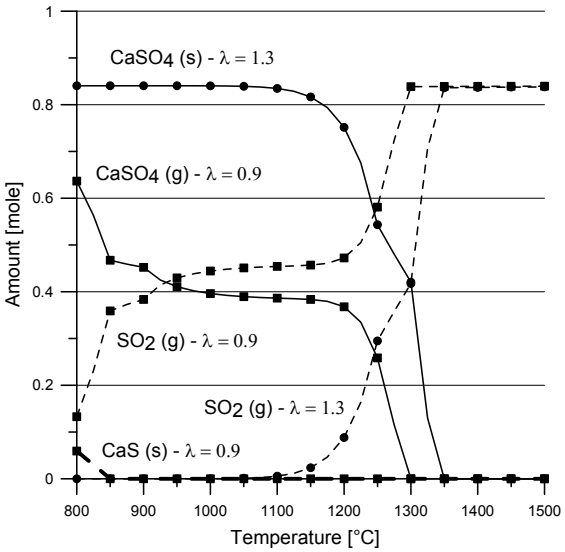

Figure 6-4: S distribution in calcined raw material. Gas atmosphere is either oxidizing with 5 vol-% O_2 ($\lambda = 1.3$) or reducing with 2 vol-% CO ($\lambda = 0.9$).

Through the equilibrium calculations it was also found that the phase distribution of Cl-containing compounds such as HCl, NaCl and KCl is not affected by the change in gas atmosphere: It remains the same whether the atmosphere is oxidizing or reducing. This result was also expected because Cl is known to be much more sensitive to temperature than to gas atmosphere (Locher and Klein, 2009).

The sulfur retention in the calcined cement raw materials will depend on the specific degree of reducing atmosphere. The equilibrium calculated sulfur retention under different atmospheres and in the temperature interval 700-1100°C is shown in Figure 6-5. This temperature interval is representative for the conditions in the material inlet end of cement rotary kilns, where fully or partly calcined raw materials enter the rotary kiln with a temperature of approximately 840-880°C and where the kiln flue gas leaves the rotary kiln with a temperature of approximately 1000-1100°C. It is observed that all sulfur is retained in the calcined raw material under oxidizing conditions with 5-21% O_2: These two curves are identical and at 100% sulfur retention in the temperature interval. Also under inert conditions with 0% O_2 the sulfur retention is observed to be 100%, except above 1050°C where a minor sulfur release is observed.
The sulfur release increases significantly when reducing conditions prevails. The sulfur release does not increase with increasing concentration of the reducing agent CO. Instead, the situation can be divided into mildly reducing conditions with 1-3% CO, and strongly reducing conditions with 4-10% CO. The sulfur release is observed to be most significant under mildly reducing conditions, where it accelerates at temperatures above 780°C. At 1% CO, a fraction of the sulfur is released due to reductive decomposition of $CaSO_4$. But most of the sulfur is still retained in the calcined raw

material. The thermodynamic calculations suggest that the sulfur is stabilized as K_2SO_4 and $K_2Ca_2(SO_4)_3$ at 1% CO. 2% CO is observed to lead to a high sulfur release, reaching 50% at 950°C. This is because the compound $K_2Ca_2(SO_4)_3$ is not stable under this reducing atmosphere, but at the same time the reducing atmosphere is not strong enough to stabilize sulfur as CaS. Thus phase equilibria are shifted towards free SO_2. The sulfur release is lower at 3% CO because this stronger reducing atmosphere favors formation of CaS. But the thermal stability of CaS decreases as the temperature increases, so at 1050°C the sulfur release reaches the same level as for 2% CO.
At strongly reducing conditions, 4-10% CO, the sulfur release is observed to be lower than under mild reducing conditions. Again, this is because sulfur is retained in the calcined raw material as CaS. But as the temperature increases and approaches 1100°C the sulfur release increases rapidly due to the thermal instability of CaS. These observations are in good correspondence with the phase diagram shown in Figure 6-3, which indicates that sulfur may be stabilized as either $CaSO_4$ at a low reducing potential or as CaS at a high reducing potential.

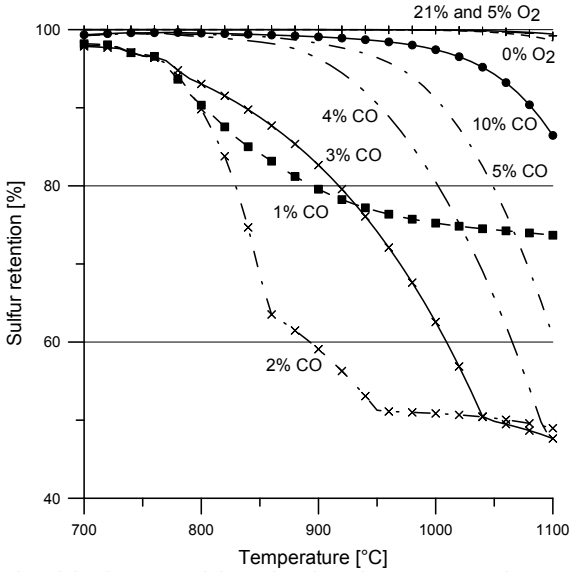

Figure 6-5: Sulfur retention in calcined raw material as a function of temperature and gas atmosphere. Note the cropped Y-axis.

6.3.4 Relative stability of sulfates towards reducing conditions

Sulfur introduced to the rotary kiln with the fully or partly calcined raw materials will mainly be in the form of sulfates, $CaSO_4$, Na_2SO_4 and K_2SO_4. The distribution is dependent on parameters such as concentrations of these individual elements, level of chlorine available to react with the alkali metals, temperature, etc. Since it is clear that the stability of sulfates is affected by the gas atmosphere, the relative stability of the sulfates $CaSO_4$, Na_2SO_4 and K_2SO_4 has been studied through equilibrium calculations.

Based on these equilibrium studies of the three dominating sulfates present in the kiln system, it is clear that reducing conditions generally shifts the equilibrium towards more SO_2 in the gas phase. The sulfates are used as an oxygen donor in the oxidation of CO to CO_2.
An interesting observation was that the relative stability of the sulfates was $Na_2SO_4 > K_2SO_4 >> CaSO_4$, an observation that is confirmed experimentally. $CaSO_4$ is thus less stable and more critical than the alkali sulfates. This observation may indicate that it is desirable to bind as much sulfur as possible as alkali sulfates, in order to keep the sulfur evaporation in the kiln system as low as possible. This has also previously been reported by e. g. Rosholm et al. (1998).

6.3.5 Concluding remarks about thermodynamic equilibrium calculations

Based on the thermodynamic equilibrium calculations it is clear that the stability of sulfates in the inlet to the rotary kiln is strongly affected by the gas atmosphere. Especially $CaSO_4$ tend to decompose at much lower temperatures under a reducing atmosphere. The alkali sulfates are also affected by a reducing atmosphere, but not as significant as $CaSO_4$.

The volatility of chlorine is not affected by the gas atmosphere, but is very sensitive to the temperature.

The equilibrium calculations indicate that high levels of alkali will help to minimize SO_2-release to the gas phase, by forming stable alkali sulfates. However, this result is only valid under equilibrium conditions, which are not necessarily present in the inlet to rotary kilns. It is possible that the alkali content in the raw material will have no, or little, effect on the sulfur volatility in the *inlet end* of the rotary kiln because the relative amount of calcium is much larger than the amount of alkali metals. Thus, formation of $CaSO_4$ is much more likely than formation of the more stable alkali sulfates.

6.4 Experimental

This section describes experiments made in order to improve the understanding of the inorganic chemistry in the material inlet end of cement rotary kilns. The first part is about laboratory scale experiments in a fixed bed tube furnace where SO_2 release from calcined raw material was studied at different temperatures, atmospheres and time intervals. The second part describes SO_2 release from raw materials under the influence of different solid fuels. These experiments with fuels are made in the high-temperature rotary drum described in chapter 5, section 5.3.2.

6.4.1 Release of SO_2 from calcined raw material

The release of sulfur from cement raw materials as a function of gas atmosphere was quantified in the temperature interval 900-1100°C. Different gas atmospheres were tested but most of the experiments were conducted with 5 vol.-% O_2 in N_2 to represent an oxidizing atmosphere and 2 vol.-% CO in N_2 to represent a reducing atmosphere. The temperature interval and gas atmospheres resemble realistic temperatures and atmospheres in the material inlet end of cement rotary kilns. The used cement raw materials were based on a mixture of pure chemicals of CaO, SiO_2, Fe_2O_3, Al_2O_3 and a sulfate such as $CaSO_4$, Na_2SO_4 or K_2SO_4. These chemicals were mixed in the right proportions to simulate a simplified calcined raw material, with a well-known content of sulfur. The compounds are also representative for the form that the elements has on entry into the rotary kiln.

6.4.1.1 Laboratory-scale tube reactor set-up

A laboratory-scale tube reactor set-up was used for the experiments. The experimental set-up is shown in Figure 6-6 and was found to be suitable for the experiments because it allowed a continuous gas flow passing a raw material sample. The set-up consists of a gas mixing panel to mix the gases in the desired concentration and flow, the electrically heated reactor in which the sample is placed, filters to remove particles and moisture, a pump and the analyzers that measure the gas concentration. Measured gas concentrations and temperatures are collected in a computer.

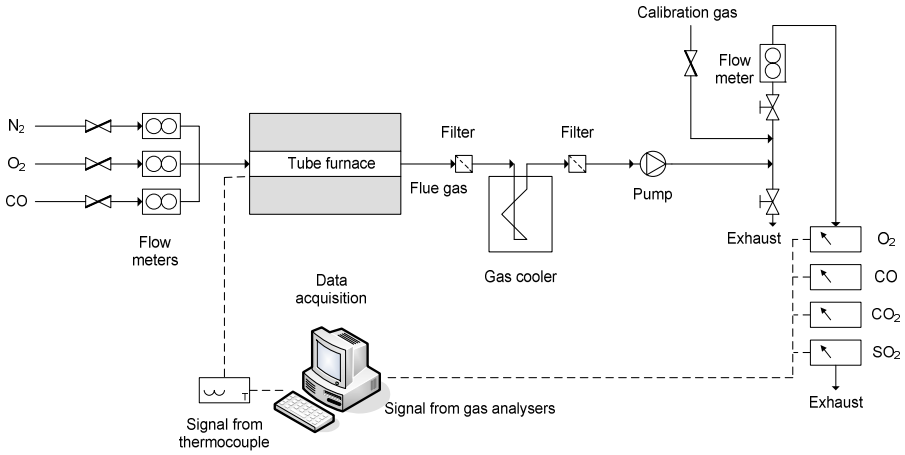

Figure 6-6: Tube reactor experimental set-up for investigation of SO_2 release from calcined cement raw materials.

The reactor depicted in Figure 6-7 is a two-zone electrically heated tube furnace in which a horizontal alumina tube is mounted, having water-cooled flanges at both ends. The tube furnace has

a maximum operating temperature of 1150°C. The internal diameter of the inner tube is 47 mm and it has a heated length of 900 mm. The sample is placed in a platinum/rhodium holder (95% Pt). The dimensions of the sample holder is HxWxL = 2x3x10 cm, corresponding to a volume of approximately 60 mL. During an experiment the sample holder is placed in the centre of the tube furnace, and the tube furnace is sealed with a stainless steel plate which contains an opening for gas inlet. The gas composition exiting the reactor is monitored on the computer. The sample will be heated from room temperature and up to the desired temperature by conduction, convection and radiation from the tube walls and gas.

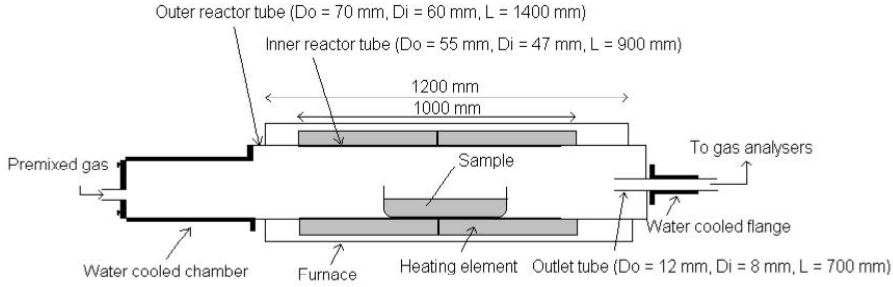

Figure 6-7: Sketch of the tube furnace reactor with size specifications of the reactor tubes (D_O = outer diameter, D_i = inner diameter, L = length).

In order to test whether the reactor set-up are producing stable and sufficient gas temperatures, center-line temperature profiles in the tube reactor were established. It is concluded that, at the position of the sample holder, the measured temperature corresponds fairly well with the reactor set point temperature.

6.4.1.2 Method

The composition of used calcined cement raw material is shown in Table 6-3. Only the main components, as well as a sulfur-containing component are included. The sulfur-containing component is $CaSO_4$, which is believed to be the dominant sulfur-containing component in calcined raw material entering cement rotary kilns, due to the excessive amounts of calcium relative to alkali metals. It should be noted that the sulfur content in the calcined raw material is relatively high (1.17 wt-%), but not unrealistic. Prior to the experiments, the synthetic calcined raw material was stored under an inert atmosphere to prevent CaO from reacting with moisture or atmospheric CO_2.

Component	Amount (wt-%)
CaO	67
SiO_2	20
Al_2O_3	5
Fe_2O_3	3
$CaSO_4$	5

Table 6-3: Composition of calcined raw material used for the experiments.

The following procedure is followed during each experiment:
5 g of the calcined raw material sample is placed in a well distributed layer in the sample holder. The sample amount is chosen to have a suitable amount of sulfur in the experiments in order to

detect sulfur releases in the ppm range 0-1000 ppm. The sample container is then placed in the tube furnace at the desired temperature. The tube furnace is sealed and the sample is heated for 10 minutes in an oxidizing atmosphere of 5% O_2 in N_2. Practically no SO_2 release was observed under the 10 minutes heating time indicating that $CaSO_4$ is stable under this oxidizing atmosphere. After 10 minutes, the gas atmosphere can be changed to the desired atmosphere whereby the experiment begins. The gas flow is maintained at 10 NL/min at all times. The gas composition is logged for subsequent evaluation of the sulfur release. In all experiments, the sulfur release was measured by integrating the SO_2-signal over time. The experiments always lasted 30 minutes, including 10 minutes heating time and 20 minutes experimental time.

In addition to the fixed gas atmosphere, experiments were also conducted with alternating gas atmosphere between oxidizing and reducing. In these experiments, two-minute intervals were used: 2 minutes with reducing conditions (2 vol.-% of the reducing agent in nitrogen) followed by 2 minutes with oxidizing conditions (5 vol.-% O_2 in N_2). This procedure was repeated over 20 minutes, which involved 5 reducing intervals and 5 oxidizing intervals.

6.4.1.3 Assumptions and uncertainties

This section discusses important assumptions and uncertainties that may influence the obtained results.

1. It has been experimentally determined that the sample is heated for approximately 2-5 minutes in the tube furnace before the sample reaches the same temperature as the tube furnace. The exact heating time depends on the sample size and temperature to be reached; a 5 g sample, which is the sample size used in the experiments, uses approximately 2 minutes to reach 900°C. In order to ensure sufficient time for sample heat up, the sample will stay 10 minutes in the furnace under oxidizing conditions before an experiment is started.

2. The gas passing through the reactor will be pure $N_2/O_2/CO/H_2/CH_4$ in different compositions. Under industrial scale conditions, the gas will also contain H_2O, CO_2, NO_x, SO_x and various volatile species such as alkali metals or trace metals. It is a foregone conclusion that the simplified gas composition used in the experiments contains the most important components, and that the other components' influence on the results can be neglected.

3. The uncertainty on the O_2, CO and CO_2 analyzers are +/- 2% of total span range of each species while it is +/- 5% of total span range on the SO_2 measurement. These uncertainties should be kept in mind when evaluating the results.

4. It is a foregone conclusion that all sulfur released from the sample will form SO_2 before leaving the reactor. This assumption has been confirmed by two mass balances over two different calcined raw material samples: After an experiment, the residual sulfur content of the sample was determined by chemical analysis and compared to the sulfur amount that was found in the flue gas as SO_2. In the first case, the sulfur mass balance was found to be 93% and in the second case, 95% of the sulfur was found in either the sample or in the flue gas as SO_2. Considering the uncertainties with sample composition, precision of analyzers and mass flow controllers, as well as the accuracy of the chemical analysis procedure, it is

fairly safe to assume that nearly all released sulfur will be in the form of SO_2. This assumption is also confirmed by equilibrium calculations with the thermodynamics software FactSage, which calculated that nearly all sulfur is present as SO_2 under the studied conditions.

5. It is known from preliminary experiments that the physical shape of the sample holder and sample mass will cause diffusion limitation of gas components such as CO to the sample. However, since all experiments are made with similar sample masses and procedures, it is a foregone conclusion that results will be comparable.

6. The flue gas composition will not change significantly in the distance between the reactor and the analyzers. To minimize this uncertainty and prevent e.g. SO_2 absorption in filters and condensers, these parts were regularly cleaned or replaced to minimize presence of compounds able to absorb SO_2. A gas with known content of SO_2 was also regularly sent through the system to test if any SO_2 was absorbed before reaching the analyzers.

7. The calcined raw material to be used in the experiments is representative for calcined raw material from an industrial plant. However, an industrial calcined raw material will contain many minor components which could have an effect on results.

6.4.1.4 Results and Discussion

Figure 6-8 shows an example of the measured concentrations during an experiment with alternating oxidizing and reducing conditions at 1100°C. The first 10 minutes is the heating period under oxidizing conditions, initially atmospheric air with 21% vol.-% O_2 followed by 4.75 vol.-% O_2 in N_2 when the tube reactor is sealed. During the heating under oxidizing conditions, no SO_2 is observed. After 10 minutes, the gas concentration is changed to 2 vol.-% CO in N_2. Since the change is rapid, some oxygen will be left in the reactor and will react with CO, forming CO_2. Thus, the CO_2-concentration is observed to increase to approximately 1.5 vol.-%. After the last O_2 in the reactor is consumed, the CO-concentration increases to approximately 1.8 vol.-%. At the same time, a dramatic increase in the SO_2-concentration is observed: From 0 ppm and up to 800 ppm. The formed CO_2 is also observed at a level of around 0.2 vol.-%. The SO_2-level drops relatively fast. When the atmosphere is again changed to oxidizing (4.75 vol.-% O_2), a new, smaller SO_2-peak is observed. The sulfur release cycle is observed to be repeated for each of the following reducing/oxidizing intervals, with a slight decrease in the SO_2 each time, because the sulfur content in the sample gradually decreases. The experiment is stopped after 30 minutes when the fifth oxidizing interval is finished and the SO_2-concentration has dropped to values close to 0 ppm. However, it should be noted that more sulfur would be released from the sample if the cycles were repeated: This was tried out and it can be concluded that the measured SO_2-level gradually decreases with time, but that it takes more than two hours before all sulfur has been released from the sample.

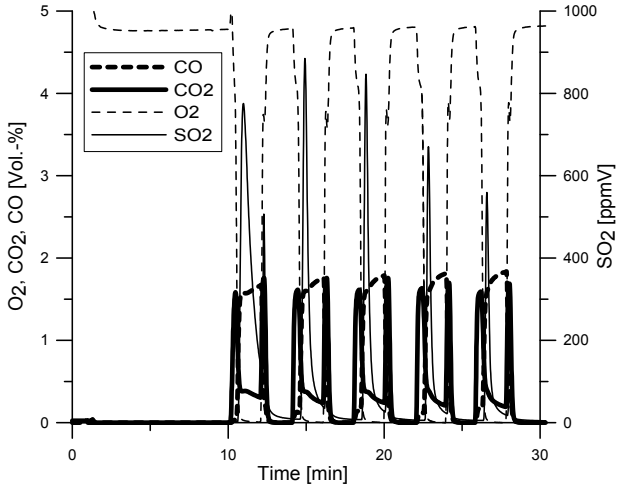

Figure 6-8: Concentrations of SO_2, O_2, CO and CO_2 during an experiment with calcined raw material under alternating oxidizing and reducing conditions. 1100°C, 10 NL/min. 20 minutes of reaction time.

It is interesting to note from Figure 6-8 that the first SO_2-peak during the reductive decomposition of $CaSO_4$ only reaches 780 ppm while the next SO_2-peak reaches 890 ppm. The first SO_2-peak is also wider than subsequent SO_2-peaks. This tendency was observed in all experiments with alternating reducing and oxidizing conditions. The same tendency has also been reported by other researchers (Wheelock and Boylan, 1960, Ghardashkhani et al., 1989, and Hansen et al., 1991). The reductive decomposition of $CaSO_4$ is initiated by an induction period which has been explained by slow desorption of SO_2 and slow rate of nucleation of CaO. Ghardashkhani et al. (1989) reported that shifting from reducing to oxidizing and back to reducing conditions during reductive decomposition of $CaSO_4$ did not give rise to a new induction period. This is in agreement with the experimental observations where the second SO_2-peak reaches larger values than the first SO_2-peak.

The characteristic SO_2-peaks observed from Figure 6-8 during alternating reducing and oxidizing conditions can be explained by the existence of phase equilibria between different sulfur species: Under oxidizing conditions sulfur is stabilized in the form of $CaSO_4$ and under reducing conditions, sulfur is partially stabilized as CaS. When the gas atmosphere changes, sulfur may be released to the gas phase as SO_2, as illustrated in Figure 6-2.

Release quantification

The release of sulfur during the experiments is calculated by integration of the gas concentration of SO_2 over the relevant time interval:

$$n_{\text{Sulfur found}} = \int_0^t y_{SO_2} dt \cdot 10^{-6} \cdot \frac{PV}{RT} \qquad (6.8)$$

where y_{SO2} is in ppmV and V is the gas flow in L/s. It should be noted that due to diffusion limitation of gas components such as CO, only experiments made with similar sample masses can be compared. The sum of sulfur found as SO_2 is divided by the total sulfur amount in the sample:

$$\text{S release} = \frac{n_{\text{sulfur found}}}{n_{\text{sulfur in sample}}} \cdot 100\% \qquad (6.9)$$

Effect of reducing atmosphere with CO

The sulfur release from calcined raw material has been studied at temperatures of 900°C, 1000°C and 1100°C. Two different atmospheres with 5% O_2 and 2% CO (pure nitrogen is the balance in both cases) as well as alternating reducing and oxidizing conditions has been studied. The results are shown in Figure 6-9. Under oxidizing conditions with 5% oxygen, the S release is approximately 0% in the studied temperature interval. This result has been found to be valid at all oxygen concentrations from 1% to 21%, indicating that $CaSO_4$ is generally stable under oxidizing conditions and temperatures below 1100°C. This finding is in agreement with the thermodynamic equilibrium calculations which did not show any decomposition of $CaSO_4$ below 1150°C.
Under reducing conditions with 2% CO, the sulfur release was still approximately 0% at 900°C, but increased to 17% at 1000°C and 19% at 1100°C. This significant increase in sulfur release under reducing conditions may be explained by the formation of CaS from $CaSO_4$ in which CaO and free SO_2 are reaction intermediates. Each experiment was repeated three times and the standard deviation was found to be +/- 2%.
Under shifting oxidizing and reducing intervals with 2 minutes of 2% CO followed by 2 minutes of 5% O_2 continuously repeated 2 · 5 times, the sulfur release is observed to be significantly higher than under constant reducing or oxidizing conditions: 14% at 900°C, 40% at 1000°C and 48% at 1100°C. Each experiment has been repeated three times and the standard deviation were found to be +/- 3%. This strong effect of alternating oxidizing and reducing conditions is in correspondence with the sulfur transformation cycle shown in Figure 6-2: Under oxidizing conditions sulfur is stabilized as $CaSO_4$ and under reducing conditions sulfur is stabilized as CaS. Every shift in atmosphere leads to formation of CaO and free SO_2. Formation of SO_2 is particularly large at higher temperatures, whereas the lowest temperature of 900°C can limit the sulfur release even under alternating oxidizing and reducing conditions.

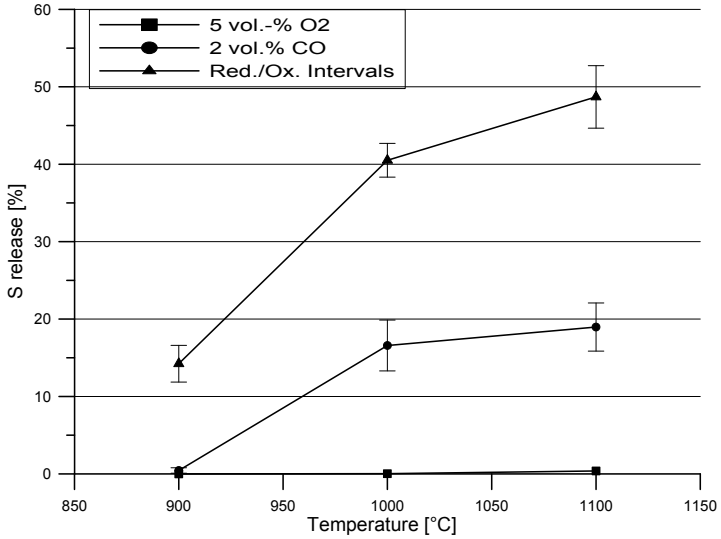

Figure 6-9: Effect of gas atmosphere on the sulfur release from calcined raw material. Sulfur release evaluated after 20 minutes of reaction time.

The results are in correspondence with previous work where sulfur release and capture have been studied under alternating oxidizing and reducing conditions: Lyngfelt and Leckner (1989) reported a decrease in the sulfur capture ability of limestone at temperatures above 880°C and reducing conditions, due to reductive decomposition of $CaSO_4$. Hansen et al. (1993) found that the competition between sulfur capture and sulfur release under alternating oxidizing and reducing conditions were shifted towards more sulfur release when the temperature increased. Tarelho et al. (2005) found a maximum sulfur capture efficiency of limestone at around 825°C. Higher temperatures reduced the sulfur capture efficiency, particularly under reducing conditions.

Effect of other reducing agents

Most investigations of reductive decomposition of $CaSO_4$ reported in literature use either CO or H_2 as reducing agent. Since combustion of alternative fuels in cement kilns may lead to formation of significant amounts of CO, H_2 and hydrocarbons such as CH_4 under sub-stoichiometric conditions, these three reducing agents have been investigated with respect to sulfur release from calcined raw material in the temperature interval 900-1100°C. The results are shown in Figure 6-10. The experimental conditions were shifting oxidizing and reducing intervals with 2 minutes of the reducing agent (2% of either CO, H_2 or CH_4) followed by 2 minutes of 5% O_2. The two-minute intervals were continuously repeated 2 · 5 times, thus 20 minutes of total reaction time. All experiments were repeated three times with a standard deviation in the order of 3%. Under these reaction conditions, the sulfur release when CO was used were 14%, 40% and 48% at 900°C, 1000°C and 1100°C, respectively. When CH_4 was used, the sulfur release was 6%, 40% and 17% at 900°C, 1000°C and 1100°C, respectively. And finally, when H_2 was used, the sulfur release was 8%, 27% and 20% at 900°C, 1000°C and 1100°C, respectively.

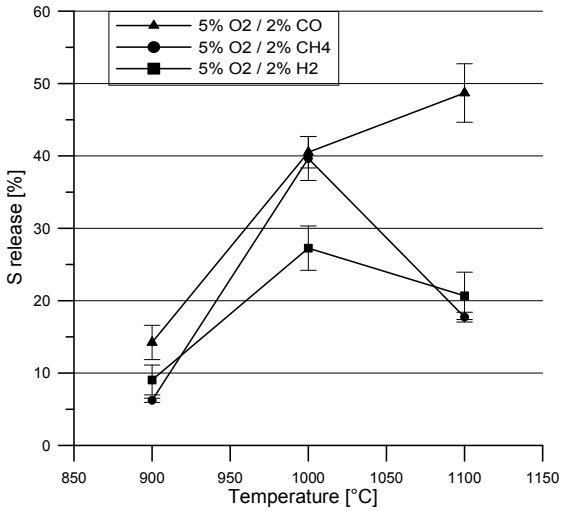

Figure 6-10: Effect of reducing agent on sulfur release from calcined raw material under alternating oxidizing and reducing conditions. Sulfur release evaluated after 20 minutes of reaction time.

While the results with CO are observed to lead to increased sulfur release as a function of temperature, the results with H_2 and CH_4 are more surprising: The sulfur release increases from 900°C to 1000°C but then decreases again at 1100°C. This was unexpected since it was assumed

that the sulfur release would increase with temperature regardless of the reducing agent. It was also expected that H_2 would lead to a higher sulfur release than CO, and CH_4 would lead to a much lower sulfur release than CO, according to Hansen's findings: Hansen (1993) found that the rate of reductive decomposition of $CaSO_4$ increased when H_2 was used instead of CO, and that CH_4 gave no reductive decomposition at all. However, the reaction conditions used in Hansen's experiments were quite different from the ones used in this investigation, since he used relatively short time intervals of 30 s / 30 s and only studied the effect of reducing agent at 850°C. In this experiment, longer time intervals of 2 min / 2 min were used and the temperature interval was 900-1100°C. This may explain why CH_4 is found to be of comparable efficiency as H_2 and CO in this investigation, while Hansen reported it to be less efficient due to slower reaction kinetics.
Regarding the lower sulfur release at 1100°C relative to 1000°C when H_2 and CH_4 were used as reducing agents, similar results have been reported by Kamphuis et al. (1993): At temperatures above 950°C, a fraction of the SO_2 was observed to be converted to H_2S which was not detected by the analysis system, when the flue gas contained H_2. Based on a series of tests with known SO_2 concentrations in a H_2/N_2 gas mixture passing through the reactor without a sample, Kamphuis et al. established a correction factor to correlate for the formed H_2S. It is likely that the same phenomenon took place in the present experiments with H_2 and CH_4 since H_2S can be formed from both reducing agents. This will explain why the found sulfur release is lower at 1100°C relative to at 1000°C. Prior to the experiments, thermodynamic equilibrium calculations had been made for the calcined raw material exposed to the reducing agents H_2 and CH_4. These thermodynamic calculations indicated that practically all released sulfur would be present as SO_2 under the experimental conditions. However, the thermodynamic calculations may be misleading since they do not consider reaction kinetics: H_2S may be formed as an intermediate species which leaves the reactor before formation of SO_2 has occurred. A sulfur mass balance should be performed in order to determine whether some sulfur has escaped from the system as H_2S or not. Since a sulfur mass balance has not been conducted for the experiments with H_2 and CH_4 it is not directly possible to quantify the effect on sulfur release as a function of the reducing agent. However, the results do indicate that all three reducing agents CO, CH_4 and H_2 have an effect on the sulfur release in the studied temperature interval.

6.4.1.5 Conclusions for sulfur release from calcined raw materials

The release of sulfur from cement raw materials under both oxidizing and reducing conditions were investigated. The investigated conditions resemble actual conditions in the material inlet end of cement rotary kilns, where local reducing conditions may occur during combustion of solid, alternative fuel particles and where solid/gas temperatures are usually between 900°C and 1100°C. The following results were obtained:

- Experimentally, a clear tendency for increasing sulfur release was observed when the gas atmosphere shifted from oxidizing to reducing: No sulfur release was observed under oxidizing conditions (5 vol.-% O_2), whereas the sulfur release increased to 19% under reducing conditions (2 vol.-% CO) at 1100°C. The sulfur release was particularly significant if the calcined raw material was exposed to alternating oxidizing and reducing conditions, which led to a sulfur release of 48% at 1100°C.
- The sulfur release from calcined raw material was observed to be dependent on the temperature: Under alternating oxidizing and reducing conditions, the sulfur release was observed to be 14% at 900°C and 48% at 1100°C.

- Sulfur release from calcined raw material was shown to take place in the presence of any of the reducing agents CO, H_2 and CH_4. However, it was not possible to directly quantify the sulfur release as a function of the reducing agent, because part of the released sulfur from the experiments with H_2 and CH_4 presumably formed H_2S which could not be detected by the analysis system.

6.4.2 Sulfur release from raw materials during combustion of solid fuels

The purpose of the experiments is to clarify how the sulfur release in the form of SO_2 is affected by different solid fuels. The release of sulfur from cement raw materials as a function of fuel type and fuel characteristics was quantified in the temperature interval from 700°C to 1000°C and at oxygen concentrations from 5 vol.-% O_2 in N_2 to 21 vol.-% O_2 in N_2. The temperature interval and oxygen concentrations up to 10 vol.-% resemble realistic material temperatures and atmospheres in the material inlet end of cement rotary kilns. The cement raw materials used were based on a synthetic mixture of quartz sand and 5 wt.-% calcium sulfate, $CaSO_4$. This represents a simplified batch of cement raw material entering the rotary kiln, but with realistic sulfur content. Quartz sand was used for practical reasons, as explained in section 5.4.1.

6.4.2.1 Experimental set-up and method

The experiments are made in the high-temperature rotary drum experimental set-up described in chapter 5, section 5.3.2.

2.5 kg of raw material in the form of quartz sand with 5 wt.-% $CaSO_4$ is placed in the rotary drum. This corresponds to a volumetric fill degree of 5%. The drum is rotated with 6 rotations per minute in order to keep the raw material in a continuous rolling motion. The raw materials are then preheated to the desired temperature, in the interval from 700°C to 1000°C. A constant flow of 100 NL/min of gas with the desired oxygen concentration is transported through the rotary drum and will pass over the raw materials in the lower part of the rotary drum. The gas has been preheated to the same temperature as the raw materials in order to obtain a uniform temperature at all positions. The temperature and oxygen concentration are monitored continuously, and when these have stabilized, a batch of solid fuel will rapidly be added into the raw materials in the rotary drum. SO_2-, O_2-, CO- and CO_2-concentrations are measured during the devolatilization and char combustion. The gas composition is logged for subsequent evaluation of the sulfur release. In all experiments, the sulfur release was measured by integrating the SO_2-signal over time.
Since many of the fuels contain sulfur that will also be released during the experiments, baseline experiments have been made, where the fuels are combusted in 2.5 kg of *pure* quartz sand, *without* $CaSO_4$. The measured SO_2 from the baseline experiments can only arise from the fuels and not from the raw material. The amount of sulfur released during the baseline experiments is subtracted from the sulfur released during the actual experiment in order to get the amount of sulfur that arises from the raw material.
All experiments were repeated at least two times to ensure the repeatability. The sulfur release values reported in the figures are the average values from the experiments. These values have been corrected for the sulfur contribution from the fuels.
Five different solid fuels have been studied; tire rubber, pine wood, polypropylene, petcoke and sewage sludge. In order to compare the sulfur release caused by each fuel with each other, the amount of fuel is chosen to obtain the same energy input. Fuel proximate and ultimate analyses as well as lower heating values are shown in Table 6-4. The lower heating values for the fuels are

quite different. Thus quite different fuel sample amounts have been used in order to have the same energy input in each experiment, regardless of the fuel. The energy input during the experiments were chosen to be in the interval 15 to 50 kJ per batch, corresponding to fuel sample sizes from 0.3 g to 4.2 g. These energy inputs were chosen to obtain a suitable level of sulfur release, thereby avoiding SO_2-peaks exceeding the analyzer range.

	Proximate analysis			**Ultimate analysis**				**LHV**
	VM	FC	Ash	C	H	N	S	MJ/kg
Tire rubber	64.6	32.6	2.8	87.4	7.1	0.3	1.2	36.9
Pine wood	75.3	24.5	0.2	38.9	5.2	0.1	-	16.2
Polypropylene	97.5	0.0	2.5	83.0	14.0	0.0	-	44.5
Petcoke	13.4	85.1	1.5	87.3	3.7	1.5	4.7	34.0
Sewage sludge	49.3	0.5	50.2	29.0	3.8	3.8	1.0	12.5

Table 6-4: Fuel analyses and lower heating values (LHV) for solid fuels used in the experiments. Units are in wt.-% as received and MJ/kg.

Several different fuel particle sizes and shapes have been used in the experiments, and these are presented in Table 6-5.

Fuel	**Shape**	**Dimensions**
Tire rubber granulate	Irregular	$D_p \approx 2$ mm
Tire rubber cylinders	Cylindrical	L = 12 mm, D_p = 9 mm
Pine wood cubes	Rectangular	Thickness ≈ 10 mm
Pine wood saw dust	Needles	Thickness ≈ 1 mm
Polypropylene flakes	Rectangular	Thickness ≈ 1 mm
Petcoke	Spherical	$D_p \approx 1$ mm
Sewage sludge	Spherical	$D_p \approx 0.5$ mm

Table 6-5: Approximate shapes and dimensions of the fuels used in the experiments.

6.4.2.2 Assumptions and uncertainties

This section discusses important assumptions and uncertainties that may influence the obtained results.

1. The temperature at which the experiment is conducted is determined as the measured temperature in the center of the rotary drum, above the raw material charge. It is a foregone conclusion that the gas temperature and raw material temperature is the same at all positions in the rotary drum. Temperature profiles have been measured at various positions in the rotary drum, and the temperature was found to deviate no more than +/- 15°C.

2. The experiments are conducted in the temperature interval from 700°C to 1000°C whereas the raw material and gas temperatures in the material inlet end of modern industrial cement rotary kilns are often in the interval 900°C to 1200°C. The temperature interval is thus only partly representative for the industrial conditions. However, it is not possible to conduct experiments above 1000°C in the used experimental set-up.

3. The gas passing through the rotary drum will be pure N_2 and O_2 in different compositions. During the devolatilization and char combustion, a fraction of the O_2 will be consumed, and the ultimate combustion products H_2O, NO, SO_2, CO and CO_2 will be formed. In addition some intermediate combustion products such as CH_4 or higher hydrocarbons, alkali species, etc. may be formed. Under industrial scale conditions, the gas will also contain the combustion products from the main kiln burner and may have an overall gas composition different from the one used in these experiments. This difference in gas composition is likely to affect the sulfur release, which is not only influenced by oxygen concentration but also by the presence of reducing agents.

4. The uncertainty on the O_2, CO and CO_2 analyzers are +/- 2% of span range for each species while it is +/- 5% of span range on the SO_2 measurement. These uncertainties should be kept in mind when the results are evaluated.

5. It is a foregone conclusion that all sulfur released from the sample will be oxidized to SO_2 before leaving the reactor. This assumption has been supported by equilibrium calculations with the thermodynamics software FactSage, which calculated that nearly all sulfur is present as SO_2 under the studied conditions.

6. The physical shape of the rotary drum reactor may cause diffusion limitation of oxygen to the fuel particles. However, since all experiments are made under similar conditions, it is a foregone conclousion that the results will be comparable.

7. The flue gas composition will not change significantly in the distance between the reactor and the analyzers. To minimize this uncertainty and prevent e.g. SO_2 absorption in filters and condensers, these parts were regularly cleaned or replaced to minimize presence of compounds able to absorb SO_2. A gas with known content of SO_2 was also regularly sent through the system to test if any SO_2 was absorbed before reaching the analyzers.

6.4.2.3 Results and discussion

General observations

Figure 6-11 shows an example of the flue gas composition during combustion of tire rubber granulate at an initial oxygen concentration of 10 vol.-%. When the devolatilization starts, the O_2-concentration drops to approximately 7 vol.-% and the CO_2-concentration increases to nearly 4 vol.-%. The CO-concentration also increases shortly to around 600 ppm. The change in flue gas composition is followed by a rapid increase in the SO_2-concentration from 0 ppm to around 2,500 ppm. The SO_2-concentration then gradually decreases towards 0 ppm again, as the CO/CO_2-concentrations gradually decrease.

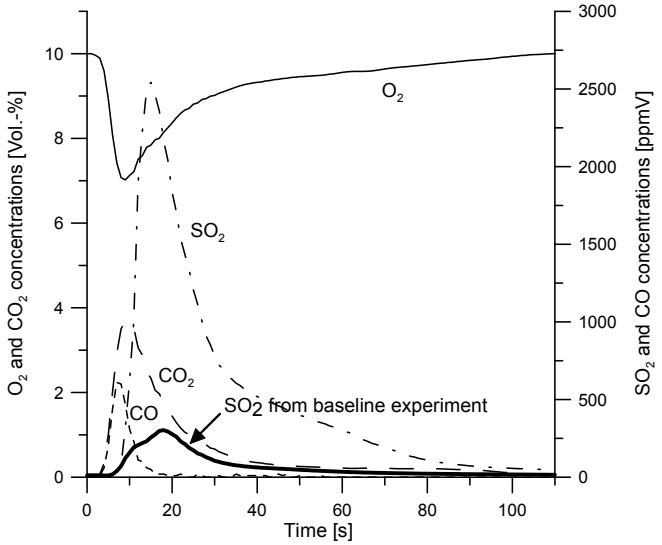

Figure 6-11: Concentrations of O_2, CO_2, CO and SO_2 during an experiment with 0.81 g tire rubber granulate corresponding to an energy input of 30 kJ. 900°C, 5% fill, 6 rpm, 100 NL/min, 10% O_2.

The sulfur release from the tire rubber and raw material is observed to begin almost immediately, during the fuel heat-up and devolatilization. This is in correspondence with the work of Díez et al. (2004) who reported that the C-S bonds in TDF will break at temperatures above 200ºC and form either H_2S or SO_2. However, baseline experiments with fuel combustion in pure quartz sand *without* $CaSO_4$ shows that only a minor fraction of the sulfur release arises from fuel-bound sulfur: Most of the sulfur is released from the raw materials, which is also shown in Figure 6-11. The reason is believed to be due to the formation of local reducing conditions near the raw material charge during fuel devolatilization which leads to reductive decomposition of $CaSO_4$. The tendency for a rapid sulfur release during fuel devolatilization was observed for all experiments regardless of the fuel.

Effect of energy input and fuel type

The sulfur release from the raw material as a function of the energy input, has been studied for five different fuels at 900°C and 10 vol.-% oxygen. The fuels were polypropylene flakes, petcoke, pine wood saw dust, tire rubber granulate and sewage sludge, see Table 6-4 and Table 6-5 for details. These fuels all have relatively similar average particle thicknesses in the interval 0.5-2.0 mm. The results are shown in Figure 6-12. For all tested fuels it is observed that the sulfur release from the raw materials increases as the energy input increases. It is also observed that the sulfur release is quite different depending on the specific fuel: tire rubber granulate and sewage sludge leads to the highest sulfur release while pine wood saw dust, petcoke and polypropylene all leads to a lower sulfur release.

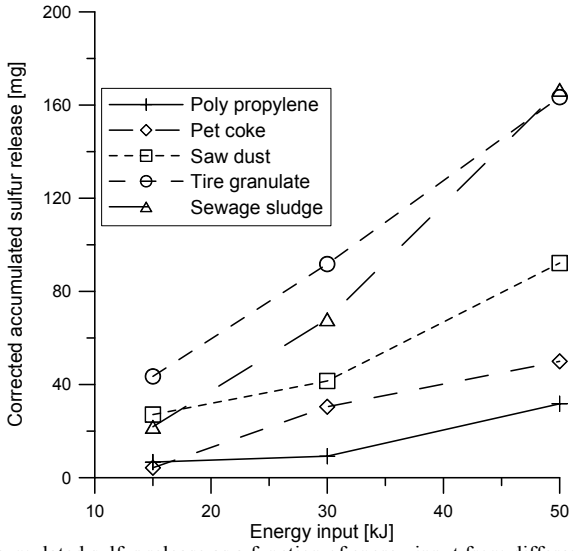

Figure 6-12: Corrected accumulated sulfur release as a function of energy input from different fuels. 900°C, 10 vol.-% O_2, 5% fill, 100 NL/min, 6 rpm.

The reason why the sulfur release increase when the energy input increases becomes clear when the flue gas compositions at each individual experiment are compared with each other: The larger the energy input, the higher the rate of decrease of oxygen concentration will be during fuel devolatilization, while both CO and CO_2 concentrations increase, thereby forming a higher degree of reducing conditions near the raw material charge. In addition, local temperatures in the bed are likely to increase when the energy input increases. Higher local temperatures may also cause an increase in sulfur release, see section 6.4.2.3.3.

The large differences in sulfur release for identical energy inputs but by different fuels are interesting. A detailed study of the flue gas concentration for each fuel type has not revealed any clear trends about degree of reducing conditions and sulfur release. The reason is probably that the exact particle sizes, shapes, densities, fuel combustion pathways and kinetics of the studied fuels are quite different and that this also has an effect on sulfur release. The approximately spherical tire rubber granulate and sewage sludge particles may for example lead to a high sulfur release because of a relatively fast devolatilization combined with a high degree of mixing with the raw material. The needle shaped saw dust particles gives a lower sulfur release than tire rubber granulate and

sewage sludge despite the fact that the saw dust also has a fast devolatilization. An explanation could be that the saw dust particles are less dense than the tire rubber and sewage sludge and that the density difference leads to a low degree of mixing of saw dust into the raw material. The polypropylene flakes have the lowest sulfur release which may be explained by a very fast devolatilization; so fast that the polypropylene devolatilization ends before it has been well mixed into the raw material. Finally, the small petcoke particles are a slow burning fuel with a volatile content of only 13%. This leads to a relatively small decrease in oxygen concentration during the fuel conversion compared to the other fuels and thereby a low degree of local reducing conditions near the raw material bed.

Effect of temperature and fuel particle size

The sulfur release is studied as a function of the temperature and fuel particle size, which is important for the devolatilization and char combustion times. Tire rubber and pine wood are used in these investigations about particle size while the investigations about temperature also include petcoke and polypropylene. The tire rubber is studied as one cylinder versus tire rubber granulate and the pine wood is studied as one pine wood particle versus saw dust. The overall energy input is the same in each experiment. Details about the fuels can be found in Table 6-4 and Table 6-5. The results are shown in Figure 6-13 with sulfur release in mg versus temperature for the different fuel particle sizes. It is observed that influence of the fuel particle size on the sulfur release at 700°C and 800°C is insignificant whereas the influence becomes more evident at 900°C and, in particular, at 1000°C: At 900°C and 1000°C the saw dust and tire granulate lead to a higher sulfur release than for the wood particle and tire particle.

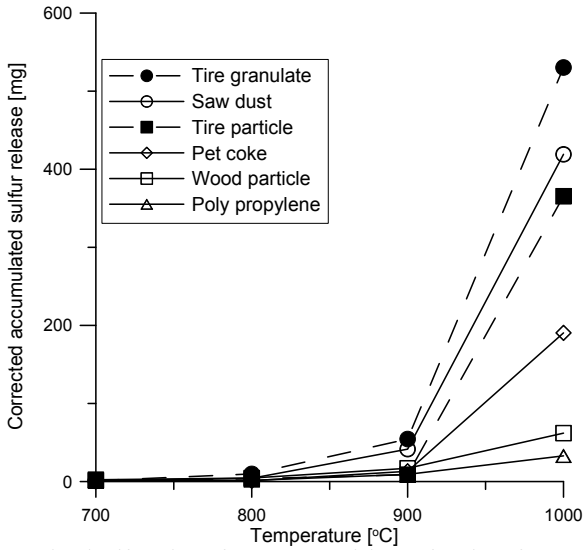

Figure 6-13: Corrected accumulated sulfur release from raw materials as a function of temperature and fuel particle size. 5% fill degree, 10 vol.-% O_2, 100 NL/min, 6 rpm. Energy input in each experiment: 30 kJ. The sulfur release from the experiments with tire granulate and saw dust at 1000°C has been estimated because the SO_2-concentration exceeded the analyzer range for these specific experiments.

The significant effect of temperature on the sulfur release was also to be expected based on the thermodynamic equilibrium calculations (see section 6.3), due to the lower thermal stability of

$CaSO_4$ at higher temperatures. In addition, a comparison of the flue gas compositions during the combustion at different temperatures shows that the CO-concentration during fuel devolatilization reaches higher values at higher temperatures than at lower temperatures. The reason is likely to be a faster release of volatiles from the fuel particles at elevated temperatures which will increase the tendency for local reducing conditions in the area around the fuel particles. This higher tendency for local reducing conditions is likely to contribute to increase the sulfur release during the fuel devolatilization.

The reason for the difference in sulfur release for different fuel particle sizes becomes clear when the flue gas composition is studied for the individual experiments: The larger total surface areas of the smaller fuel particles lead to a fast devolatilization and thus a fast release of volatiles. This leads to significantly higher CO-concentrations and thus a higher reductive decomposition of $CaSO_4$ during devolatilization. An example is illustrated in Figure 6-14 which show flue gas compositions during wood particle and saw dust combustion, respectively, at 1000ºC. At the wood particle combustion, the CO-peak during devolatilization reaches 180 ppm and the SO_2-peak reaches 1350 ppm. At the saw dust combustion, the CO-peak is significantly larger and reaches 27000 ppm (2.7 vol.-%) which leads to a SO_2-peak well above the analyzer detection range of 3500 ppm. The changes in O_2-concentration are from the initial 10 vol.-% to 5 vol.-% for the saw dust and to 7 vol.-% for the pine wood particle. Similar trends were observed for the experiments with one tire particle versus tire granulate.
Since the experiments with saw dust and tire granulate at 1000°C led to SO_2-peaks well above the SO_2-analyzer range, it has been necessary to estimate the total sulfur release from these two experiments. This induces some uncertainty on the exact amount of released sulfur in these two cases at 1000°C.

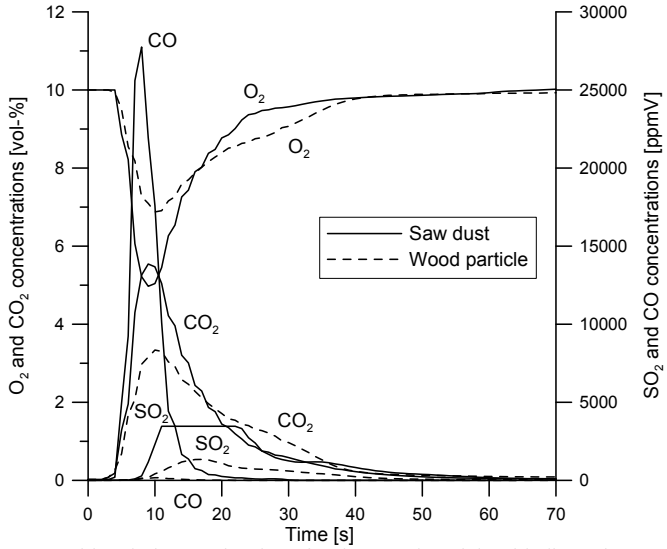

Figure 6-14: Flue gas composition during combustion of a pine wood particle with dimensions 30x15x10 mm and pine wood saw dust with particle size < 1 mm. 10 vol.-% O_2, 5% fill degree, 1000°C, 100 NL/min, 6 rpm.

Figure 6-15 shows the sulfur release versus the total surface area of the fuel particles tire rubber and pine wood at 900°C. The sulfur release is observed to increase approximately linearly as a function

of surface area for tire rubber. The sulfur release for pine wood is less significant than for tire rubber but also may also be characterized as linear as a function of surface area. The large difference in sulfur release between pine wood and tire rubber for the same surface area may be due to factors such as devolatilization rate of the fuels and density. These factors are likely to affect to what extent the raw materials will be exposed to local reducing conditions during fuel combustion. But it is required to explore the reasons in greater details before any clear conclusions can be made.

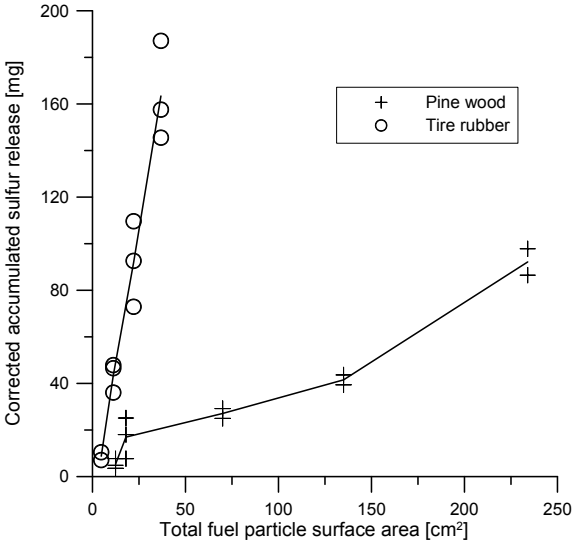

Figure 6-15: Corrected accumulated sulfur release versus the total surface area of pine wood and tire rubber fuel particles. 900°C, 10 vol.-% O_2, 5% fill degree, 6 rpm, 100 NL/min.

Effect of bulk oxygen concentration

The sulfur release has been studied as a function of the inlet oxygen concentration in the freeboard gas above the raw material bed. The investigation has been conducted with polypropylene, petcoke, pine wood cubes and tire rubber granulate, see Table 6-5 for details. The results are shown in Figure 6-16 with the sulfur release expressed in mg pure sulfur versus the oxygen concentration expressed in vol.-%. It is observed that the sulfur release increases for all tested fuels when the oxygen concentration decreases. Particularly the tire rubber granulate leads to an increase in sulfur release of nearly a factor 8 when the oxygen concentration changes from 21 vol.-% O_2 to 5 vol.-% O_2.

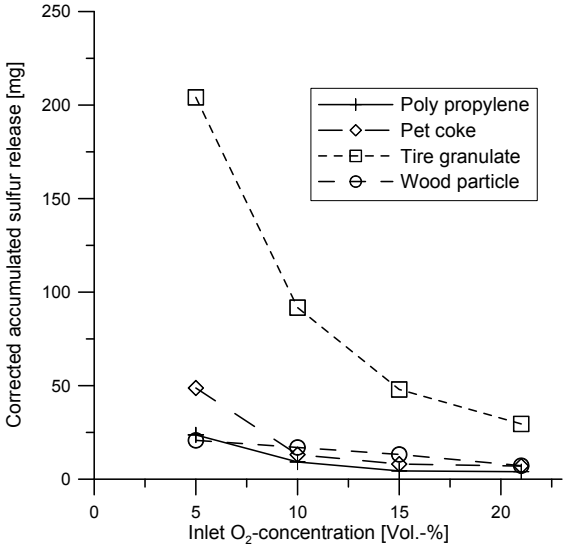

Figure 6-16: Corrected accumulated sulfur release as a function of inlet oxygen concentration for four different fuels. 5% fill degree, 900°C, 100 NL/min, 6 rpm. Energy input in each experiment: 30 kJ.

The reason for this high dependency of the oxygen concentration on the sulfur release becomes clear when considering the changes in flue gas composition. Figure 6-17 shows the combustion of tire rubber granulate at 21 vol.-% and 5 vol.-%, respectively. It is observed that the CO- and SO_2-concentrations reach approximately 500 ppm and 350 ppm, respectively, at 21 vol.-% O_2, while the CO- and SO_2-concentrations reaches approximately 5700 ppm and 2900 ppm, respectively, at 5 vol.-% O_2. Thus, the formation of the reducing agent CO is accompanied by a reductive decomposition of $CaSO_4$ to SO_2, and the degree of this reductive decomposition seems to be directly related to the CO-concentration. The same trend was observed for the other tested fuels.

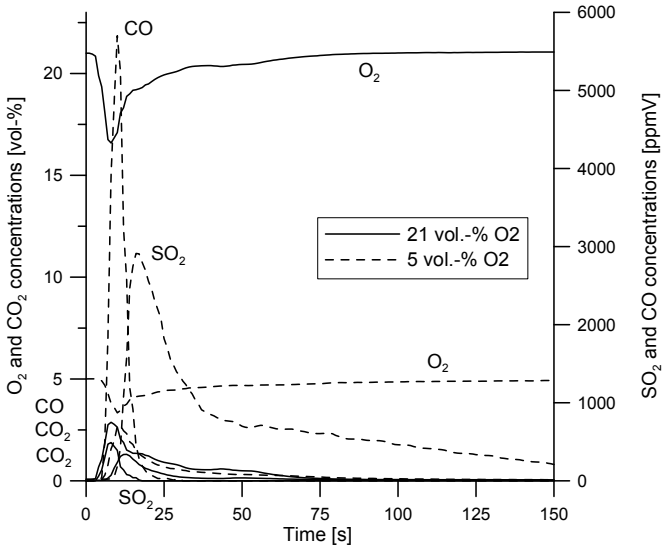

Figure 6-17: Flue gas composition during combustion of 0.81 g (30 kJ) of tire rubber granulate at 5 and 21 vol.-% O_2. 5% fill degree, 900°C, 100 NL/min, 6 rpm.

6.4.2.4 Practical implications

The experiments with sulfur release during solid fuel combustion indicate that the sulfur release from raw materials in the material inlet end of rotary kilns may be reduced by keeping the temperature as low as possible and the oxygen concentration as high as possible, particularly during fuel devolatilization. The results indicate that it may be advantageous to utilize relatively large fuel particles because this will lead to longer fuel devolatilization times and thus reduce the tendency for sudden formation of large CO-peaks followed by high sulfur release from the raw materials.

The experiments also gave an indication that the type of fuel was important for the extent of sulfur release. The sequence was found to be tire rubber granulate > sewage sludge > pine wood saw dust > petcoke > polypropylene flakes. However, it should be noted that the fuel particle size, and possibly shape, is of high importance for the degree of sulfur release and other fuel particle sizes may give quite different results.

6.4.2.5 Conclusions for experiments with sulfur release during fuel combustion

Sulfur release from cement raw materials during combustion of solid fuels has been studied experimentally in a high-temperature rotary drum. The fuels were tire rubber, pine wood, petcoke, sewage sludge and polypropylene. The sulfur release from the raw materials was observed to increase when:

1. The inlet oxygen concentration decreased.
2. The temperature increased.
3. The total surface area of the fuel particles increased.

These three parameters all had the potential of increasing the formation of local reducing conditions in the raw material bed, as indicated by elevated levels of CO during fuel devolatilization. The sulfur release is thus likely to increase as a consequence of the reducing conditions.

The type of fuel also had a significant effect on the sulfur release. The sequence was found to be tire rubber granulate > sewage sludge > pine wood saw dust > petcoke > polypropylene flakes. However, the sulfur release was significantly lower when the fuel was one tire rubber particle or one wood particle, indicating the significant effect of fuel particle size and shape on the sulfur release from the raw materials.

6.5 Conclusions for chapter 6

Volatile, inorganic elements such as sulfur, chlorine, potassium and sodium circulate to a high degree in the rotary kiln, calciner and preheater due to evaporation-condensation reactions. Chlorine, in particular, is a very volatile element with an evaporation factor close to 1. If utilization of alternative fuels increases the input of particularly Cl it is often necessary to install a bypass to remove a fraction of this volatile element, thereby preventing deposit build-ups.
The evaporation factor of sulfur depends on the amount of alkali metals available to form stable alkali sulfates and/or alkali-calcium sulfates in the rotary kiln burning zone. Similarly, the evaporation factor of alkali metals depends on the distribution between the stable sulfates and the more volatile chlorides.

Local reducing conditions in the material inlet end of the rotary kiln have no direct effect on the release of chlorine species to the gas phase: Chlorine release is to a very high degree influenced by temperature and not by gas atmosphere.

By contrast, the release of sulfur is influenced by local reducing conditions in the material inlet end: Sulfates present in the calcined raw material will be reductively decomposed by the presence of reducing agents. Sulfur is mainly released as SO_2. Thus, gas phase SO_2-concentration increases which may lead to increased deposit build-ups in rotary kiln, riser duct or lower cyclone stage.

The sulfur release was shown to be significantly higher under alternating reducing and oxidizing conditions than under constant reducing conditions. It was also shown that sulfur release under reducing conditions was particularly critical at high temperatures.

Experiments with sulfur release from raw materials during solid fuel combustion showed that the fuel particle size was very important for the extent of sulfur release: Many small fuel particles led to a higher sulfur release than few large fuel particles due to a faster devolatilization of the small fuel particles.

The results indicate that problematic deposit build-ups caused by high SO_2 concentrations in the gas phase may be reduced by minimizing the direct, physical contact between fuel particles and raw material. Local reducing conditions in the raw material should be minimized by ensuring a high excess air ratio in the rotary kiln and by optimizing the fuel-gas mixing.
Also, if temperatures in the material inlet end of rotary kilns can be kept relatively low, less sulfur is expected to be released from the raw material during fuel devolatilization.

6.6 References

Aho, M. and Ferrer, E.; Importance of coal ash composition in protecting the boiler against chlorine deposition during combustion of chlorine-rich biomass, Fuel, 84, 201-212, 2005.

Ayllón, M., Aznar, M., Sánchez, J. L., Gea, G. and Arauzo, J.; Influence of temperature and heating rate on the fixed bed pyrolysis of meat and bone material, Chem. Eng. Journal, 121 85-96, 2006.

Barin, I.; Thermochemical Data of Pure Substances. 3rd ed., VCH, Germany, 1995. ISBN: 3-527-28745-0.

Bhatty, J. I., Miller, F. MacG. and Kosmatka, S. H.; Innovations in Portland Cement Manufacturing, Portland Cement Association, Illinois, USA, Chapter 3.4, 2004. ISBN 0-89322-235-1.

Choi, G.-S. and Glasser, F. P.; The sulphur cycle in cement kilns: Vapour pressures and solid-phase stability of the sulphate phases. Cement and Concrete Research, Vol. 10, 367-374, 1988.

Dam-Johansen, K., Hansen, P. F. B. and Østergaard, K.; High-temperature reaction between sulphur dioxide and limestone – III. A grain-micrograin model and its verification. Chem. Eng. Sci., Vol. 46, No. 3, 847-853, 1991.

Davidsson, K. O., Stojkova, B. J. and Pettersson, J. B. C.; Alkali emission from birchwood particles during rapid pyrolysis, Energy & Fuels, 16, 1033-1039, 2002.

Diaz-Bossio, L. M., Squier, S. E. and Pulsifer, A. H.; Reductive decomposition of calcium sulfate utilizing carbon monoxide and hydrogen, Chem. Eng. Sci., 40, 3, 319-324, 1985.

Díez, C., Martínez, O., Calvo, L. F., Cara, J. and Morán, A.; Pyrolysis of tyres. Influence of the final temperature of the process on emissions and the calorific value of the products recovered, Waste Management, 24, 463-469, 2004.

Farag, L. M. and Kamel, H. M.; Effect of high intakes of chlorine, sulfur and alkalies on cement kiln operation. ZKG, 10, 586-590, 1994.

FLSmidth; Overcoming side effects of alternative fuels on pyro process. Highlights, 28, November 2008.

Ghardashkhani, S., Ljungström, E. and Lindquist, O.; Release of sulphur dioxide from calcium sulphate under reducing conditions. 10th Int. Conf. of fluidized bed combustion, 611-615, 1989.

Hansen, P. F. B., Dam-Johansen, K., Bank, L. H. and Østergaard, K; Sulphur retention on limestone under fluidized bed combustion conditions – An experimental study. Proceedings of the international conference on fluidized bed combustion, 1 73-82, 1991.

Hansen, P. F. B, Dam-Johansen, K. and Østergaard, K.; High temperature reaction between sulphur dioxide and limestone – V. The effect of periodically changing oxidizing and reducing conditions. Chem. Eng. Sci., Vol. 48, No. 7, 1325-1341 1993.

Hansen, J. P.; SO_2 Emissions from Cement Production. PhD Thesis, Technical University of Denmark, Department of Chemical Engineering, 2003. ISBN 87-90142-96-9.

Hewlett, P. C. (Editor); Chemistry of Cement and Concrete; 4th edition, John Wiley & Sons Inc., New York, 1998. ISBN 0-340-56589-6.

FLSmidth; Overcoming side effects of alternative fuels on pyro process. Highlights, 28, FLSmidth, Valby, Denmark, November 2008.

Jensen, P. A., Frandsen, F. J., Dam-Johansen, K. and Sander, B.; Experimental investigation of the transformation and release to gas phase of potassium and chlorine during straw pyrolysis, Energy & Fuels, 14, 1280-1285, 2000.

Jøns, E.; Personal communication, FLSmidth, Valby, Denmark, January 2010.

Kamphuis, B., Potma, A. W., Prins, W. and Van Swaaij, W. P. M.; The reductive decomposition of calcium sulphate – I. Kinetics of the apparent solid-solid reaction. Chem. Eng. Sci., Vol. 48, 1, 105-116, 1993.

Knudsen, J. N., Jensen, P. A. and Dam-Johansen, K.; Transformation and release to the gas phase of Cl, K and S during combustion of annual biomass, Energy & Fuels, 18, 1385-1399, 2004.

Knudsen, J. N., Jensen, P. A., Lin, W., Frandsen, F. J. and Dam-Johansen, K.; Sulfur transformations during thermal conversion of herbaceous biomass, Energy & Fuels, 18, 810-819, 2004.

Kobyashi, N., Itaya, Y., Piao, G., Mori, S., Kondo, M., Hamai, M. and Yamaguchi, M; The behavior of flue gas from RDF combustion in a fluidized bed, Powder Technology, 151 87-95, 2005.

Locher, G. and Klein, H.; Modelling circulating sulfur, chlorine and alkali systems in the clinker burning process; Part 2: Theory and discussion. Cement International, Vol. 7, 4, 64-75, 2009.

Lyngfelt, A. and Leckner, B.; Sulphur capture in fluidized bed boilers: The effect of reductive decomposition of CaSO4. The Chem. Eng. Journal, 40, 59-69, 1989.

Lyngfelt, A. and Leckner, B.; SO_2 capture in fluidized-bed boilers: Re-emission of SO_2 due to reduction of CaSO4. Chem. Eng. Sci., Vol. 44, No. 2, 207-213, 1989.

Lyngfelt, A. and Leckner, B.; Sulphur capture in circulating fluidized-bed boilers: Can the efficiency be predicted? Chem. Eng. Sci., 54, 5573-5584, 1999.

Masaki, K., Suzuki, M. and Maki, I.; Burning and nodulization process of clinker in the rotary kiln as viewed from the fine textures of the constituent minerals. Cement and Concrete Research, 32, 1039-1044, 2002.

Miller, F. M. and Tang, F. J.; The distribution of sulphur in present-day clinkers of variable sulphur content. Cement and Concrete Research, 26, No. 12, 1821-1829, 1996.

Rasmussen, M. H.; Low SO2 emission preheaters for cement production. PhD Thesis, Department of Chemical and Biochemical Engineering, Technical University of Denmark, 2011.

Rosholm, P., Mortensen, A. H. and Hintsteiner, E. A.; Converting two kiln lines to 100% high sulphur petroleum coke firing, ZKG International, February and April, 1998.

Sutou, K., Harada, H. and Ueno, N.; Concentration is the key, International Cement Review, 36-41, June 1999.

Tarelho, L. A. C., Matos, M. A. A. and Pereira, F. J. M. A.; The influence of operational parameters on SO_2 removal by limestone during fluidised bed coal combustion. Fuel Processing Technology, 86, 1385-1401 2005.

Taylor, H. F. W.; Distribution of sulfate between phases in Portland cement clinkers, Cement and Concrete Research, 29, 1173-1179, 1999.

Tian, H. and Guo, Q.; Investigation into the behavior of reductive decomposition of calcium sulfate by carbon monoxide in chemical-looping combustion. Ind. Eng. Chem. Res., 48, 5624-5632, 2009.

Tsoumeleas, C. I., Katsioti, M., Georgali, B. and Marinos, J.; Thermal stabilisation of $CaSO_4$, World Cement, 57-61 November, 2000.

Turkdogan, E. T. and Vinters, J. V.; Reduction of calcium sulphate by carbon, Trans. Inst. Min. Metall. Sec. C, vol. 85, c113-123, 1976.

Twomey, C., Birkinshaw, C. and Breen, S.; The identity of the sulphur-containing phases present in cement clinker manufactured using a high sulphur petroleum coke fuel. J. Chem. Technol. Biotechnol., 79, 486-490, 2004.

Wheelock, T. D. and Boylan, D. R.; Reductive decomposition of gypsum by carbon monoxide. Ind. Eng. Chem. 52, 3, 215-218, 1960.

Zevenhoven, R., Axelsen, E. P. and Hupa, M.; Pyrolysis of waste-derived fuel mixtures containing PVC, Fuel, 81 507-510, 2002.

7 Analysis of industrial experience and combustion model for industrial rotary kilns

The purpose of this chapter is to briefly describe and analyze industrial experience with alternative fuel utilization in the material inlet end of rotary kilns. In addition, a full-scale model for fuel combustion is suggested, based on the pilot-scale combustion experiments described in chapter 5. Finally, the chapter gives a short evaluation of different alternative fuels regarding their utilization in the material inlet end of cement rotary kilns.
The industrial experience, the full-scale model, and results from chapter 4 and 6 regarding fuel/raw material mixing and sulfur release during fuel combustion may be used as a basis to suggest how rotary kilns should be designed if it is desired to fire a fraction of the total energy into the material inlet end while reducing negative impact on process stability or product quality.

7.1 Industrial experience with combustion of large fuel particles

This section summarizes observations and analyses that have been made for combustion of solid alternative fuels in various FLSmidth rotary kiln systems. The aim is to provide insight into the industrial scale experience with coarse alternative fuels fired into the rotary kiln, either directly or indirectly through the calciner.
Initially, experience in wet kiln systems without preheater will briefly be described. Secondly, Suspension Preheater (SP) kilns will be analyzed. It is relatively common to fire coarse alternative fuels into the material inlet end of SP kilns. Finally, experience in modern calciner kilns will be analyzed. Relatively little experience is available about alternative fuels firing into the material inlet end of calciner kilns.

7.1.1 Wet process kilns

Wet process kilns are rarely constructed today due to a high energy consumption compared to modern, dry process kiln systems. However, there are still many old wet kilns in operation, e.g. at the Danish Aalborg Portland cement plant. The wet kilns are typically very long, with L/D ratios around 40. The raw materials enter in one end of the rotary kiln as slurry with high water content. All the processes of water evaporation, preheating, calcination and clinker reactions take place within the long kiln.

Many wet process kilns (and long dry process kilns) uses mid-kiln firing of alternative fuels. The fuel is typically tires. The fuel drops into the hot rotary kiln through a sluice which is installed in the kiln shell. The technology has proven to work well on several long rotary kilns. Energy input through mid-kiln firing may be in the order of 20% of the total energy fired (Hess, K. et al., 2008). The technology has not been utilized in modern preheater or calciner kilns with shorter rotary kilns, where firing in the calciner or in the material inlet end are preferred solutions.

7.1.2 SP kilns

The Suspension Preheater kiln (SP kiln) system consists of raw material preheating in 4-6 preheater cyclones prior to calcination and clinker reactions in the rotary kiln. SP rotary kilns are relatively long because calcination takes place in the first section.

Many SP kilns fire 10-15% of their total energy input as coarse, solid fuels fed into the material inlet end of the rotary kiln. This is a relatively high percentage, compared to calciner kilns, see section 7.1.3. The reason why it works well is believed to be that the raw meal is only partly calcined when it enters the rotary kiln – typically 30-40% calcined. The heat developed under the fuel combustion can therefore be directly used in the endothermic calcination process, thereby efficiently controlling the local temperature and thereby the sulfur release.

The theoretically possible fuel quantity is normally limited to below 25% of total energy input because of the limitation of excess air that can be passed through the burning zone. The typical oxygen concentration in the material inlet end is quite low, about 2-3 vol.-%. Oxygen enrichment in the material inlet end of the rotary kiln may be a feasible way to increase oxygen concentration without having higher excess air ratios in the rotary kiln burning zone. This approach has long been recognized, but has only become attractive in recent years due to the availability of cheaper production methods of oxygen (Bhatty et al., 2004).

In practice, most SP kilns cannot fire more than 10-15% of their total energy input in the rotary kiln material inlet end due to the risk of local reducing conditions and increasing temperatures that may affect process and product stability. However, one European SP kiln produced by FLSmidth is reported to be able to fire up to 35% of its energy input as whole tires in the material inlet end of the rotary kiln. This extraordinary high percentage is due to low sulfur content in the feed streams to the kiln system which minimizes problems in terms of deposit build-ups. But it should be noted that a relatively large fraction of the production is “reduced clinker” which have to be discarded. This specific cement factory accepts to discard a significant part of the production because it have access to cheap alternative fuels in the form of whole tires as well as low-sulfur waste fuels for firing through the kiln main burner (Rosholm, 2009).

Experiments made in a SP kiln with whole tires and tire chips indicate that whole tires are more attractive than tire chips: The tendency to deposit build-ups and reduced clinker was less severe with whole tires relative to the situation with tire chips (Jannerup, 2009). These results indicate that the smaller tire chips can more easily be buried in the material bed and create local reducing conditions. The larger whole tires will to a larger degree stay above the bed and be exposed to higher temperatures as well as to higher oxygen concentrations from the freeboard gas. These results have to the author’s knowledge never been published but they are important since they prove that there is no reason to shred the tires before firing them into the rotary kiln. Furthermore, the results are in fine correspondence with the results from the mixing experiments presented in chapter 4, where it was also observed that large fuel particles maintained a better contact with the gas above the raw material bed than smaller fuel particles.

7.1.3 Calciner kilns

In modern cement plants, raw meal is preheated to calcination temperature in a multi-stage cyclone preheater and most of the calcination process takes place in a separately fired calciner. The In-Line Calciner (ILC) is an example of such a modern kiln system. Alternative fuels are today widely used in calciner kilns. But it is most common to fire the fuels in the traditional firing points in the calciner and main burner. Firing with coarse alternative fuels directly into the rotary kiln is generally restricted to small percentages of the total energy input, due to low oxygen concentrations about 2-7 vol.-% and high calcination degrees above 90% of raw meal entering into the kiln. These conditions create a high risk for local reducing conditions in the material charge and/or increasing temperatures in the rotary kiln material inlet or riser pipe.

In the following, full-scale experience with alternative fuel firing in the material inlet end of calciner kilns at eight different cement plants will be described.

Plant 1

This cement factory is of the ILC type pyrolysis tires in a separate gasifier, whereafter the tire char is introduced into the kiln riser duct and, subsequently, into the rotary kiln material inlet. Besides tire char coal and petcoke are fired in the calciner and main burner. Plastic waste is also fired in the main burner. Despite a relatively high O_2-concentration in the kiln material inlet of 4-6 vol.-%, it is clear from flue gas measurements that the SO_2-concentration increases significantly when tire char is fired into the kiln material inlet. This is illustrated in Figure 7-1. When neither tire char nor plastic is fired in the kiln system, the SO_2-concentration in the flue gas is around 1800 ppm. When plastic is co-fired through the burner along with coal and petcoke, the SO_2-concentration increases to 3000-5000 ppm. Also, small CO peaks are seen. And when both plastic and tire char is fired simultaneously, the SO_2-concentration increases above 10000 ppm, which is the detection limit for the analyzer. The oxygen concentration fluctuates around 4-6 vol.-% most of the time. However, a sudden drop in the oxygen-concentration is observed with intervals, simultaneously with increasing CO-concentrations. This indicates that there are some irregularities in the alternative fuel combustion, and that local reducing conditions have been present in the material charge. This type of situation with CO peaks and increasing SO_2-concentrations is often reported from cement plants that fire solid fuels into the material inlet end of the rotary kiln.

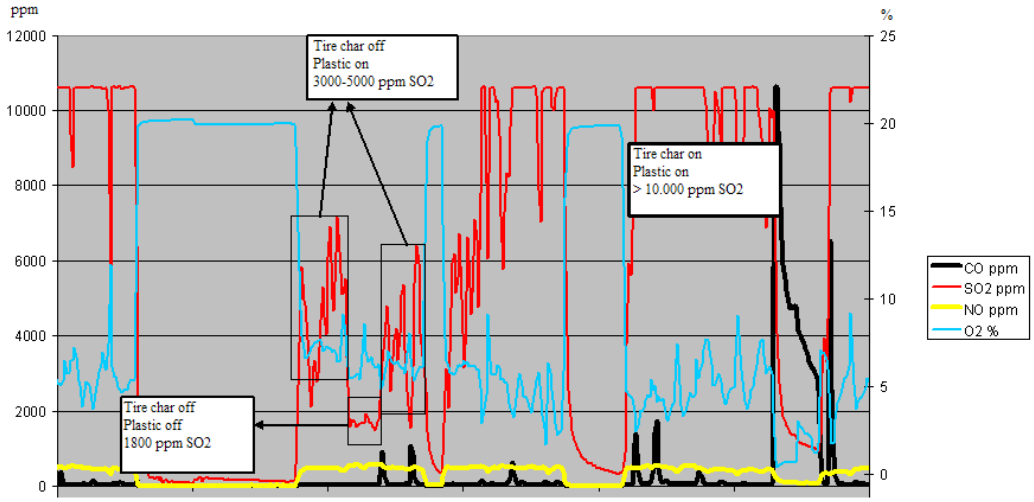

Figure 7-1: Flue gas analysis in kiln material inlet (Jøns, 2007).

Plant 2

This cement plant of the ILC-type fires approximately 10% of the total energy consumption as whole tires fired into the material inlet end of the rotary kiln. This is a relatively high energy percentage for an ILC kiln, but despite this, none of the typical problems associated with local reducing conditions have been observed. The remaining 90% of the energy is supplied from heavy fuel oil fired in the main burner and calciner. The ILC kiln is similar to other ILC kilns in most ways, so it is not directly possible to point out a particular reason why this plant is able to fire a large percentage of fuel in the kiln material inlet end. But several possibilities exist: The rotary kiln has a small length-to-diameter ratio of 11. The kiln inner diameter is 5 m which is relatively large for a typical clinker production around 3200 tpd. This means that the material filling degree is only around 6%. The combination of a low material filling degree and a large fuel particle in the form of a whole tire is likely to provide good fuel-air contact in the rotary kiln. Thus, the tendency for local reducing conditions in the material charge may be minimized. Another possibility may be that the whole tires are delivered continuously, on a kg-per-hour basis. Thus, fluctuations in energy input to the rotary kiln can be minimized. A third possibility may be the rather unusual main fuel, heavy fuel oil. Oil consists of hydrocarbons and during the combustion process it will produce more water vapour than coal. Thus the flue gas in the rotary kiln will contain high water content. It is well known that OH radicals from water accelerate the oxidation of CO (Turns, 2006). This phenomenon could consequently decrease the degree of local reducing conditions in the material charge.

Plant 3

Another ILC rotary kiln fires 15-20% of the total energy as tire chips into the middle of the calciner, see Figure 7-2. The tire chips are in sizes of up to 10 cm in length and width. It is estimated that 10-20% of the tire chips falls through the kiln riser duct and into the kiln material inlet end where the combustion is completed (Green-Andersen, 2008). The kiln operation is not reportedly affected by these tire chips in the form of local reducing problems in the kiln inlet. But another challenge is formation of so-called "bird nests" in the kiln riser duct: Steel wires from the tire chips get stuck in the riser duct and dust transferred with the kiln gas accumulates in the network of steel wires. This creates deposits in the kiln riser duct that have to be manually removed. At this particular plant, the main challenge associated with firing tires in the calciner, riser duct and kiln inlet is thus the steel wires from the tires and not local reducing conditions.

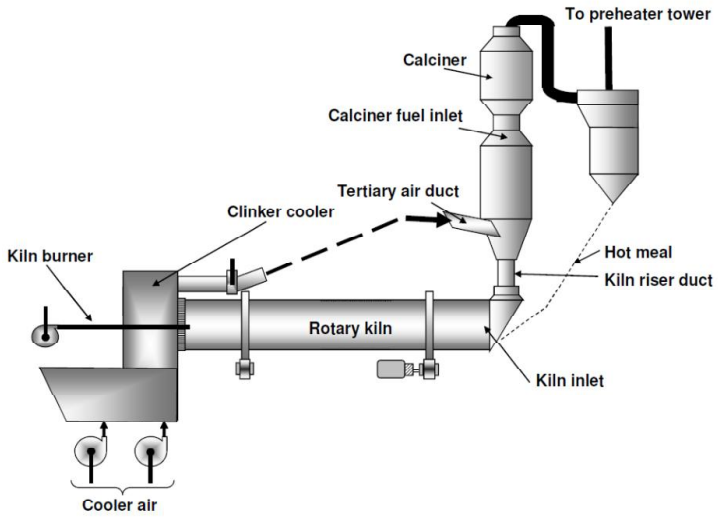

Figure 7-2: ILC kiln with TDF chip firing in the middle of the calciner. The TDF chips drop into the kiln inlet before reaching full conversion.

Plant 4

This cement plant of the SLC-D (Separate Line Calciner – Downdraft) type has experience with firing of many different alternative fuels: The plant has during the last 10 years fired different hazardous solid and liquid waste fuels such as pesticides, organic solvents, cyanide – and during the last three years, whole tires (Paone, 2009). The fuels are fired into the lower part of the preheater tower and are fully or partly combusted before reaching the rotary kiln material inlet. The plant has due to the various alternative fuels experienced substantial fluctuations in the input levels of sulfur and chlorine, as well as other elements. This has been compensated for by mixing different fuel types in order to keep a fairly constant input level of different elements. Experience from the plant is that the energy percentage in this position should not exceed 10% of total energy fired in the plant. The remaining 90% energy is fired in either the kiln main burner or in the calciner.

Plant 5

This cement plant of the ILC type has experience with firing of 1-2 energy-% of the alternative fuel "criolita" into the kiln riser pipe: Criolita is a waste product from the aluminium producer Alcoa where it is used as an electrode in aluminium production. It is – in addition to the high carbon content, a potential source of fluor which is an important mineralizer in cement production. However, during trial tests it was observed that firing of criolita in the kiln riser pipe caused increased formation of "gypsum-rings" in the kiln inlet. The same tendency had been observed with previous tests with firing of petcoke in the kiln riser pipe. The tests were cancelled and it was decided not to fire criolita in the kiln riser pipe due to the risk of kiln rings. It should be noted that the kiln operation was generally unstable with low oxygen and NO concentrations in the kiln inlet, as well as frequent CO peaks (Nielsen and Jøns, 2000). It is possible that a higher excess air ratio in the kiln inlet would be sufficient to avoid increased formation of kiln rings when fuels are combusted in the kiln riser duct.

Plant 6

This ILC kiln has a production capacity of 3000 tpd and uses several different fuels: Petcoke, Liquid Waste Derived Fuel (LWDF), whole tires and shredded solid industrial waste. The plant was able to fire 1 tph of whole tires into the lower calciner part. Here the whole tires were held by a fork in the hot gas stream from the tertiary air duct and rotary kiln before being pushed into the kiln riser duct and kiln inlet. However, after installation of a chloride by-pass, the process conditions in the kiln riser duct changed with less dust entrained in the flue gas and gas temperatures increasing from approximately 1000°C to 1050-1100°C (Lewis and Shenk, 2009). This led to build up problems in the kiln riser duct unless the tire feeding was reduced to 0.5 tph. Since whole tires were the cheapest fuel in the cement plant it was desirable to maintain the feed rate at 1 tph. Attempts were made to increase the oxygen concentration in the kiln material inlet from 3-3.5% to 6-7% and install additional air blasters in the kiln riser duct. These two modifications were proven to be successful in removing build ups in the kiln riser duct. The overall pressure drop over the preheater tower was noted to decrease due to less build up in the riser duct. Consequently, the plant is able to run at higher production capacity as a result of increased draft capacity.

Plant 7

Another cement plant of the ILC-type utilizes both whole tires and 300x300 mm tire chips in the material inlet end of the rotary kiln (Lund, 2010). The experience from this cement plant is that whole tires has less negative impact on process stability, presumably because the tire chips devolatilize too rapidly due to their higher surface area. This leads to high CO concentrations in the material inlet end. The cement plant still accepts to receive tire chips because transportation costs is cheaper: Tire chips can be packed better than whole tires, making it possible to transport more on each truck. When whole tires are used, the capacity is around 3.6 t/h which corresponds to 12-14% of the total energy requirement. This amount of tires can replace 3-5 t/h of coal. However, it is only possible to utilize whole tires some of the time due to deposit build-up formation in the riser duct, which must be manually removed. The daily average energy supplied by tires are around 7% of the total energy requirement (Lund, 2010).

Plant 8
This plant of the ILC type has a production capacity of 3300 tpd in a rotary kiln with a length of 69 m and a diameter of 4.6 m, corresponding to an L/D ratio of 15 (Valchev, 2010). The cement plant utilizes a variety of alternative fuels, mainly solid refuse derived fuels, whole tires, meat and bone meal and flower shells. The average alternative fuel share is 51-55% of the total energy requirement. Approximately 3 t/h of whole tires and 3 t/h of meat and bone meal is fed to the material inlet end of the rotary kiln, and occasionally automobile interior components and waste wood are also fed to the material inlet (Valchev, 2010). The cement plant has experienced several problems with deposit build-ups, but have optimized the process stability by installation of a chlorine bypass. However, it is still necessary to remove deposits in bottom stage cyclones, riser duct and material inlet of the rotary kiln. Cleaning is done with cardox and air blasters as well as by manual cleaning 6 to 10 times a day by one or two workers. Manual cleaning is done with long metal pipes and pressurized air (Valchev, 2010).

7.1.4 Conclusions for industrial experience

This section summarized experience with combustion of large solid fuel particles in the material inlet end of rotary kilns. Firing of fuels into the kiln material inlet end is most common in long wet or dry rotary kilns, or in SP kilns where it is common to feed 10-15% of the total energy in this position.
In modern calciner kilns (ILC or SLC kilns) it is generally regarded as problematic to feed solid fuels into the kiln material inlet end. However, some calciner kilns do feed up to 10% of the total energy in the kiln material inlet end. Experience has shown that higher feed ratios may result in local reducing conditions, and consequently CO peaks, increased SO_2-concentration in the rotary kiln exit gas and heavier deposit formations in the kiln and riser duct.
The reason why long wet and dry rotary kilns and SP kilns are believed to be better suited for firing in the kiln material inlet end is because the raw material in the kiln material inlet end is only partly calcined. Thus, the raw material may be able to take up heat from the fuel combustion so that high temperatures are minimized, thereby minimizing sulfur release. Another theory is that during the calcination, CO_2 is released from the raw material and this creates a bubbling, dynamic environment similar to that in the calciner. This environment promotes heat and mass transfer between the material charge and the freeboard gas, thereby minimizing risk of local reducing conditions in the material charge.

Most experience with alternative fuel utilization in the material inlet end is based on combustion of tires which is a very common alternative fuel in the cement industry. It is possible that solid fuels with different volatile/char contents and fuel conversion pathways can be fed into the kiln material inlet end in higher ratios due to less impact on the inorganic chemistry.

It is interesting to note that experience with higher oxygen concentrations in the kiln inlet and lower material filling degrees in the rotary kiln seems to have a positive effect on the process stability during combustion of fuels in the kiln material inlet end. Experience with tires in two different rotary kilns also indicates that the particle size is of importance: Whole tires seem to have less negative impact on process stability than tire chips which become buried in the bed.

7.2 Modeling combustion of solid fuels in industrial rotary kilns

The drying, devolatilization and char oxidation models developed in chapter 5 is now used to estimate conversion times of solid tire particles in industrial rotary kilns. Tires are used in the model because there is industrial experience with tire combustion, as described in section 7.1. Thus it is possible to compare model results with industrial experience. But the same model approach may be used for other fuels as well. The aims of these simulations are to:

a) Predict drying, devolatilization and char oxidation times for the fuels during their transport into the rotary kiln.
b) Predict oxygen consumption in the rotary kiln during fuel conversion in the material inlet end.
c) Predict approximate gas and bed temperatures during fuel conversion in the material inlet end.

These model predictions may be useful in determining how large quantities of fuels that can be accepted in the material inlet of the rotary kiln based on fuel characteristics and operational parameters.

Figure 7-3 illustrates qualitatively how deep into the rotary kiln solid fuels will reach during drying, devolatilization and char oxidation. In addition, the figure illustrates how temperature and oxygen concentrations with and without fuel combustion in the material inlet end may be. As shown on the figure, the temperature of both gas and bed will increase with solid fuels entering the material inlet. And the oxygen concentration will decrease to a lower level in the material inlet end of the rotary kiln.

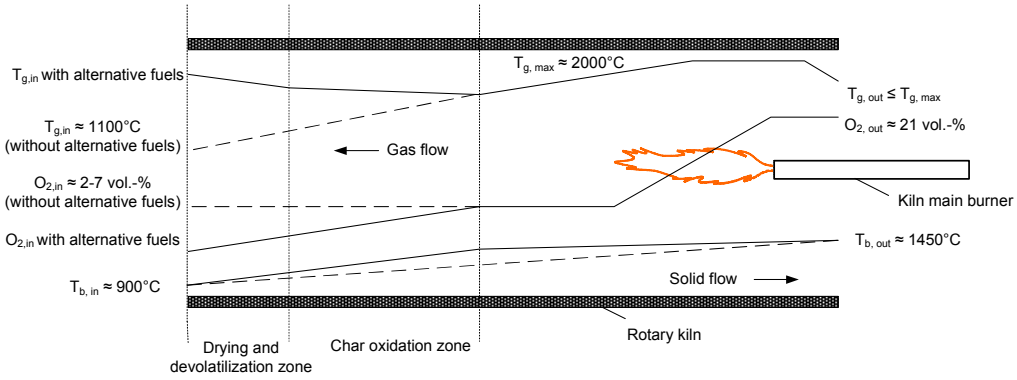

Figure 7-3: Temperature and oxygen concentration profiles in a rotary kiln with and without alternative fuel utilization in the material inlet end.

Before the temperature, oxygen and fuel conversion models are developed, the following main assumptions are made:

1) The oxygen profile in the gas phase is assumed to be evenly distributed over the radial cross section.
2) Heat effects of calcinations reactions in the rotary kiln inlet are neglected.
3) Heat transfer through the kiln wall is neglected.
4) The gas and bed temperatures are modelled by a simple linear correlation. Conductive, convective and radiative heat exchange is assumed contained in this correlation.

At conditions pertinent to the material inlet of rotary kilns, the oxygen concentration is expected to be more important for fuel conversion than temperature. Consequently, the relatively simple assumptions regarding the energy balance are considered to provide satisfactory model results in terms of point a) and b) above.

The models for gas and bed temperatures along the kiln length and during fuel combustion are included in Appendix E. Stoichiometric calculations (see Appendix F) coupled with the fuel conversion profiles are used to determine the axial oxygen profile.

The used dimensions and values are summarized in Appendix B and G. The calculations are based on a modern FLSmidth ROTAX 2 kiln with a clinker production of 3,500 tpd.

7.2.1 Selected full scale model results

Figure 7-4 shows the estimated degree of conversion of tire-derived fuel (TDF) fed to the material inlet end of a rotary kiln at a rate of 0.076 kg/s corresponding to around 2% of the total thermal energy input necessary to produce cement clinker. The time for devolatilization is fast, around 30 s, compared to the time for char oxidation which is around 1600 s. In the studied case, this corresponds to 2 m of kiln length for the devolatilization and 56 m for the char conversion. Thus 58 m of kiln length is required for the total conversion of the TDF. The long conversion time for the char is due to mass transfer limitations of oxygen to the fuel, both from the bulk gas to the bed surface and from the bed surface into the active layer of the bed. It may be shown that the conversion time is roughly halved if the oxygen concentration is doubled, or if the fuel amount is halved.

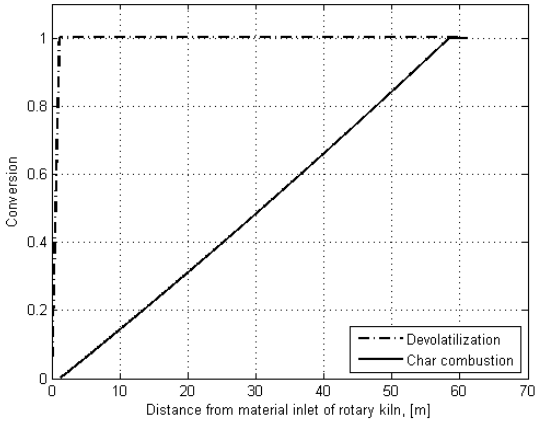

Figure 7-4: Degree of conversion for TDF as a function of kiln length in the material inlet end of a 60 m long rotary kiln. 5 vol.% O_2 in kiln burner flue gas. Tire rubber average particle diameter = 11 mm. Fuel amount: 0.076 kg/s corresponding to 2% of the total energy input to the kiln system.

Figure 7-5 shows the gas and bed temperature profiles through the rotary kiln during the tire char combustion. The gas temperature is observed to decrease linearly from an average gas temperature of 1600°C in the burning zone to approximately 2 m from the material inlet end. Here, the fuel devolatilization begins, thereby changing the slope of the temperature profile due to the heat release from the volatile combustion. Similarly, the bed temperature is observed to increase fastest from 900°C in the first two meters of the material inlet and then increase at a slower rate during the rest of the rotary kiln.

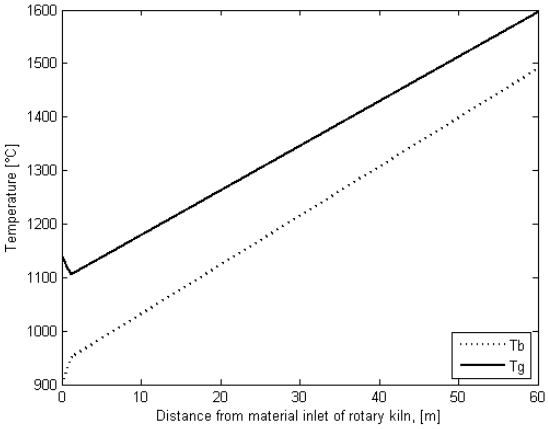

Figure 7-5: Temperature profiles through rotary kiln during combustion of TDF in a 60 m long rotary kiln. 5 vol.-% O_2 in kiln burner flue gas. Tire rubber average particle diameter = 11 mm. Fuel amount: 0.076 kg/s corresponding to 2% of the total energy input to the kiln system.

Figure 7-6 shows the changes in bulk gas oxygen concentration through the rotary kiln when TDF is combusted in the material inlet end of the rotary kiln. The oxygen concentration in the flue gas from the kiln burner is 5 vol.-% corresponding to an excess air ratio of 1.33. This oxygen concentration decreases slightly to 4.8 vol.-% during the char oxidation. And then it decreases fast to 4.3 vol.-% during fuel devolatilization. Overall the change in oxygen concentration is around 0.7 vol.-% through the rotary kiln. This indicates that the slow char oxidation is not only due to lack of oxygen but also mass transfer of oxygen to the char: Most of the oxygen does not reach the char before leaving the rotary kiln. If the rotary kiln is longer, the fuel amount can be increased because the longer retention time will ensure more time for char oxidation.

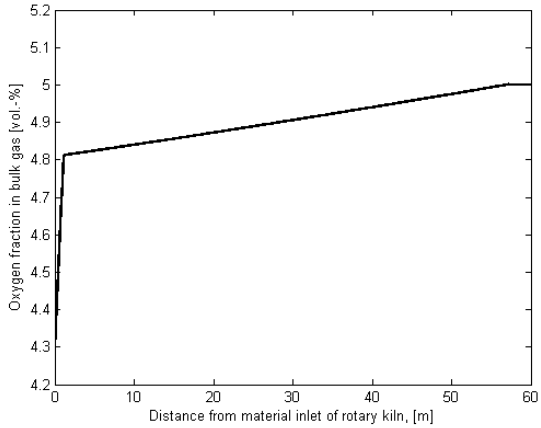

Figure 7-6: Oxygen fraction in bulk gas through rotary kiln during combustion of TDF in a 60 m long rotary kiln. 5 vol.-% O_2 in kiln burner flue gas. Tire rubber average particle diameter = 11 mm. Fuel amount: 0.076 kg/s corresponding to 2% of the total energy input to the kiln system.

The long conversion time for the tire char reduces the energy input in the material inlet end to no more than 2% if complete conversion of the tire char is required in the rotary kiln. This low figure is not in correspondence with the industrial experience from some calciner kilns, where it is possible to feed around 10% of the total energy into the material inlet end of the rotary kiln. It may indicate that the model under-estimates mass transfer of oxygen in the rotary kiln. Other reasons for the deviation between model predictions and industrial experience may be that some of the char is entrained in the flue gas and transported back towards the material inlet end of the rotary kiln. Or it may be that a fraction of the char leaves the rotary kiln with the clinker and is fully oxidized in the clinker cooler where the clinker is cooled with ambient air. The material residence time in the clinker cooler is up to 30 min and the oxygen concentration is 21 vol.-%, which provide good conditions for oxidation of unburned chars from the rotary kiln. However, the material temperature will decrease from around 1450°C to 100°C through the clinker cooler, which may entail considerable reduction of the char oxidation rate.

The model may be used to estimate the required kiln length in order to reach full conversion for different fuel loads, and under different conditions. Figure 7-7 is an example where the required kiln length is showed versus the energy percentage of the total required energy necessary to produce cement. The fuel is tire-derived fuel, TDF. Values used in the model are summarized in Appendix B and G. Four different excess air ratios from the main burner are shown, and the corresponding oxygen concentrations in the flue gas from the main burner are shown in parenthesis. At the lowest excess air ratio of 1.14, it is observed that 94 m and 142 m of kiln length is required to reach full conversion of 1% and 2.5% TDF, respectively. Thus at low excess air ratios, it is only possible to utilize small amounts of TDF in the material inlet end. But if the bulk oxygen concentration increases, the energy share in the material inlet end can be increased significantly. For the highest studied excess air ratio of 1.95, the energy share by TDF may be up to 26% in a 150 m long rotary kiln or around 7% in a 50 m long rotary kiln.

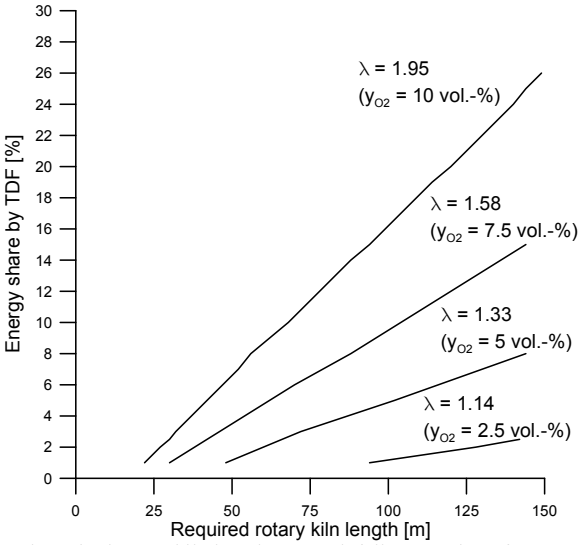

Figure 7-7: Model predicted required rotary kiln lengths to reach full conversion of TDF at different energy loads in the material inlet end of rotary kilns. The fuel is TDF with average particle diameter of 11 mm. Different oxygen concentrations are specified in the figure.

7.2.2 Conclusions for modeling solid fuel combustion in industrial rotary kilns

The fuel conversion model has been applied on an industrial rotary kiln to predict the conversion time for tire rubber. The results may be used to estimate how far different fuel particles will be transported into the rotary kiln as a function of particle size and key process parameters.

From the models results it is clear that the fuel devolatilization is a relatively fast process, taking place in the first part of the material inlet end of the rotary kiln. By contrast, the char conversion time is significantly longer and the char will thus be transported deep into the rotary kiln before reaching full conversion. The reason for the slow char conversion is mass transfer limitations of oxygen to the char particles.

The models may be used to estimate how large a share of the total energy input to the kiln system that can be utilized into the material inlet end by considering e.g. the excess air ratio and conversion time. However, when comparing full-scale experience with model predicted possible energy shares in the material inlet, it seems that the model under-estimates the mass transfer of oxygen to the char and thus, under-estimates how large fuel amounts it is possible to utilize in the material inlet end.

Ideally, the models should be validated against experimental data from a cement plant. It is, however, a complicated task to determine the conversion times of solid fuels fired into the material inlet of a cement rotary kiln due to the extreme environment and poor accessibility. It is also of interest to further develop the model regarding heat transfer between gas, wall and bed along the kiln length in order to obtain more realistic predictions of temperature profiles.

7.3 Suggestions for alternative fuel utilization

It was shown in section 7.2 that the fuel devolatilization is a fast process while the char oxidation is slow due to mass transfer limitations in rotary kilns. This was also confirmed by the experimental results with tire rubber and pine wood combustion described in chapter 5. In addition, the results from chapter 6 clearly showed that sulfur release from raw materials during fuel combustion primarily took place during fuel devolatilization. It was also shown that the sulfur release was most significant for several small fuel particles relative to few large fuel particles due to a faster devolatilization, a result that corresponds well with industrial experience. From these results the following recommendations regarding fuel utilization in the material inlet end are:

1) The fuel should have a high volatile content.
2) Few large fuel particles are preferred rather than several small fuel particles. However, the fuel particle size may be limited in order to keep the conversion time shorter than the residence time in the rotary kiln.
3) The fuel and cement raw materials should be in minimum physical contact during fuel devolatilization and/or the raw material temperature should be as low as possible during fuel devolatilization.
4) Chars should preferably be of the crackling type in order to produce small char particles that require shorter residence times than larger char particles. This corresponds to pathway f in Figure 5-3 in chapter 5.

In the following, different relevant fuel types are considered with respect to the above mentioned criteria. Please refer to table 3-2 in chapter 3 for details about each fuel type.

Tire-derived fuels (TDF)
TDF is a suitable fuel: It contains around 54-66 wt.-% volatiles and the char rapidly cracks into smaller char particles, leading to an overall short conversion time. In addition, a high heating value of 31-33 MJ/kg means that the required fuel mass is quite low. TDF contains around 1.5 wt.-% sulfur and will therefore increase the sulfur input to the kiln system, which may affect process stability. As shown in section 7.1, TDF is an often used alternative fuel in the material inlet end of cement rotary kilns.

Plastics
Plastics, except PVC, are excellent fuels since their volatile content approaches 100 wt.-% leading to very short conversion times. Their heating values are also typically 40-44 MJ/kg, which is very high and attractive.

Wood/biomass
Wood and different types of biomass have high volatile contents around 75-83 wt.-%. But their char and ash matrix structures are often quite stable, leading to conversion according to the shrinking particle or unreacted shrinking core mechanism, pathways G and H in Figure 5-3 in

chapter 5. This may lead to quite long char conversion times thereby limiting the fuel amounts to be utilized in rotary kilns. In addition, the heating values are relatively low, around 18-19 MJ/kg, and the moisture content may be very high. Pre-treatment in the form of drying or shredding may be required in order to utilize large amounts of wood and biomass.

Meat and bone meal (MBM)
Meat and bone meal has a high volatile content around 65-72 wt.-%. The fixed carbon content is typically low, in the order of 7-10 wt.-% which may make MBM an advantageous fuel. However, the ash content is high, around 17-28 wt.-%, and the ash contains relatively high amounts of sulfur, chlorine and phosphorous which may affect the process stability and product quality. In addition, the heating value is relatively low, around 16-20 MJ/kg.

Refuse derived fuel (RDF)
RDF is a mixture of different materials and may exhibit great variations in volatile, char, ash, moisture and chlorine content. Heating values for RDF are often also low, around 14 MJ/kg. The utilization of RDF in rotary kilns should therefore be based on a worst case scenario to allow flexibility for fluctuations in composition and amounts.

Sewage sludge (SS)
Sewage sludge has typically a high volatile content of 48-64 wt.-% and a low fixed carbon content of 0-6 wt.-%. This has the consequence that sewage sludge burns fast in the rotary kiln material inlet end, leaving only small amounts of char to be transported into the rotary kiln. Sewage sludge may be characterized as a suitable fuel in the material inlet. However, the high ash content of 17-50 wt.-% may affect the clinker quality in the form of e.g. phosphorous or coarse silicate grains from the sewage sludge being mixed into the clinker, see section 3.4.1. The lower heating value is typically 14-19 MJ/kg which is relatively low.

7.4 Conclusions for chapter 7

Industrial experience with alternative fuel utilization in the material inlet end of cement rotary kilns indicates that the energy share in this point may be around 10% in modern ILC calciner kilns, without jeopardizing process stability. A higher energy share may be achieved in long wet and dry kilns or in SP kilns due to longer residence times in the rotary kiln and lower temperatures in the material inlet end compared to ILC kilns.
A model has been developed to predict fuel combustion times for solid alternative fuels. The model predicts quite long conversion times for TDF which will limit the amounts of fuels to be used in the material inlet end. By comparison with industrial experience it is likely that the model under-estimates mass transfer of oxygen to fuel chars in industrial rotary kilns, thereby predicting too long conversion times.

References

Bhatty, J. I., Miller, F. McGregor and Kosmatka, S. H.; Innovations in Portland Cement Manufacturing, Portland Cement Association, ISBN: 0-89312-234-3, 2004.

Green-Andersen, P.; Kiln Performance Study, Internal Report, FLSmidth, Valby, Denmark, June 2008.

Hess, K., Omar, H., Rivera. L., Stubenbort, B. and Stutsman, B.; Pyroprocessing Audit, FLSmidth, Bethlehem PA, USA, October 2008.

Jannerup, H.-E.; Personal communication, FLSmidth, Valby, Denmark, September 2009.

Nielsen, K. P. and Jøns, E.; Internal report, FLSmidth, Valby, Denmark, September 2000.

Jøns, E.; Behaviour of volatile matter, Lecture 05-02, International Cement Production Seminar, FLSmidth, Denmark, 2007.

Larsen, M. B.; Alternative Fuels in Cement Production; PhD Thesis, Department of Chemical Engineering, Technical University of Denmark, 2007. ISBN 978-87-91435-49-8.

Lewis, B. and Shenk, R.; Internal report, FLSmidth, Bethlehem PA, USA, June 2009.

Lund, J. E.; Direct communication. Plant Director, Cemex Philippines, Tinaan, Naga, Cebu, Philippines, 2010.

Paone, P.; Personal communiation, FLSmidth, USA, September 2009.

Rosholm, P.; Personal communication, FLSmidth, Valby, Denmark, September 2009.

Sønderborg, H. R.; The International Cement Production Seminar 2007, Volume IA, Lecture 05-01; FLSmidth A/S, Valby, Denmark, 2007.

Turns, S. R.; An introduction to combustion. McGraw-Hill Int. Ed.2nd ed., 2006. ISBN: 978-007-126072-5.

Valchev, P.; Personal communication, HOLCIM, Beli Izvor, Bulgaria, July 2010.

8 Final conclusions

An improved understanding of utilization of solid alternative fuels in the material inlet end of cement rotary kilns has been gained through this PhD project. This has been obtained through literature studies, experimental investigations, mathematical modeling, analysis of existing process equipment and industrial experience.

8.1 Concluding trends

The main conclusions to be drawn from the literature review are:

1) Cement production is a very energy-intensive industry, accounting for approximately 2% of the world's primary energy consumption and being responsible for around 5% of the world's total CO_2 emissions.
2) The cement industry has a great interest in replacing fossil fuels with alternative fuels in order to a) reduce overall production costs and b) minimize CO_2 emissions.
3) Solid alternative fuels utilization requires new solutions in the form of combustion equipment or modifications of existing plant layout due to the fact that common alternative fuels have different physical and chemical properties than traditional solid fossil fuels.
4) The use of alternative fuels may influence clinker quality and/or process stability: The clinker quality may be affected by minor components from the fuel ashes or from unburned carbon leaving the rotary kiln with the clinker. The process stability may be affected by increased circulation of inorganic volatiles, particularly sulfur and chlorine, in the kiln system. Sulfur and chlorine containing species are known to cause deposit build-ups in the kiln system, restricting gas and material flows.

The main trends regarding alternative fuel utilization in the material inlet end of cement rotary kilns are:

1) Solid alternative fuel particles are rapidly mixed into cement raw materials. Thus, heat transfer by conduction from the cement raw materials to the fuel particles must be expected to be a major heat transfer mechanism rather than convection or radiation from the freeboard gas above the material bed. Consequently, the temperature of the cement raw materials becomes of great importance for the heating of the fuel particles. In addition, it must be expected that mass transfer of oxygen from the freeboard gas to the fuel particles will be hindered by the cement raw materials covering the fuel particles. The mixing process depends on several parameters such as fuel particle size and shape, fuel particle density, bed fill degree and kiln rotational speed, making the mixing process complicated to model.
2) Heating, drying and devolatilization of solid alternative fuels are fast processes which primarily depend on temperature and fuel particle size. The volatile content of alternative fuels is typically high. Consequently, a large fraction of the energy from the alternative fuels will be released rapidly in the material inlet end of the rotary kiln. This creates a

risk for increasing local temperatures and reducing conditions in the raw material charge, which consequently may lead to increased sulfur release from the raw materials, followed by increased formation of deposit build-ups in the kiln system. The sulfur release may be kept low during fuel devolatilization by minimizing the physical contact between fuel and raw materials, increasing fuel particle size, increasing the bulk oxygen concentration or by lowering the raw material temperature in the material inlet end of the rotary kiln.

3) Char oxidation is a slow process and therefore has a great influence on the amounts of fuel to be utilized, due to limited residence time in cement rotary kilns. Several parameters control the rate of char oxidation: a) bulk oxygen concentration, b) mass transfer rate of oxygen to char particles, c) conversion pathway, d) bed material fill degree and e) char particle size and shape. Parameters such as temperature and rotational speed only have a minor influence on char oxidation under the conditions in cement rotary kilns.
4) When considering alternative fuel utilization in the material inlet end of cement rotary kilns, the key parameters are a) overall input of the inorganic volatiles Cl, S, K and Na to the kiln system, b) volatile and char content of the fuel, c) (char) conversion pathway and d) fuel particle size and shape. Rotary kiln specific parameters such as length, inner diameter, bed fill degree, solids residence time and gas velocity has great influence on the amounts of fuel it is possible to utilize.

8.2 Suggestions for further work

Much effort has been spent on the development of a new, high-temperature experimental set-up, capable of simulating the conditions in the material inlet end of a cement rotary kiln. This work has been at the expense of the time available to make experiments in the rotary drum. The rotary drum is a unique experimental set-up which enables us to study several interesting parameters, such as combustion behavior of solid fuels and inorganic chemistry under well-defined conditions. It is therefore strongly recommended to further explore the many opportunities and continue the experimental work in the rotary drum set-up.

The char combustion model presented in this work has not been optimized with respect to predicting the effect of bed fill degree and temperature on the conversion time. A comparison between the model and full-scale experience also seems to imply that the model over-estimates the time for external mass transfer of oxygen to the char. Hence it will be necessary to further optimize the char combustion model. Ideally, the model should be validated against full-scale data.

Results from the fuel/raw material mixing experiments indicated that insertion of mixing devices in rotary kilns could help to optimize fuel-gas contact, thereby enhancing mass transfer of oxygen to fuel chars. This opportunity should be further investigated, e.g. by experiments in the rotary drum set-up or by full-scale tests.

List of symbols

Roman nomenclature

A	Area	m^2
Bi	Biot number	-
C_0	Moisture content	g water/g dry fuel
C_p	Specific heat capacity	J/(kg K)
C_2S	Belite	-
C_3S	Alite	-
C_4AF	Ferrite	-
C_3A	Aluminate	-
D	Diameter of drum/kiln	m
D	Diffusion coefficient	m^2/s
d	Particle diameter	m
E_a	Activation energy	J/mol
F	Bed fill degree	- (%)
FC	Fixed carbon	wt.-%
g	Gravitational speed	m/s^2
h	Heat transfer coefficient	$W/(m^2 K)$
h	Height	m
ILC	In-Line calciner	-
k_p	Thermal conductivity	W/(m K)
k_g	Mass transfer coefficient	m/s
k_0	Rate constant	s^{-1}
L	Length	m
LHV	Lower heating value	MJ/kg
m	Mass	g (kg)
M	Molar weight	mol/kg
MBM	Meat and bone meal	-
n	Rotational speed	min^{-1}
n	Moles	Mol
R	Universal gas constant	8.314 J/(mol K)
R	Radius of drum/kiln	m
r	Particle radius	m
r	Rate	mol O_2/ (m^2 s)
RDF	Refuse derived fuel	-
Re	Reynolds number	-
P	Pressure	Pa
P	Probability	%
PE	Poly ethylene	-
PVC	Poly vinyl chloride	-
Sc	Schmidt number	-
Sh	Sherwood number	-
SLC	Separate Line calciner	-
SP	Suspension preheater	-
t	Time	s or min
T	Temperature	K or °C
TDF	Tire-derived fuel	-
V	Degree of devolatilization	-

List of symbols

V	Volume	m^3
VM	Volatile matter	wt.-%
Y	Distribution factor in bed	-
y	Mole fraction	-
X	Degree of conversion	-
x	Distance	m

Greek nomenclature

α	Thermal diffusitivity	m^2/s
α	Mol C in fuel	Mol C/kg fuel
β	Mol H in fuel	Mol H/kg fuel
β_i	Positive solutions to equation	-
ε	Porosity	-
ε	Emissitivity	-
ρ	Density	kg/m^3 or mol/m^3
δ	Mol N in fuel	Mol N/kg fuel
φ	Mol O in fuel	Mol O/kg fuel
θ	Sphericity	-
λ	Excess air ratio	-
λ	Heat of vaporization	Cal/g
γ	Mol S in fuel	Mol S/kg fuel
ω	Rotational speed	rad/s
σ	Stefan-Boltzmann constant	$5.6704 \cdot 10^{-8}$ $W/(m^2 K^4)$
ζ	CO/CO_2 product ratio	-
ζ	Mol Cl in fuel	Mol Cl/kg fuel
τ	Total time	s
τ	Tortuosity	-
μ	Mol H_2O in fuel	Mol H_2O/kg fuel

Subscripts

a	Average
b	Bed
c	Char
e	Wet/dry interface
Cond	Conduction
Conv	Convection
Devol	Devolatilization
eff	Effective
g	Gas
p	Particle
Rad	Radiation
Sph	Spherical
Vol	Volatiles
w	Wall
0	Initial value

Appendixes

Appendix A – Sensitivity analysis on estimated fuel conversion

Several random errors may affect the predicted degree of fuel conversion. The impact of these accumulated random errors is analyzed with the accumulation law of uncertainties (Larsen and Hellesen, 1998). The degree of fuel conversion is estimated from the ideal gas law:

$$X_{Fuel}(t) = \frac{M_{carbon}}{m_{carbon,total}} \cdot \frac{P \cdot V}{R \cdot T} \cdot \int_0^t y_{CO} + y_{CO_2} dt \qquad \text{(A-1)}$$

When calculating the degree of fuel conversion a series of calculated and measured values is used and the fuel conversion may be expressed as a function of these values:

$$X_{Fuel} = X_{Fuel}\left(T, V, y_{CO}, y_{CO_2}\right) \qquad \text{(A-2)}$$

The uncertainty on the determined fuel conversion, $\sigma(X_{Fuel})$, is then predicted with the accumulation law of uncertainties:

$$\sigma\left(X_{Fuel}\right) = \sqrt{\left(\frac{\partial X_{Fuel}}{\partial T} \cdot \sigma\left(T\right)\right)^2 + \left(\frac{\partial X_{Fuel}}{\partial V} \cdot \sigma\left(V\right)\right)^2 + \left(\frac{\partial X_{Fuel}}{\partial y_{CO}} \cdot \sigma\left(y_{CO}\right)\right) + \left(\frac{\partial X_{Fuel}}{\partial y_{CO_2}} \cdot \sigma\left(y_{CO_2}\right)\right)^2} =$$

$$\frac{M_{carbon}}{m_{carbon,total}} \cdot \sqrt{\left(\frac{-PV}{RT^2} \cdot \int_0^t y_{CO} + y_{CO_2} dt \cdot \sigma\left(T\right)\right)^2 + \left(\frac{P}{RT} \cdot \int_0^t y_{CO} + y_{CO_2} dt \cdot \sigma\left(V\right)\right)^2 + \left(\frac{PV}{RT} \cdot \left(y_{CO} + \int_0^t y_{CO_2} dt\right) \cdot \sigma\left(y_{CO}\right)\right)^2 + \left(\frac{PV}{RT} \cdot \left(y_{CO_2} + \int_0^t y_{CO} dt\right) \cdot \sigma\left(y_{CO_2}\right)\right)^2} \qquad \text{(A-3)}$$

In the estimation of the overall uncertainty, the temperature is assumed to fluctuate ± 1%, the gas flow is assumed to fluctuate ± 3% and the uncertainties on measured gas species is assumed to fluctuate ± 1% for each species. The pressure P is assumed to be constant.

The total uncertainty on the fuel conversion has been estimated for typical experiments with combustion of tire rubber and pine wood. The uncertainty for one of these experiments with pine wood is presented at different fuel conversion degrees in Table A-1. It is observed that the total uncertainty increases with time, and reaches ± 0.059 at full fuel conversion, corresponding to a relative uncertainty of ± 5.9%. The measured gas flow has the greatest impact on overall uncertainty. It accounts for 87% of the total uncertainty.

X_{Fuel}	0.25	0.5	0.75	1.0
$\sigma(X_{Fuel})$	0.033	0.043	0.051	0.059

Table A-1: Total uncertainty of fuel conversion at different conversion degrees.

Appendix A references:

Larsen, M. O. and Hellesen, B.; Statistik 1, Institut for Anvendt Kemi, 3rd ed., 1998. Technical University of Denmark. (in Danish).

Appendix B – Data used in the combustion models

Property	TDF	Pine wood	References
Specific heat capacity, C_p, [J/(kg · K)]	2,000	1,500	Larsen et al., 2006 Leon et al., 2000
Initial particle density, ρ_p, [kg/m^3]	1,150	690	Yang et al., 1995 Leon et al., 2000
k_p, virgin fuel thermal conductivity, [W/(m · K)]	0.30	0.2	Sellassie et al., 2007 Leon et al., 2000
Conductive heat transfer coefficient, h_{CBP}, [W/(m^2 · K)]	250	250	Linjewile et al., 1993
Convective heat transfer coefficient, h_{CBP}, [W/(m^2 · K)]	150	150	Tscheng and Watkinson, 1979

Table B-1: Fuel specific data used in the devolatilization models.

Fuel	TDF	Pine wood	References
Property			
ρ_p [kg/m^3]	1,100	690	Larsen et al., 2006 Leon et al., 2000
k_0 [1/s]	1.5 (± 5.1) · 10^{10}	1.19 · 10^8	Larsen et al., 2007 Kastanaki and Vamvuka, 2006
Ea [kJ/mol]	193±28	140±10	Larsen et al., 2007 Kastanaki and Vamvuka, 2006
Exponent m	0.63	0.89	Larsen et al., 2007 Kastanaki and Vamvuka, 2006
LHV [MJ/kg]	37	14	From analysis

Table B-2: Fuel specific data used in the char oxidation models.

Appendix B references

Kastanaki, E. and Vamvuka, D.; A comparative reactivity and kinetic study on the combustion of coal-biomass char blends. Fuel, Vol. 85, 1186-1193, 2006.

Larsen, M. B., Schultz, L., Glarborg, P., Skaarup-Jensen, L., Dam-Johansen, K., Frandsen, F. and Henriksen, U.; Devolatilization characteristics of large particles of tyre rubber under combustion conditions. Fuel, vol. 85, 1335-1345, 2006.

Larsen, M. B., Hansen, M. L., Glarborg, P., Skaarup-Jensen, L., Dam-Johansen, K. and Frandsen, F.; Kinetics of tyre char oxidation under combustion conditions. Fuel, vol. 86, 2343-2350, 2007.

Leon, G., Cruz-de-Leon, J. and Villasenor, L.; Thermal characterization of pine wood by photoacoustic and photothermal techniques. Holz als Roh- und Werkstoff, 58, 241-246, 2000.

Linjewile, T. M., Hull, A. S. and Agarwal, P. K.; Heat transfer to a large mobile particle in gas-fluidized beds of smaller particles. Chem. Eng. Sci., 48, 21, 3671-3675, 1993.

Sellassie, K. G., Moo-Young, H. K. and Lioyd, T. B.; Determination of the thermal conductivity of shredded tyres by utilizing a hot plate apparatus. Int. J. Environment and Waste Management, Vol. 1, Nos. 2/3, 179-191, 2007.

Tscheng, S. H. and Watkinson, A. P.; Convective heat transfer in a rotary kiln. Can. J. Chem. Eng., Vol. 57, 433-443, August 1979.

Yang, J., Tanguy, P. A. and Roy, C.; Heat transfer, mass transfer and kinetics study of the vacuum pyrolysis of a large used tire particle. Chem. Eng. Sci., Vol. 50, No. 12, 1909-1922, 1995.

Appendix C – Calculation of values used in the char model

The char particle density, ρ_p, is calculated based on knowledge of the virgin fuel density as well as volatile and ash content:

$$\rho_p = \left(1 - Volatiles - Ash\right) \cdot \rho_{p,0} \qquad \text{(C-1)}$$

The gas phase O_2-concentration, C_{O2}, is assumed to be constant in the rotary kiln freeboard cross section due to turbulent flow conditions, and is found from the ideal gas law:

$$C_{O_2} = \frac{y_{O_2} \cdot P}{R \cdot T} \qquad \text{(C-2)}$$

where P is the pressure in Pa, R is the gas constant and T is the temperature in Kelvin. y_{O2} is the mole fraction of O_2 in the gas phase.

The binary diffusion coefficient, D_{O2}, for oxygen in nitrogen is temperature dependent. The value at a specific temperature can be predicted with an accuracy of 5% by use of the Chapman-Enskog kinetic theory (Bird et al., 2002):

$$D_{O_2} = 0.0018583 \sqrt{T^3 \left(\frac{1}{M_{O_2}} + \frac{1}{M_{N_2}} \right)} \frac{1}{P\sigma^2 \Omega} \qquad \text{(C-3)}$$

where T is the temperature in Kelvin, M is the molar masses of oxygen and nitrogen, respectively, P is the pressure in atm, σ is the collision diameter in Ångstrøm and Ω is the collision integral for diffusion. The unit of D_{O2} will be cm^2/s.
By using table values from Bird et al., the so-called Lennard-Jones parameters, σ and ε/κ, can be calculated (Bird et al., 2002):

$$\sigma = ½\left(\sigma_{O_2} + \sigma_{N_2}\right) = ½\left(3.433 + 3.667\right) \mathring{A} = 3.55 \cdot 10^{-10} m \qquad \text{(C-4)}$$

$$\frac{\varepsilon}{\kappa} = \sqrt{\frac{\varepsilon_{O_2}}{\kappa} \frac{\varepsilon_{N_2}}{\kappa}} = \sqrt{113 \cdot 99.8} = 106.2K \qquad \text{(C-5)}$$

The collision integral Ω can be calculated from the expression:

$$\Omega = \frac{1.06036}{T^{*0.1561}} + \frac{0.193}{\exp(0.47635T^*)} + \frac{1.03587}{\exp(1.52996T^*)} + \frac{1.76474}{\exp(3.89411T^*)} \qquad \text{(C-6)}$$

where $T^* = \frac{\kappa T}{\varepsilon}$ (C-7)

By using these expressions, D_{O2} can be calculated at any given temperature.

Appendix C references

Bird, R. B., Stewart, W. E. and Lightfoot, E. N.; Transport Phenomena, 2nd edition, John Wiley & Sons, 2002. ISBN: 0-471-41077-2.

Appendix D – Species included in the equilibrium calculations

For the equilibrium calculations, gas phase compounds, pure solid phases, and pure liquid phases were included from the FactSage 6.0 compound database. The species included from the compound database are listed below.

Gas phase components

N_2	N_2O	H	OAlOH
CO_2	HONO	HNO	OAlCl
H_2O	ONCl	K	CaCl
O_2	CO	$O_2S(OH)_2$	$(FeCl)_2$
HCl	SO_3	NaO	NaH
KCl	K_2SO_4	NO_3	N
$(KCl)_2$	O	$(NaOH)_2$	SO_2Cl_2
$(NaCl)_2$	Na_2SO_4	$(KOH)_2$	FeO
NO	H_2	KO	CaOH
Cl	HOOH	Cl_2O	HNCO
NO_2	$FeCl_2$	$KAlCl_4$	NH_2
Cl_2	$NaFeCl_4$	$NaAlCl_4$	KH
OH	$HONO_2$	$AlCl_3$	$SOCl_2$
HOCl	$FeCl_3$	N_2O_3	NH
$CaCl_2$	$Ca(OH)_2$	COCl	N_2O_5
KOH	Na	$COCl_2$	FeCl
NaOH	$Fe(OH)_2$	HCOOH	$(FeCl_3)_2$
ClO	O_3	NH_3	$AlCl_2$
SO_2	NO_2Cl	SO	N_3
HOO	ClO_2	N_2O_4	HCO
CaO	SCl	NS	$SiHCl_3$
H_2CO	HCN	NaCN	$SiCl_2$
Fe	S	$SiCl_3$	CH_2Cl_2
Na_2	AlO_2	KCN	N_2H_4
NCO	Ca	AlO	CH_3OH
$SiCl_4$	AlOH	Al_2Cl_6	CaH
HNNH	AlCl	CCl_4	SSO
SCl_2	HS	$CHCl_3$	CH_3Cl
K_2	H_2S	CCl_3	AlOH
ClCN	COS	CN	CH_4
$AlCl_6Fe$	SiO	CCl_2	CNN
S_2Cl	C_2HCl	CS_2	CH_3CH_2OH
C_2O	Si	CH_3NC	C_2H_5Cl
CS	CH_3NH_2	CH_2CHCl	$CH_3N_2H_3$
CaS	Al_2O	$(KCN)_2$	C_2H_6
$(AlO)_2$	SiH_3Cl	C_2H_4O	AlC
SiCl	C_2Cl_4	CH_3SH	AlN
CH	C_2H_4	C_2H_4	Ca_2
ClSSCl	$CHClCCl_2$	C_2Cl_6	$(NaCN)_2$

CH_3COOH	SiH	C_2Cl_5H	C_2
C_3O_2	C_2H_4O	S_3	CH_3CHCl_2
HCNS	SiS	SiH_4	SiN
$(CN)_2$	AlS	C_2H_3	CH_3COCl
C_2Cl_2	C_2N	$CHCl_2CHCl_2$	C_2H
H_2S_2	CH_2CCl_2	CHCl2CH_2Cl	$SiCH_3Cl_3$

Pure solid phases

Ca_2SiO_4	NaOH	$NaNO_2$	Fe
$CaSO_4$	FeOCl	$Fe_2O_3(H_2O)$	$KAlSi_3O_8$
$Ca_2Al_2SiO_7$	$Ca_3Al_2Si_3O_{12}$	KNO_3	$NaAlSi_3O_8$
$Ca_2Fe_2O_5$	SiO_2	$NaHCO_3$	K
$CaAl_2O_4$	$Ca_3Fe_2Si_3O_{12}$	$CaOCl_2$	$Al_6Si_2O_{13}$
$KCaCl_3$	$CaAl_{12}O_{19}$	$FeSiO_3$	$(FeO)_2(SiO_2)$
NaCl	KAl_9O_{14}	$FeCl_2$	$K_2(OH)(NO_3)$
KCl	Fe_2O_3	$Na_2Al_{12}O_{19}$	$(FeO)_2(SiO_2)$
Ca_2SiO_4	KOH	$FeCO_3$	$NaAlSi_3O_8$
$CaAl_4O_7$	$(CaSO_4)_2(H_2O)$	$FeCl_2$	$FeSiO_3$
$CaFe_2O_4$	$(Na_2O)(SiO_2)$	$CaAl_2Si_2O_8$	$FeCl_3$
CaO	$Na_3(OH)(SO_4)$	$FeSiO_3$	K_2O_2
$CaCO_3$	$K_2Ca(CO_3)_2$	$KFeCl_4$	$KAl(SO_4)_2$
Ca_3SiO_5	$NaAl_9O_{14}$	$KHCO_3$	$H_2Si_2O_5$
$Ca_3Al_2O_6$	K_2CO_3	$NaAlSi_2O_6$	$KAlCl_4$
$CaCl_2$	$CaAl_2Si_2O_8$	H_2SiO_3	$NaAlSi_2O_6H_2O$
$Ca_3Si_2O_7$	$NaAlSiO_4$	$Al(OH)_3$	H_4SiO_4
Al_2O_3	$Na_2Ca_2Si_3O_9$	$(Na_2O)(SiO_2)_2$	$Na_2Ca_3Si_6O_{16}$
Na_2SO_4	Al_2SiO_5	$Fe(OH)_2$	SO_3
$CaSiO_3$	H_2O	$CaFeSi_2O_6$	K_2O
Fe_2O_3	Al_2SiO_5	$K_2Si_2O_5$	$Na_6Si_2O_7$
$CaSiO_3$	$K_2Ca_2(CO_3)_3$	$FeSO_4$	$Na_3(OH)_2(NO_3)$
K_2SO_4	$Ca_2FeSi_2O_7$	$K_2Si_2O_5$	$Ca(NO_3)_2$
$K_2Ca_2(SO_4)_3$	$(CaSO_4)_2(H_2O)$	$Ca_2Al_3Si_3O_{12}(OH)$	$NaAlCl_4$
$KAlO_2$	$CaSO_3$	$CaSO_4(H_2O)_2$	NaH
$CaFe_4O_7$	OAlCl	Na_2SO_3	$KAl_3Si_3O_{10}(OH)_2$
CaO_2	$Al_2O_3(H_2O)$	$Na_4CaSi_3O_9$	C
$CaAl_2SiO_6$	$Al_2O_3(H_2O)$	Fe_3O_4	$CaAl_2Si_2O_7(OH)_2(H_2O)$
$NaAlO_2$	$KAlSi_2O_6$	$(Na_2O)_2(SiO_2)$	$KClO_4$
$K_3Na(SO_4)_2$	K_2SiO_3	$Fe(OH)_3$	KH
$Al_2Fe_2O_6$	K_2SiO_3	$NaFeCl_4$	$NaAl_3Si_3O_{12}H_2$
$Ca(OH)_2$	K_2FeCl_4	Na_2O	$AlCl_3$
$NaAlSiO_4$	NaO_2	Na_2O_2	$KClO_4$
$KAlSiO_4$	$K_2Al_{12}O_{19}$	$AlCH_2NaO_5$	$CaSO_3(H_2O)_2$
Na_2CO_3	$KFeCl_3$	K_2SO_3	$Al_2O_3(H_2O)_3$
Na_2CO_3	KO_2	Na_2O_2	$K_2Si_4O_9$
$KAlSiO_4$	$NaNO_2$	Na	$(CaO)_6(SiO_2)_6(H_2O)$
FeO	KNO_3	$(FeO)_2(SiO_2)$	$Na_2CaSi_5O_{12}$

Fe_3O_4	$NaNO_3$	Na_2OHNO_3	$K_2Si_4O_9$
NaOH	$(Na_2O)(Fe_2O_3)$	$CaAl_4Si_2O_{10}(OH)_2$	$NaClO_4$
$FeAl_2O_4$	$NaNO_3$	$KAlSi_3O_8$	$(CaO)(SiO_2)_2(H_2O)_2$
S	$CaC_2O_4(H_2O)$	$(Al_2O_3)(SiO_2)_2$	Ca
AlN	N_2O_4	$H_6Si_2O_7$	$(CaO)_8(SiO_2)_6(H_2O)_3$
$(CaO)_3(SiO_2)_2(H_2O)_3$	$(Al_2O_3)(SiO_2)_2(H_2O)_2$	CaS	$(Al_2O_3)(SiO_2)_2(H_2O)_2$
NH_4Cl	$KFe_3AlSi_3O_{10}(OH)_2$	$CaCl_2(H_2O)_6$	$(CaO)_5(SiO_2)_6(H_2O)_3$
$(Al_2O_3)(SiO_2)_2(H_2O)_2$	Fe_2N	$K_4C_2O_6(H_2O)_3$	NH_4NO_3
$Fe_3Al_2Si_3O_{12}$	FeS	Al	$Ca(NO_3)_2(H_2O)_3$
$Al_2Si_4O_{10}(OH)_2$	$Fe_2(SO_4)_3$	K_2S	NH_4HCO_3
N_2O_5	$Al_2(SO_4)_3$	$(CaO)_3(Al_2O_3)(H_2O)_6$	Si
NaCN	$Ca(NO_3)_2(H_2O)_2$	CaH_2	$Na_6Si_8O_{19}$
KCN	Na_2S	$Fe_2Al_4Si_5O_{18}$	$Ca(NO_3)_2(H_2O)_4$
AlS	FeSi	$FeAl_2Cl_8$	FeS_2
$NH_4Al(SO_4)_2$	NH_4ClO_4	Na_2S_2	SiS
$(CaO)_{12}(SiO_2)_6(H_2O)_7$	$CO(NH_2)_2$	$AlCl_3(H_2O)_6$	$FeSO_4(H_2O)_7$
NH_4ClO_4	NaS_2	$(CaO)_4(SiO_2)_6(H_2O)_5$	SiC
Fe_4N	AlH_3	Fe_3C	CaC_2
$(NH_4)_2(SO_4)$	CaSi	NH_4HS	$(CaO)_4(Al_2O_3)(H_2O)_{13}$
C_2Na_2	$Na_2SO_4(H_2O)_{10}$	$Na_2CO_3(H_2O)_{10}$	$Al_2(SO_4)_3(H_2O)_6$
CH_3NH_3Cl	Ca_3N_2	$Ca(ClO_4)_2(H_2O)_4$	NH_2CH_2COOH
SiS_2	$(CaO)_2(Al_2O_3)_2(SiO_2)_8$	Fe_3Si	Na_2S_3

Pure liquid phases

KCl	Na_2SO_4	H_2O	KOH
NaCl	K_2SO_4	Al_2O_3	SiO_2
$CaSO_4$	CaO	NaOH	K_2CO_3
$CaCl_2$	$NaAlO_2$	$KAlO_2$	$(Na_2O)(SiO_2)$
$CaAl_2O_4$	$CaAl_4O_7$	FeO	Fe_3O_4
$NaNO_3$	$NaNO_2$	K_2SiO_3	$K_2Si_2O_5$
K_2SO_3	KNO_3	$(Na_2O)(SiO_2)_2$	Na_2SO_3
$FeCl_3$	Na	Na_2O	$(Na_2O)_2(SiO_2)$
HOOH	$KAlCl_4$	$NaAlCl_4$	$AlCl_3$
K	$HONO_2$	$O_2S(OH)_2$	$Na_6Si_2O_7$
Fe	SO_3	K_2O	$H_2SO_4(H_2O)$
HCOOH	N_2O_4	$H_2SO_4(H_2O)_2$	NH_4Cl
$K_2Si_4O_9$	S	Ca	$H_2SO_4(H_2O)_3$
NaCN	$H_2SO_4(H_2O)_6$	Al	CH_2Cl_2
KCN	HCN	K_2S	N_2H_4
$SiCl_4$	Na_2S	$CHCl_3$	CH_3OH
SCl_2	$H_2SO_4(H_2O)_4$	CCl_4	AlS
FeS	Na_2S_2	$SiHCl_3$	$(NH_4)_2O$
CH_3NO_2	ClSSCl	H_2S_2	CH_3NH_2
NaS_2	CH_3COOH	CH_3COCl	C_2Cl_4
$CHClCCl_2$	Fe_3C	CH_2CCl_2_cis-12	CH_2CCl_2_trans-12
CaC_2	C_2H_4O	CH_2CCl_2	C_2Na_2

CS_2	CH_3SH	$CHCl_2CHCl_2$	CH_3CHCl_2
CH_3NC	C_2H_4O	$(CH_2OH)_2$	C_2H_5Cl
CH_3CH_2OH	SiS_2	$CH_3N_2H_3$	Na_2S_3

Appendix E – Gas and bed temperatures through the rotary kiln

Gas and bed temperatures through the rotary kiln are assumed to change according to the following equations:

$$\frac{dT_g}{dt} = \frac{T_{g,out} - T_{g,in}}{\tau} - \frac{(1-Y)}{C_{p,g}} \cdot \left(\frac{dV}{dt} \frac{\dot{m}_{fuel} \cdot y_{Vol} \cdot LHV_{Vol}}{\left(\dot{m}_{fuel} \cdot y_{Vol} \cdot V(t) + \dot{m}_g \right)} + \frac{dX}{dt} \frac{\dot{m}_{fuel} \cdot y_{Char} \cdot LHV_{Char}}{\left(\dot{m}_{fuel} \cdot y_{Char} \cdot X(t) + \dot{m}_g \right)} \right) \quad \text{(E-1)}$$

$$\frac{dT_b}{dt} = \frac{T_{b,out} - T_{b,in}}{\tau} + \frac{Y}{C_{p,b}} \cdot \left(\frac{dV}{dt} \cdot \frac{\dot{m}_{fuel} \cdot y_{Vol} \cdot LHV_{Vol}}{\left(\dot{m}_{fuel} \cdot y_{Vol} \cdot V(t) + \dot{m}_b \right)} + \frac{dX}{dt} \cdot \frac{\dot{m}_{fuel} \cdot y_{Char} \cdot LHV_{Char}}{\left(\dot{m}_{fuel} \cdot y_{Char} \cdot X(t) + \dot{m}_b \right)} \right) \quad \text{(E-2)}$$

These equations describe that the gas and bed temperatures through the rotary kiln changes linearly, but are affected by the heat release from both the volatile and char content of the fuels that are fed to the material inlet end. $T_{g,out}$ and $T_{b,out}$ are gas and bed temperatures in the material outlet end of the rotary kiln, and $T_{g,in}$ and $T_{b,in}$ are gas and bed temperatures in the material inlet end of the rotary kiln. τ is the mean solid residence time in the rotary kiln, and is estimated by the empirical formula:

$$\tau = \frac{11.2 \cdot L}{n \cdot D \cdot s} \quad \text{(E-3)}$$

where L is the rotary kiln length, n is the rotary kiln speed, D is the inner kiln diameter and s is the rotary kiln inclination. This empirical formula can only be used to give a rough estimate of the mean solid residence time in the rotary kiln, since it does not consider physical properties of the solids. However, the mean residence time predicted by the formula is in good correspondence with experimentally measured mean residence times in a cement rotary kiln reported by Strauβ et al. (1987) and experiments with sand in a pilot-scale rotary kiln, reported by Liu and Specht (2006).
Y is the fraction of heat that is released to the bed relative to the heat released to the gas, see section 5.1 in chapter 5. V is the dimensionless devolatilization degree, and the change with time is estimated from equation 5.6 or 5.9 in chapter 5:

$$\frac{dV}{dt} = \frac{1}{\tau_{Devol}} \quad \text{(E-4)}$$

X is the dimensionless char oxidation degree, and the change with time is estimated from equation 5.27 in chapter 5. m_{fuel}, m_g and m_b are the mass flows of fuel, gas and raw material bed in kg/s. y_{Vol} and y_{Char} are the volatile and char fractions in the fuel, respectively. LHV_{Vol} and LHV_{Char} are the lower heating values of volatiles and char, respectively. LHV_{Char} is found from

the reaction enthalpy for oxidation of carbon to CO_2, while LHV_{Vol} is found by subtracting LHV_{Char} from the fuel lower heating value, LHV:

$$LHV_{Vol} = \frac{LHV - y_{Char} \cdot LHV_{Char}}{y_{Vol}} \qquad \text{(E-5)}$$

The first term in equations (E-1) and (E-2) refers to the situation in a rotary kiln without alternative fuel utilization in the material inlet end, where it is assumed that bed and gas temperatures change linearly along the kiln length. This is a simplification of actual conditions in a rotary kiln where gas and bed temperatures will also be affected by gas-bed heat transfer, gas-wall heat transfer and wall-bed heat transfer. These heat transfer mechanisms should be included in the equations as well in order to obtain more realistic temperature profiles along the kiln length. It is therefore important to point out that equation (E-1) and (E-2) should be further developed to include the entire heat transfer mechanism between gas-bed, bed-wall, gas-wall and heat loss to the surroundings. This work has not been made in the present study because char oxidation is assumed to be the slowest and most critical part of the fuel combustion in industrial rotary kilns, regarding conversion times: Temperature is expected to be of minor importance for the fuel char oxidation which is more dependent on oxygen mass transfer to the char particles.

$T_{g,\,in}$ is calculated from the expression:

$$T_{g,in} = T_{g,in,0} + \frac{(1-Y) \cdot LHV \cdot \dot{m}_{fuel}}{C_{p,g} \cdot \left(\dot{m}_{fuel} + \dot{m}_{g} \right)} \qquad \text{(E-6)}$$

where $T_{g,\,in,0}$ is the gas inlet temperature if there is no fuel utilization in the material inlet end.

Appendix E references

Liu, X. Y. and Specht, E.; Mean residence time and hold-up of solids in rotary kilns. Chem. Eng. Sci., 61, 5176-5181, 2006.

Strauß, F., Steinbiß, E. and Wolter, A.; Measurement of retention times in cement burning systems with the aid of radionuclides. ZKG-International, 9, 441-446, 1987.

Appendix F – Stoichiometric calculations on flue gas composition

The following formula is used to describe the reaction of the fuel with oxygen from the combustion air:

$$C_\alpha H_\beta S_\gamma N_\delta O_\varphi Cl_\xi \cdot (H_2O)_\mu + \lambda(\alpha + \frac{\beta}{4} + \gamma + \frac{\delta}{2} - \frac{\varphi}{2}) \cdot \left(O_2 + \frac{79}{21} N_2 \right) \rightarrow$$
$$\alpha CO_2 + (\frac{\beta}{2} + \mu) H_2O + \gamma SO_2 + \delta NO + \frac{\xi}{2} Cl_2 + (\alpha + \frac{\beta}{4} + \gamma + \frac{\delta}{2} - \frac{\varphi}{2}) \cdot \left((\lambda - 1) O_2 + \frac{79}{21} \lambda N_2 \right) \quad \text{(F-1)}$$

where λ is the excess air ratio. The stoichiometric numbers α, β, etc., have the unit mol/kg fuel. The reaction can be divided into one reaction equation for devolatilization and one for char oxidation. The volatile fraction in the fuel is assumed to be all non-carbon compounds and the amount of carbon needed to reach the volatile weight fraction, y_{Vol}:

$$C_{\alpha,Vol} H_\beta S_\gamma N_\delta O_\varphi Cl_\xi \cdot (H_2O)_\mu + \lambda(\alpha_{Vol} + \frac{\beta}{4} + \gamma + \frac{\delta}{2} - \frac{\varphi}{2}) \cdot \left(O_2 + \frac{79}{21} N_2 \right) \rightarrow$$
$$\alpha_{Vol} CO_2 + (\frac{\beta}{2} + \mu) H_2O + \gamma SO_2 + \delta NO + \frac{\xi}{2} Cl_2 + (\alpha_{Vol} + \frac{\beta}{4} + \gamma + \frac{\delta}{2} - \frac{\varphi}{2}) \cdot \left((\lambda - 1) O_2 + \frac{79}{21} \lambda N_2 \right)$$
(F-2)

where α_{Vol} is found from:

$$\alpha_{Vol} = \frac{y_{Vol} - \left(\beta \cdot M_H + \gamma \cdot M_S + \delta \cdot M_N + \phi \cdot M_O + \xi \cdot M_{Cl} + \mu \cdot M_{H_2O} \right)}{M_C} \quad \text{(F-3)}$$

The reaction equation for the char oxidation becomes:

$$C_{\alpha,Char} + \lambda \cdot \alpha_{Char} \cdot \left(O_2 + \frac{79}{21} N_2 \right) \rightarrow$$
$$\alpha_{Char} CO_2 + \alpha_{Char} \cdot \left((\lambda - 1) O_2 + \frac{79}{21} \lambda N_2 \right) \quad \text{(F-4)}$$

where α_{Char} is found from:

$\alpha_{Char} = \alpha - \alpha_{Vol}$ (F-5)

The minimum amount of air, $N_{air,min}$, needed for the fuel combustion and the minimum amount of produced flue gas, $N_{FG,min}$, is estimated from:

$$N_{air,\min} = \frac{\alpha + \frac{\beta}{4} + \gamma + \frac{\delta}{2} - \frac{\phi}{2}}{y_{O_2}^{air}} \quad \text{(F-6)}$$

$$N_{FG,\min} = N_{air,\min} + \frac{\beta}{4} + \mu + \frac{\delta}{2} + \frac{\phi}{2} + \frac{\xi}{2} \qquad \text{(F-7)}$$

The excess air ratio is the actual amount of combustion air relative to the minimum amount:

$$\lambda = \frac{N_{air}}{N_{air,\min}} \qquad \text{(F-8)}$$

The actual amount of produced flue gas is determined as:

$$N_{FG} = N_{FG,\min} + (\lambda - 1) N_{air,\min} \qquad \text{(F-9)}$$

The mole fraction of oxygen in the flue gas is estimated from:

$$y_{O_2}^{FG} = \frac{(\lambda - 1) N_{air,\min} \cdot y_{O_2}^{air}}{N_{FG}} \qquad \text{(F-10)}$$

The flue gas oxygen fraction in the kiln material inlet end may be described as:

$$y_{O_2,in}^{FG} = y_{O_2,\text{ burner}}^{FG} - \frac{(\alpha + \frac{\beta}{4} + \gamma + \frac{\delta}{2} - \frac{\varphi}{2}) \cdot \dot{m}_{fuel}}{\dot{n}_{FG,in}} \qquad \text{(F-11)}$$

where $y_{O2,burner}$ is the oxygen fraction in the flue gas leaving the kiln main burner. $n_{FG,in}$ is the total moles of flue gas per second.

The change in oxygen concentration along the kiln length can be estimated from the expression:

$$y_{O_2}(t) = y_{O_2,in} + \frac{(\alpha_{Vol} + \frac{\beta}{4} + \gamma + \frac{\delta}{2} - \frac{\varphi}{2}) \cdot \dot{m}_{fuel} \cdot V(t)}{\dot{n}_{FG,in} - (\frac{\beta}{4} + \mu + \frac{\delta}{2} - \frac{\varphi}{2}) \cdot \dot{m}_{fuel} \cdot V(t)} + \frac{\alpha_{Char} \cdot \dot{m}_{fuel} \cdot X(t)}{\dot{n}_{FG,in} - (\frac{\beta}{4} + \mu + \frac{\delta}{2} - \frac{\varphi}{2}) \cdot \dot{m}_{fuel} \cdot V(t) - \alpha_{Char} \cdot \dot{m}_{fuel} \cdot X(t)} \qquad \text{(F-12)}$$

Appendix G – Data used in the industrial model

Variable	Industrial kiln
Kiln length, m	60
Inner refractory diameter, m	4.35
Speed of rotation, min^{-1}	3
Angle of tilt, °	1.8
Solids flow, tpd (kg clinker/s)	3,500 (40.51)
Gas flow rate from burner, Nm^3/kg clinker	0.42
Gas temperature, material inlet end, °C	1,100
Gas temperature, material outlet end, °C	1,600
Bed temperature, material inlet end, °C	900
Bed temperature, material outlet end, °C	1,450
Pressure, atm	1
Gas molar weight, g/mol	31.5
Excess air ratio at main burner, λ	1,33 (5 vol.-% O_2 in flue gas from main burner)

Table F-1: Dimensions of kiln and operation conditions.

Parameter	Value
Stefan-Boltzmann constant, σ, $W/(m^2K^4)$	$5.6704 \cdot 10^{-8}$
ε_W	0.9
ε_p	0.9
ρ_B, kg/m^3	1650
$C_{p,bed}$, J/(kg-K)	800
Porosity, bed	0.5
h_{COND}, bed-char particle, $W/(m^2K)$	300
ΔH_r, C to CO, 25°C, J/mol	-110520
$T_{p,0}$, surface temperature, initial char ox., °C	1,050
Y (fuel contact ratio between gas and bed)	0.5

Table F-2: Values used in the calculations.

Appendixes

Paper A - Mixing large and small particles in a pilot-scale rotary kiln

Published in Powder Technology, 210, 273-280, 2011.

Paper B – High-temperature release of SO_2 from calcined cement raw materials

Published in Energy & Fuels, 25, 2917-2926, 2011.

Paper C – Sulfur release from cement raw materials during solid fuel combustion

Published in Energy & Fuels, 25, 3917-3924, 2011.

Paper D – Devolatilization and combustion of tire rubber and pine wood in a pilot scale rotary drum

Published in Energy & Fuels, 26, 854-868, 2012.

Powder Technology 210 (2011) 273–280

Contents lists available at ScienceDirect

Powder Technology

journal homepage: www.elsevier.com/locate/powtec

Mixing large and small particles in a pilot scale rotary kiln

Anders Rooma Nielsen [a,b,*], Rasmus Wochnik Aniol [a,b], Morten Boberg Larsen [a], Peter Glarborg [b], Kim Dam-Johansen [b]

[a] FLSmidth A/S, Vigerslev Allé 77, DK-2500 Valby, Denmark
[b] Department of Chemical Engineering, CHEC Research Centre, Technical University of Denmark (DTU), DK-2800 Lyngby, Denmark

ARTICLE INFO

Article history:
Received 5 October 2010
Received in revised form 23 November 2010
Accepted 27 March 2011
Available online 5 April 2011

Keywords:
Rotary kiln
Mixing
Alternative fuels
Cement
Heating
Combustion

ABSTRACT

The mixing of solid alternative fuel particles in cement raw materials was studied experimentally by visual observation in a pilot scale rotary kiln. Fuel particles were placed on top of the raw material bed prior to the experiment. The percentage of particles visible above the bed as a function of time was evaluated with the bed predominantly in the rolling bed mode. Experiments were conducted to investigate the effects of fuel particle size and shape, fuel particle density, rotary kiln fill degree and rotational speed. Large fuel particles and low-density fuel particles appeared more on top of the bed than smaller particles and high-density fuel particles. Fuel particle dimensions and sphericity were important parameters for the percentage of visible particles. Increasing bed fill degree and/or increasing rotational speed decreased the percentage of particles visible on top of the bed.

Results can be up-scaled to industrial conditions in cement rotary kilns and show that even relatively large fuel particles will predominantly be covered by raw material after less than 30 s in the rotary kiln. This affects the heating and combustion mechanisms for the fuel particles.

1. Introduction

Cement production is energy intensive with an energy usage of approximately 3 MJ per kg cement clinker produced [1]. Traditionally, cement production has mainly depended on fossil fuels such as coal, oil and natural gas. Due to fierce competition in the cement market, increasing fossil fuel prices and environmental concerns, many cement producers have increased the utilization of alternative fuels as a substitute for fossil fuels in order to achieve the most economic fuel mix. In this context, "alternative fuels" cover all non-fossil fuels and waste from other industries. Popular alternative fuels in the cement industry are tire-derived fuels, biomass residues and different commercial and industrial wastes.

It is attractive to feed coarse, solid alternative fuels into the material inlet end of cement rotary kilns in order to save expenses for shredding of the fuels to smaller particle sizes and to increase fuel flexibility. High temperatures in the rotary kiln and material retention times of several minutes provide good combustion conditions.

Rotary kilns are widely used in the cement industry where they are well suited for the cement clinker burning processes that require high temperatures at near-atmospheric pressure. The basic purpose of a rotary kiln is to a) transfer heat from the kiln gasses and walls to the solid particles in the rotary kiln bed and b) mix the solid particles in order to facilitate the cement clinker reactions. Because the particles on the outside of the bed insulate those on the inside, the rate of heat transfer is directly related to the rate of mixing of particles within the bed. Much research has been done to describe mixing of uniform particles in rotary kilns or rotary drums [2–5]. Less information is available about the mixing of particles with different sizes, shapes and densities. This is relevant when large alternative fuel particles are mixed with raw material particles of much smaller particle size. The degree of mixing of these fuel particles is important since their burnout behavior depends on mass and heat transfer. Most of the current research about mixing of particles with different sizes has been made with spherical balls of different materials, and typically with size ratios of less than 5 [6–13].

This article studies the mixing of different fuel particles and cement raw materials in order to predict combustion behavior. The study was carried out under ambient conditions in a pilot scale rotary kiln.

1.1. Bed behaviour

As a rotary kiln turns on its axis the solid bed inside is subjected to transverse motion. The bed motion can take many forms, depending on variables such as rotational speed, kiln diameter, fill degree, bed/wall friction and bed particle characteristics. For conditions relevant for clinker nodulization in cement rotary kilns, the characteristic bed motion is the rolling bed motion [14]. This article will therefore focus on the rolling mode. It should be noted however, that other bed motions are

* Corresponding author at: FLSmidth A/S, Vigerslev Allé 77, DK-2500 Valby, Denmark. Tel.: +45 36181000; fax: +45 36182647.
E-mail address: arni@flsmidth.com (A.R. Nielsen).

0032-5910/$ – see front matter © 2011 Elsevier B.V. All rights reserved.
doi:10.1016/j.powtec.2011.03.029

possible, particularly in the material inlet end of the rotary kiln where the partially calcined raw material particles enter with particle sizes typically in the order of 5–90 μm with average sizes around 20 μm.

Henein et al. have performed extensive work to establish bed behavior diagrams for a number of compounds [15]. This type of bed behavior diagrams is useful to predict mode of bed motion based on bed depth and Froude number (rotational speed). The Froude number is here defined as:

$$Fr = \frac{\omega^2 R}{g} = \frac{\left(\frac{2\pi n}{60}\right)^2 R}{g} \tag{1.1}$$

where ω has the unit rad/s and n has the unit min^{-1}. R is the drum radius and g is the gravitational acceleration in m/s^2. Mellmann investigated different operating regimes based on the Froude number [16]. He found that rolling beds typically occur for Froude numbers between $10^{-4}<Fr<10^{-2}$ for fill degrees higher than 10%. This result is in good correlation with Froude numbers reported by Henein et al. from experiments in a rotary drum with limestone and sand [15].

Henein et al. found useful correlations for scale up. The bed behavior is not only characterized by bed fill degree and Froude number for a given material. Particle size and shape must also be considered. For particles with the same shape and for rotary kilns with the same diameter and fill degree (and same bed/wall friction), the bed motion from one particle size to another can be described as [15]:

$$Fr_1\left(\frac{D}{d_p}\right)_1^{1/2} = Fr_2\left(\frac{D}{d_p}\right)_2^{1/2}. \tag{1.2}$$

This correlation is also valid for scaling of bed behavior from one drum diameter to another, for the same particle shape and size, and has been used in this study to estimate the relevant rotational speeds when scaling from an industrial rotary kiln to a pilot scale rotary kiln.

1.2. Fuel particle mixing

Cement rotary kilns are always slightly inclined with the raw materials entering in the upper end and flowing by gravity and kiln rotation to the lower end. A large fuel particle will spend some of its time in the active layer, on the bed surface, and the remainder of the time in the passive layer, below the bed surface. The time that the fuel particle will be present in the active layer relative to the time in the passive layer, depends on a number of parameters, such as bed fill degree, rotational speed, raw material characteristics, fuel particle size, shape and density.

Although mixing occurs in both the axial and transverse direction, mixing in the transverse direction is much more rapid [17]. This is true for mixing in both industrial rotary kilns as well as in horizontal, rotary drums.

The theoretical probability, P, of a large fuel particle to be present on top of the bed rather than being buried in the bed may be described as proportional to the volume occupied by the fuel particles relative to the total available volume:

$$P \propto \frac{1}{\theta}\frac{V_{fuel}}{V_{total}} \propto \frac{1}{\theta}\frac{V_{fuel}}{V_{fuel}+V_{raw\ material}} \propto \frac{1}{\theta}\frac{V_{fuel}}{V_{fuel}+\frac{\pi}{4}\cdot L\cdot D^2\cdot F}\cdot 100\% \tag{1.3}$$

where V_{fuel} is the volume of each fuel particle multiplied by the number of fuel particles in the bed, L and D are the kiln length and diameter, respectively, and F is the bed fill degree. θ is the sphericity which is a measure for the non-sphericity of the fuel particle, defined as:

$$\theta = \left(\frac{\text{Surface of sphere}}{\text{Surface of particle}}\right)_{\text{of same volume}}. \tag{1.4}$$

With this definition, $\theta = 1$ for spherical particles and $0<\theta<1$ for all other particle shapes. The sphericity is included because the shape of the particles is likely to affect the degree of visibility, because for particles of the same volume, the external particle surface area increases when the sphericity decreases. This may be illustrated with the three particle shapes shown in Fig. 1. All three particles have a volume of 1 cubic unit, but their external surface areas are quite different depending on their shape. The surface area increases with decreasing sphericity and thus the particle is more likely to be fully or partly visible in the bed.

Eq. (1.3) includes the kiln dimensions, bed fill degree, volume and sphericity of the fuel particle. The probability increases as the fuel volume increases. However, parameters such as rotational speed, fuel density and raw material density are not included, even though they are likely to have an effect. Attempts have been made to correlate experimental values for mixing with the operating parameters and properties of granular material. Sherrit et al. provide a review of such correlations [17]. However, these correlations are based on mixing of particles with the same or similar particle sizes. A similar correlation can be derived from experiments to yield a correlation of the form:

$$P = \frac{1}{\theta^a}\cdot\frac{V_{fuel}}{V_{fuel}+\frac{\pi}{4}D^2LF^b}\cdot Fr^c\cdot\left(\frac{\rho_{raw\ material}}{\rho_{fuel}}\right)^d\cdot 100\% \tag{1.5}$$

where a, b, c and d are the experimentally determined fitting parameters. Fr is the Froude number which includes the rotational speed. $\rho_{raw\ material}$ and ρ_{fuel} are the density of raw material and fuel particles, respectively.

2. Material and methods

2.1. Experimental setup

A pilot scale rotary kiln with inner diameter and length of 50 cm was used for the experiments, see Fig. 2. The kiln walls were made of a deck plate with a thickness of 5 mm, and a rough inner surface. The two end walls consisted of 600 mm diameter plexi glass plates with a thickness of 5 mm, which was mounted with butterfly screws for easy removal during loading and unloading of the pilot scale rotary kiln. The pilot scale rotary kiln was placed on rollers connected to a motor with variable speed. The rotary kiln was positioned horizontally with no inclination.

2.2. Materials

The experiments were all made with cement raw materials with physical and chemical properties as shown in Table 1. The raw material has a particle size that is significantly smaller than that of the fuel particles.

The 15 fuel particles used in the experiments are presented in Table 2.

These fuel particles all have different shapes, sphericities, sizes, volumes, weights and solid densities, given in the table per particle. The sphericity is defined in Eq. (1.4). As indicated by Table 2 some of the fuel particles have significantly larger dimensions than the raw material, and the size ratio may be as high as 10^4. The size ratio is, however, realistic, since solid fuels used in industrial cement rotary kilns may also have dimensions up to 1–2 m, whereas the cement raw material particle sizes generally are below 100 μm.

2.3. Methods

The desired fill degree is obtained by filling the pilot scale rotary kiln with the desired volume of raw material. The fill degree is here defined as the percentage of the kiln cross sectional area that is covered by raw

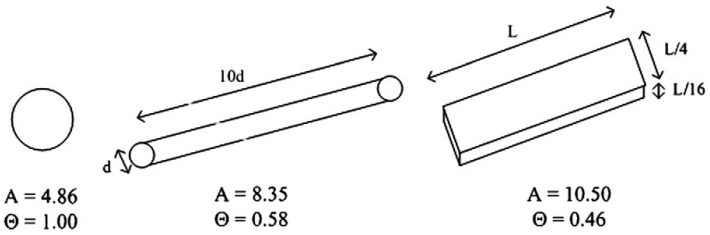

Fig. 1. External surface areas and sphericities for three particles with the same volume.

material. A fixed number of fuel particles are placed on top of the raw material, along the center line: 20 fuel particles were used in each experiment, except for the experiments with the largest fuel particles, sample no. 9 and no. 12 in Table 2. For these experiments with the two largest fuel particles, only 10 fuel particles were used. The rotation is started with the desired rotational speed. The rotational speed used in the experiments is varied between 3 and 16 rpm. It should here be noted that a rotational speed of 13 rpm in the experimental setup corresponds to approximately 5 rpm in an industrial rotary kiln with a 4 m diameter, if the scaling correlations found by Henein et al. are used [15].

A video camera was used to record the mixing in order to document the experiments. At time intervals of 30 s the rotation is stopped and the number of fuel particles visible on top of the bed are counted. Then the rotation is started again. This start–stop cycle is repeated until there are only random changes in the number of visible particles, or for at least 180 s. All fuel particles visible on the top of the bed are included, even if a significant fraction of the fuel particle is buried in the bed.

2.4. Assumptions and uncertainties

This section discusses the main differences between the pilot scale rotary kiln and industrial rotary kilns. The discussion presents assumptions that have to be made in order to account for uncertainties when results may be transferred from the pilot scale rotary kiln and to industrial scale conditions.

1. The experiments are made at ambient temperature. It is assumed that the fuel particle/raw material mixing at ambient temperature is the same as at high temperature conditions. This assumption is based on particle characteristics such as density which is virtually independent on temperature. An uncertainty, however, is the surface properties of the particles which may be quite different at ambient and high temperature conditions. At high temperatures the raw materials may stick to the fuel particles and e.g. affect sphericity and flowability of the fuel particles.
2. The pilot scale rotary kiln is not inclined. It is assumed that the lack of material transport in the axial direction has no significant effect on the overall mixing process since mixing in the transverse plane is dominating [17].
3. It is assumed that the dimensions of the pilot scale rotary kiln are sufficiently large to allow up-scale to industrial rotary kilns without introducing too much uncertainty. This assumption is based on the fact that several researchers have used similar rotary drums to simulate industrial conditions, and in many cases experimental results have been successfully validated against published full scale data [15,16].
4. It is assumed that Henein et al.'s scaling principles of rotational speed for rolling beds can be applied for the conditions used in these experiments [15]. This assumption is confirmed by visual observations of bed motion prior to the experiments, where the rolling motion is seen to be dominating.
5. It is assumed that the bed–wall friction coefficient in the pilot scale rotary kiln is of comparable size as to industrial kilns: The steel wall used in the pilot scale rotary kiln has a rough surface. In addition, the kiln walls are covered by a thin layer of raw material that adheres to the surface. This is assumed to be comparable to an industrial kiln where the wall is typically covered by a coating layer consisting of raw materials.

3. Results and Discussion

3.1. General observations

The mixing was generally observed to be a fast process that was completed in less than 30 s, or after a few kiln rotations. After this initial mixing, a steady state was reached where the percentage of visible particles did not change significantly. This observation is in correspondence with Cantelaube et al. who also reported that the mixing process of large particles appeared very quickly after the start of drum rotation, typically in less than one drum revolution [10].

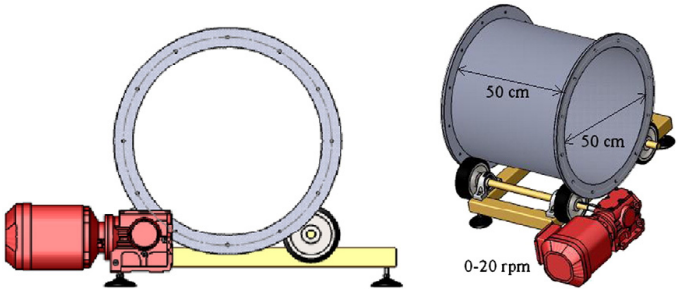

Fig. 2. Sketch of pilot scale rotary kiln used in the experiments.

Table 1
Composition and physical properties of cement raw material used in the experiments.

Chemical composition	
$CaCO_3$	78.4 wt.%
SiO_2	13.5 wt.%
Fe_2O_3	2.3 wt.%
Al_2O_3	3.3 wt.%
Minor components	2.6 wt.%
Bulk density	1200 kg/m^3
Number mean particle size	18 μm
Sieve interval, μm	
0–5	21.4 wt.%
5–10	13.3 wt.%
10–20	19.0 wt.%
20–30	12.5 wt.%
30–60	18.9 wt.%
60–90	8.2 wt.%
90–400	6.6 wt.%

The rotational velocity is varied from 3 rpm to 16 rpm, corresponding to approximately 1 to 6 rpm in an industrial, 4 m diameter rotary kiln according to the scaling correlations found by Henein et al. [15]. The bed behavior should be in the rolling regime under these conditions. The rolling bed behavior was also observed to be dominant.

Henein et al. reported that the dynamic angle of repose should be between 30° and 50° for cement raw materials in the rolling motion [15]. They also reported that the angle of repose is independent of fill degree and rotational speed when the rolling motion dominates [15]. In the experiments the angle of repose was generally measured to be between 30° and 40°, and thus in good correspondence with the findings of Henein et al. [15].

All experiments have been repeated three times. The repeatability is generally good with standard deviations of the experiments generally within 4–8%.

Based on all the experimental data, optimal values for the fitting parameters a, b, c and d used in Eq. (1.5) were determined. The optimal fitting parameters are shown in Table 3.

The visibility predicted by the correlation will be shown graphically in Figs. 4 to 7.

3.2. Effect of fuel particle size and shape

The effect of particle size and shape on the mixing efficiency has been investigated for fill degrees between 5% and 30% and rotational speeds between 3 rpm and 16 rpm. 12 samples with different sizes and shapes were used in the experiments, see Table 2 The sphericity is defined in Eq. (1.4). As indicated in Table 2 some of the fuel particles have significantly larger dimensions than the raw material, and the size ratio may be as high as 10^4. The size ratio is, however, realistic, since solid fuels used in industrial cement rotary kilns may also have dimensions up to 1–2 m, whereas the cement raw material particle sizes generally are below 100 μm.

Table 2
Fuel particles used in the experiments. Size, volume and weight are per particle. The density is the solid density.

Sample No.	Particle type	Shape/ sphericity	Size [cm]	Volume [cm^3]	Weight [g]	Density [kg/m3]
1	Charcoal	Oval/0.95	5.5×5.5×3.0	56.8	45	792
2	Charcoal	Oval/0.95	5.5×2.8×3.0	29.0	23	792
3	Charcoal	Irregular/0.89	2.8×2.8×3.0	10.1	8	792
4	Ceramic	Spherical/1.0	D=0.6	0.11	0.32	2829
5	Wood	Cubic/0.81	2×2×2	8.0	3.3	470
6	Wood	Cylindric/0.87	D=2.2, L=2	7.6	5.1	665
7	Wood	Cylindric/0.84	D=2.2, L=4	15.2	10	665
8	Wood	Rectangular/0.67	1.8×4.5×8.1	66.0	31	470
9	Wood	Rectangular/0.56	1.8×4.5×16.5	134.0	78	470
10	Tire rubber	Rectangular/0.78	2.5×2.0×4.0	20.0	22	1100
11	Tire rubber	Rectangular/0.75	2.5×5.0×6.0	75.0	82.5	1100
12	Tire rubber	Rectangular/0.59	2.5×8.0×17.0	340.0	374	1100
13	Plastic	Cylindric/0.73	D=1.3, L=5.3	7.0	2.4	341
14	Plastic	Cylindric/0.73	D=1.3, L=5.3	7.0	4.0	569
15	Plastic	Cylindric/0.73	D=1.3, L=5.3	7.0	7.7	1095

Table 3
Fitting parameters used in the correlation between percent visible particles and experimental data.

a	b	c	d
1.5 ± 0.2	1.2 ± 0.3	−0.09 ± 0.01	0.77 ± 0.2

See Table 2 for details. An example for a fill degree of 10% and a rotational speed of 13 rpm is shown in Fig. 3. It is observed that particles, regardless of size and shape, decrease rapidly from 100% percent visibility to significantly lower values. The mixing takes place within the first 30 s, corresponding to 1–8 kiln rotations. After this, the particles are to a large degree covered by raw material and only appear on top of the bed randomly.

It is noted that the large, rectangular samples numbers 9 and 12 are significantly more visible on top of the bed: After 30 s approximately 47% and 58% of these particles are still visible, respectively. And these percentages are more or less constant with time. On the contrary, the smallest particles which are the spherical ceramic particles denoted sample 4, drop from 100% to 0% during the first 30 s. Thereafter, the small particles are not observed more on top of the bed, during the 180 s that the experiment runs. The largest and most visible fuel particles numbers 9 and 12 are also the least spherical particles, whereas the smallest and least visible fuel particles are also the only truly spherical particles used in the experiments. These results indicate that not only the fuel particle dimensions but also the fuel particle shape, expressed as sphericity, is important for the visibility above the bed. This effect of sphericity is further confirmed by comparing samples numbers 1 and 8 which have similar volumes of 57 cm^3 and 66 cm^3, respectively, but quite different sphericities of 0.95 and 0.67. It is observed that the least

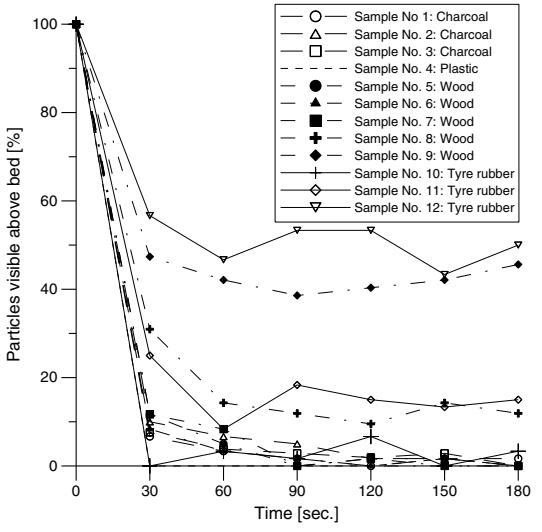

Fig. 3. Example of raw data: Percent particles visible above bed as a function of time. 10% fill degree and 13 rpm.

spherical particle is the most visible. However, the density of the two samples is not identical and this may affect the visibility as well. In order to determine the effect of shape with greater accuracy, it is required to conduct more experiments with fuel particles of similar volumes and densities but different shapes.

The experiments have been repeated for different fill degrees and rotational speeds and the tendency is the same under all conditions: Fuel particles with large dimensions have a higher probability to be visible on top of the bed relatively to smaller particles that are to a higher degree buried in the bed. This geometric effect on the degree of visibility was also predicted by Eqs. (1.3) and (1.5).

Fig. 4 shows the visibility of all the different fuel particles at steady state, sample no. 1 to sample no. 12, as a function of the fuel particle volume. Steady state is here defined as the time interval between 30 s and 180 s, where the percent visibility is relatively constant.

The small ceramic spheres, sample no. 4, had the smallest volume of 0.11 cm^3 per particle, and has a steady state visibility of close to 0%. Several of the tested fuel particles had volumes around 10 to 60 cm^3, but different sphericities and densities. The steady state visibility is still low, around 3–7%. For fuel particles with volumes larger than 100 cm^3 the percent visibility increases significantly, up to 50% for the largest particle with a volume of 340 cm^3. The standard deviation varied from 0% to 8% during the experiments, and was observed to be greatest for the largest fuel particles.

Fig. 4 also shows the estimated probability for the particles to be visible based on Eqs. (1.3) and (1.5). Even though Eq. (1.3) does not take the effect of density and rotational speed into account, a fairly good consistency is seen between the theoretical and experimental values, for volumes up to around 100 cm^3. But for the largest particles, Eq. (1.3) under-estimates the probability: This is particularly observed for the particle with a volume of 134 cm^3, where the observed visibility is 43% but the theoretical probability is only 21%. The reason why Eq. (1.3) fails to give a good estimation of the theoretical visibility for the largest particles may be that it becomes increasingly difficult for the largest particles to be fully buried in the bed, as their dimensions increase. Thus the degree of visibility will deviate more and more from the theoretical predictions as the particle dimensions increases.

Eq. (1.5) which includes correlations for rotational speed and density and the experimentally determined fitting parameters presented in Table 3 give a good consistency between theoretical and experimental values. The greatest deviation is for the particle with a volume of 57 cm^3 which deviates 4% from the experimental value. But it is also observed that sample no. 10 and sample no. 1 with volumes of 20 cm^3 and 57 cm^3, respectively, lie on a slightly lower visibility than the other particles with volumes in the range 10–70 cm^3. A reason can be that these two particles have a high density, see Section **3.5**. However, as indicated by the standard deviations, the reason may also simply be due to uncertainties.

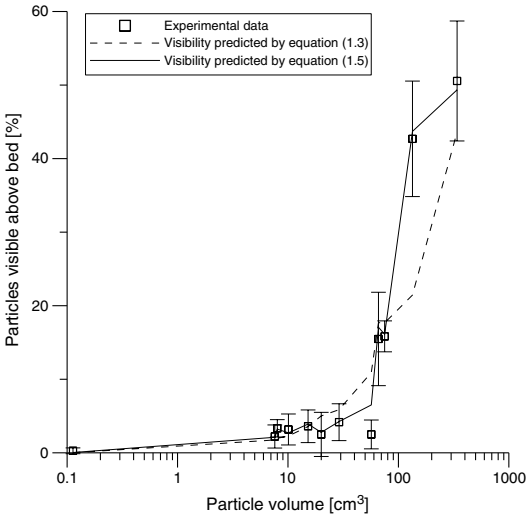

Fig. 4. Percent visible particles at steady state versus particle volume. 10% fill degree, 13 rpm. Eq. (1.3) is predictive while Eq. (1.5) has been adapted on the experimental data.

The observations regarding fuel particle size and the degree of visibility above the bed is in good correspondence with the theory about void filling presented by Savage and Lun [18]: During mixing of several layers of particles in a bed, void spaces between the particles are undergoing continual random changes. If a void space is large enough, then a particle from the above layer can fall into it as the layers move relative to each other. The probability of finding a void space that a small (raw material) particle can fall into is larger than the probability for finding a void space that a large (fuel) particle can fall into. Thus, this gravity-induced size-dependent void filling mechanism creates a tendency for small particles to end at the bottom and large particles to end at the top.

The observations may also be considered as a pure geometric effect where increasing dimensions of the fuel particles imply a decreasing probability that the fuel particles will be fully covered by the raw material bed.

3.3. Effect of bed fill degree

The raw material bed fill degree has been varied for all samples in the following range: 5%, 10%, 15% and 20%. This range of fill degrees covers the situation in industrial cement rotary kilns, where fill degrees typically are 8–15%.

Fig. 5 shows the effect of fill degree for tire rubber particles of three different sizes and thus with three different volumes, as specified in Table 2. For all three particle sizes are the percent visibility observed to decrease with increasing fill degrees.

The large particles are around 80% visible at the 5% fill degree. At 10% fill degree and 15% fill degree the percentages are around 50% and 40%, respectively.

It was found that the fill degree is an important parameter for the percentage of fuel particles that is present on top of the bed. Especially small particles will, regardless of shape, rapidly be buried in the bed. Larger particles will, due to their proportions, only be partly buried in the bed whereas part of the particles will be sticking out in the freeboard above the bed.

The degree of visibility predicted by Eq. (1.5) is shown with solid lines for each of the three particle sizes. The correlation fits the experimental data well with deviations generally less than 3%.

3.4. Effect of bed rotational speed

Fig. 6 shows the effect of rotational speed on the mixing of tire rubber particles, samples no. 10, 11 and 12 in Table 2. The rotational speed is expressed in terms of the dimensionless Froude number. It is observed that the percentage of visible particles decreases when the Froude number increases: Approximately 28% of the medium sized particles are visible at the lowest Froude number of 0.0024, whereas only 9% are visible at the highest Froude number of 0.0702. For the largest particles, 68% of the particles are visible at the lowest Froude number and 48% are visible at the highest Froude number. The smallest particles, however, do not show any particular dependence of Froude number. The same tendencies were also observed for other fill degrees and other particles.

The degree of visibility predicted by Eq. (1.5) is shown with solid lines for each of the three particle sizes. The correlation fits the experimental data well with deviations generally less than 3%.

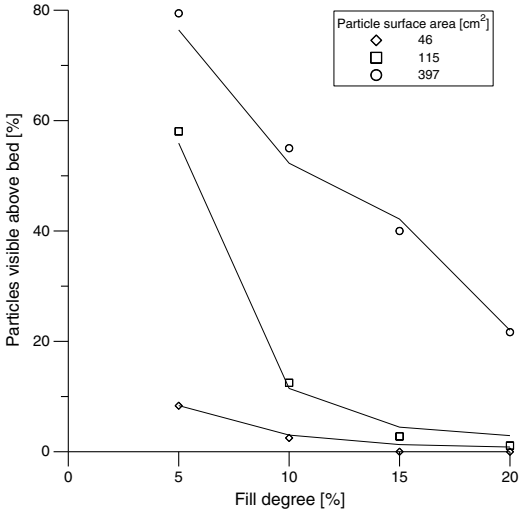

Fig. 5. Percent visible tire rubber particles versus bed fill degree for three different particle sizes. Predicted values are shown with solid lines and experimental values are shown with symbols. 10 rpm.

The effect of the rotational speed on percentage of visible particles can be explained by the fact that a high rotational speed is equal to more bed revolutions and thus a more efficient mixing process relative to a lower rotational speed [15]. It should, however, be noted that the percent visibility of particles seems to stabilize at a certain percentage for each rotational speed. These differences in steady state visibility at different rotational speeds may be due to the changes in centrifugal forces acting on the fuel particles which may affect the fuel particle distribution in the raw material bed.

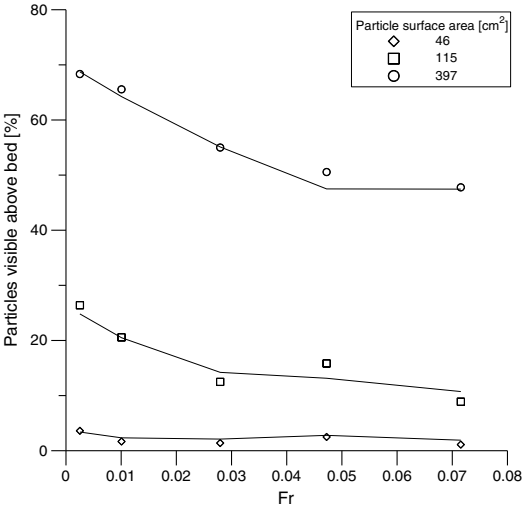

Fig. 6. Percent visible tire rubber particles versus Froude number for three different particle sizes. 10% fill degree. Predicted values are shown with solid lines and experimental values are shown with symbols.

Thomas and Cantelaube et al. also studied the effect of rotational speed on the segregation of particles up to 3 mm and 20 mm in diameter, respectively [11,13]. They found no effect of the rotational speed for these particle sizes, which are in correspondence with the observations in this study, for the smallest particles.

3.5. Effect of fuel density

The effect of particle density was studied by filling plastic containers of identical size and shape with materials of different weight. Thus, the outer dimensions of the particles were identical, but the densities were varied from low, medium and high, see Table 2 for details.

Fig. 7 shows the percentage of visible particles versus the raw material/fuel particle density ratio for fill degrees of 5%, 10% and 15%, and rotational speeds of 3, 10 and 16 rpm. Standard deviations on the results presented in Fig. 7 were between 2% and 6%. It is observed that the greatest effect of particle density appears with the 5% fill degree and 3 rpm: The low-density particles stabilize at a level around 45% visible particles, the medium-density particles stabilize at a level around 43% visible particles, whereas the high-density particles are only 28% visible. The same effect of particle density is also observed at 10% fill degree and 3 rpm. It is generally observed that the lowest rotational speed of 3 rpm results in the highest percentage of visible particles. The effect of density is observed to decrease as the fill degree and/or rotational speed increases.

Fig. 7 also shows the values predicted from Eq. (1.5), with solid lines and symbols. Eq. (1.5) predicts the visibility reasonably well, except for the two cases with the lowest rotational speed of 3 rpm: In these two cases the deviations are as high as 20%, which is a significantly higher deviation than observed for any other combinations of density, rotational speed, fill degree and fuel particle size and shape. There is thus a poor relationship between the fitting parameter for density, and some combinations of operational parameters.

The effect of particle density on the percent visibility is in good correspondence with the “push-away” theory presented by Tanaka,

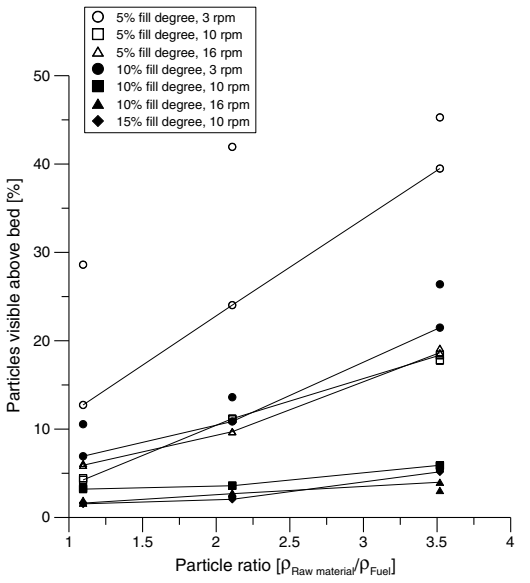

Fig. 7. Percent particles visible above bed at steady state versus particle density. Estimated values are shown with solid lines and symbols while experimental values are shown with symbols only.

which states that dense particles are more likely to push away other particles and sink to the bottom [19].

4. Practical implications

Eq. (1.5) is applied to conditions of an industrial rotary kiln in order to estimate the effect of fuel particle volume and sphericity on the percent visibility above the raw material bed. Typical values for a cement rotary kiln are shown in Table 4.

Two selected fuels, tire rubber and wood are studied. The fuel densities will decrease rapidly during the heating and devolatilization process in the material inlet where raw material temperatures and gas temperatures are typically 900 °C and 1100 °C, respectively. It is assumed that the fuel char densities are representative during the mixing process. The char density of tire rubber is assumed to be 340 kg/m^3 and the char density of wood is assumed to be 160 kg/m^3.

Fig. 8 shows the percent visibility of tire rubber char and wood char particles as a function of the fuel particle volume and for three different fuel particle sphericities of 0.5, 0.75 and 1.0, respectively. The volume of fuel particles is assumed to be distributed over the first 10 m of the material inlet end of the rotary kiln, where the combustion is assumed to take place. The percent visibility is observed to increase linearly with the fuel particle volume. It is interesting to note that the sphericity of the fuel particles has a great effect on the percent visibility: A pure spherical fuel particle ($\theta = 1.0$) is least visible due to its compact shape which leads to a high degree of fuel coverage by raw materials. As the fuel particle sphericity decreases, the percent visibility increases due to the larger dimensions of the fuel particles. The increasing dimensions of fuel particles of the same volume but decreasing sphericity are illustrated in Fig. 1. The tendency with sphericity and visibility is the same for tire rubber char and wood char but it is observed that the wood char is considerably more visible than tire rubber char due to its lower density.

An important practical implication for combustion processes in industrial rotary kilns can be concluded to be the shape of the fuel particles, because low sphericity fuel particles are expected to be in better contact with the gas phase, which may improve the combustion process. Also the fuel particle density will have an effect on the gas–fuel contact.

Full scale experience at two different cement plants with combustion of whole automobile tires and tire chips have shown that the tendency for undesirable effects on process stability and cement clinker quality due to reducing conditions in the raw material bed was less severe with whole tires relative to the situation with tire chips [20,21]. These results indicate that the smaller tire chips are to a higher degree buried in the raw material bed and create local reducing conditions. The larger whole tires will to a larger degree stay above the bed and be exposed to higher temperatures as well as to improved oxygen mass transfer from the freeboard gas. The industrial experience is in line with the experimental results in this study regarding the tendency for large fuel particles to be in better contact with the freeboard gas above the raw material bed relative to smaller fuel particles.

Table 4
Typical data for a modern cement rotary kiln (FLSmidth one string ROTAX 2 kiln).

Rotary kiln	
Inner diameter, m	4.35
Total rotary kiln length, m	51
Material inlet section length, m	10
Rotational speed, min^{-1}	4
Angle of tilt, °	3
Raw material flow, tpd (kg clinker/s)	3500 (40.51)
Mean raw material residence time, min	11
Mean raw material fill degree,%	11
Raw material density, kg/m^3	1200

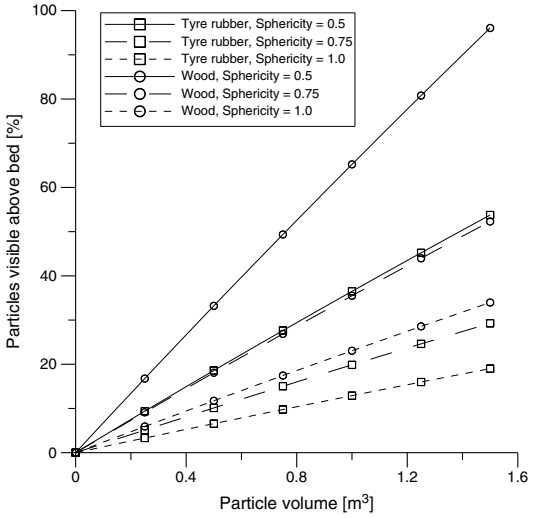

Fig. 8. Estimated degree of visibility of tire rubber char and wood char particles as a function of fuel particle volume and sphericity. Estimated by Eq. (1.5).

5. Conclusions

During experiments in a pilot scale rotary kiln distribution of large solid fuel particles in cement raw materials were studied. The results were evaluated as the percentage of fuel particles visible above the bed at specific time intervals.

The fuel particles were to a large degree buried in the cement raw materials within less than 30 s. After this, the percentage of visible fuel particles stabilized at a specific level, depending on fuel particle size. There was a clear tendency that large fuel particles were more visible than smaller fuel particles. Fuel particle dimensions and sphericity are important parameters for the degree of visibility.

Low-density fuel particles were more present above the bed than high-density fuel particles which were to a higher degree buried in the bed. The influence of density was particularly pronounced at low fill degrees and/or low rotational speeds.

The bed fill degree is of major importance for the percentage of visible fuel particles in the bed. Small bed fill degrees favor the number of fuel particles visible above the bed.

There is a tendency that an increase in rotational speed reduces the number of fuel particles visible above the bed. However, the effect of rotational speed was not as significant as the effect of bed fill degree.

A correlation for the percentage of visible fuel particles and the operating parameters was presented and compared with the experimental results. The correlation did generally predict the degree of visibility within 3%. However, the correlation failed to give good predictions in the cases with the lowest rotational speed of 3 rpm and density as a variable parameter.

Acknowledgments

The work described in this article is part of a research platform on future cement technology financed by The Danish National Advanced Technology Foundation, Technical University of Denmark and FLSmidth A/S.

References

[1] M. Schneider, VDZ Activity Report 2007–2009, Germany, 2009.
[2] G.R. Woodle, J.M. Munro, Particle motion and mixing in a rotary kiln, Powder Technol. 76 (1993) 241–245.
[3] A. Santomaso, M. Olivi, P. Canu, Mixing kinetics of granular materials in drums operated in rolling and cataracting regime, Powder Technol. 152 (2005) 41–51.
[4] D.R. van Puyvelde, Comparison of discrete elemental modelling to experimental data regarding mixing of solids in the transverse direction of a rotating kiln, Chem. Eng. Sci. 61 (2006) 4462–4465.
[5] M. Kwapinska, G. Saage, E. Tsotsas, Mixing of particles in rotary drums — a comparison of discrete element simulations with experimental results and penetration models for thermal processes, Powder Technol. 161 (2006) 69–78.
[6] S. Tallon, C.E. Davies, In-situ monitoring of axial particle mixing in a rotating drum using bulk density measurements, Powder Technol. 186 (2008) 22–30.
[7] A.V. Orpe, D.V. Khakhar, Scaling relations for granular flow in quasi-two-dimensional rotating cylinders, Phys. Rev. E 64 (031302) (2001) 1–13.
[8] S.K. Hajra, D.V. Khakhar, Sensitivity of granular segregation of mixtures in quasi-two-dimensional fluidized layers, Phys. Rev. E 031304 (2004) 1–4.
[9] E. Clément, J. Rajchenbach, J. Duran, Mixing of a granular material in a bidimensional rotating drum, Europhys. Lett. 30 (1995) 7–12.
[10] F. Cantelaube, D. Bideau, Radial segregation in a 2d drum: an experimental analysis, Europhys. Lett. 30 (1995) 133–138.
[11] F. Cantelaube, D. Bideau, S. Roux, Kinetics of segregation of granular media in a two-dimensional rotating drum, Powder Technol. 93 (1997) 1–11.
[12] M. Alonso, M. Satoh, K. Miyanami, Optimum combination of size ratio, density ratio and concentration to minimize free surface segregation, Powder Technol. 68 (1991) 145–152.
[13] N. Thomas, Reverse and intermediate segregation of large beads in dry granular media, Phys. Rev. E 62 (2000) 961–974.
[14] A.A. Boateng, Rotary Kilns, Elsevier Inc., USA978-0-7506-7877-3, 2008.
[15] H. Henein, J.K. Brimacombe, A.P. Watkinson, Experimental study of transverse bed motion in rotary kilns, Metall. Trans. B 14B (1983) 191–205.
[16] J. Mellmann, The transverse motion of solids in rotating cylinders — forms of motion and transition behaviour, Powder Technol. 118 (2001) 251–270.
[17] R.G. Sherritt, J. Chaouki, A.K. Mehrotra, L.A. Behie, Axial dispersion in the three-dimensional mixing of particles, Chem. Eng. Sci. 58 (2003) 401–415.
[18] S.B. Savage, C.K.K. Lun, Particle size segregation in inclined chute flow of dry cohesionless granular solids, J. Fluid. Mech. 189 (1988) 311–335.
[19] T. Tanaka, Segregation models of solid mixtures composed of different densities and particle sizes, Ind. Eng. Chem. Process Des. Develop. 10 (1971) 332–340.
[20] H.-E. Jannerup, Personal Communication, FLSmidth A/S, Valby, Denmark, September 2009.
[21] J.E. Lund, Personal Communication, Cemex Philippines, Tinaan, Naga, Cebu, Philippines, June 2010.

energy&fuels

ARTICLE

pubs.acs.org/EF

High-Temperature Release of SO_2 from Calcined Cement Raw Materials

Anders R. Nielsen,*[,†,‡] Morten B. Larsen,[†] Peter Glarborg,[‡] and Kim Dam-Johansen[‡]

[†]FLSmidth A/S, Vigerslev Allé 77, DK-2500 Valby, Denmark

[‡]Department of Chemical Engineering, CHEC Research Centre, Technical University of Denmark (DTU), DK-2800 Lyngby, Denmark

ABSTRACT: During combustion of alternative fuels in the material inlet end of cement rotary kilns, local reducing conditions may occur and cause reductive decomposition of sulfates from calcined cement raw materials. Decomposition of sulfates is problematic because it increases the gas-phase SO_2 concentration, which may cause deposit formation in the kiln system. In this study, the release of sulfur from calcined cement raw materials under both oxidizing and reducing conditions is investigated. The investigations include thermodynamic equilibrium calculations in the temperature interval of 800−1500 °C and experiments in a tube furnace reactor in the temperature interval of 900−1100 °C. The investigated conditions resemble actual conditions in the material inlet end of cement rotary kilns. It was found that the sulfates $CaSO_4$, K_2SO_4, and Na_2SO_4 were all stable under oxidizing conditions but began to decompose under reducing conditions. Particularly, $CaSO_4$ was sensitive to reducing conditions. The sulfur release was most significant if the gas atmosphere frequently shifted between oxidizing and reducing conditions. An increasing temperature from 900 to 1100 °C under alternating oxidizing and reducing conditions was also observed to increase the sulfur release from the calcined raw materials by a factor of 3, from 14 to 48%.

INTRODUCTION

Cement production is energy-intensive, with an energy usage of approximately 3 MJ/kg of cement clinker produced.[1] With an annual global cement production of 2.83 billion tons of cement, the cement industry is responsible for approximately 2% of the world's primary energy consumption.[2,3]

Fuel consumption accounts for about 30−40% of the total cement clinker production costs.[4] Traditionally, cement production has mainly depended upon the fossil fuels coal, oil, and natural gas. Because of fierce competition in the cement market, increasing fossil fuel prices, and environmental concerns, cement producers have increased the use of alternative fuels as a substitute for fossil fuels to achieve the most economic fuel mix. In this context, "alternative fuels" cover all nonfossil fuels and waste from other industries. Popular alternative fuels in the cement industry are tire-derived fuels, biomass residues, and different commercial and industrial wastes.

It is attractive to use coarse, solid alternative fuels in the material inlet end of cement rotary kilns to save expenses for shredding of the fuels to smaller particles and to increase fuel flexibility of the system. High temperatures in the rotary kiln and material retention times of several minutes provide good conditions for fuel burnout.

Figure 1 shows a simplified flow diagram and main sulfur reactions of a rotary kiln and calciner. Preheated cement raw materials are admitted to the calciner from the preheater (the preheater above the calciner is not shown). Because the raw materials have been preheated to around 800 °C, only inorganic-bound sulfur is present in the raw materials, mainly in the form of sulfates. Besides sulfur input from the cement raw materals, sulfur may also be introduced with the fuels in either calciner or rotary kiln. Sulfur from the fuel may be either organic- or inorganic-bound, and in Figure 1, sulfur input via the fuels is indicated by a S in parentheses.

The calciner acts as a fluidized-bed reactor where good contact between hot gas from the rotary kiln or tertiary air duct and raw materials from the preheater provide optimal conditions for gas−solid heat transfer and fuel combustion that drives the endothermic calcination of limestone.

$$CaCO_3(s) \leftrightarrow CaO(s) + CO_2(g) \quad (1)$$

Besides calcination of limestone, the conditions in the calciner with temperatures in the range of 800−900 °C, good gas−solid mixing, and excessive amounts of CaO also favor the SO_2 capture reaction.[5]

$$CaO(s) + SO_2(g) + \frac{1}{2}O_2(g) \leftrightarrow CaSO_4(s) \quad (2)$$

Because of the efficient SO_2 capture by CaO in the calciner, SO_2 emissions because of sulfur oxidation in the rotary kiln are negligible at modern cement plants equipped with a calciner. SO_2 emissions from cement plants are mainly due to oxidation of pyrite, Fe_2S, from the cement raw materials in the early stages of the preheater.[6] An exception, however, are cement plants operating with a bypass, where a fraction of the kiln gases are released to the atmosphere without being transported through the calciner. This may result in increased SO_2 emissions.

The partially calcined raw materials from the calciner are admitted to the material inlet end of the rotary kiln, where the calcination reaction is completed. In this paper, fully or partly calcined cement raw materials will be denoted calcined raw meal.

Sulfur present in the calcined raw meal is mainly bound as $CaSO_4$ or as alkali sulfates. The calcined raw meal is then

Received: April 20, 2011
Revised: May 23, 2011
Published: May 24, 2011

dx.doi.org/10.1021/ef2006222 | *Energy Fuels* 2011, 25, 2917–2926

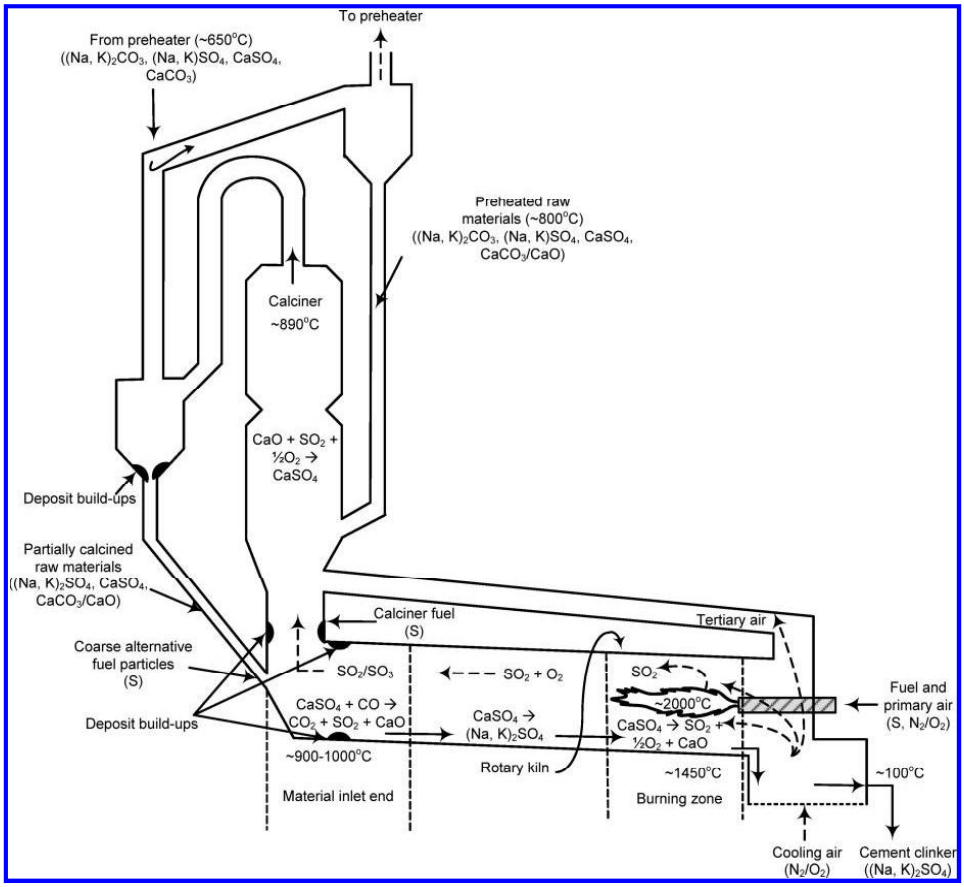

Figure 1. Simplified flow diagram of a rotary kiln, calciner, and material flows from a preheater, showing sulfur balances. Arrows indicate the flow direction, and the principal reactions are shown.

transported by the rotational movement and slight inclination of the rotary kiln toward the hot burning zone, where flame temperatures are in the range of 2000 °C and material temperatures are around 1450 °C. The clinker reactions take place during the gradual heating of the calcined raw meal as it is transported through the rotary kiln. During the gradual heating of the calcined raw meal, a sulfate melt is formed, which facilitates the formation of alkali sulfates, Na_2SO_4 and K_2SO_4, which are more thermodynamically stable than $CaSO_4$.[7] $CaSO_4$ will decompose at the high temperatures present in the burning zone and form SO_2.

$$CaSO_4(s) \leftrightarrow SO_2(g) + \frac{1}{2}O_2(g) + CaO(s) \qquad (3)$$

The fraction of $CaSO_4$ that decomposes in the burning zone depends upon parameters such as retention time, clinker and gas temperatures, gas composition, and clinker nodule size. High SO_2 concentrations in the gas phase suppress dissociation of $CaSO_4$ to CaO and SO_2 in the calcined raw meal.[7,8]

SO_2 formed in the rotary kiln is transported with the kiln gases to the calciner, where the previously described sulfur capture on CaO takes place. Thus, an internal sulfur cycle in the rotary kiln and calciner is established. The fraction of sulfur released as SO_2 depends upon the sulfur/alkali ratio in the rotary kiln. High levels of alkali metals will favor the formation of alkali sulfates rather than the formation of free SO_2.[9]

After the rotary kiln, the cement clinker is quench-cooled by ambient air as cooling air. Sulfur in the cement clinker is mainly bound as Na_2SO_4, K_2SO_4, or $3K_2SO_4 \cdot Na_2SO_4$. However, it may also be present as $CaSO_4$.[10]

The main challenge with respect to alternative fuel use in the material inlet end of rotary kilns is that the solid fuel particles will be in physical contact with the calcined raw meal. During the fuel devolatilization, reducing agents, such as CO, H_2, and/or hydrocarbons, are formed. These reducing agents may react with minor elements in the calcined raw meal before they are oxidized to their ultimate combustion products, H_2O and CO_2. In addition, if the fuel particles are fully or partly covered by calcined raw meal, mass transfer of oxygen to the fuel char will be hindered. Sub-stoichiometric amounts of oxygen will lead to incomplete oxidation of the fuel char, forming reducing agents in form of CO, H_2, and/or hydrocarbons.

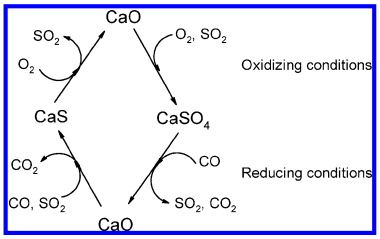

Figure 2. Sulfur transformation during periodically changing oxidizing and reducing conditions.[17]

It is widely accepted that Portland cement should be burnt under oxidizing combustion conditions.[11] The reason is that the existence of local reducing conditions in the calcined raw meal charge may affect the product quality and process stability of the kiln system. The product quality can be influenced by calcined raw meal components, such as Fe^{III}, being reduced to Fe^{II}. Fe^{II} catalyzes alite ($3CaO \cdot SiO_2$) decomposition, the main strength-giving component in cement.[11] The process stability is affected by the increased release of sulfur from the calcined raw meal, mainly by reductive decomposition of $CaSO_4$.

$$CaSO_4(s) + CO(g) \leftrightarrow CaO(s) + CO_2(g) + SO_2(g) \quad (4)$$

This reaction is shown in the material inlet end of the rotary kiln (see Figure 1). Increasing amounts of SO_2 in the cement kiln system are problematic because SO_2 promotes the formation of sulfospurrite [$2(2CaO \cdot SiO_2) \cdot CaSO_4$] and calcium sulfoaluminate ($3CaO \cdot 3Al_2O_3 \cdot CaSO_4$), some of the principal constituents of deposit buildups found in rotary kilns and kiln riser ducts[12] (see Figure 1). These sulfur-containing deposit buildups can lead to blockages that need to be removed, sometimes by a temporary plant shutdown.

With respect to local reducing conditions caused by alternative fuel combustion in the material inlet end of cement kilns, the most important challenge is assumed to be process stability because of sulfur release from the calcined raw materials and to a lesser degree product quality. Product quality is mainly affected by local reducing conditions in the kiln burning zone, which is a different situation.

The aim of this work is to obtain quantitative data on the release of SO_2 from calcined cement raw materials under conditions that resemble those in the material inlet end of rotary kilns. The purpose is to document the impact of variations in the local stoichiometry on the sulfur release. This type of information is useful in the prediction of effects on sulfur release during use of solid alternative fuels in the material inlet end of cement rotary kilns. The work includes both thermodynamic calculations on phase equilibria and experiments in a high-temperature tube furnace reactor. As described in the next section, most related knowledge is obtained under fluidized-bed conditions, where both temperatures and Ca/S ratios are typically lower than in the material inlet end of cement rotary kilns.

HIGH-TEMPERATURE REACTIONS BETWEEN SO_2 AND LIMESTONE

Absorption of SO_2 on limestone under fluidized-bed conditions has been studied extensively during the last few decades.[6,13−18] Even though these investigations are not directly applicable to describe the conditions in the material inlet end of cement rotary kilns, they do include relevant descriptions of mechanisms for sulfur release and capture by limestone at temperatures up to 1200 °C and under oxidizing as well as reducing atmospheres. An important point to note however is that these investigations only include reactions between limestone and sulfur species, whereas a full investigation of the reactions taken place in cement rotary kilns should also include other major components present in the calcined cement raw materials because they may affect the sulfur chemistry. In addition, the Ca/S molar ratio studied under fluidized-bed conditions was typically in the range of 1:1−4:1 which differs from the conditions in cement rotary kilns, where there is a massive excess of Ca relative to sulfur. The Ca/S molar ratio in the calcined raw meal that enters the rotary kiln is typically higher than 10:1.[19]

Table 1. Calcined Raw Meal Composition Used in the Equilibrium Calculations

calcined raw meal	wt %	mol/kg of clinker
SiO_2	18.00	3.000
Al_2O_3	4.76	0.467
Fe_2O_3	2.30	0.144
CaO	56.80	10.128
K_2O	2.50	0.266
Na_2O	0.20	0.032
S total	2.66	0.829
Cl	1.17	0.330

The following reaction mechanism for reductive decomposition of $CaSO_4$ has been proposed:[17]

$$CaSO_4(s) + CO(g) \leftrightarrow CaSO_3(s) + CO_2(g) \quad (5)$$

$$CaSO_3(s) \leftrightarrow CaO(s) + SO_2(g) \quad (6)$$

CO is believed to react directly on $CaSO_4$, giving $CaSO_3$ and CO_2. CO_2 is rapidly desorbed, while $CaSO_3$ disproportionates and forms CaO and SO_2. $CaSO_3$ is believed to be an important reaction intermediate. The formed CaO is subsequently sulfidized to CaS according to

$$CaO(s) + SO_2(g) + 3CO(g) \leftrightarrow CaS(s) + 3CO_2(g) \quad (7)$$

Returning to oxidizing conditions, CaS is oxidized to CaO by the reaction

$$CaS(s) + 1.5O_2(g) \leftrightarrow CaO(s) + SO_2(g) \quad (8)$$

The CaS oxidation is a rapid and very exothermal reaction, which may lead to a temperature increase.[20] The final step is the formation of $CaSO_4$ by the reaction of CaO, SO_2, and O_2, which is also an exothermal reaction[20]

$$CaO(s) + SO_2(g) + \frac{1}{2}O_2(g) \leftrightarrow CaSO_4(s) \quad (9)$$

Hansen et al.[16,17] studied phase equilibria for the SO_2−CaO−$CaSO_4$−CaS−CO−CO_2 system. They performed experiments in an electrically heated laboratory-scale fixed-bed reactor developed to simulate the changing oxidizing and reducing conditions similar to the conditions that particles will experience in a fluidized-bed reactor. They found that any transformation between $CaSO_4$ and CaS takes place via CaO. This transformation cycle is shown in Figure 2, which also illustrates the competition between sulfur capture and sulfur release. This competition depends upon parameters such as partial pressures of SO_2, CO, and CO_2 (see the phase

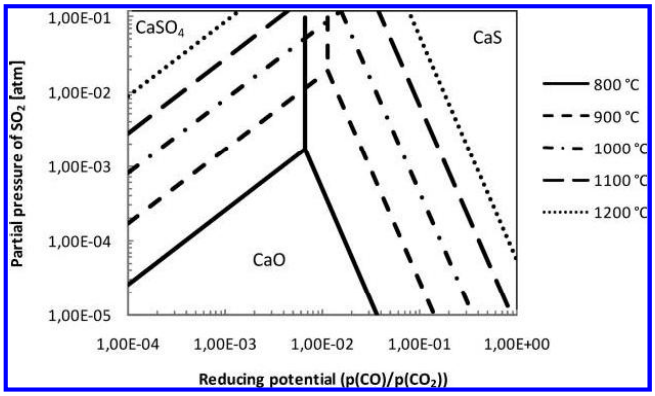

Figure 3. Phase diagram for the $SO_2-CaO-CaSO_4-CaS-CO-CO_2$ system (on the basis of thermochemical data from Barin).[21]

diagram in Figure 3). The temperature is a very important parameter. An increase in the temperature in the interval of 800−1200 °C will shift the equilibrium toward CaO and release more SO_2.[16]

During devolatilization and combustion of alternative fuels in an oxygen-lean environment, several reducing agents may be formed: CO, H_2, CH_4, as well as other hydrocarbons. It is well-documented that reducing agents, such as CO and H_2, can promote reductive decomposition of $CaSO_4$.[16,17,22] Hansen et al.[17] studied the rate of reductive decomposition with three reducing agents, CO, H_2, and CH_4. It was observed that the rate of decomposition was fastest with H_2 as a reducing agent. This is in agreement with earlier findings, which showed that the rate was increased by a factor 2 or 3 when the reducing agent was H_2 instead of CO.[23] Also, Diaz-Bossio et al. reported that the rate of reductive decomposition was fastest with H_2 relative to CO.[23] Hansen et al. did not detect any reductive decomposition of $CaSO_4$ with CH_4 as a reducing agent, even though the reaction is thermodynamically feasible.[17] It was assumed to be because reductive decomposition of $CaSO_4$ with CH_4 is a very slow process that did not have sufficient time to proceed during the 30 s intervals used in the experiments.

Turkdogan and Vinters also showed that elemental carbon could be used as a reducing agent.[24] The conversion rate of $CaSO_4$ to SO_2 and/or CaS was reported to be determined by the rate of oxidation of carbon to CO, which then rapidly reduced $CaSO_4$.

THERMODYNAMIC EQUILIBRIUM CALCULATIONS

To provide the basis for a better understanding of the inorganic chemistry in the rotary kiln material inlet, thermodynamic equilibrium calculations were performed using the commercially available software FactSage 6.0. This program uses the principle of minimization of the total Gibbs free energy to calculate the equilibrium composition of a chemical system with known total elemental composition, temperature, and pressure.

Input Data. The equilibrium calculations are based on the composition of calcined cement raw meal and the flue gas leaving the rotary kiln. These compositions are shown in Tables 1 and 2. It should be noted that the calcined raw meal used in the calculations contains a relatively high amount of chlorine and sulfur, relative to the guidelines for a stable kiln operation.

The following input data were used: (1) Chemical compositions of calcined raw meal and flue gas are as specified in Tables 1 and 2. All elements are inserted as mol/kg of clinker. (2) It is assumed that there is 1 kg of calcined raw meal and 0.5 N m^3 flue gas for each kilogram of clinker produced. (3) The following elements were included: C, H, N, O, S, Cl, K, Na, Ca, Si, Fe, and Al. (4) The flue gas is either oxidizing (λ = 1.3) or reducing (λ = 0.9). (5) Temperature = 800−1500 °C, with a step size of 25 °C. (6) Pressure = 1 atm.

Table 2. Flue Gas Compositions Used in the Equilibrium Calculations

oxidizing conditions (λ = 1.3)	vol %	mol/kg of clinker	reducing conditions (λ = 0.9)	vol %	mol/kg of clinker
CO_2	25.00	5.580	CO_2	25.00	5.580
H_2O	5.00	1.116	H_2O	5.00	1.116
O_2	5.00	1.116	O_2	0.00	0.000
CO	0.10	0.022	CO	2.00	0.446
SO_2	0.05	0.011	SO_2	0.05	0.011
N_2	64.85	14.475	N_2	67.95	15.167
total	100.00		total	100.00	

For the equilibrium calculations, ideal gas-phase compounds, solid-phase compounds, and liquid-phase compounds were included from the FactSage 6.0 compound database.

Limitations. The equilibrium model has the following limitations, which should be considered when comparing the results to actual conditions: (1) The model does not consider mass-transfer and kinetic limitations. In an industrial rotary kiln, the residence time may be too short for the species to come in contact with each other and for reactions to take place. Furthermore, the residence time may be too short for the transformation or decomposition of some compounds. Therefore, the predicted formation of compounds may exceed that occurring in reality. (2) The model does not take into account in which form the elements are initially present in the calcined raw meal and flue gas. In reality, the elements may be bound in different minerals and be released at different temperatures. This may affect the distribution of the element between the solid, liquid, and gas phase. It may also affect the compounds formed and the phase distribution of other elements.

Because of these limitations, the results of the equilibrium calculations cannot be used for a quantitative comparison to

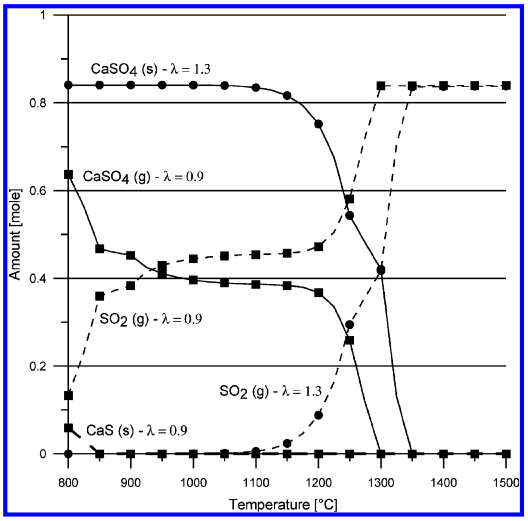

Figure 4. Equilibrium calculations for S distribution in calcined raw meal. The gas atmosphere is either oxidizing with 5 vol % O_2 ($\lambda = 1.3$) or reducing with 2 vol % CO ($\lambda = 0.9$).

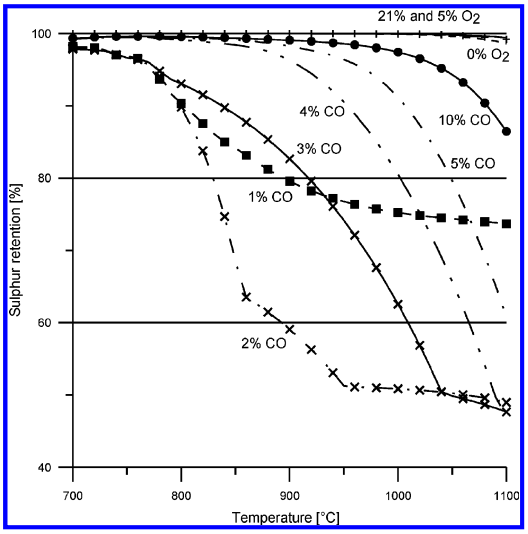

Figure 5. Sulfur retention in calcined raw meal as a function of the temperature and gas atmosphere. Note the cutted *y* axis.

experimental data but only to determine which species are likely to be formed under different gas atmospheres.

Influence of Reducing Conditions. To investigate the effect of changing the atmosphere from oxidizing to reducing, the calcined raw meal is exposed to (a) an atmosphere with 5 vol % oxygen and (b) an atmosphere with 0 vol % oxygen and 2 vol % CO. The exact composition of calcined raw meal and flue gas is given in Tables 1 and 2.

The equilibria for oxidizing and reducing conditions are shown in Figure 4. Only the main sulfur-containing compounds are included for clarity. The figure shows the sulfur distribution between $CaSO_4$, CaS, and SO_2 at various temperatures and under either oxidizing or reducing atmosphere. It is noted that no alkali sulfates are formed in the studied case, because the formation of alkali chlorides is thermodynamically favored.

The most important observation from Figure 4 is that the decomposition of $CaSO_4$ to CaO and SO_2 takes place at lower temperatures when reducing conditions are prevailing. Under oxidizing conditions, $CaSO_4$ is stable until approximately 1100 °C. At temperatures between 1100 and 1350 °C, $CaSO_4$ is gradually decomposed, forming CaO and SO_2. Above 1350 °C, $CaSO_4$ is not thermodynamically stable and all sulfur is released as SO_2. The situation is very different under reducing conditions, where $CaSO_4$ is observed to be partly reductively decomposed already at temperatures below 800 °C. The reductive decomposition continues until approximately 1300 °C. At higher temperatures, all sulfur is present as SO_2. The reductive decomposition of $CaSO_4$ takes place because sulfates can be used as an oxygen donor under reducing conditions. It should also be noted that a fraction of the sulfur is present as CaS under reducing conditions. However, CaS is only stable at temperatures below 850 °C, and the sulfur is released as SO_2 at higher temperatures. This is in correspondence with the $CaSO_4-CaS-CaO-SO_2-O_2-CO$ phase diagram in Figure 3.

Through the equilibrium calculations, it was also found that the phase distribution of Cl-containing compounds, such as HCl, NaCl, and KCl, is not affected by the change in the gas atmosphere. It is identical whether the atmosphere is oxidizing or reducing. This result was also expected because Cl is known to be much more sensitive to the temperature than to the gas atmosphere.[25]

The sulfur retention in the calcined cement raw materials will depend upon the specific degree of reducing atmosphere. The sulfur retention under different atmospheres and in the temperature interval of 700−1100 °C is shown in Figure 5. This temperature interval is representative for the conditions in the material inlet end of cement rotary kilns, where fully or partly calcined raw materials enter the rotary kiln with a temperature of approximately 900 °C and where the kiln flue gas leaves the rotary kiln with a temperature of approximately 1000−1100 °C. It is observed that all sulfur is retained in the calcined raw meal under oxidizing conditions with 5−21% O_2. These two curves are identical and at 100% sulfur retention in the temperature interval. Also, under inert conditions with 0% O_2, the sulfur retention is observed to be 100%, except above 1050 °C, where a minor sulfur release is observed.

The sulfur release increases significantly when reducing conditions prevail. The sulfur release does not increase with an increasing concentration of the reducing agent CO. Instead, the situation can be divided into mildly reducing conditions with 1−3% CO and strongly reducing conditions with 4−10% CO. The sulfur release is observed to be most significant under mildly reducing conditions, where it accelerates at temperatures above 780 °C. At 1% CO, a fraction of the sulfur is released because of reductive decomposition of $CaSO_4$. However, most of the sulfur is still retained in the calcined raw meal. The thermodynamic calculations suggest that the sulfur is stabilized as K_2SO_4 and $K_2Ca_2(SO_4)_3$ at 1% CO. The 2% CO is observed to lead to a high sulfur release, reaching 50% at 950 °C. This is because the compound $K_2Ca_2(SO_4)_3$ is not stable under this reducing atmosphere, but at the same time, the reducing atmosphere is not strong enough to stabilize sulfur as CaS. Thus, phase equilibria are shifted toward free SO_2.

dx.doi.org/10.1021/ef2006222 |*Energy Fuels* 2011, 25, 2917–2926

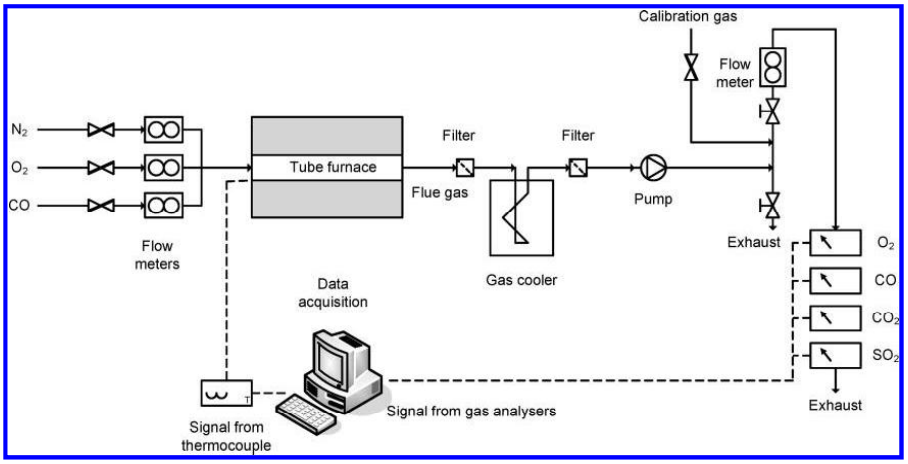

Figure 6. Experimental setup.

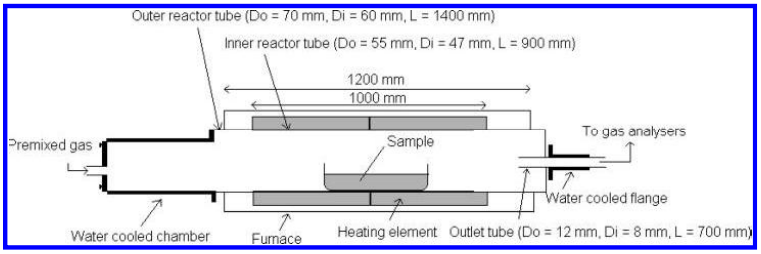

Figure 7. Sketch of the tube furnace reactor with size specifications of the reactor tubes (D_o, outer diameter; D_i, inner diameter; and L, length).

Table 3. Composition of Calcined Raw Meal Used for the Experiments

component	amount (wt %)
CaO	67
SiO_2	20
Al_2O_3	5
Fe_2O_3	3
$CaSO_4$	5

The sulfur release is lower at 3% CO because this stronger reducing atmosphere favors the formation of CaS. However, the thermal stability of CaS decreases as the temperature increases; therefore, at 1050 °C, the sulfur release reaches the same level as for 2% CO.

At strongly reducing conditions, 4−10% CO, the sulfur release is observed to be lower than under mild reducing conditions. This is again because sulfur is retained in the calcined raw meal as CaS. However, as the temperature increases and approaches 1100 °C, the sulfur release increases rapidly because of the thermal instability of CaS. These observations are in good correspondence with the phase diagram shown in Figure 3, which indicates that sulfur may be stabilized as either $CaSO_4$ at a low reducing potential or CaS at a high reducing potential.

Relative Stability of Sulfates toward Reducing Conditions. Sulfur introduced to the kiln system with the fully or partly calcined raw materials will mainly be in the form of sulfates, $CaSO_4$, Na_2SO_4, and K_2SO_4. The distribution is dependent upon parameters such as concentrations of these individual elements, level of chlorine available to react with the alkali metals, temperature, etc. Because it is clear that the stability of sulfates is affected by the gas atmosphere, the relative stability of the sulfates has been studied through equilibrium calculations.

On the basis of these equilibrium studies of the three dominating sulfates present in the kiln system, it is clear that reducing conditions generally shift the equilibrium toward more SO_2 in the gas phase. The sulfates are used as an oxygen donor in the oxidation of CO to CO_2.

An interesting observation was that the relative stability of the sulfates was $Na_2SO_4 > K_2SO_4 \gg CaSO_4$, an observation that was later confirmed experimentally. $CaSO_4$ is thus less stable and more critical than the alkali sulfates. This observation may indicate that it is desirable to bind as much sulfur as possible as alkali sulfates, to keep the sulfur evaporation in the kiln system as low as possible.

EXPERIMENTAL SECTION

The release of sulfur from cement raw materials as a function of the gas atmosphere was quantified in the temperature interval of 900−1100 °C. Different gas atmospheres was tested, but most of the experiments were conducted with 5 vol % O_2 in N_2 to represent an oxidizing atmosphere and 2 vol % CO in N_2 to represent a reducing atmosphere. The temperature interval and gas atmospheres resemble realistic temperatures and atmospheres in the material inlet end of cement rotary kilns. The used cement raw materials

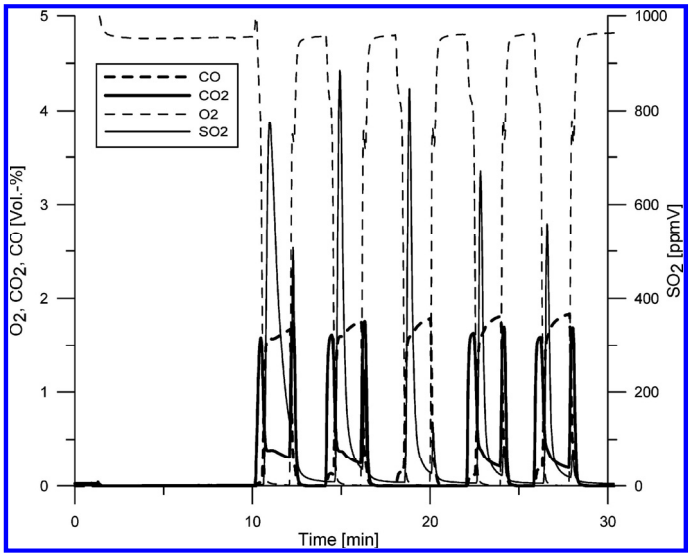

Figure 8. Concentrations of SO_2, O_2, CO, and CO_2 during an experiment with calcined raw meal under alternating oxidizing and reducing conditions at 1100 °C and gas flow = 10 NL/min.

were based on a synthetic mixture of pure chemicals of CaO, SiO_2, Fe_2O_3, Al_2O_3, and a sulfate, such as $CaSO_4$, Na_2SO_4, or K_2SO_4. These chemicals were mixed in the right proportions to simulate a simplified calcined raw meal, with a well-known content of sulfur. The compounds are also representative for the form that the elements have when they enter the rotary kiln.

Laboratory-Scale Tube Reactor Setup. A laboratory-scale tube reactor setup was used for the experiments (see Figure 6). It consists of a gas mixing panel to mix the gases in the desired concentration and flow, the electrically heated reactor in which the sample is placed, filters to remove particles and moisture, a pump, and the analysers that measure the gas concentration. Measured gas concentrations and temperatures are collected in a computer.

The reactor depicted in Figure 7 is a two-zone electrically heated tube furnace in which a horizontal alumina tube is mounted, having water-cooled flanges at both ends. The tube furnace has a maximum operating temperature of 1150 °C. The internal diameter of the inner tube is 47 mm, and it has a heated length of 900 mm. The sample is placed in a platinum/rhodium holder (95% Pt). The dimensions of the sample holder are $H \times W \times L = 2 \times 3 \times 10$ cm, corresponding to a volume of approximately 60 mL. During an experiment, the sample holder is placed in the center of the tube furnace and the tube furnace is sealed with a stainless-steel plate, which contains an opening for gas inlet. The gas composition exiting the reactor is monitored on the computer. The sample will be heated from room temperature to the desired temperature by conduction, convection, and radiation from the tube walls and gas.

To test whether the reactor setup are producing stable and sufficient gas temperatures, center-line temperature profiles in the tube reactor were established. It is concluded that, at the position of the sample holder, the measured temperature is within ±5 °C of the reactor set point temperature. The mass flow controllers were calibrated prior to the experiments. The actual gas flows were found to be within ±4% of the set point values on the mass flow controllers. The uncertainty on the O_2, CO, and CO_2 analysers is ±2% of the total span range of each species, while it is ±5% on the SO_2 measurement.

Method. The composition of used calcined cement raw meal is shown in Table 3. Only the main components as well as a sulfur-containing component are included. The sulfur-containing component is $CaSO_4$, which is believed to be the dominant sulfur-containing component in calcined raw meal entering cement rotary kilns, because of the excessive amounts of calcium relative to alkaline metals. It should be noted that the sulfur content in the calcined raw meal is relatively high (1.17 wt %) but not unrealistic. Prior to the experiments, the synthetic calcined raw meal was stored under an inert atmosphere to prevent CaO from reacting with moisture or atmospheric CO_2.

The following procedure is followed during each experiment: A total of 5 g of the calcined raw meal sample is placed in a well-distributed layer in the sample container. The sample amount is chosen to have a suitable amount of sulfur in the experiments to detect sulfur releases in the parts per million (ppm) range of 0−1000 ppm. The sample container is then placed in the tube furnace at the desired temperature. A thermocouple is placed in the center of the sample container to continuously log the temperature. The tube furnace is sealed, and the sample is heated for 10 min in an oxidizing atmosphere of 5% O_2 in N_2. Practically no SO_2 release was observed under the 10 min heating time. After 10 min, the gas atmosphere can be changed to the desired atmosphere, whereby the experiment begins. The gas flow is kept at 10 NL/min at all times. The gas composition is logged with 1 s intervals for subsequent evaluation of the sulfur release. In all experiments, the sulfur release was measured by integrating the SO_2 signal over time. The experiments always lasted 20 min, not including the 10 min heating time. The SO_2 concentration was measured in parts per million by volume (ppmV), while O_2, CO_2, and CO concentrations were measured in volume percentages (vol %).

In addition to the fixed gas atmosphere, experiments were also conducted with an alternating gas atmosphere between oxidizing and reducing. In these experiments, 2 min intervals were used: 2 min with reducing conditions (2 vol % of the reducing agent in nitrogen), followed by 2 min with oxidizing conditions (5 vol % O_2 in N_2). This procedure was repeated over 20 min, which gave time for five reducing intervals and five oxidizing intervals.

Assumptions and Uncertainties. This section discusses important assumptions and uncertainties that may influence the obtained results. (1) It has been experimentally determined that the sample is

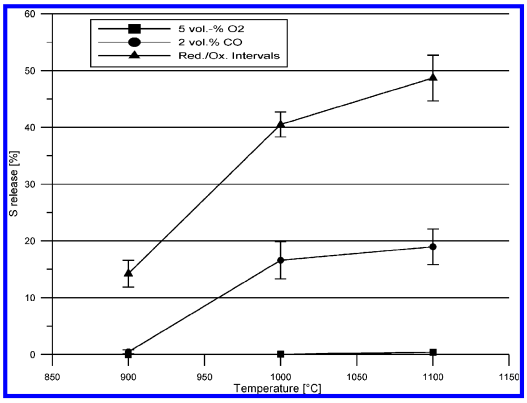

Figure 9. Effect of the gas atmosphere on the sulfur release from calcined raw meal. Sulfur release was evaluated after 20 min of reaction time.

heated for approximately 2−5 min in the tube furnace before the sample reaches the same temperature as the tube furnace. The exact heating time depends upon the sample size and temperature to be reached; a 5 g sample, which is the sample size used in the experiments, uses approximately 2 min to reach 900 °C. To ensure sufficient time for sample heat up, the sample will stay 10 min in the furnace under oxidizing conditions before an experiment is started. (2) The gas passing through the reactor will be pure $N_2/O_2/CO/H_2/CH_4$ in different compositions. Under industrial-scale conditions, the gas will also contain H_2O, CO_2, NO_x, SO_x, and various volatile species, such as alkaline metals or trace metals. It is assumed that the simplified gas composition used in the experiments contains the most important components and that the influence of the other components on the results can be neglected. (3) It is assumed that all sulfur released from the sample will form SO_2 before leaving the reactor. This assumption has been confirmed by two mass balances over two different calcined raw meal samples. After an experiment, the residual sulfur content of the sample was determined by chemical analysis and compared to the sulfur amount that was found in the flue gas as SO_2. In the first case, the sulfur mass balance was found to be 93%, and in the second case, 95% of the sulfur was found in either the sample or the flue gas as SO_2. Considering the uncertainties with sample composition, precision of analysers and mass flow controllers, as well as accuracy of the chemical analysis procedure, it is fairly safe to assume that nearly all released sulfur will be in the form of SO_2. This assumption is also confirmed by equilibrium calculations with the thermodynamic software FactSage, which calculates that nearly all sulfur is present as SO_2 under the studied conditions. (4) It is known from earlier experiments that the physical shape of the sample holder and sample mass will cause diffusion limitation of gas components, such as CO, to the sample. However, because all experiments are made with similar sample masses and procedures, it is assumed that results will be comparable. (5) The flue gas composition will not change significantly in the distance between the reactor and the analysers. To minimize this uncertainty and prevent, e.g., SO_2 absorption in filters and condensers, these parts were regularly cleaned or replaced to minimize the presence of compounds able to absorb SO_2. A gas with a known content of SO_2 was also regularly sent through the system to test if any SO_2 was absorbed before reaching the analysers. (6) The calcined raw meal to be used in the experiments is representative for calcined raw meal from an industrial plant. However, an industrial calcined raw meal will contain many minor components, which could have an effect on results.

RESULTS AND DISCUSSION

Figure 8 shows an example of the measured concentrations during an experiment with alternating oxidizing and reducing conditions at 1100 °C. The first 10 min is the heating period under oxidizing conditions, initially atmospheric air with 21 vol % O_2, followed by 4.75 vol % O_2 in N_2 when the tube reactor is sealed. During the heating under oxidizing conditions, no SO_2 is observed. After 10 min, the gas concentration is changed to 2 vol % CO in N_2. Because the change is rapid, some oxygen will be left in the reactor and will react with CO, forming CO_2. Thus, the CO_2 concentration is observed to increase to approximately 1.5 vol %. After the last O_2 in the reactor is consumed, the CO concentration increases to approximately 1.8 vol %. At the same time, a dramatic increase in the SO_2 concentration is observed from 0 to 800 ppm. The formed CO_2 is also observed at a level of around 0.2 vol %. The SO_2 level drops relatively fast. When the atmosphere is again changed to oxidizing (4.75 vol % O_2), a new, smaller SO_2 peak is observed. The sulfur release cycle is observed to be repeated for each of the following reducing/oxidizing intervals, with a slight decrease in SO_2 each time, because the sulfur content in the sample gradually decreases. The experiment is stopped after 30 min when the fifth oxidizing interval is finished and the SO_2 concentration has dropped to values close to 0 ppm. However, it should be noted that more sulfur would be released from the sample if the cycles were repeated. This was tried out, and it can be concluded that the measured SO_2 level gradually decreases with time but that it takes more than 2 h before all sulfur has been released from the sample.

It is interesting to note from Figure 8 that the first SO_2 peak during the reductive decomposition of $CaSO_4$ only reaches 780 ppm, while the next SO_2 peak reaches 890 ppm. The first SO_2 peak is also wider than subsequent SO_2 peaks. This tendency was observed in all experiments with alternating reducing and oxidizing conditions. The same tendency has also been reported by other researchers.[16,23,26] The reductive decomposition of $CaSO_4$ is initiated by an induction period, which has been explained by the slow desorption of SO_2 and slow rate of nucleation of CaO. Ghardashkhani et al. reported that shifting from reducing to oxidizing and back to reducing conditions during reductive decomposition of $CaSO_4$ did not give rise to a new induction period.[26] This is in agreement with the experimental observations, where the second SO_2 peak reaches larger values than the first SO_2 peak.

The characteristic SO_2 peaks observed from Figure 8 during alternating reducing and oxidizing conditions can be explained by the existence of phase equilibria between different sulfur species. Under oxidizing conditions, sulfur is stabilized in the form of $CaSO_4$, and under reducing conditions, sulfur is stabilized as CaS. When the gas atmosphere changes, sulfur may be released to the gas phase as SO_2, as illustrated in Figure 2.

Release Quantification. The release of sulfur during the experiments is calculated by integration of the gas concentration of SO_2 over the relevant time interval

$$n_{\text{sulfur found}} = \int_0^t y_{SO_2} dt \times 10^{-6} \times \frac{PV}{RT} \qquad (10)$$

where y_{SO_2} is in ppmV and V is the gas flow in L/s. It should be noted that, because of diffusion limitation of gas components, such as CO, only experiments made with similar sample masses can be compared. The sum of sulfur found as SO_2 is divided by

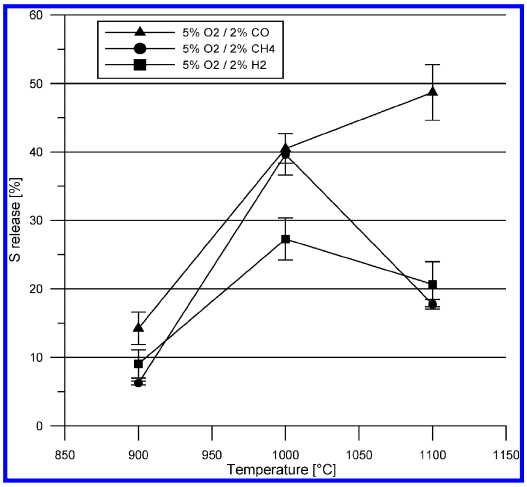

Figure 10. Effect of the reducing agent on sulfur release from calcined raw meal under alternating oxidizing and reducing conditions. Sulfur release was evaluated after 20 min of reaction time.

the total sulfur amount in the sample

$$\text{S release} = \frac{n_{\text{sulfur found}}}{n_{\text{sulfur in sample}}} \times 100\% \qquad (11)$$

Effect of the Reducing Atmosphere with CO. The sulfur release from calcined raw meal has been studied at the temperatures of 900, 1000, and 1100 °C. Two different atmospheres with 5% O_2 and 2% CO (pure nitrogen is the balance in both cases) as well as alternating reducing and oxidizing conditions have been studied. The results are shown in Figure 9. Under oxidizing conditions with 5% oxygen, the S release is approximately 0% in the studied temperature interval. This result has been found to be valid at all oxygen concentrations from 1 to 21%, indicating that $CaSO_4$ is generally stable under oxidizing conditions and temperatures below 1100 °C. This finding is in agreement with the thermodynamic equilibrium calculations, which did not show any decomposition of $CaSO_4$ below 1150 °C.

Under reducing conditions with 2% CO, the sulfur release was still approximately 0% at 900 °C but increased to 17% at 1000 °C and 19% at 1100 °C. This significant increase in sulfur release under reducing conditions may be explained by the formation of CaS from $CaSO_4$, in which CaO and free SO_2 are reaction intermediates. Each experiment was repeated 3 times, and the standard deviation were found to be ±2%.

Under shifting oxidizing and reducing intervals with 2 min of 2% CO, followed by 2 min of 5% O_2 continuously repeated 2 × 5 times, the sulfur release is observed to be significantly higher than under constant reducing or oxidizing conditions: 14% at 900 °C, 40% at 1000 °C, and 48% at 1100 °C. Each experiment has been repeated 3 times, and the standard deviation was found to be ±3%. This strong effect of alternating oxidizing and reducing conditions is in correspondence with the sulfur transformation cycle shown in Figure 2. Under oxidizing conditions, sulfur is stabilized as $CaSO_4$, and under reducing conditions, sulfur is stabilized as CaS. Every shift in atmosphere leads to the formation of CaO and free SO_2. The formation of free SO_2 is particularly large at higher temperatures, whereas the lowest temperature of 900 °C can limit the sulfur release even under alternating oxidizing and reducing conditions.

The results are in correspondence with previous work, where sulfur release and capture has been studied under alternating oxidizing and reducing conditions. Lyngfelt and Leckner reported a decrease in the sulfur capture ability of limestone at temperatures above 880 °C and reducing conditions, because of reductive decomposition of $CaSO_4$.[5] Hansen et al. found that the competition between sulfur capture and sulfur release under alternating oxidizing and reducing conditions was shifted toward more sulfur release when the temperature increased.[17] Tarelho et al. found a maximal sulfur capture efficiency of limestone at around 825 °C. Higher temperatures reduced the sulfur capture efficiency, particularly under reducing conditions.[18]

Effect of Other Reducing Agents. Most investigations of reductive decomposition of $CaSO_4$ reported in the literature use either CO or H_2 as the reducing agent. Because combustion of alternative fuels in cement kilns may lead to the formation of significant amounts of CO, H_2, and hydrocarbons, such as CH_4, under substoichiometric conditions, these three reducing agents have been investigated with respect to sulfur release from calcined raw meal in the temperature interval of 900−1100 °C. The results are shown in Figure 10. The experimental conditions were shifting oxidizing and reducing intervals with 2 min of the reducing agent (2% of either CO, H_2, or CH_4), followed by 2 min of 5% O_2. The 2 min intervals were continuously repeated 2 × 5 times, thus 20 min of total reaction time. All experiments were repeated 3 times with a standard deviation in the order of 3%. Under these reaction conditions, the sulfur release when CO was used was 15, 40, and 48% at 900, 1000, and 1100 °C, respectively. When CH_4 was used, the sulfur release was 6, 40, and 17% at 900, 1000, and 1100 °C, respectively. Finally, when H_2 was used, the sulfur release was 8, 27, and 20% at 900, 1000, and 1100 °C, respectively.

While the results with CO are observed to lead to increased sulfur release as a function of the temperature, the results with H_2 and CH_4 are more surprising. The sulfur release increases from 900 to 1000 °C but then decreases again at 1100 °C. This was unexpected because it was assumed that the sulfur release would increase with the temperature, regardless of the reducing agent. It was also expected that H_2 would lead to a higher sulfur release than CO and CH_4 would lead to a much lower sulfur release than CO, according to Hansen's findings. Hansen found that the rate of reductive decomposition of $CaSO_4$ increased when H_2 was used instead of CO and that CH_4 gave no reductive decomposition at all.[17] However, the reaction conditions used in Hansen's experiments were quite different from the ones used in this investigation, because he used relatively short time intervals of 30 s/30 s and only studied the effect of the reducing agent at 850 °C. In this experiment, longer time intervals of 2 min/2 min were used and the temperature interval was 900−1100 °C. This may explain why CH_4 is found to be of comparable efficiency as H_2 and CO in this investigation, while Hansen reported it to be less efficient because of slower reaction kinetics.

With regard the lower sulfur release at 1100 °C relative to 1000 °C when H_2 and CH_4 were used as reducing agents, similar results have been reported by Kamphuis et al. At temperatures above 950 °C, a fraction of SO_2 was observed to be converted to H_2S, which was not detected by the analysis system, when the flue gas contained H_2.[27] On the basis of a series of tests with known SO_2 concentrations in a H_2/N_2 gas mixture passing

through the reactor without a sample, Kamphuis et al. established a correction factor to correlate for the formed H_2S. It is likely that the same phenomenon took place in the present experiments with H_2 and CH_4 because H_2S can be formed from both reducing agents. This will explain why the found sulfur release is lower at 1100 °C relative to 1000 °C. Prior to the experiments, thermodynamic equilibrium calculations had been made for the calcined raw meal exposed to the reducing agents H_2 and CH_4. These thermodynamic calculations indicated that practically all released sulfur would be present as SO_2 under the experimental conditions. However, the thermodynamic calculations may be misleading because they do not consider reaction kinetics. H_2S may be formed as an intermediate species, which leaves the reactor before the formation of SO_2 occurred. A sulfur mass balance should be performed to determine whether some sulfur has escaped from the system as H_2S or not. Because a sulfur mass balance has not been conducted for the experiments with H_2 and CH_4, it is not directly possible to quantify the effect on sulfur release as a function of the reducing agent. However, the results do indicate that all three reducing agents, CO, CH_4, and H_2, have an effect on the sulfur release in the studied temperature interval.

CONCLUSION

The release of sulfur from cement raw materials under both oxidizing and reducing conditions was investigated. The investigations included thermodynamic equilibrium calculations in the temperature interval of 800−1500 °C and experiments in a tube furnace reactor in the temperature interval of 900−1100 °C. The investigated conditions resemble actual conditions in the material inlet end of cement rotary kilns, where local reducing conditions may occur during combustion of solid, alternative fuel particles and where solid/gas temperatures are usually between 900 and 1100 °C. The following results were obtained: (1) The thermodynamic equilibrium calculations showed that the stability of sulfates present in calcined cement raw meal is strongly affected by the gas atmosphere. Especially, $CaSO_4$ tends to decompose at much lower temperatures under a reducing atmosphere. K_2SO_4 and Na_2SO_4 are also affected by a reducing atmosphere but not as significant as $CaSO_4$. (2) Experimentally, a clear tendency for increasing sulfur release was observed when the gas atmosphere shifted from oxidizing to reducing. No sulfur release was observed under oxidizing conditions (5 vol % O_2), whereas the sulfur release increased to 19% under reducing conditions (2 vol % CO) at 1100 °C. The sulfur release was particularly significant if the calcined raw meal was exposed to alternating oxidizing and reducing conditions, which led to a sulfur release of 48% at 1100 °C. (3) The sulfur release from calcined raw meal was observed to be dependent upon the temperature. Under alternating oxidizing and reducing conditions, the sulfur release was observed to be 14% at 900 °C and 48% at 1100 °C. (4) Sulfur release from calcined raw meal was shown to take place in the presence of any of the reducing agents CO, H_2, and CH_4. However, it was not possible to directly quantify the sulfur release as a function of the reducing agent, because part of the released sulfur from the experiments with H_2 and CH_4 presumably formed H_2S, which could not be detected by the analysis system.

AUTHOR INFORMATION

Corresponding Author
*Telephone: +45-45252831. E-mail: arn@kt.dtu.dk.

ACKNOWLEDGMENT

The work described in this paper is part of a research platform on future cement technology financed by The Danish National Advanced Technology Foundation, Technical University of Denmark (DTU) and FLSmidth A/S.

REFERENCES

(1) Verein Deutscher Zementwerke (VDZ). *Activity Report 2007−2009*, 2009; http://www.vdz-online.de (accessed on April 20, 2011).
(2) Cembureau. *Activity Report 2008*; http://www.cembureau.be (accessed on April 20, 2011).
(3) BP. *Statistical Review of World Energy*, June 2009; http://www.bp.com (accessed on April 20, 2011).
(4) Cembureau. *Alternative Fuels in Cement Manufacture*, 1997; http://www.cembureau.be (accessed on April 20, 2011).
(5) Lyngfelt, A.; Leckner, B. *Chem. Eng. J.* **1989**, *40*, 59–69.
(6) Hansen, J. P. SO_2 emissions from cement production. Ph.D. Thesis, Department of Chemical Engineering, Technical University of Denmark (DTU), Lyngby, Denmark, 2003; ISBN: 87-90142-96-9.
(7) Choi, G.-S.; Glasser, F. P. *Cem. Concr. Res.* **1988**, *18*, 367–374.
(8) Farag, L. M.; Kamel, H. M. *ZKG Int.* **1994**, *10*, 586–590.
(9) Rosholm, P.; Mortensen, A. H.; Hintsteiner, E. A. *ZKG Int.* **1998**, *51* (2/4), 19.
(10) Twomey, C.; Birkinshaw, C.; Breen, S. *J. Chem. Technol. Biotechnol.* **2004**, *79*, 486–490.
(11) Klauss, J. *ZKG Int.* **2000**, *53* (3), 132–144.
(12) Sylla, H.-M. *ZKG Int.* **1974**, *10*, 499–508.
(13) Lyngfelt, A.; Leckner, B. *Chem. Eng. Sci.* **1989**, *44* (2), 207–213.
(14) Lyngfelt, A.; Leckner, B. *Chem. Eng. Sci.* **1999**, *54*, 5573–5584.
(15) Dam-Johansen, K.; Hansen, P. F. B.; Østergaard, K. *Chem. Eng. Sci.* **1991**, *46* (3), 847–853.
(16) Hansen, P. F. B.; Dam-Johansen, K.; Bank, L. H.; Østergaard, K. *Proc. Int. Conf. Fluid. Bed Combust.* **1991**, *1*, 73–82.
(17) Hansen, P. F. B; Dam-Johansen, K.; Østergaard, K. *Chem. Eng. Sci.* **1993**, *48* (7), 1325–1341.
(18) Tarelho, L. A. C.; Matos, M. A. A.; Pereira, F. J. M. A. *Fuel Process. Technol.* **2005**, *86*, 1385–1401.
(19) *Chemistry of Cement and Concrete*, 4th ed.; Hewlett, P. C., Ed.; John Wiley and Sons, Inc.: New York, 1998; ISBN: 0-340-56589-6.
(20) Tian, H.; Guo, Q. *Ind. Eng. Chem. Res.* **2009**, *48*, 5624–5632.
(21) Barin, I. *Thermochemical Data of Pure Substances*, 3rd ed.; VCH: Weinheim, Germany, 1995; ISBN: 3-527-28745-0.
(22) Diaz-Bossio, L. M.; Squier, S. E.; Pulsifer, A. H. *Chem. Eng. Sci.* **1985**, *40* (3), 319–324.
(23) Wheelock, T. D.; Boylan, D. R. *Ind. Eng. Chem.* **1960**, *52* (3), 215–218.
(24) Turkdogan, E. T.; Vinters, J. V. *Trans. Inst. Min. Metall., Sect. C* **1976**, *85*, 113–123.
(25) Locher, G.; Klein, H. *Cement Int.* **2009**, *7* (4), 64–75.
(26) Ghardashkhani, S.; Ljungström, E.; Lindquist, O. *Proc. Int. Conf. Fluid. Bed Combust.* **1989**, 611–615.
(27) Kamphuis, B.; Potma, A. W.; Prins, W.; Van Swaaij, W. P. M. *Chem. Eng. Sci.* **1993**, *48* (1), 105–116.

energy&fuels

ARTICLE

pubs.acs.org/EF

Sulfur Release from Cement Raw Materials during Solid Fuel Combustion

Anders R. Nielsen,[†,‡,*] Morten B. Larsen,[†] Peter Glarborg,[‡] and Kim Dam-Johansen[‡]

[†]FLSmidth A/S, Vigerslev Allé 77, DK-2500 Valby, Denmark

[‡]Department of Chemical and Biochemical Engineering, CHEC Research Centre, Technical University of Denmark (DTU), DK-2800 Lyngby, Denmark

ABSTRACT: During combustion of solid fuels in the material inlet end of cement rotary kilns, local reducing conditions can occur and cause decomposition of sulfates from cement raw materials. Decomposition of sulfates is problematic because it increases the gas-phase SO_2 concentration, which may cause deposit formation in the kiln system. SO_2 release from cement raw materials during combustion of solid fuels has been studied experimentally in a high temperature rotary drum. The fuels were tire rubber, pine wood, petcoke, sewage sludge, and polypropylene. The SO_2 release from the raw materials was observed to increase when (a) the inlet oxygen concentration decreased, (b) the temperature increased, and (c) when the total surface area of the fuel particles increased. The type of fuel also had a significant effect on the SO_2 release. The sequence of SO_2 release for fuel particles in the size interval 1−2 mm was found to be tire rubber granulate > sewage sludge > pine wood sawdust > petcoke > polypropylene flakes. The SO_2 release was generally observed to increase when formation of local reducing conditions near the raw material bed increased, as indicated by elevated levels of CO during the fuel devolatilization.

INTRODUCTION

Fuel consumption accounts for a significant fraction of the total cement clinker production costs.[1] Traditionally, cement production has mainly depended on the fossil fuels coal, oil, and natural gas. Due to competition in the cement market, rising fossil fuel prices, and environmental concerns, cement producers have increased the utilization of alternative fuels as a substitute for fossil fuels in order to achieve the most economic fuel mix. In this context, "alternative fuels" cover all nonfossil fuels and waste from other industries. Popular alternative fuels in the cement industry are tire-derived fuels, biomass residues, and different commercial and industrial wastes.

It is attractive to utilize coarse, solid alternative fuel particles in the material inlet end of cement rotary kilns in order to save the expense of shredding of the fuels to smaller particles and to increase fuel flexibility of the system. High temperatures in the rotary kiln and material retention times of several minutes provide good conditions for fuel burnout. Figure 1 show how coarse, solid alternative fuels can be introduced into the material inlet end of a cement rotary kiln.

Sulfur is introduced to cement rotary kilns as inorganic bound sulfur in the preheated and calcined cement raw materials or with the fuels (see Figure 1). A detailed description of sulfur species and the main sulfur reactions in rotary kilns and calciners is described elsewhere.[2,3]

Sulfur present in the calcined raw material is mainly bound as $CaSO_4$ or as alkali sulfates. The calcined raw material is transported by the rotational movement and slight inclination of the rotary kiln toward the hot burning zone, where flame temperatures are in the range of 2000 °C and material temperatures are around 1450 °C. The clinker reactions take place during the gradual heating of the calcined raw material as it is transported through the rotary kiln. During the gradual heating of the calcined raw material, a sulfate melt is formed that facilitates formation of alkali sulfates, Na_2SO_4 and K_2SO_4, which are more thermodynamically stable than $CaSO_4$.[3] $CaSO_4$ will decompose at the high temperatures present in the burning zone and form SO_2 or alkali sulfates.

The main challenge with respect to alternative fuel utilization in the material inlet end of rotary kilns is that solid fuel particles will be in physical contact with the calcined raw material: During the fuel devolatilization, reducing agents such as CO, H_2, and/or hydrocarbons are formed. These reducing species may react with elements in the calcined raw material before they are oxidized to their ultimate combustion products, H_2O and CO_2. In addition, if the fuel particles are fully or partly covered by calcined raw material, mass transfer of oxygen to the fuel char will be hindered. Substoichiometric amounts of oxygen will lead to incomplete oxidation of the fuel char, forming reducing agents in the form of CO, H_2, and/or hydrocarbons. The process stability of the kiln system may be affected by increased release of sulfur from the calcined raw material, mainly by reductive decomposition of $CaSO_4$:

$$CaSO_4(s) + CO(g) \leftrightarrow CaO(s) + CO_2(g) + SO_2(g) \quad (1)$$

Increasing amounts of SO_2 in the cement kiln system is problematic because SO_2 promotes formation of sulfospurrite ($2(2CaO \cdot SiO_2) \cdot CaSO_4$) and calcium sulfoaluminate ($3CaO \cdot 3Al_2O_3 \cdot CaSO_4$), some of the principal constituents of deposit buildups found in rotary kilns and kiln riser ducts.[4]

Received: July 1, 2011
Revised: August 15, 2011
Published: August 15, 2011

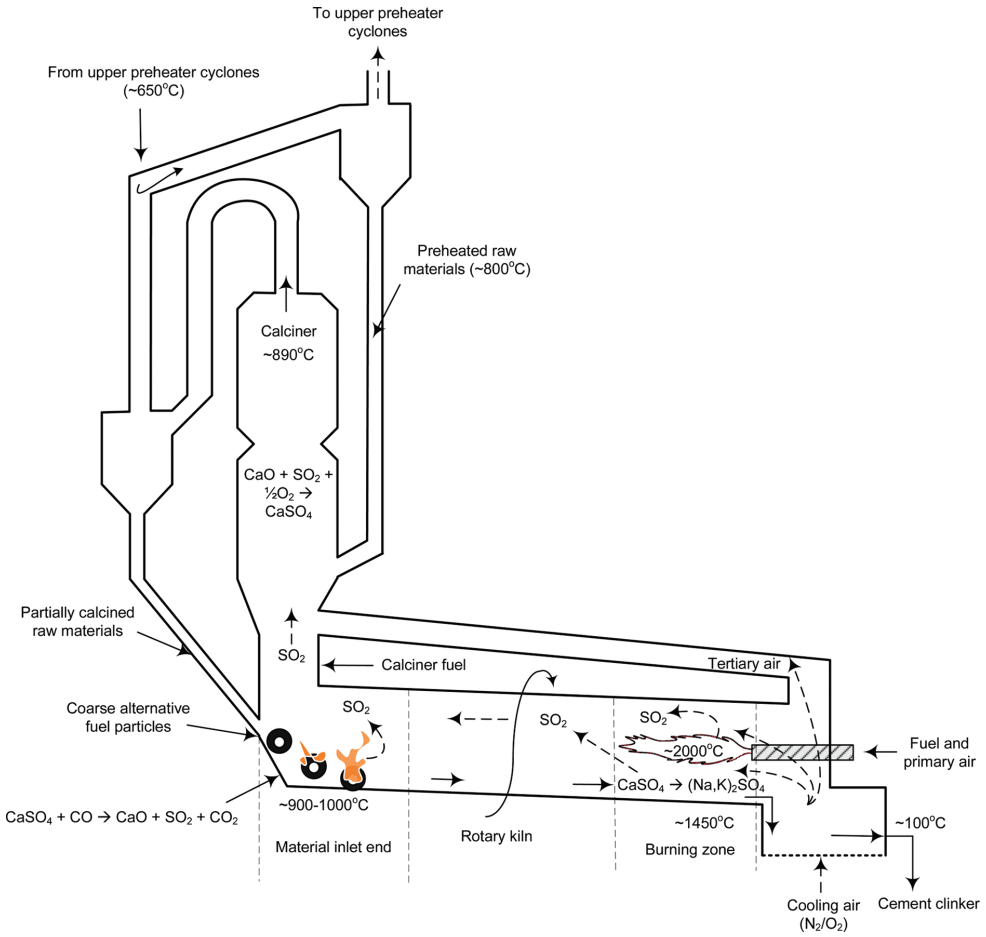

Figure 1. Illustration of alternative fuel utilization in the material inlet end of a cement rotary kiln. The calciner and two lowest preheater cyclones are also shown.

These sulfur-containing deposits can lead to blockages that need to be removed, sometimes by a temporary plant shutdown.

Relatively little information is available in the literature about SO_2 release from cement raw materials during utilization of solid fuels. However, adsorption and release of SO_2 for the $SO_2-CaO-CaSO_4-CaS-CO-CO_2$ system under fluidized bed conditions has been studied extensively during the last decades.[5−11] Even though these investigations are not directly applicable to describe the conditions in the material inlet end of cement rotary kilns, they do include relevant descriptions of mechanisms for SO_2 release and capture by limestone at temperatures up to 1200 °C and under oxidizing as well as reducing atmospheres.

Hansen et al.[9,10] studied phase equilibria for the $SO_2-CaO-CaSO_4-CaS-CO-CO_2$ system. They performed experiments in an electrically heated laboratory scale fixed bed reactor developed to simulate the changing oxidizing and reducing conditions similar to the conditions particles will experience in a fluidized bed reactor. They found that any transformation between $CaSO_4$ and CaS takes place via CaO. This competition

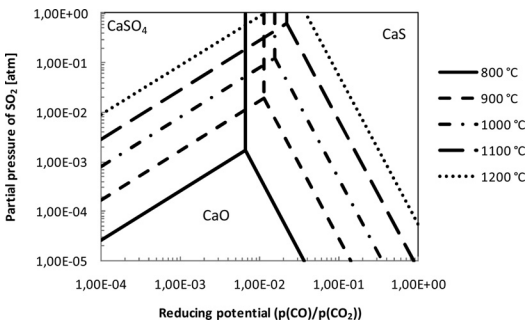

Figure 2. Phase diagram for the $SO_2-CaO-CaSO_4-CaS-CO-CO_2$ system (based on thermochemical data from Barin).[12]

between sulfur capture and sulfur release depends on parameters such as partial pressures of SO_2, CO, and CO_2 (see the equilibrium

dx.doi.org/10.1021/ef200963v |*Energy Fuels* 2011, 25, 3917–3924

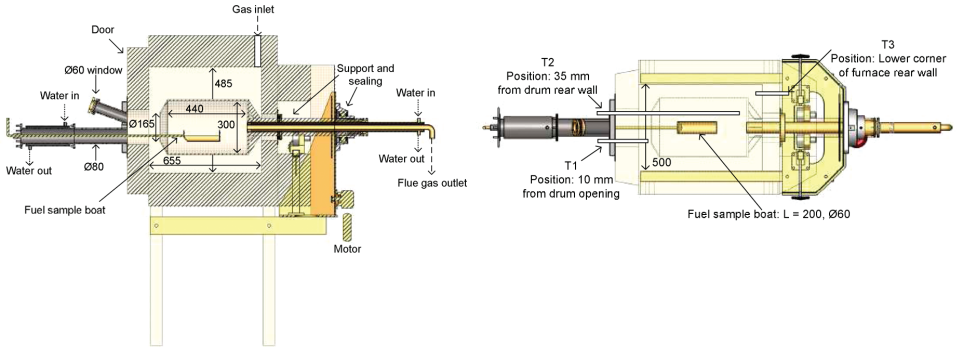

Figure 3. High-temperature rotary drum: (left) side view and (right) top view.

phase diagram in Figure 2). Temperature is a very important parameter: An increase in temperature in the interval 800−1200 °C will shift the equilibrium toward CaO and release more SO_2.[9]

The aim of this work is to obtain quantitative data on the release of SO_2 from calcined cement raw materials under conditions that resemble those in the material inlet end of rotary kilns. The purpose is to document the impact on SO_2 release during utilization of solid alternative fuels, in the material inlet end of cement rotary kilns.

■ EXPERIMENTAL SECTION

The purpose of the experiments is to clarify how the sulfur release in the form of SO_2 is affected by different solid fuels and reaction conditions. The release of sulfur from cement raw materials as a function of fuel type and fuel characteristics was quantified in the temperature interval from 700 to 1000 °C and at oxygen concentrations from 5 to 21 vol %. The temperature interval and oxygen concentrations up to 10 vol % resemble realistic material temperatures and atmospheres in the material inlet end of cement rotary kilns. The used cement raw materials were based on a synthetic mixture of quartz sand and 5 wt % calcium sulfate, $CaSO_4$. This represents a simplified batch of cement raw material entering the rotary kiln, with a high, but realistic, sulfur content.

Experimental Setup. The experiments were made in a high-temperature rotary drum in a commercially available chamber furnace (see Figure 3). The setup can reach an operating temperature of 1000 °C. It is electrically heated by heating elements embedded in two side walls and the floor. The steel drum is supported by a steel tube on rollers that passes through the rear wall. This steel tube is connected to a motor by means of a roller chain, in order to rotate the drum. The part of the steel tube that is outside the chamber furnace is water cooled in order to protect the rollers, roller chain, and gas seals against the high temperatures.

Gas can be transported to the chamber furnace through a hole in the roof. The furnace has been designed to achieve sufficient heating of the reactant gas before it enters the rotary drum; this was verified by temperature measurements. The gas is transported into the rotating steel drum due to an externally placed gas pump that pumps the gas through the rotating drum and steel tube, after which the gas exits the reactor for subsequent cooling and analysis.

The chamber furnace door is equipped with a window for visual inspection, two holes for thermocouples, and a centrally placed water-cooled tube for solid fuel addition. The solid fuels are placed in a sample container that can be pushed into the hot rotary drum or pulled out to the water-cooled tube.

The experimental setup is shown in Figure 4. The gas supply can be up to 500 NL/min of air and nitrogen. The gas is transported to the rotary drum reactor during the experiments, but may also be bypassed during calibration of flow controllers, leakage tests, etc.

The temperature is measured in three different positions in the rotary drum reactor: at the rear wall in the chamber furnace (T1), in the center of the rotary drum (T2), and at the door just in front of the rotary drum (T3). A pump transports the flue gas out of the rotary drum reactor. Before passing the pump, the flue gas is cooled in a heat exchanger, and soot particles are captured in a filter. After having passed the pump, the flue gas is sent directly either to the stack or to the gas analyzers for measurement of O_2, CO, CO_2, SO_2, and NO. The fraction of the flue gas that is transported to the analyzers will pass another two filters, a gas cooler for condensation of water, and a sample gas pump before reaching the gas analyzers.

Materials and Methods. A 2.5 kg portion of raw material in the form of quartz sand with 5 wt % $CaSO_4$ is placed in the rotary drum. This corresponds to a volumetric fill degree of 5%. The drum is rotated at 6 rpm in order to keep the raw material in a continuous rolling motion. The raw materials are then preheated to the desired temperature, in the interval from 700 to 1000 °C. A constant flow of 100 NL/min of gas with the desired oxygen concentration is transported through the rotary drum and will pass over the raw materials in the lower part of the rotary drum. The gas is preheated to the same temperature as the raw materials in order to obtain a uniform temperature at all positions. The temperature and oxygen concentration are monitored continuously, and when these have stabilized, a batch of solid fuel is rapidly added into the raw materials in the rotary drum. SO_2, NO, O_2, CO, and CO_2 concentrations are measured during the devolatilization and char combustion. The gas composition is logged for subsequent evaluation of the sulfur release. In all experiments, the sulfur release was measured by integrating the SO_2 signal over time:

$$m_{\text{sulfur}} = \int_0^t y_{SO_2}\, dt \times 10^{-6} \times MW_{\text{sulfur}} \times \frac{PV}{RT} \qquad (2)$$

where y_{SO_2} is the mole fraction in ppmV, MW_{sulfur} is the molar weight of sulfur in g/mol, and V is the gas flow in L/s.

Since many of the fuels contain sulfur that will also be released during the experiments, baseline experiments have been made, where the fuels are combusted in 2.5 kg of *pure* quartz sand, *without* $CaSO_4$. The measured SO_2 from the baseline experiments can only arise from the fuels and not from the raw material. The amount of sulfur released during the baseline experiments is subtracted from the sulfur released during the actual experiment in order to get the corrected accumulated amount of sulfur that arises from the raw material.

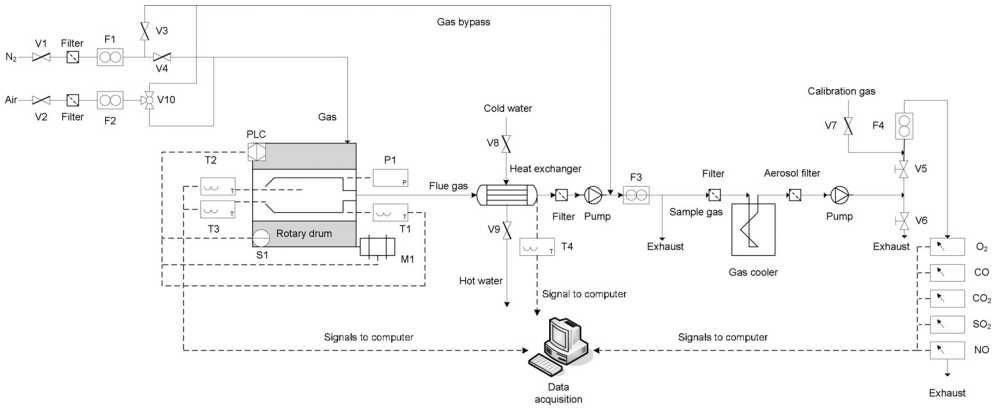

Figure 4. Sketch of the high-temperature rotary drum experimental setup.

Table 1. Fuel Analyses and Lower Heating Values (LHV) for Solid Fuels Used in the Experiments

	proximate analysis[a]			ultimate analysis[a]				
	VM	FC	ash	C	H	N	S	LHV (MJ/kg)
tire rubber	64.6	32.6	2.8	87.4	7.1	0.3	1.2	36.9
pine wood	75.3	24.5	0.2	38.9	5.2	0.1	–	16.2
polypropylene	97.5	0.0	2.5	83.0	14.0	0.0	–	44.5
petcoke	13.4	85.1	1.5	87.3	3.7	1.5	4.7	34.0
sewage sludge	49.3	0.5	50.2	29.0	3.8	3.8	1.0	12.5

[a] Units are weight percent as received.

Table 2. Approximate Shapes and Dimensions of the Fuels Used in the Experiments

fuel	shape	dimensions
tire rubber granulate	irregular	$D_p \approx 2$ mm
tire rubber cylinders	cylindrical	$L = 12$ mm, $D_p = 9$ mm
pine wood cubes	rectangular	thickness ≈ 10 mm
pine wood sawdust	needles	thickness ≈ 1 mm
polypropylene flakes	rectangular	thickness ≈ 1 mm
petcoke	spherical	$D_p \approx 1$ mm
sewage sludge	spherical	$D_p \approx 0.5$ mm

All experiments were repeated at least two times to ensure the repeatability. The sulfur release values reported in the figures are the average values from the experiments, corrected for the sulfur contribution from the fuels.

Five different solid fuels have been tested: tire rubber, pine wood, polypropylene, petcoke, and sewage sludge. In order to compare the sulfur release between fuels, the amount of fuel is chosen to obtain the same energy input. Fuel proximate and ultimate analyses as well as lower heating values are shown in Table 1. The lower heating values for the fuels are quite different. Thus, quite different fuel sample amounts have been used in order to have the same energy input in each experiment, regardless of the fuel. The energy input during the experiments was chosen to be in the interval 15−50 kJ per batch, corresponding to fuel sample sizes from 0.3 to 4.2 g. These energy inputs were chosen to obtain a suitable level of sulfur release, thereby avoiding SO_2 peaks exceeding the analyzer range.

Several different fuel particle sizes and shapes have been used in the experiments, and these are presented in Table 2.

Assumptions, Limitations, and Uncertainties. This section discusses important assumptions, limitations, and uncertainties that may influence the obtained results.

(1) The temperature at which the experiment is conducted is determined as the measured temperature in the center of the rotary drum, above the raw material charge. It is assumed that the gas temperature and raw material temperature is the same at all positions in the rotary drum. Temperature profiles have been measured at various positions in the rotary drum, and the temperature was found to deviate no more than ±15 °C.

(2) The experiments are conducted in the temperature interval from 700 to 1000 °C, whereas the raw material and gas temperatures in the material inlet end of modern industrial cement rotary kilns are typically 900 °C and 1000−1200 °C, respectively. The temperature interval is thus only partly representative for the industrial conditions. However, it is not possible to conduct experiments above 1000 °C in the present experimental setup.

(3) The gas passing through the rotary drum is pure mixtures of N_2 and O_2. During the devolatilization and char combustion, a fraction of the O_2 will be consumed, and the combustion products H_2O, NO, SO_2, CO, and CO_2 will be formed. In addition, some intermediate products such as CH_4 or higher hydrocarbons, alkali species, etc. may be formed. Under industrial conditions, the gas will also contain the combustion products from the main kiln burner and may have overall gas compositions different from the one used in these experiments. This difference in gas composition is likely to affect the sulfur release to some extent.

(4) The uncertainty on the O_2, CO, and CO_2 analyzers are ±2% of span range for each species, while it is ±5% on the SO_2 measurement. These uncertainties should be kept in mind when the results are evaluated.

(5) It is assumed that all sulfur released from the sample will be oxidized to SO_2 before leaving the reactor. This assumption is supported by equilibrium calculations with the thermodynamics software FactSage, which predicts that nearly all sulfur is present as SO_2 under the studied conditions.[2]

(6) The physical shape of the rotary drum reactor may cause a diffusion limitation of oxygen to the fuel particles, since oxygen must be transported from the drum center line to the fully or partly

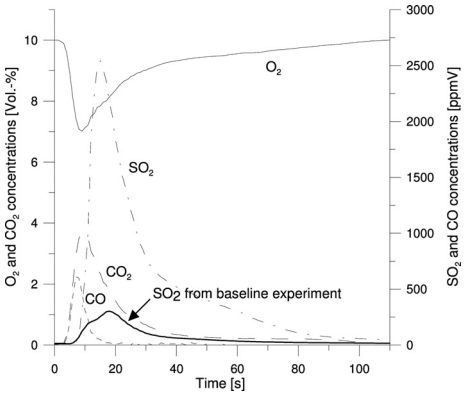

Figure 5. Concentrations of O_2, CO_2, CO, and SO_2 during an experiment with 0.81 g of tire rubber granulate corresponding to an energy input of 30 kJ. Conditions: 900 °C, 5% fill, 6 rpm, 100 NL/min, 10% O_2.

buried fuel particles in the raw material bed. However, since all experiments are made under similar conditions, it is assumed that results will be comparable.

(7) The flue gas composition will not change significantly in the distance between the reactor and the analyzers. To minimize this uncertainty and prevent, for example, SO_2 absorption in filters and condensers, these parts were regularly cleaned or replaced to minimize the presence of compounds able to absorb SO_2. A gas with known content of SO_2 was also regularly sent through the system to test if any SO_2 was absorbed before reaching the analyzers.

■ RESULTS AND DISCUSSION

General Observations. Figure 5 shows an example of the flue gas composition during combustion of tire rubber granulate at an initial oxygen concentration of 10 vol %. When the devolatilization starts, the O_2 concentration drops to approximately 7 vol % and the CO_2 concentration increases to nearly 4 vol %. The CO concentration also increases shortly to around 600 ppm. The change in flue gas composition is followed by a rapid increase in the SO_2 concentration from 0 ppm to around 2500 ppm. The SO_2 concentration then gradually decreases toward 0 ppm again, as the CO/CO_2 concentrations gradually decrease.

The sulfur release from the tire rubber and raw material is observed to begin almost immediately during the fuel heat up and devolatilization. Baseline experiments with fuel combustion in pure quartz sand *without* $CaSO_4$ shows that only a minor fraction of the sulfur release arises from fuel-bound sulfur; most of the sulfur is released from the raw materials, which is also shown in Figure 5. The sulfur release is presumably facilitated by the formation of local reducing conditions near the raw material charge during the fuel devolatilization, leading to reductive decomposition of $CaSO_4$. The tendency for a rapid sulfur release during the fuel devolatilization was observed for all experiments regardless of the fuel.

Effect of Energy Input and Fuel Type. The sulfur release from the raw material as a function of the energy input has been studied for five different fuels at 900 °C and 10 vol % oxygen. The fuels were polypropylene flakes, petcoke, pine wood sawdust, tire rubber granulate, and sewage sludge (see Tables 1 and 2 for details). These fuels all have relatively similar average particle

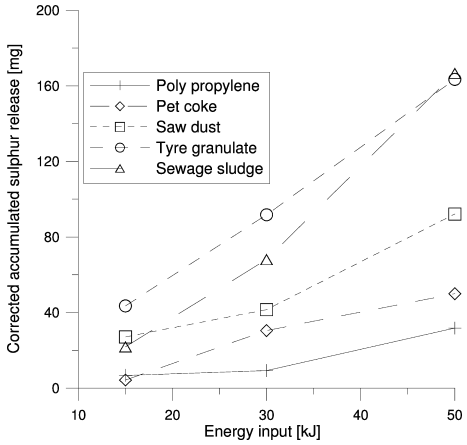

Figure 6. Corrected accumulated sulfur release as a function of energy input from different fuels. Conditions: 900 °C, 10 vol % O_2, 5% fill, 100 NL/min, 6 rpm.

thicknesses in the interval 0.5−2.0 mm. The results are shown in Figure 6. For all tested fuels it is observed that the sulfur release from the raw materials increases as the energy input increases. It is also observed that the sulfur release is quite different depending on the specific fuel: tire rubber granulate and sewage sludge leads to the highest sulfur release, while pine wood, petcoke, and polypropylene all leads to a lower sulfur release.

The reason why the sulfur release increases with increasing energy input becomes clear when the flue gas compositions at each individual experiment are compared with each other: The larger the energy input, the more the oxygen concentration will decrease during the fuel devolatilization, while both CO and CO_2 concentrations increase, thereby forming a higher degree of reducing conditions near the raw material charge.

The large differences in sulfur release for identical energy inputs but by different fuels are interesting. A detailed study of the flue gas composition for each fuel type has not revealed any clear trends about the degree of reducing conditions and sulfur release. The reason is probably that the exact particle sizes, shapes, densities, fuel combustion pathways, and kinetics of the studied fuels are quite different and that this also has an effect on sulfur release. The approximately spherical tire rubber granulate and sewage sludge particles may for example lead to a high sulfur release because of a relatively fast devolatilization combined with a high degree of mixing with the raw material. The needle-shaped sawdust particles yield a lower sulfur release than tire rubber granulate and sewage sludge, even though the sawdust also has a fast devolatilization. An explanation could be that the sawdust particles are less dense than the tire rubber and sewage sludge and that the density difference leads to a low degree of mixing of sawdust into the raw material. The polypropylene flakes have the lowest sulfur release, which may be explained by a very fast devolatilization, so fast that the polypropylene devolatilization ends before it has been well mixed into the raw material. Finally, the small petcoke particles are a slow burning fuel with a volatile content of only 13%. This leads to a relatively small decrease in oxygen concentration during the fuel conversion compared to

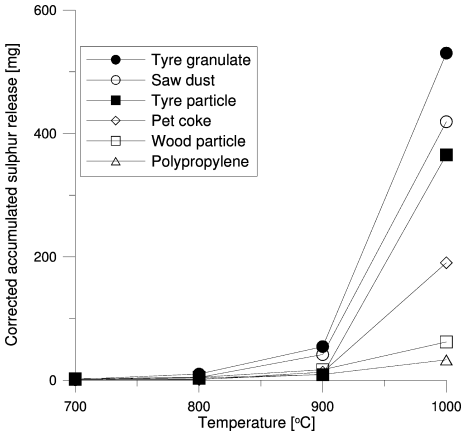

Figure 7. Corrected accumulated sulfur release from raw materials as a function of temperature and fuel particle size. Conditions: 5% fill degree, 10 vol % O_2, 100 NL/min, 6 rpm. Energy input in each experiment: 30 kJ. Sulfur release for tire granulate and sawdust at 1000 °C has been estimated because the SO_2 concentration exceeded the analyzer range for these two specific experiments.

the other fuels and thereby a low degree of local reducing conditions near the raw material bed.

Effect of Temperature and Fuel Particle Size. The sulfur release is studied as a function of the temperature and fuel particle size, which are both important for the devolatilization and char combustion times. Tire rubber and pine wood are used in the investigations about particle size while the investigations about temperature also include petcoke and polypropylene. The tire rubber is fed as cylinders or tire rubber granulates, while the pine wood is in the form of one pine wood particle or as sawdust. The overall energy input is the same in each experiment. Details about the fuels can be found in Tables 1 and 2. The results are shown in Figure 7 with sulfur release in milligrams versus temperature for the different fuel particle sizes. It is observed that the fuel particle size is insignificant for the sulfur release at 700 and 800 °C, while the influence becomes more evident at 900 °C and, in particular, at 1000 °C: At 900 and 1000 °C the sawdust and tire granulate lead to a higher sulfur release than for the wood particle and tire particle.

The significant effect of temperature on the sulfur release was also to be expected due to the lower thermal stability of $CaSO_4$ at higher temperatures (see the phase diagram in Figure 2). In addition, comparison of the flue gas compositions during the combustion at different temperatures shows that the CO concentration during the fuel devolatilization reaches higher values at higher temperatures than at lower temperatures. This can be attributed to be a faster release of volatiles from the fuel particles at elevated temperatures, thereby increasing the tendency for local reducing conditions in the area around the fuel particles. Local reducing conditions will augment the sulfur release during the fuel devolatilization.

The reason for the difference in sulfur release for different fuel particle sizes becomes clear when the flue gas composition is studied for the individual experiments: The larger total surface areas of the smaller fuel particles leads to a fast devolatilization and thus a fast release of volatiles. This leads to significantly

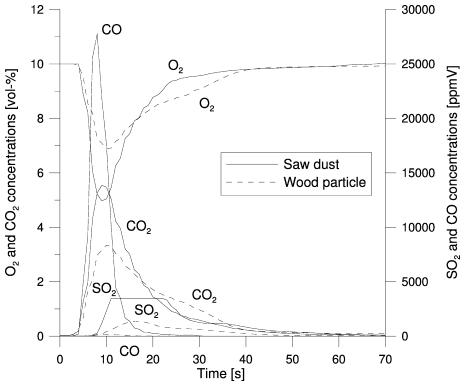

Figure 8. Flue gas composition during combustion of a pine wood particle with dimensions 30 × 15 × 10 mm and pine wood sawdust with particle size <1 mm. Conditions: 10 vol % O_2, 5% fill degree, 1000 °C, 100 NL/min, 6 rpm.

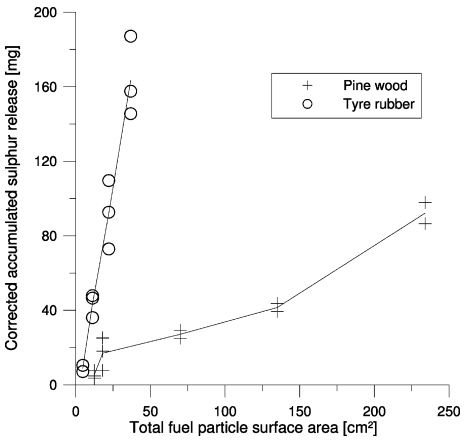

Figure 9. Corrected accumulated sulfur release versus the total surface area of pine wood and tire rubber fuel particles. Conditions: 900 °C, 10 vol % O_2, 5% fill degree, 6 rpm, 100 NL/min.

higher CO concentrations and thus a higher reductive decomposition of $CaSO_4$ during the devolatilization. An example is illustrated in Figure 8, which shows flue gas compositions during wood particle and sawdust combustion, respectively, at 1000 °C. During wood particle combustion, the CO peak during devolatilization reaches 180 ppm and the SO_2 peak reaches 1350 ppm. During sawdust combustion, the CO peak is significantly larger and reaches 27 000 ppm (2.7 vol %) which leads to a SO_2 peak well above the analyzer detection range of 3500 ppm. The changes in O_2 concentration are from the initial 10 to 5 vol % for the sawdust and to 7 vol % for the pine wood particle. Similar trends were observed for the experiments with one tire particle versus tire granulate.

Since the experiments with sawdust and tire granulate at 1000 °C led to SO_2 peaks well above the SO_2 analyzer range, it has been necessary to estimate the total sulfur release from these two experiments. This induces some uncertainty on the exact amount of released sulfur in these two cases at 1000 °C.

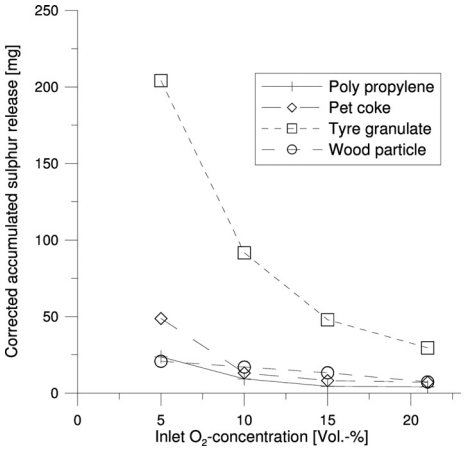

Figure 10. Corrected accumulated sulfur release as a function of inlet oxygen concentration for four different fuels. Conditions: 5% fill degree, 900 °C, 100 NL/min, 6 rpm. Energy input in each experiment was 30 kJ.

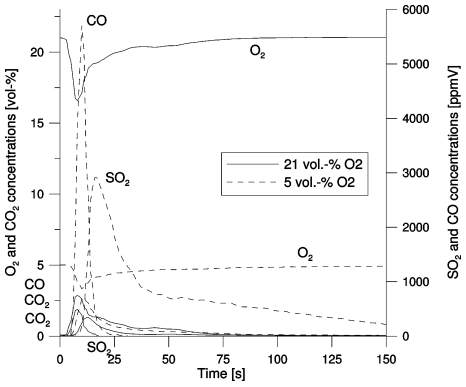

Figure 11. Flue gas composition during combustion of 0.81 g (30 kJ) of tire rubber granulate at 5 and 21 vol % O_2. Conditions: 5% fill degree, 900 °C, 100 NL/min, 6 rpm.

Figure 9 shows the sulfur release versus the total surface area of the tire rubber and pine wood fuel particles at 900 °C. The sulfur release is observed to increase approximately linearly as a function of surface area for tire rubber. It should be noted that the fuel mass, and thus energy input, also increases when the surface area increases. This increase in sample mass will also lead to more sulfur release, as shown in Figure 6. The sulfur release for pine wood is less significant than for tire rubber but also may also be characterized as linear as a function of surface area.

Effect of Bulk Oxygen Concentration. The sulfur release has been studied as a function of the inlet oxygen concentration in the freeboard gas above the raw material bed. The investigation has been conducted with polypropylene, petcoke, pine wood cubes, and tire rubber granulate (see Table 1 for details). The results are shown in Figure 10 with the sulfur release expressed in milligrams of pure sulfur versus the oxygen concentration expressed in volume percent. It is observed that the sulfur release increases for all tested fuels when the oxygen concentration decreases. Particularly, the tire rubber granulate leads to an increase in sulfur release of nearly a factor 8 when the oxygen concentration changes from 21 to 5 vol % O_2.

The reason for the high dependency of the oxygen concentration on the sulfur release becomes clear when the changes in flue gas composition are considered. Figure 11 shows the combustion of tire rubber granulate at 21 and 5 vol %, respectively. It is observed that the CO and SO_2 concentrations reaches approximately 500 and 350 ppm, respectively, at 21 vol % O_2, while the CO and SO_2concentrations reach approximately 5700 and 2900 ppm, respectively, at 5 vol % O_2. Thus, the formation of the reducing agent CO is accompanied by a reductive decomposition of $CaSO_4$ to SO_2, and the degree of this reductive decomposition is directly related to the CO concentration. The same trend was observed for the other tested fuels.

■ CONCLUSIONS

Sulfur release from cement raw materials during combustion of solid fuels has been studied experimentally in a high-temperature rotary drum experimental setup. The fuels were tire rubber, pine wood, petcoke, sewage sludge, and polypropylene. The sulfur release from the raw materials was observed to increase when (a) the inlet oxygen concentration decreased, (b) the temperature increased, and/or (c) the total surface area of the fuel particles increased. These three parameters all had the potential of augmenting local reducing conditions in the raw material bed, as indicated by elevated levels of CO during the fuel devolatilization. The sulfur release increased as a consequence of the reducing conditions, due to the lower stability of $CaSO_4$.

The type of fuel also had a significant effect on the sulfur release. The sequence was found to be tire rubber granulate > sewage sludge > pine wood sawdust > petcoke > polypropylene flakes. However, the sulfur release was significantly lower when the fuel was one tire rubber particle or one wood particle, indicating that fuel particle size has a great effect on the sulfur release from the raw materials.

In order to minimize sulfur release from cement raw materials during solid fuel combustion in the material inlet end of the rotary kiln, it is recommended to have as high a bulk oxygen concentration as possible. This could for example be achieved by a high excess air ratio in the rotary kiln main burner. The temperature of the cement raw materials should be kept as low as possible during the fuel devolatilization. This can be achieved by introducing partially calcined raw materials from the calciner rather than completely calcined raw materials: The very endothermic calcination process can absorp heat from the fuels, thereby helping to maintain a relatively low bed temperature during fuel devolatilization in the rotary kiln material inlet. Finally, use of coarse fuel particles can slow the fuel devolatilization rate and thereby the rapid formation of reducing agents. Thus, use of coarse fuel particles in the material inlet end of cement rotary kilns is likely to reduce the tendency for local reducing conditions relative to the situation with fine fuel particles.

■ AUTHOR INFORMATION

Corresponding Author

*E-mail: arn@kt.dtu.dk. Telephone: +45 45252831.

■ ACKNOWLEDGMENT

The work described in this paper is part of a research platform on future cement technology financed by The Danish National

Advanced Technology Foundation, Technical University of Denmark (DTU) and FLSmidth A/S.

■ REFERENCES

(1) Verein Deutscher Zementwerke (VDZ), Activity Report 2007–2009, Düsseldorf, Germany, http://www.vdz-online.de. Obtained July 1, 2011.
(2) Nielsen, A. R.; Larsen, M. B.; Glarborg, P.; Dam-Johansen, K. *Energy Fuels* **2011**, *25*, 2917–2926.
(3) Choi, G.-S.; Glasser, F. P. *Cem. Concr. Res.* **1988**, *18*, 367–374.
(4) Sylla, H.-M. *ZKG* **1974**, *10*, 499–508.
(5) Hansen, J. P. *SO_2 Emissions from Cement Production*. Ph.D. Thesis, Technical University of Denmark, Department of Chemical Engineering, 2003; ISBN 87-90142-96-9.
(6) Lyngfelt, A.; Leckner, B. *Chem. Eng. Sci.* **1989**, *44* (2), 207–213.
(7) Lyngfelt, A.; Leckner, B. *Chem. Eng. Sci.* **1999**, *54*, 5573–5584.
(8) Dam-Johansen, K.; Hansen, P. F. B.; Østergaard, K. *Chem. Eng. Sci.* **1991**, *46* (3), 847–853.
(9) Hansen, P. F. B.; Dam-Johansen, K.; Bank, L. H.; Østergaard, K. *Proc. Int. Conf. Fluid. Bed Combust.* **1991**, *1*, 73–82.
(10) Hansen, P. F. B; Dam-Johansen, K.; Østergaard, K. *Chem. Eng. Sci.* **1993**, *48* (7), 1325–1341.
(11) Tarelho, L. A. C.; Matos, M. A. A.; Pereira, F. J. M. A. *Fuel Process. Technol.* **2005**, *86*, 1385–1401.
(12) Barin, I. *Thermochemical Data of Pure Substances*, 3rd ed.; VCH: Weinheim, Germany, 1995; ISBN 3-527-28745-0.

energy&fuels

Article

pubs.acs.org/EF

Devolatilization and Combustion of Tire Rubber and Pine Wood in a Pilot Scale Rotary Kiln

Anders R. Nielsen,*[,†,‡] Morten B. Larsen,[†] Peter Glarborg,[‡] and Kim Dam-Johansen[‡]

[†]FLSmidth A/S, Vigerslev Allé 77, DK-2500 Valby, Denmark

[‡]Department of Chemical Engineering, CHEC Research Centre, Technical University of Denmark (DTU), DK-2800 Lyngby, Denmark

ABSTRACT: Cement production is highly energy intensive and requires large quantities of fuels. For both economical and environmental reasons, there is an increasing tendency for utilization of alternative fuels in the cement industry, examples being tire derived fuels, waste wood, or different types of industrial waste. In this study, devolatilization and combustion of large particles of tire rubber and pine wood with equivalent diameters of 10 mm to 26 mm are investigated in a pilot scale rotary kiln able to simulate the process conditions present in the material inlet end of cement rotary kilns. Investigated temperatures varied from 700 to 1000 °C, and oxygen concentrations varied from 5% v/v O_2 to 21% v/v O_2. The devolatilization time of tire rubber and pine wood were found to mainly depend on temperature and particle size and were within 40 to 170 s. Rate limiting parameters for char oxidation of tire rubber and pine wood were found to be bulk oxygen concentration, mass transfer rate of oxygen, raw material fill degree, raw material characteristics, and temperature. Kiln rotational speed only had a minor effect on the char oxidation when the raw material bed was in a rolling motion. Initial fuel particle size also influenced the char conversion time for pine wood char but had no influence on tire char conversion time, because the tire rubber crackled into several smaller char fragments immediately after devolatilization. The char conversion times were from 40 to 480 s for tire char and from 30 to 1300 s for pine wood char, depending on the conditions. Models for devolatilization and char oxidation of tire rubber and pine wood are validated against experimental results.

INTRODUCTION

The cement industry is responsible for approximately 2% of the world's primary energy consumption.[1−3] Fuel consumption accounts for about 30−40% of the total cement clinker production costs.[4] Due to competition in the cement market, increasing fossil fuel prices, and environmental concerns, cement producers have increased the utilization of alternative fuels as a substitute for fossil fuels in order to achieve the most economic fuel mix. In this context, "alternative fuels" cover all nonfossil fuels and waste from other industries. Popular alternative fuels in the cement industry are tire-derived fuels (TDF), biomass residues, and different commercial and industrial wastes.

It is attractive to utilize coarse, solid alternative fuel particles directly in the material inlet end of cement rotary kilns in order to save expenses for shredding of the fuels to smaller particles and to increase fuel flexibility of the system. High temperatures in the rotary kiln and material retention times of several minutes provide good conditions for fuel burnout. Combustion of solid fuels in the material inlet end may, however, have negative impact on the process stability of the kiln system in the form of increased tendency for deposit build-ups. The mechanism behind formation of deposit build-ups is described elsewhere.[5] The influence of alternative fuel utilization in the material inlet end of the rotary kiln on process stability often limits how large quantities of fuel are possible to use in this way. Little information is available in the literature about combustion of large fuel particles under the conditions in the material inlet end of rotary kilns, and it is possible that a systematic investigation can optimize the utilization of alternative fuels in the material inlet end of rotary kilns. Figure 1 shows utilization of large fuel particles in the form of whole tires in the material inlet end of the rotary kiln. The raw material bed temperature is typically around 900 °C and increases toward 1450 °C in the burning zone. The gas temperature is around 1000−1200 °C in the material inlet end and may be above 2000 °C in the burner flame in the burning zone. Bulk oxygen concentration in the material inlet end is typically quite low, 2−7% v/v. Solids and gas residence times in the rotary kiln are typically 15−30 min and 5−10 s, respectively.

Devolatilization of large TDF particles have been studied by several researchers.[6−12] In addition, studies have been made with micro thermogravimetric analysis (micro-TGA) on small TDF samples to determine reaction kinetics and composition of oil, gas, and char.[13−15] Devolatilization times of cylindrical tire rubber particles with diameters from 7 to 22 mm and heights of 35 mm at 840 °C in an inert atmosphere are reported to be 75 to 300 s when increasing the particle diameter from 7.5 to 22 mm.[11] Devolatilization times of tire rubber particles with thicknesses in the range of 6−12 mm in air and in the temperature interval from 700 to 1000 °C were found to be 30−100 s depending on thickness and temperature.[12] Generally, results reported in literature about devolatilization of large TDF particles show clear tendencies for devolatilization time to increase with increasing particle size and decrease with increasing temperature and/or oxygen concentration.

Received: September 8, 2011
Revised: December 20, 2011
Published: December 20, 2011

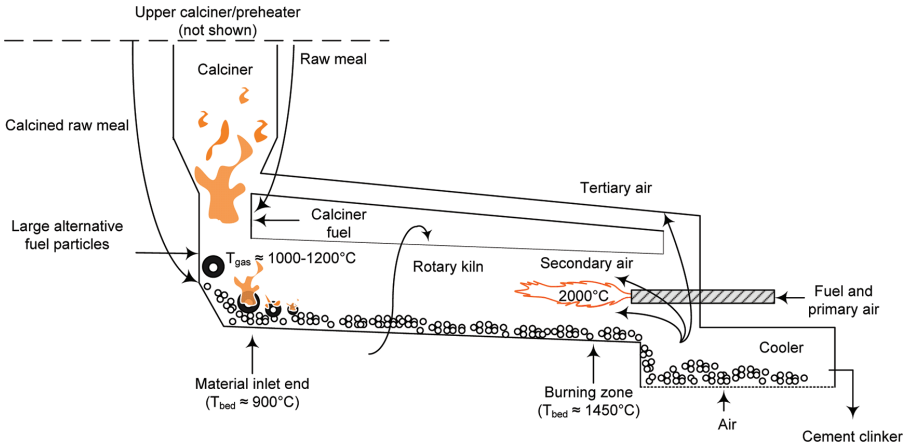

Figure 1. Utilization of large solid alternative fuel particles in the material inlet end of cement rotary kilns. Typical gas and bed temperatures shown for clarity.

Previous work about tire char combustion has been made with a few mg of tire char particles in the 100−500 μm size in thermogravimetric analyzers (TGA reactors) and drop tube reactors.[13,14,16−18] Char conversion times are reported to be well below 1 s in air and at 1200 °C for tire char with particle size of around 500 μm.[16] Oxidation time for tire char with particle size between 102 and 212 μm at 10% v/v O_2 were found to be from 9 s at 750 °C to 4 s at 850 °C.[18] Masi et al. found that a TDF char particle with a diameter of 100 μm reached full conversion after 6 s at 5% v/v O_2 and 850 °C.[17] According to Masi et al., a medium rank coal char would require 100 s to reach full conversion under the same conditions.[17] Masi et al. also compared intrinsic TDF char reactivity with the intrinsic char reactivity of refuse derived fuels (RDF) and biomass (Robinia Pseudoacacia) and found that the TDF char was most reactive.[17] Atal and Levendis also reported that tire char burned 2−4 times faster than bituminous coal char.[16] Larsen et al. concluded that the TDF chars were very reactive at temperatures of 850 °C and higher.[18] As a consequence, intraparticle kinetics were concluded to be less important because the reaction would take place at the outer particle surface. In addition, the ash layer formed on the particle surface was observed to be very porous and could easily be removed by slight mechanical interaction of the particle with tweezers. In the rotary kiln, the rotational movement of the kiln is assumed to remove the ash layer rapidly, leaving an unconverted char particle.

Devolatilization of large wood particles has also been studied by several researchers.[19−24] Winter et al. measured temperature profiles in spherical 3−20 mm diameter beech wood particles at oxygen concentrations from 0 to 21% v/v and temperatures from 700 to 950 °C. The experiments were made in a fluidized bed with silica sand as bed material. The devolatilization time of a 10 mm diameter beech wood particle at 800 °C and oxygen concentration of 10% v/v was approximately 55 s.[19] Devolatilization of nonspherical pine wood particles with equivalent diameters, d_{eff}, in the range of 10 to 45 mm and in the temperature interval of 650 to 850 °C has been investigated by de Diego et al.[21,22] The reported devolatilization times for 10 to 30 mm diameter particles were, for example, from 30 to 150 s at 850 °C. The devolatilization was reported to be only slightly affected by a change in atmosphere from air to nitrogen.[21,22] Di Blasi and Branca studied temperature profiles in cylindrical beech wood particles with lengths of 20 mm and diameters from 2 to 10 mm.[23] The experimental setup was a fluidized bed with sand as bed material and an inert atmosphere of nitrogen. Bed temperatures were from 439 to 834 °C. An empirical correlation was suggested for the devolatilization time, and the devolatilization time for a 10 mm diameter beech wood particle at 834 °C was, for example, found to be approximately 40 s.[23] Jand and Foscolo studied the pyrolysis of spherical beech wood particles with diameters from 5 to 20 mm and in the temperature interval of 560−740 °C, in a fluidized bed gasifier with sand as bed material. The devolatilization times at 740 °C were from 40 to 140 s, depending on the particle diameter.[24]

The results reported in literature about devolatilization of large wood particles are as indicated above, typically based on experiments in fluidized bed reactors with sand as bed material and at temperatures in the interval of 400−1000 °C. The wood types are either beech wood or pine wood. The general tendencies are that devolatilization times increase with increasing particle size and decrease with increasing temperatures. The effect of the atmosphere seems to be of minor importance.

Most studies with wood char combustion are made with wood chars with particle sizes in the μm range.[25−27] These studies typically use TGA experiments to obtain information about char intrinsic kinetics. Jand and Foscolo studied the char combustion of large spherical beech wood char particles with diameters from 5 to 20 mm at 740 °C and in air in a fluidized bed reactor.[24] The char oxidation times were found to be approximately 150 s for a 5 mm diameter char particle and 500 s for a 20 mm diameter char particle.

The aim of this work is to obtain quantitative data on the devolatilization and combustion of large particles of tire rubber and pine wood under conditions that resemble those in the material inlet end of rotary kilns. The purpose is to develop models for fuel conversion times in cement rotary kilns.

EXPERIMENTAL SECTION

Experimental Setup. The experiments were made in a high temperature pilot scale rotary kiln in a commercially available chamber

dx.doi.org/10.1021/ef201353t | *Energy Fuels* 2012, 26, 854−868

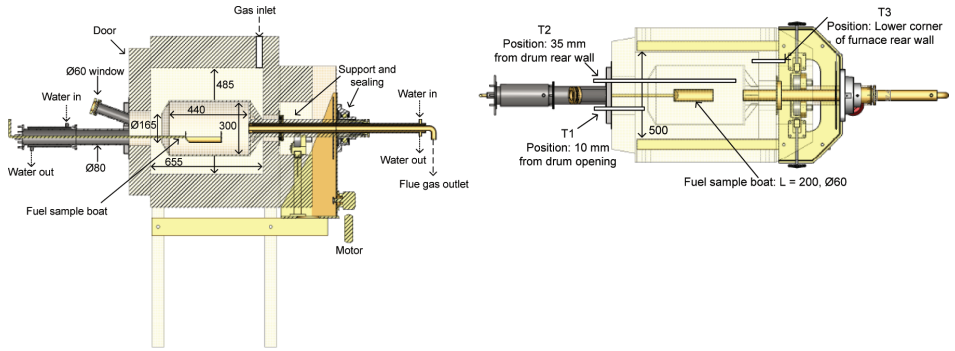

Figure 2. High temperature pilot scale rotary kiln. Left: Side view. Right: Top view.

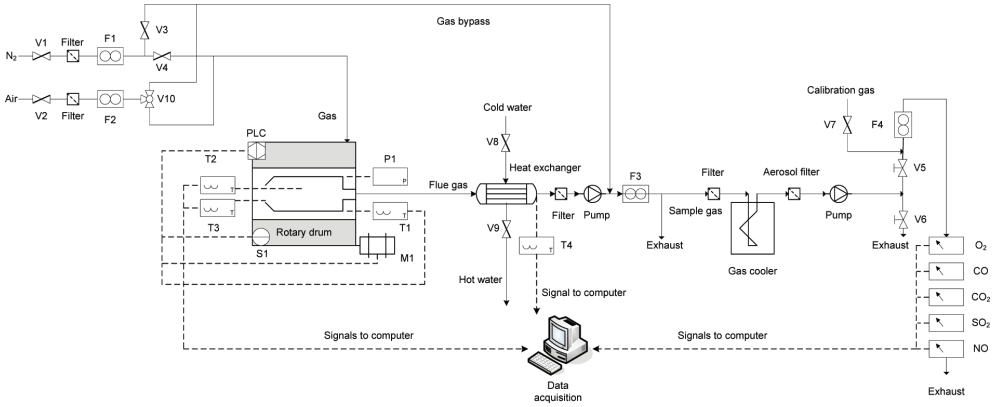

Figure 3. Sketch of the high temperature pilot scale rotary kiln experimental setup.

furnace; see Figure 2. The setup can reach an operating temperature of 1000 °C. It is electrically heated by heating elements embedded in two side walls and the bottom. The steel kiln is supported by a steel tube on rollers which passes through the rear wall. This steel tube is connected to a motor by means of a roller chain, in order to rotate the kiln. The part of the steel tube that is outside the chamber furnace is water cooled in order to protect the rollers, roller chain, and gas seals against the high temperatures.

Gas can be transported to the chamber furnace through a hole in the roof. The furnace has been designed to achieve sufficient heating of reactant gas before entering the pilot scale rotary kiln, which was also verified by temperature measurements. The gas is transported into the rotating steel kiln due to an externally placed gas pump that pumps the gas through the rotating kiln and steel tube where after the gas exits the reactor for subsequent cooling and analysis.

The chamber furnace door is equipped with a window for visual inspection, two holes for thermocouples, and a centrally placed water cooled tube for solid fuel addition. The solid fuels are placed in a sample container which can be pushed into the hot pilot scale rotary kiln or pulled out to the water cooled tube.

The experimental setup is shown in Figure 3. The gas supply can be up to 500 NL/min of air and nitrogen. The gas is transported to the pilot scale rotary kiln reactor during the experiments but may also be bypassed during calibration of flow controllers, leakage tests, etc.

The temperature is measured in three different positions in the pilot scale rotary kiln reactor: at the rear wall in the chamber furnace (T1), in the center of the pilot scale rotary kiln (T2), and at the door just in front of the pilot scale rotary kiln (T3). A pump transports the flue gas out of the pilot scale rotary kiln reactor. Before passing the pump, the flue gas is cooled in a heat exchanger and soot particles are captured in a filter. After having passed the pump, the flue gas is sent directly either to the stack or to the gas analyzers for measurement of O_2, CO, CO_2, SO_2, and NO. The fraction of the flue gas that is transported to the analyzers will pass another two filters, a gas cooler for condensation of water, and a sample gas pump before reaching the gas analyzers.

Materials and Methods. Proximate and ultimate analyses as well as lower heating values for the tested fuel samples are shown in Table 1.

Table 1. Fuel Analyses and Lower Heating Values (LHV) for Solid Fuels Used in the Experiments[a]

	proximate analysis			ultimate analysis				
	VM	FC	Ash	C	H	N	S	LHV (MJ/kg)
tire rubber	64.6	32.6	2.8	87.4	7.1	0.3	1.2	36.9
pine wood	75.3	24.5	0.2	38.9	5.2	0.1		16.2

[a]Units are in wt % as received and MJ/kg.

Tire rubber and pine wood are cut into cylindrical and rectangular shapes, respectively.

Raw materials are placed in the kiln to obtain the desired volumetric fill degree. The reactor door is closed, and the reactor is heated to the desired temperature. The kiln rotates always when the reactor is heated and keeps the raw materials in a rolling motion, with an angle

of repose of approximately 30−40°. It is the thermocouple T2 in the center of the pilot scale rotary kiln that is used to determine the temperature prior and during the experiments. The fuel sample is placed in the sample boat, and the sample boat is then positioned in the water cooled tube. The water cooled tube is closed in the end, in order to obtain a controlled atmosphere inside the pilot scale rotary kiln reactor. The gas to the reactor is adjusted to the desired flow and oxygen concentration. The temperature at T2 and oxygen concentration at the O_2 analyzer is monitored. When a stable temperature and oxygen concentration are reached, the fuel sample boat is pushed into the pilot scale rotary kiln, turned 180° and pulled out in the water cooled tube again. The fuel sample will thus drop into the preheated raw materials and immediately be heated, followed by devolatilization and char oxidation. Temperatures and flue gas compositions are continuously logged during the experiments.

An example from a typical experiment with combustion of one tire rubber cylinder is shown in Figure 4. The oxygen concentration is

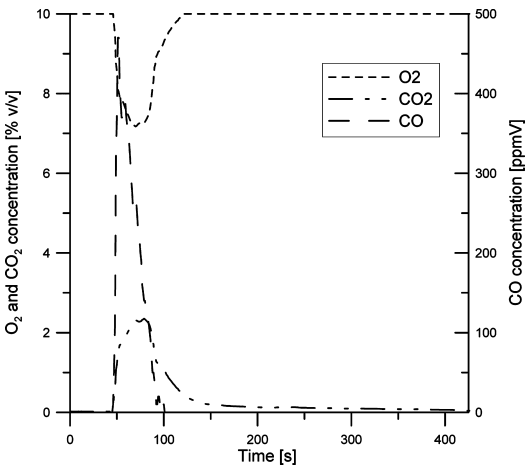

Figure 4. Example of experiment with combustion of a tire rubber cylinder. 900 °C and 10% v/v O_2. 5% volumetric kiln fill with coarse sand, 6 rpm, 100 NL/min. Particle dimensions: D = 9 mm and L = 25 mm.

observed to decrease from 10 toward 7% v/v when the devolatilization starts. At the same time, the CO concentration increases from 0 ppmV to approximately 500 ppmV, and the CO_2 concentration increases from 0 to 2.5% v/v during the devolatilization. The char oxidation is assumed to be finished when the CO_2 concentration becomes lower than 0.04% v/v. This assumption is in good agreement with the visual observations during the experiment where red-glowing char particles can be observed in the bed until the CO_2 concentration reaches values below around 0.04% v/v CO_2. Furthermore, since the experiments are made with air/nitrogen mixtures, the CO_2 concentration for experiments with pure air will never decrease below approximately 0.04% v/v, which is the CO_2 concentration in Earth's atmosphere.[28]

The degree of fuel conversion against time is derived, assuming that the fuel conversion is proportional to the carbon conversion, by integration of the concentration profiles of CO_2 and CO:[18]

$$X(t) = \frac{\int_0^t y_{CO} + y_{CO_2} dt}{\int_0^\infty y_{CO} + y_{CO_2} dt} \quad (1)$$

The repeatability of the experiments is generally found to be acceptable. Nearly all experiments were repeated at least three times to ensure the repeatability. The filters in the experimental setup have been cleaned regularly in order to avoid increases in pressure drop over the system, which were observed to affect the repeatability of individual experiments. A sensitivity analysis based on the accumulation law of uncertainties was conducted to estimate the uncertainty on the degree of fuel conversion.[29] In the estimation of the overall uncertainty, the temperature is assumed to fluctuate ±1%, the gas flow is assumed to fluctuate ±3%, and the uncertainties on each of the species CO and CO_2 are assumed to fluctuate ±1% on each species. The pressure P is assumed to be constant. The sensitivity analysis indicates an overall relative uncertainty on the estimated degree of fuel conversion in the order of ±6%.

■ RESULTS AND DISCUSSION

General Observations. During the experiments, it was possible to follow the devolatilization and char oxidation visually through the window. This gave a good impression of the main reaction pathways for the different fuels. For all the fuels, a flame front surrounding the fuel particles were observed almost immediately after insertion into the pilot scale rotary kiln, indicating the start of the devolatilization.

The tire rubber particles were observed to predominantly keep the particle shape under the devolatilization but with some degree of fragmentation. After the devolatilization, the tire char fragmented into several smaller char particles. The pine wood particles kept their shape during the devolatilization and, to a large extent, also during the char oxidation.

The experiments have been made with coarse sand as the raw material. This raw material was chosen because (1) it is inert and (2) it gives the desired rolling motion of the bed. It was attempted to use real cement raw material but without success due to the sticky nature of the raw material which partly resulted in a thick coating layer on the inner kiln wall and partly in clinker nodulization.

Effect of Fuel Sample Mass. The effect of fuel sample mass has been investigated with tire rubber. Figure 5 shows the

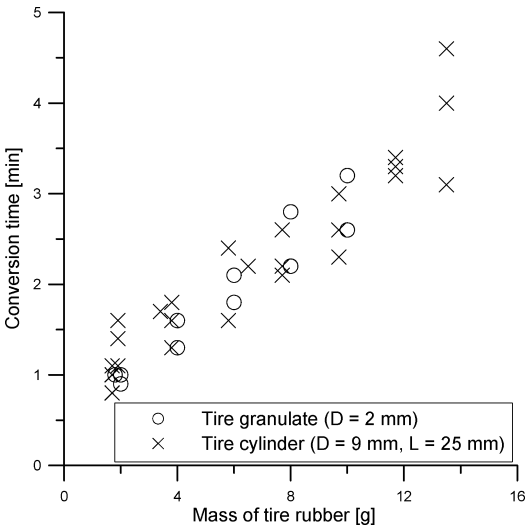

Figure 5. Conversion time versus mass for tire rubber granulate and cylinders. 10 % v/v O_2. Empty pilot scale rotary kiln, 900 °C, 6 rpm, 100 NL/min. Conversion times evaluated as 80% carbon conversion.[18]

conversion time versus mass for tire rubber cylinders with dimensions D = 9 mm and L = 25 mm and roughly spherical

dx.doi.org/10.1021/ef201353t | Energy Fuels 2012, 26, 854−868

tire rubber granulate particles with D = 2 mm. The masses are in the interval 1.8 to 15 g, and the results shown are made at 900 °C and 10% v/v O_2 and in an empty pilot scale rotary kiln. The conversion times are evaluated at 80% carbon conversion rather than at full conversion: This is to avoid the consequences of dispersion and time delay between the experimental setup and the gas analyzers which makes the time for full conversion uncertain.[18] It is observed that the conversion time increases linearly with mass for the tire cylinders as well as for the tire granulate. It is furthermore observed that there are no particular differences in conversion time for the tire cylinders and tire granulates when the total mass is the same. Thus, the initial fuel particle size of the tire rubber does not have any particular effect on the conversion time. This result is in good correspondence with the visual observation that the tire rubber rapidly cracks into several small fragments after the devolatilization, so conversion time will be a function of overall tire rubber mass rather than tire rubber particle size. The results are quite different with pine wood where the conversion time was observed to be a function of both particle size and sample mass, indicating that these fuels follow another conversion pathway than tire rubber.

Effect of Fuel Particle Size and Shape. The effect of fuel particle size has been studied with cylindrical tire rubber particles and rectangular wood particles. The rectangular wood particles are also used to study the effect of fuel particle shape. Figure 6 left shows the conversion curves for three tire rubber cylinders of different diameters (and different masses) at 900 °C and 10% v/v oxygen. The overall conversion time is observed to increase when the particle diameter (and mass) increases. It should be noted that the devolatilization time also increases when the particle diameter increases. However, on the basis of the study of fuel sample mass shown in Figure 5, it must be concluded that the increase in overall tire rubber conversion time is due to the increase in mass rather than the increase in particle diameter, since the tire char rapidly fragments into several smaller char particles.

Figure 6 right shows the carbon conversion versus time for five pine wood particles with different masses, sizes, and shapes. Four of the particles have a thickness of 10 mm while the fifth particle has a thickness of 20 mm. It is observed that the devolatilization time is approximately 1 min for the four 10 mm thick particles whereas the devolatilization time is around 2 min for the 20 mm particle; the exact devolatilization times are shown in the Model Analysis section. The char oxidation times are generally observed to increase when the mass of char increases, but it is also observed that the shape influences the char oxidation time. Three of the particles have approximately the same mass of 7 g but different char oxidation times: The longest of the 10 mm thick particles, with dimensions 120 × 15 × 10 mm, is fully combusted after approximately 11 min while the shorter, more compact particles with dimensions 60 × 30 × 10 mm and 30 × 30 × 20 require approximately 16 and 18 min for full conversion, respectively. Regarding particles with similar mass but different shapes, the reason for the difference in conversion times may be explained by the external surface area of the particles, which is largest for the particle that reaches full conversion first. Overall, the results indicate that particle thickness and external surface area have an effect on both the devolatilization time and the char combustion time.

Effect of Raw Material Bed Fill Degree. The effect of the raw material bed fill degree on the conversion time has been investigated. Figure 7 left shows the conversion time for cylindrical tire rubber particles at volumetric fill degrees of 0% (empty pilot scale rotary kiln), 5%, and 10% at 900 °C and 10% v/v oxygen. The overall carbon conversion times are observed to be highly influenced by the fill degree: In an empty pilot scale rotary kiln, the conversion time is around 100 s while it is around 200 s at 5% fill degree. For the highest fill degree of 10%, the conversion time is 600 s, significantly longer for the other two cases. It is also interesting to note that the shape of the curves are quite different, indicating that the fraction of volatile carbon and char carbon are different depending on the kiln fill degree. The reason may be differences in the heating mechanism, depending on whether the tire cylinder is buried in the bed or only exposed to the wall and freeboard gas. It has previously been reported that the heating rate of tire rubber has

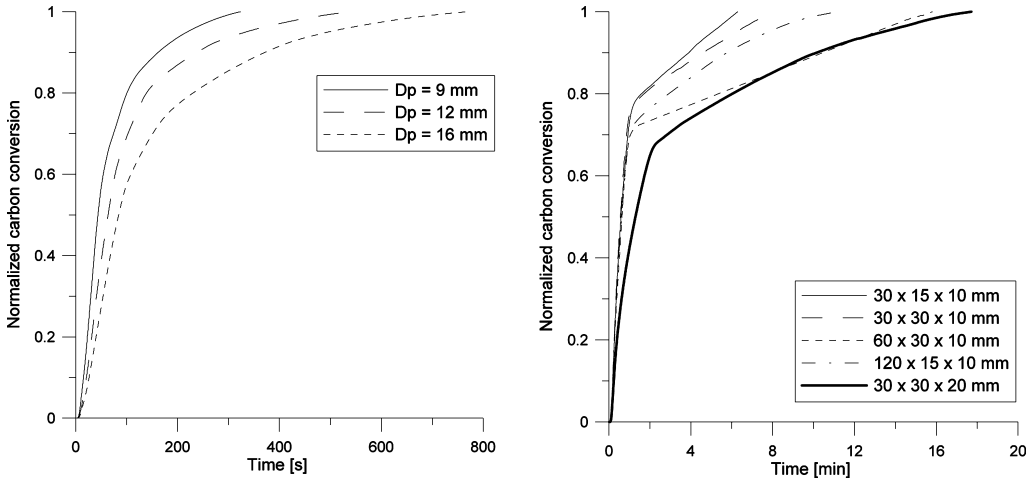

Figure 6. Left: Carbon conversion for three different tire rubber cylinders. $L_{Cylinder}$ = 25 mm. Right: Carbon conversion for pine wood particles of different sizes. T = 900 °C, 5% fill, coarse sand, 10% v/v O_2, 6 rpm, 100 NL/min.

dx.doi.org/10.1021/ef201353t | Energy Fuels 2012, 26, 854–868

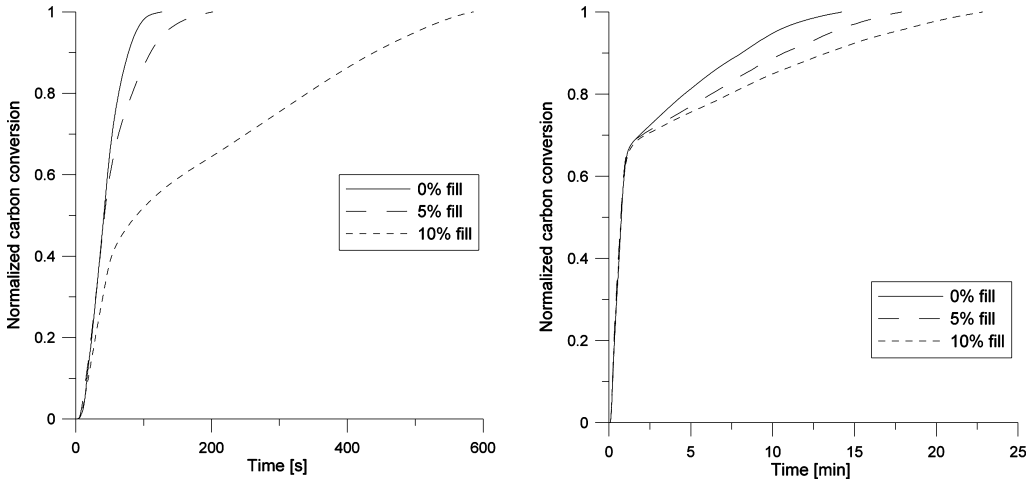

Figure 7. Carbon conversion as a function of raw material fill degree. Left: Tire rubber particle with dimensions: D = 9 mm, L = 25 mm. Right: Pine wood particle with dimensions: 60 × 30 × 10 mm. Coarse sand. T = 900 °C, 10% O_2, 6 rpm, 100 NL/min.

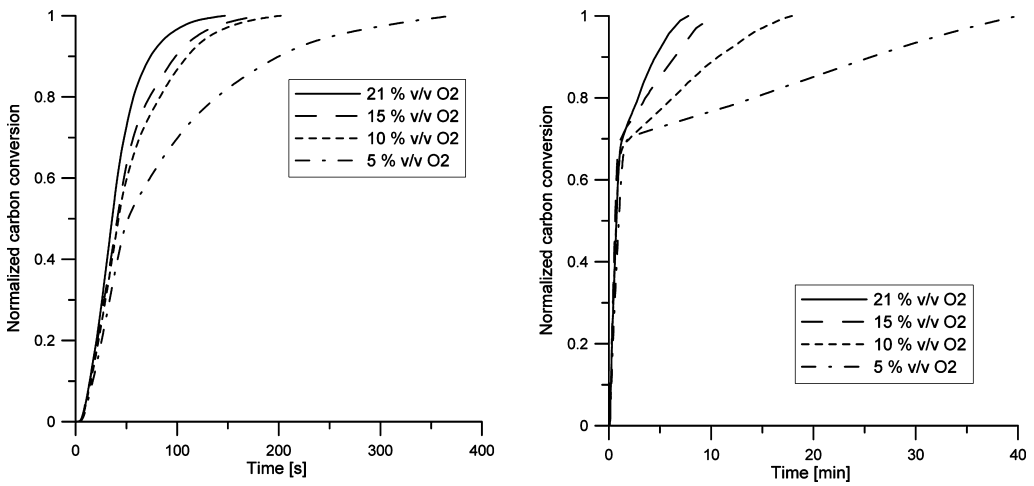

Figure 8. Carbon conversion as a function of oxygen concentration. Left: Tire rubber particle with dimensions: D = 9 mm, L = 25 mm. Right: Pine wood particle with dimensions: 60 × 30 × 10 mm. Coarse sand, 5% fill. T = 900 °C, 6 rpm, 100 NL/min.

a significant effect on the devolatilization and char combustion process.[14]

Figure 7 right shows the conversion time for a pine wood particle at fill degrees of 0% (empty pilot scale rotary kiln), 5%, and 10%. The devolatilization time is observed to be identical for the three cases while the char oxidation time increases with increasing fill degree. Thus, the raw material fill degree is of importance for the char oxidation time, which is likely to be due to diffusion limitations of oxygen to the char particle when fully or partly covered with raw materials.

Effect of Oxygen Concentration. The effect of the oxygen concentration on the conversion time has been investigated in the interval 5% v/v to 21% v/v. Figure 8 left shows the conversion time for cylindrical tire rubber particles as a function of the oxygen concentration. It is seen that the conversion time increases when the oxygen concentration decreases. The increase is approximately linear with conversion times of 140, 170, 200, and 380 s at 21, 15, 10, and 5% v/v O_2.

Figure 8 right shows the conversion time for pine wood particles as a function of the oxygen concentration. It is observed that the oxygen concentration has practically no effect on the devolatilization time but a significant effect on the char oxidation time. Full conversion is reached in less than 10 min at the highest oxygen concentrations of 21% and 15% O_2, respectively. At 10% O_2, the conversion time is 18 min, and at 5% O_2, the conversion time is 40 min. Thus, the oxygen concentration clearly has a significant effect on the conversion time of pine wood char, and the conversion time increases approximately linearly as the oxygen concentration decreases.

Effect of Rotational Speed. The effect of kiln rotational speed on the conversion time has been studied. Figure 9 left shows the conversion time for cylindrical tire rubber particles as

dx.doi.org/10.1021/ef201353t | Energy Fuels 2012, 26, 854–868

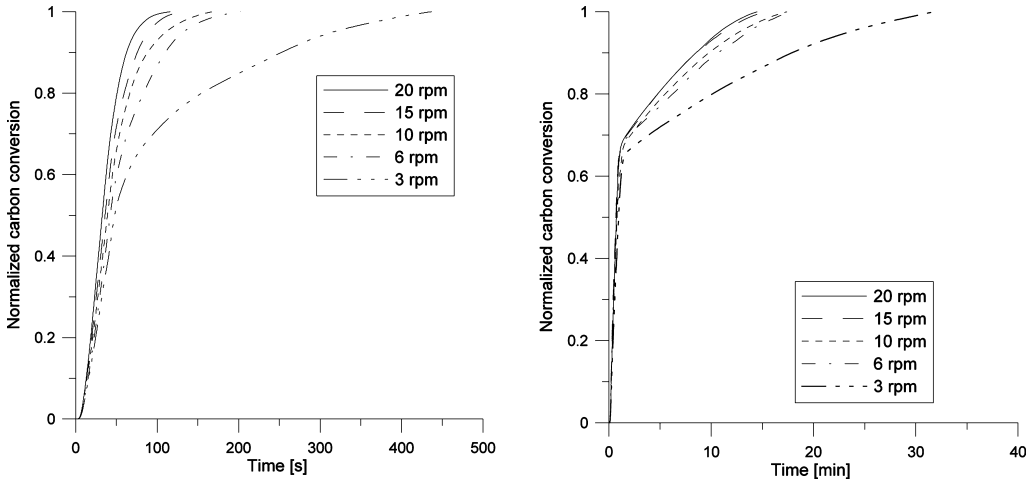

Figure 9. Carbon conversion as a function of rotational speed. Left: Tire rubber particle with dimensions: D = 9 mm, L = 25 mm. Right: Pine wood particle with dimensions: 60 × 30 × 10 mm. Coarse sand, 5% fill. T = 900 °C, 10% O_2, 100 NL/min.

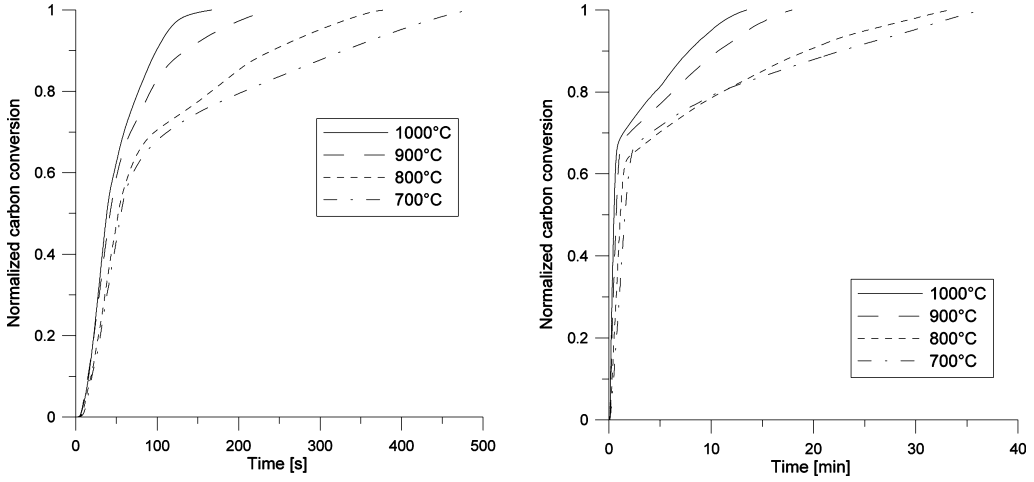

Figure 10. Carbon conversion as a function of temperature. Left: Tire particle with dimensions: D = 9 mm, L = 25 mm. Right: Pine wood particle with dimensions: 60 × 30 × 10 mm. Coarse sand, 5% fill. 6 rpm, 10% O_2, 100 NL/min.

a function of rotational speed in a bed with 5% fill degree at 900 °C and 10% v/v O_2. It is observed that the conversion time increases when the rotational speed decreases. The conversion time is, e.g., 100 s at 20 rpm and 200 s at 6 rpm, a factor 2 in difference. The conversion time increases dramatically to 440 s at the lowest rotational speed of 3 rpm. The reason is likely to be a change in bed behavior, which could also be observed visually: The bed motion is slumping at 3 rpm while it is rolling at 6 rpm and higher rotational speeds. This difference in bed motion affects the mixing process and thus the conversion time of the fuel particles. It is also possible that the fuel particle breakdown is more significant at higher rotational speeds due to stronger forces acting on the fuel particles.

Figure 9 right shows the conversion time for pine wood particles as a function of rotational speed in a bed with 5% fill degree at 900 °C and 10% v/v O_2. It is observed that there is no difference for the devolatilization time. For the char oxidation, the conversion time increases slightly when the rotational speed is decreased in the interval of 20 to 6 rpm. However, when the rotational speed is lowered to 3 rpm, the conversion time is increased significantly (33 min relative to 17 min at 6 rpm). This large effect at the lowest rotational speed is due to a change in bed behavior, from rolling to slumping.

Effect of Temperature. The effect of temperature on the conversion time has been investigated for the temperatures 700 °C, 800 °C, 900 °C, and 1000 °C. Figure 10 left shows the conversion time of tire rubber as a function of temperature. It is observed that both the devolatilization time and the char oxidation time decreases when the temperature increases. The conversion time at 1000 °C is observed to be around 160 s, while it is 490 s at 700 °C.

dx.doi.org/10.1021/ef201353t | *Energy Fuels* 2012, 26, 854–868

Figure 10 right shows the conversion time for pine wood particles as a function of temperature in the temperature interval of 700 °C to 1000 °C. Both the devolatilization time and the char oxidation time increases when the temperature decreases. However, the time difference for the char oxidation at 700 °C and 800 °C is quite small, 0 to 1 min, whereas the time is significantly shorter at 900 °C and 1000 °C.

Conclusions on Experimental Parameter Study. A parameter study has been conducted for tire rubber and pine wood. The main findings were:

For pine wood, fuel mass, particle thickness, and external surface area are important for the conversion time, both regarding devolatilization and char oxidation. For tire rubber, however, the tire char rapidly fragments into smaller particles. Consequently, the initial dimensions of the tire rubber are of little importance for the tire char conversion time. For the char oxidation part of tire rubber and pine wood, the parameters char mass, oxygen concentration, temperature, and raw material fill degree are all important parameters, but also rotational speed was observed to have an effect on the conversion time.

MODEL ANALYSIS

This section seeks to develop and verify mathematical models for devolatilization and char oxidation of selected alternative fuels. The models are to be used under conditions similar to those in the material inlet end of cement rotary kilns.

Model for Devolatilization. The heat up of a large, spherical particle may be derived by solving the unsteady heat transfer differential equation:[30,31]

$$\frac{\partial T_p}{\partial t} = \frac{1}{r^2}\frac{\partial}{\partial r}\left(r^2 \frac{k_p}{\rho_p C_p}\frac{\partial T_p}{\partial r}\right) \tag{2}$$

with the following boundary and initial conditions:

$$k_p\frac{\partial T_p}{\partial r} = Y h_{Cond}(T_b - T_p) + (1 - Y)\left(h_{Conv}(T_g - T_p) + \sigma\varepsilon_p(\varepsilon_g T_g^{\,4} - \alpha_g T_p^{\,4}) + \sigma\varepsilon_p(\varepsilon_w T_w^{\,4} - \alpha_w T_p^{\,4})\right) \quad \text{for} r = R \tag{3}$$

$$\frac{\partial T_p}{\partial r} = 0 \quad \text{for} r = 0 \tag{4}$$

where R is the initial radius of the particle, k_p is the thermal conductivity of the particle, ρ_p is the virgin fuel density, and C_p is the specific solid heat capacity. h_{Cond} and h_{Conv} are the heat transfer coefficients for conduction and convection, respectively. T_p, T_b, T_g, and T_w are temperatures of particle, bed, bulk gas, and inner kiln walls, respectively. Y is the dimensionless distribution of fuels in the bed, which is 1 if the fuel particles are fully covered by raw materials and 0 if the fuel particles are fully exposed to the gas phase. Equation 3 expresses that all heat transferred to the surface of the particle is conducted into the particle, and eq 4 expresses that the gradient at the particle center is zero due to symmetry. Equation 3 must be solved numerically. However, if radiation is neglected, an analytical solution can be found.[31]

$$\frac{T_a - T_p}{T_a - T_{p,0}} = 2\sum_{i=1}^{\infty}\frac{\sin\beta_i - \beta_i\cos\beta_i}{\beta_i - \sin\beta_i\cos\beta_i}\left[\frac{\sin\left[\beta_i\frac{r_p}{r_{p,0}}\right]}{\left[\beta_i\frac{r_p}{r_{p,0}}\right]}\right] e^{-(\beta_i^{\,2}\alpha t/r_{p,0}^{\,2})} \tag{5}$$

where T_a is the mean average temperature surrounding the particle. T_a may be estimated as $T_a = Y \cdot T_b + (1 - Y) \cdot T_g$. α is the thermal diffusivity, $\alpha = k_p/(\rho_p C_p)$.

The β_i's are the positive solutions to the equation:

$$\beta\cdot\cos\beta = (1 - Bi)\cdot\sin\beta \tag{6}$$

where Bi is the Biot number. An efficient heat transfer coefficient, h_{eff}, is used to calculate Bi, where $h_{eff} = Y \cdot h_{Cond} + (1 - Y) \cdot (h_{Conv} + h_{rad})$ and $h_{rad} = \varepsilon_g\sigma \cdot (T_g^{\,2} + T_p^{\,2}) \cdot (T_g + T_p)$.[32]

The time, τ_{devol}, required for complete devolatilization corresponds to the time needed for the fuel particle center to reach the upper devolatilization temperature, T_{Vol2}. This time is determined from eq 5 using $T_p(0, t) = T_{Vol2}$.[33] However, eq 5 should only be used to determine the devolatilization time for an initially dry particle, since the equation does not take the particle moisture content into consideration. The moisture content of a fuel particle may influence the devolatilization time considerably.[21,22,31,33]

Validation of Devolatilization Model. If the temperature required for complete devolatilization, T_{Vol2}, is known, e.g., from TGA measurements reported in the literature, eq 5 may be used to determine the time required for full devolatilization. Table 2 shows the temperatures for initial and final devolatilization temperatures for the fuels tire rubber and pine wood.

Table 2. Temperatures for Initial and Final Devolatilization of Tire Rubber and Pine Wood

fuel	T_{Vol1} [K]	T_{Vol2} [K]	reference
tire rubber	523	773	12
pine wood	473	773	34

Experiments with nonspherical tire rubber and pine wood particles of different size and shapes have been conducted to study the devolatilization time. Since the model assumes that the fuel particles are spherical, it is required to represent the nonspherical fuel particles as spherical particles of diameter, d_{eff}, characterized by the nonspherical and spherical particles having the same total surface area:[35]

$$d_{eff} = \theta\cdot d_{sph} \tag{7}$$

where d_{sph} is the equivalent spherical diameter, defined as the diameter of a sphere with the same volume as the particle. θ is the sphericity defined as:

$$\theta = \left(\frac{\text{Surface of sphere}}{\text{Surface of particle}}\right)_{\text{of same volume}} \tag{8}$$

The experimentally found devolatilization times are determined by means of the normalized carbon conversion curves for the fuels. Figure 11 shows an example with pine wood, where the devolatilization time is observed to begin at

dx.doi.org/10.1021/ef201353t | Energy Fuels 2012, 26, 854–868

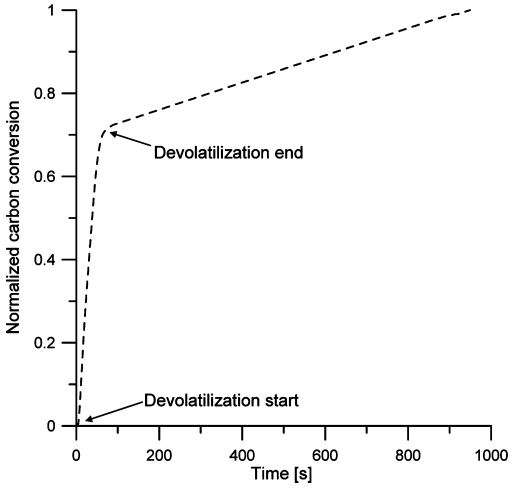

Figure 11. Determination of devolatilization time for a pine wood particle at 900 °C and 10% v/v O_2. 5% volumetric fill, coarse sand, 100 NL/min, 6 rpm. Particle dimensions: 60 × 30 × 10 mm (7.0 g).

time 0 s and end at time 80 s. The devolatilization ends when the slope of the conversion curve is observed to decrease significantly, indicating the start of the slower char oxidation.

Devolatilization of Tire Rubber. A comparison between experimental values and values predicted by the model for tire rubber is shown in Figure 12. Values used in the model are summarized in Table 3.

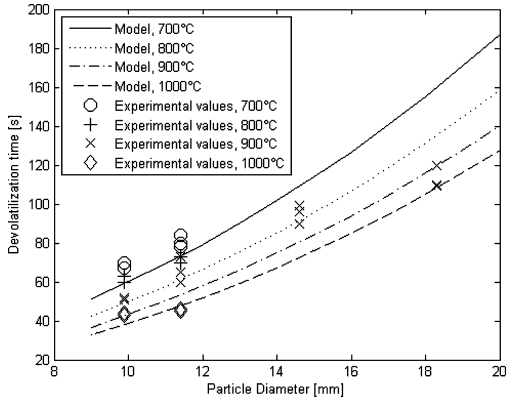

Figure 12. Comparison of tire rubber devolatilization time predicted by the model and by experimentally found values. 10% O_2. 5% volumetric fill degree in pilot scale rotary kiln. $Y = 0.2$. $\alpha = 1.25 \cdot 10^{-7}$ m^2/s.

In the model, the fraction of the fuel particle surface that is covered by raw materials, Y, is 0.2. This fraction was chosen on the basis of visual observations during the experiments, where the cylindrical tire rubber particle was observed to be free of the raw material bed during most of the devolatilization. The experimental values were obtained for four different tire rubber particle diameters from 10 mm to 18.5 mm and at 900 °C. The two smallest tire rubber particles were also studied at 700 °C, 800 °C, and 1000 °C. The model is in acceptable agreement with the experimental values, which were found to have devolatilization times from approximately 40 to 120 s, depending on temperature and tire rubber particle size. The model generally overestimates the effect of temperature compared to the experimental findings: For the two smallest fuel particles, the difference in experimentally found devolatilization times were smaller than that predicted by the model.

Table 3. Fuel Specific Data Used in the Devolatilization Models

property	TDF	pine wood	references
specific heat capacity, C_p, [J/(kg · K)]	2000	1500	11
			36
initial particle density, ρ_p, [kg/m^3]	1150	690	8
			36
k_p, virgin fuel thermal conductivity, [W/(m · K)]	0.3	0.2	37
			36
conductive heat transfer coefficient, h_{CBP}, [W/(m^2 · K)]	250	250	38
convective heat transfer coefficient, h_{CBP}, [W/(m^2 · K)]	150	150	39

Chinyama and Lockwood studied the devolatilization times of tire rubber particles with thicknesses in the range of 6−12 mm and in the temperature interval from 700 to 1000 °C.[12] The devolatilization times were found to be 30−100 s, depending on thickness and temperature, which were typically 20 s longer than the values found in this study for the same particle sizes and temperatures. This difference in time may be due to different heat transfer mechanisms at the two experimental conditions: In the experiments conducted by Chinyama and Lockwood, heat transfer to the tire rubber particles were exclusively by convection and radiation, whereas heat transfer in this study was also partly by conduction from the raw materials and kiln wall. Another reason may be the mechanical influence from the pilot scale rotary kiln in this study, which is likely to increase fragmentation of the fuel particle during devolatilization; in fact, the tire rubber particles were observed to fragment a little during the experiments, thereby leading to smaller fuel particle sizes.

Larsen et al. also studied the devolatilization of cylindrical tire rubber particles with diameters from 7 to 22 mm and heights of 35 mm at temperatures up to 840 °C in an inert atmosphere.[11] The reported devolatilization times at 840 °C were 75 to 300 s when increasing the particle diameter from 7.5 to 22 mm. These devolatilization times are approximately twice as long as indicated by the results from this study. The reason for the deviations may again be differences in the heat transfer mechanisms due to different experimental conditions as well as the mechanical influence in this study. In addition, the experiments conducted by Larsen et al. were made under an inert atmosphere while the present study was made under oxidizing conditions which are likely to have accelerated the devolatilization.

Devolatilization of Pine Wood. A comparison between experimentally found values and values predicted by the model for pine wood is shown in Figure 13. Values used in the model can be found in Table 3. The experimental values were obtained for five different pine wood particle diameters from 12 mm to 26 mm and at 900 °C. The pine wood particles of diameters 15 mm and 20 mm were also studied at 700 °C, 800 °C,

dx.doi.org/10.1021/ef201353t | Energy Fuels 2012, 26, 854−868

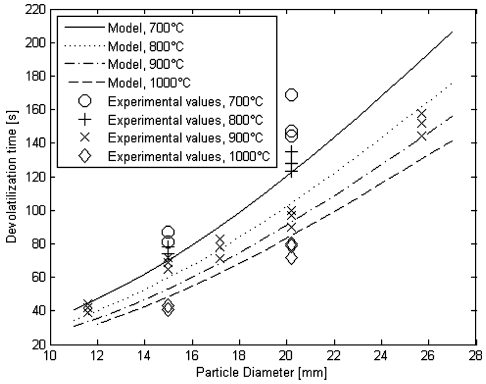

Figure 13. Comparison of pine wood devolatilization time predicted by the model and by experimentally found values. 10% O_2, 5% volumetric fill degree in kiln. $Y = 0.2$. $\alpha = 1.9 \cdot 10^{-7}$ m^2/s.

and 1000 °C. The model is observed to be in acceptable agreement with the experimental values, which were found to have devolatilization times from approximately 40−170 s, depending on temperature and particle size. However, the experiments conducted at 700 °C and 800 °C are generally 20−30 s longer than the devolatilization times predicted by the model, and in one case, with a particle diameter of 20 mm and at 700 °C, the deviation is 50 s.

Devolatilization of nonspherical pine wood particles with equivalent diameters, d_{eff}, in the range of 10 mm to 45 mm and in the temperature interval of 650 °C to 850 °C has been investigated by de Diego et al.[21,22] The reported devolatilization times were in good correspondence with the values found in the present study. For example, at 850 °C, the devolatilization times for 10 mm to 30 mm diameter particles were reported to be from 30 s to 150 s, whereas the results from this study indicates devolatilization times from 25 s to 180 s at 850 °C. These minor differences in devolatilization times may be due to different characteristics of the pine wood used in the experiments. The found devolatilization times for pine wood are also in relatively good consistency with devolatilization times for beech wood particles of similar size as reported by Di Blasi and Branca[23] and Jand and Foscolo;[24] see the literature study in the Introduction.

Model for Char Combustion. The aim of this section is to derive a model for char conversion in the pilot scale rotary kiln, including the main rate limiting parameters for char conversion. The char combustion model will be validated against experimental results. The model may be modified into a realistic char conversion model for the material inlet end of industrial rotary kilns. The char conversion model may be used in combination with models for drying and devolatilization of virgin fuel particles, or it may stand alone to simulate the fate of char particles dropping from calciners through the kiln riser duct and into the material inlet end of rotary kilns.

Figure 14 shows a rotary kiln where char particles are buried in the raw material bed. The bulk oxygen volume fraction is denoted $y_{O2,\infty}$, and the oxygen volume fraction at the bed surface is called $y_{O2,surf}$. The oxygen volume fraction at the char particle surface is called $y_{O2,part}$. The mixing of large particles into a bed of smaller particles has previously been shown to be a fast process, typically taking only a few bed revolutions.[40]

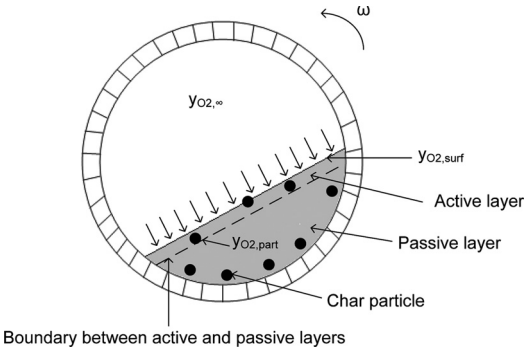

Figure 14. Oxygen mass transfer to char particles in a bed of cement raw materials in a rotary kiln.

In a cement rotary kiln, it may be assumed that mass transfer of oxygen into the active layer is fast while oxygen mass transfer into the passive layer takes place by a relatively slow diffusion; see Figure 14. Since the char particles will continuously be transported through the active and passive layers, respectively, it may be assumed that char oxidation primarily takes place when the char particles are present in the active layer.

With the above-mentioned considerations in mind, a model for char oxidation applicable for the conditions in the material inlet end of a rotary kiln should include the following: (1) external mass transfer of oxygen to bed surface, (2) mass transfer of oxygen through the active layer, (3) diffusion of oxygen into the char particle, and (4) chemical reaction of char and oxygen.

The external mass transfer of oxygen to the bed surface can be written as the mass transfer coefficient k_g multiplied by the driving force:[41]

$$r = k_g \cdot \frac{P}{RT_g} \cdot (y_{O_2,\infty} - y_{O_2,surf}) \left[\frac{\text{mol } O_2}{m^2 \cdot s}\right] \tag{9}$$

where k_g is found from a Sherwood correlation. For the pilot scale rotary kiln, where the gas flow is in the laminar regime, the following correlation is used[42]

$$Sh = \frac{k_g L}{D_{O_2}} = 0.646 Re^{1/2} Sc^{1/3} \tag{10}$$

where Re is calculated from the pilot scale rotary kiln length, L. This correlation is valid for laminar flow over a flat plate, which is roughly similar to the situation with gas flow above the bed surface.

In case of a pilot scale rotary kiln without raw materials and few fuel particles, the mass transfer coefficient may be found from a Sherwood correlation for flow past single spheres:[42]

$$Sh = \frac{k_g \cdot d_p}{D_{O_2}} = 2 + 0.6 \cdot Re_{d_p}^{1/2} \cdot Sc^{1/3}$$
$$2 \le Re_{d_p} \le 800,\ 0.6 \le Sc \le 2.5 \tag{11}$$

The mass transfer of oxygen from the bed surface into the active layer can be written as the mass transfer coefficient in the active layer, k_{AL}, multiplied by the driving force and the probability that the char particles are in the active layer, P_{AL}, at

dx.doi.org/10.1021/ef201353t | Energy Fuels 2012, 26, 854−868

any given time:

$$r = P_{AL} \cdot k_{AL} \cdot \frac{P}{RT_b} \cdot (y_{O_2,surf} - y_{O_2,part\ surf}) \left[\frac{mol\ O_2}{m^2 \cdot s}\right] \quad (12)$$

The probability for the char particles to be in the active layer may be estimated by the experimentally determined correlation suggestion by eq 13, which provides a correlation for the percentage of visible fuel particles at the bed surface:[40]

$$P_{AL} = \frac{1}{\theta^{1.5}} \cdot \frac{V_{fuel}}{V_{fuel} + \frac{\pi}{4} D^2 L F^{1.2}} \cdot Fr^{-0.09} \cdot \left(\frac{\rho_{raw\ material}}{\rho_{fuel}}\right)^{0.77} \cdot 100\% \quad (13)$$

This correlation may be used since the active layer thickness is quite small, and it therefore may be assumed that the number of fuel particles in the active layer is practically the same as the number of fuel particles that are visible above the bed surface. A bulk density of 1200 kg/m^3 is used for the raw material. The dimensionless Froude number is defined as:

$$Fr = \frac{\left(\frac{2\pi\omega}{60}\right)^2 R}{9.81\,m/s^2} \quad (14)$$

The mass transfer coefficient in the active layer, k_{AL}, has been determined by Heydenrych:[43]

$$k_{AL} = \sqrt{D_{O_2,eff} \frac{6(1-\varepsilon) \cdot Sh \cdot D_{O_2}}{d_p^{\,2}}}, \quad Sh = 3.8 \quad (15)$$

where $D_{O2,\ eff}$ is the effective diffusion coefficient of oxygen:

$$D_{O_2,eff} = \frac{\varepsilon}{\tau} D_{O_2} \quad (16)$$

D_{O_2} is the diffusion coefficient for oxygen in air, τ is the bed tortuosity, and ε is the bed porosity or void fraction available for gas flow. Dias et al. found that the tortuosity, τ, of a mixed bed of granular particles could be described as $\tau = 1/\varepsilon^n$, where n depends on the particle packing but usually is in the range of 0.4−0.5.[44]

The rate of oxygen diffusion into the char particle may be estimated by the expression:

$$r = \frac{D_{O_2,part}}{r_p(t)} \cdot \frac{P}{RT_p} \cdot (y_{O_2,part\ surf} - y_{O_2,part\ core}) \left[\frac{mol\ O_2}{m^2 \cdot s}\right] \quad (17)$$

where $D_{O2,\ part}$ is the intraparticle oxygen diffusion coefficient, r_p is the particle radius, $y_{O2,\ part\ surf}$ and $y_{O2,\ part\ core}$ are the oxygen volume fractions at the particle surface and at the intraparticle ash/char interface, respectively. $D_{O2,\ part}$ may be calculated from:

$$D_{O_2,part} = \frac{\varepsilon_{part}}{\tau_{part}} D_{O_2,eff} = \frac{1 - y_{Vol} - y_{ash}}{\tau_{part}} D_{O_2,eff} \quad (18)$$

where the char particle porosity, ε_{part}, is calculated by subtraction of the weight fractions of volatiles and ash, y_{Vol} and y_{ash}. The char particle tortuosity for chars is typically around 3 to 5.[45]

The rate of reaction at the unreacted char outer surface between char and oxygen is found from the intrinsic rate expression multiplied with the total moles and divided by the char surface area and product distribution ratio between CO and CO_2:

$$r = \frac{n_C}{A_{char} \cdot \zeta} \cdot k_0 \cdot \exp\left(-\frac{E_a}{RT_p}\right) \cdot y_{O_2,part\ core}^{\ n} \cdot (1-X)^m \left[\frac{mol\ O_2}{m^2 \cdot s}\right] \quad (19)$$

where ζ is the product distribution ratio between CO and CO_2, X is the char fractional conversion degree, and A_{char} is the char surface area. A correlation between temperature and the CO/CO_2 ratio, ζ, during combustion of different coal chars has been reported by Arthur:[46]

$$\zeta = \frac{CO}{CO_2} = 10^{3.4} \cdot \exp\left(-\frac{51916\,J/mol}{R \cdot T}\right) \quad (20)$$

This correlation may be used to estimate ζ at different temperatures under the assumption that it is representative for other chars than coal chars.

At pseudo steady state, the O_2 flux balances the consumption at the char particle surface and the char conversion may be expressed as:

$$\frac{dn_C}{dt} = \zeta \cdot A_{surf} \cdot r \left[\frac{mol\ C}{s}\right] \quad (21)$$

The conversion may also be expressed in terms of fractional conversion, X, instead of moles, n_C, by inserting:

$$X = 1 - \frac{n_C}{n_{C,0}} \quad (22)$$

and

$$dX = \frac{1}{n_{C,0}} dn_C \quad (23)$$

The following expression is then obtained:

$$\frac{dX}{dt} = \frac{\zeta \cdot A_{surf} \cdot r}{n_{C,0}} \quad (24)$$

The unknown oxygen concentrations $y_{O2,surf}$, $y_{O2,part\ surf}$, and $y_{O2,part\ core}$ may be found by solving the four eqs 9, 12, 17, and 19 for the four unknowns r, $y_{O2,surf}$, $y_{O2,part\ surf}$, and $y_{O2,partcore}$. This is easily done for $n = 1$ in eq 19, whereas a numerical solution procedure is required for $n \neq 1$. For $n = 1$, the following expression for char conversion is derived

dx.doi.org/10.1021/ef201353t | Energy Fuels 2012, 26, 854−868

$$\frac{dX}{dt} = \frac{A_{surf}\cdot\zeta}{n_{C,0}}\cdot\frac{y_{O_2,\infty}}{\frac{R\cdot T_g}{k_g\cdot P} + \frac{R\cdot T_b}{P_{AL}\cdot k_{AL}\cdot P} + \frac{r_{p,0}\cdot(1-X)^{1/3}\cdot R\cdot T_p}{D_{O_2,part}\cdot P} + \frac{\zeta\cdot A_{char}}{n_{C,0}\cdot(1-X)^{m+1}\cdot k_0\cdot\exp\left(-\frac{E_a}{R\cdot T_p}\right)}} \quad (25)$$

This expression includes the "resistances" external oxygen transport, oxygen transport into the bed, diffusion into the char particle, and chemical reaction between char and oxygen. The intraparticle diffusion term may be omitted for small char particles or for char particles that rapidly fragment into many smaller char particles. It may also be shown that the term for char oxidation kinetics becomes negligible at high temperatures above 900 °C. Fuel specific, kinetic data, and densities used in the model are summarized in Table 4.

Analysis and Comparison of Char Combustion Model. This section analyses the char combustion model under the experimental conditions in the pilot scale rotary kiln and compares the model predictions with experimental results. The purpose is to study effects of mass, oxygen concentration, bed fill degree, and temperature on the char conversion time.

Table 4. Fuel Specific Data Used in the Char Oxidation Models

fuel property	TDF	pine wood	references
ρ_p [kg/m^3]	1100	690	11
			36
k_0 [1/s]	1.5 (±5.1) · 10^{10}	1.19 · 10^8	18
			47
E_a [kJ/mol]	193 ± 28	140 ± 10	18
			47
exponent m	0.63	0.89	18
			47
LHV [MJ/kg]	37	14	from analysis

Figure 15 left shows the char conversion times for three different pine wood char particles of masses of 0.12 g, 0.24 g, and 0.88 g, respectively. The initial fuel particle dimensions are 30 × 10 × 8 mm, 30 × 10 × 15 mm, and 60 × 30 × 10 mm, respectively. The oxygen concentration is 5% v/v, 10% v/v, or 21% v/v O_2. It is observed that the model, shown with solid lines, predicts a linear relationship between conversion time, char mass, and oxygen concentration. The experimental data also confirm this linear relationship: The conversion time for the 0.88 g char particle is, for example, around 300 s, 600 s, and 1300 s at oxygen concentrations of 21% v/v, 10% v/v, and 5% v/v O_2. The model is generally observed to give a good fit to the experimental data in the experiments with different char masses and oxygen concentrations.

Figure 15 right shows the char conversion time as a function of volumetric bed fill degree and temperature. The fill degrees are 0% (only char in the reactor), 5%, or 10% and the temperatures are 700 °C, 800 °C, 900 °C, or 1000 °C. It is observed that the char conversion time increases when the bed fill degree increases. The model shows the same tendencies in temperature dependence as the experimental results. However, the experimental data show greater differences in conversion time as a function of temperature compared to the model, particularly at 700 °C where the deviation is up to 350 s at 10% fill degree corresponding to a deviation of around 30%.

Figure 16 left shows the char conversion time for three different tire rubber char cylinders with masses of approximately 0.6 g, 1.4 g, and 2.0 g, respectively. The oxygen concentration is 5% v/v, 10% v/v, or 21% v/v O_2. The model, shown with solid lines, predicts a linear increase in conversion time with char mass and a linear decrease with oxygen

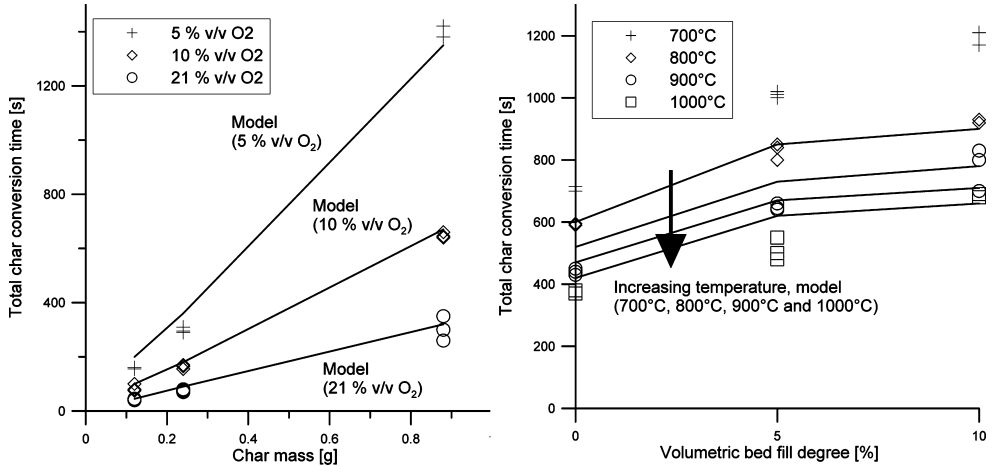

Figure 15. Comparison of experimental data with model predictions for pine wood. Left: Effect of char mass and oxygen concentration on the char conversion time. 900 °C, 5% fill degree, 100 NL/min. Initial particle dimensions: 30 × 10 × 8 mm, 30 × 10 × 15 mm and 60 × 30 × 10 mm. Right: Effect of raw material fill degree and temperature on model predicted char conversion time for a pine wood char particle with initial dimensions of 60 × 30 × 10 mm. Char mass = 0.88 g. 10 % v/v O_2, 100 NL/min. Char conversion evaluated at 80% conversion degree.[18]

dx.doi.org/10.1021/ef201353t | Energy Fuels 2012, 26, 854–868

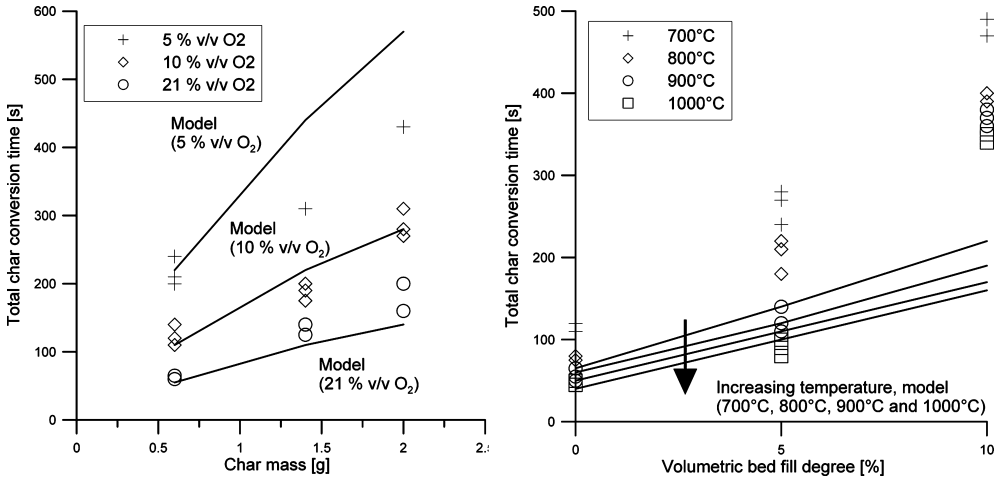

Figure 16. Left: Comparison between model predictions and experimental data for char conversion time of three different tire rubber char cylinders with lengths of 25 mm and initial diameters of 9 mm, 12 mm, and 16 mm, respectively. 900 °C, 5% raw material fill, 100 NL/min. Char masses and oxygen concentrations indicated on figure. Right: Effect of raw material fill degree and temperature on model predicted char conversion time for tire char cylinder with a length of 25 mm and initial diameter of 9 mm. Char mass = 0.6 g. 10 % v/v O_2, 100 NL/min. Char conversion evaluated at 80% conversion degree.[18]

concentration. For example, the predicted conversion time for 2 g of char is observed to be halved from 570 to 280 s when the oxygen concentration is doubled from 5% v/v to 10% v/v. Thus, the model predicts that external mass transfer of oxygen from gas to fuel particle is a main rate limiting parameter. The model gives the best agreement with the experimental values at 10% v/v and 21% v/v O_2, where the deviation is generally within ±50 s, but the model fails to give good agreement with the experiments at 5% v/v O_2 and char masses of 1.4 g and 2.0 g. In these cases, the deviations are up to nearly 30%.

Figure 16 right shows the predicted effect of raw material fill degree in the interval of 0−10% and in the temperature interval of 700−1000 °C for a cylindrical tire rubber char particle. Experimental values are also compared with the model. Both experimental values and the model show that the char conversion time increases with volumetric bed fill degree and decreases when the temperature increases. The model only fits the experimental values in the case with a fill degree of 0%, corresponding to a situation with only char in the pilot scale rotary kiln and no cement raw materials. However, the experimental values at 700 °C and 0% fill show longer conversion times than predicted by the model: 120−130 s relative to 65 s, respectively. At 5% fill degree, the model only fits the experimental values at 900 °C and 1000 °C but underestimates the conversion times at 700 °C and 800 °C by a factor of 2, and at a fill degree of 10%, the model underestimates the effect of fill degree and temperature by a factor of 2.5 to 3, depending on temperature. The effect of fill degree seems to increase more with fill degree for tire rubber than for pine wood. The reason for these differences may be related to the chemical and physical properties of the different chars: Tire char fragments into several small particles while the wood char to a high degree retains its size and shape.

Conclusions on Char Conversion Model. A model for char conversion has been suggested and compared with experimental data for large particles of tire char and pine wood char. The model includes the four resistances: external oxygen diffusion to raw material bed, oxygen transport into the bed, intraparticle oxygen diffusion, and chemical reaction at the char surface.

The model is in good correspondence with the observed conversion times for pine wood char. However, it underestimates the effect of bed fill degree for tire char. The model also underestimates the effect of the lowest temperatures of 700 °C and 800 °C on the conversion time for both pine wood char and tire char. Regarding the effect of material fill degree on the char conversion time, it is required to make more experiments with different fuel chars and particle sizes/shapes to obtain a better basis for model validation.

■ CONCLUSIONS

Experiments with tire rubber and pine wood in a high temperature pilot scale rotary kiln have been conducted in order to quantify the effect of key process parameters such as bed fill degree, kiln rotational speed, temperature, etc. on the fuel conversion time. The process conditions have been chosen to simulate the process conditions in the material inlet end of a modern cement rotary kiln. Investigated temperatures varied from 700 °C to 1000 °C, oxygen concentrations varied from 5% v/v O_2 to 21% v/v O_2, volumetric raw material bed fill degrees varied from 0% to 10%, and kiln rotational speeds varied from 3 rpm to 20 rpm.

The results showed that devolatilization of tire rubber and pine wood was mainly influenced by the temperature and fuel particle size. The devolatilization times were from 40 s for a 10 mm diameter tire rubber particle at 1000 °C to 170 s for a 20 mm diameter pine wood particle at 700 °C. The char oxidation was influenced by all investigated parameters fuel sample mass, particle size, temperature, oxygen concentration, bed fill degree, and rotational speed. Rotational speed, however, was only of importance if there was a shift in bed motion, e.g., from slumping to rolling. For changes in rotational speed where the

dominant bed motion was maintained as the rolling motion, the effect of rotational speed was of minor importance.

The tire char was observed to fragment into smaller particles during the char oxidation, leading to shorter conversion times than for pine wood char which predominantly behaved as one shrinking particle during the char oxidation. The found char conversion times were from 40 s to 480 s for tire char and from 30 s to 1300 s for pine wood char, depending on the conditions.

Devolatilization and char oxidation models have been developed and compared with experimental results and published data. These models may be further modified to predict fuel conversion times in industrial cement rotary kilns.

AUTHOR INFORMATION

Corresponding Author

*E-mail: arni@flsmidth.com. Telephone: +45 36181970.

ACKNOWLEDGMENTS

The work described in this Article is part of a research platform on future cement technology financed by The Danish National Advanced Technology Foundation, Technical University of Denmark (DTU), and FLSmidth A/S.

NOMENCLATURE

A = Surface area (m^2)
Bi = Biot number (-)
C_p = Specific heat capacity (J/(kg·K))
D = Diameter (mm or m)
D_{O2} = Diffusion coefficient (m^2/s)
E_a = Activation energy (J/mol)
F = Fill degree (-)
FC = Fixed Carbon (wt %)
Fr = Froude number (-)
h = Heat transfer coefficient ($W/(m^2K)$)
k = Mass transfer coefficient (m/s)
k_p = Thermal conductivity (W/(m·K))
k_0 = Pre-exponential factor (1/s)
L = Length (m)
LHV = Lower Heating Value (MJ/kg)
n = Moles (Mole)
P = Pressure (Pa) or probability (%)
r = Radius (mm or m) or rate (mol/m^2s)
R = Universal gas constant (J/(mol·K)
Sc = Schmidt number (-)
Sh = Sherwood number (-)
t = Time (s or min)
T = Temperature (°C or K)
Y = Distribution between bed and gas (-)
X = Degree of conversion (-)
V = Volume (m^3)
VM = Volatile Matter (wt %)
α = Thermal diffusivity (m^2/s)
β = Positive solutions (-)
ε = Emissivity or Porosity (-)
σ = Stefan−Boltzmanns constant ($5.72 \cdot 10^{-8}$ $W/(m^2K^4)$)
ρ = Density (kg/m^3)
τ = Tortuosity (-)
ζ = CO/CO_2 distribution ratio (-)
ω = Rotational speed (min^{-1})

Subscripts

a = Average
AL = Active Layer
b = Bed
cond = Conduction
conv = Convection
eff = Effective
g = Gas
p = Particle
part = Particle surface
rad = Radiation
sph = Spherical
surf = Surface
Vol = Volatile
w = Wall
∞ = Surroundings

REFERENCES

(1) VDZ, *Activity Report 2007−2009*; 2009, http://www.vdz-online.de. Obtained April 20, 2011.
(2) Cembureau, *Activity Report 2008*; http://www.cembureau.be. Obtained April 20, 2011.
(3) *BP Statistical Review of World Energy*; June 2009, http://www.bp.com. Obtained April 20, 2011.
(4) Cembureau, *Alternative Fuels in Cement Manufacture*; 1997, http://www.cembureau.be. Obtained April 20, 2011.
(5) Nielsen, A. R.; Larsen, M. B.; Glarborg, P.; Dam-Johansen, K. *Energy Fuels* **2011**, *25*, 2917−2926.
(6) Bouvier, J. M.; Charbel, F.; Gelus, M. *Resour. Conserv.* **1987**, *15*, 205−214.
(7) Yang, J.; Tanguy, P. A.; Roy, C. *AIChE J.* **1995**, *41* (6), 1500−1512.
(8) Yang, J.; Tanguy, P. A.; Roy, C. *Chem. Eng. Sci.* **1995**, *50* (12), 1909−1922.
(9) Schmidthals, H. *Luftvergasung von Altreifen zur integrierten stofflichen und energetischen Nutzung im Klinkerbrennprozess*; Doktor-Ingenieur Dissertation, Fakultät für Maschinenbau, Ruhr-Universität Bochum, Germany, 2001.
(10) Giddings, D.; Pickering, S. J.; Simmons, K.; Eastwick, C. N. *J. Energy Inst.* **2002**, *75*, 91−99.
(11) Larsen, M. B.; Schultz, L.; Glarborg, P.; Skaarup-Jensen, L.; Dam-Johansen, K.; Frandsen, F.; Henriksen, U. *Fuel* **2006**, *85*, 1335−1345.
(12) Chinyama, M. P. M; Lockwood, F. C. *J. Energy Inst.* **2007**, *80* (3), 162−167.
(13) Conesa, J. A.; Font, R.; Fullana, A.; Caballero, J. A. *Fuel* **1998**, *77* (13), 1469−1475.
(14) Leung, D. Y. C; Wang, C. L. *J. Anal. Appl. Pyrolysis* **1998**, *45*, 153−169.
(15) Kyari, M.; Cuncliffe, A.; Williams, P. T. *Energy Fuels* **2005**, *19*, 1165−1173.
(16) Atal, A.; Levendis, Y. A. *Fuel* **1995**, *74* (11), 1570−1581.
(17) Masi, S.; Salatino, S.; Senneca, O. *Fluidised Bed Combust.* **1997**, *1*, 135−143.
(18) Larsen, M. B.; Hansen, M. L.; Glarborg, P.; Skaarup-Jensen, L.; Dam-Johansen, K.; Frandsen, F. *Fuel* **2007**, *86*, 2343−2350.
(19) Winter, F.; Prah, M. E.; Hofbauer, H. *Combust. Flame* **1997**, *108*, 302−314.
(20) Di Blasi, C. *Chem. Eng. Sci.* **2000**, *55*, 5999−6013.
(21) De Diego, L. F.; García-Labiano, F.; Gayán, P; Abad, A.; Adánez, J. *J. Anal. Appl. Pyrolysis* **2002**, *65*, 173−184.
(22) De Diego, L. F.; García-Labiano, F.; Gayán, P; Abad, A; Adánez, J. *Ind. Eng. Chem. Res.* **2002**, *41*, 3642−3650.
(23) Di Blasi, C.; Branca, C. *Energy Fuels* **2003**, *17*, 247−254.
(24) Jand, N.; Foscolo, P. U. *Ind. Eng. Chem. Res.* **2005**, *44*, 5079−5089.
(25) Janse, A. M. C.; de Jonge, H. G.; Prins, W.; van Swaaij, W. P. M *Ind. Eng. Chem. Res.* **1998**, *37*, 3909−3918.
(26) Senneca, O. *Fuel Proc. Technol.* **2007**, *88*, 87−97.
(27) Shen, D. K.; Gu., S.; Luo, K. H.; Bridgwater, A. V.; Fang, M. X. *Fuel* **2009**, *88*, 1024−1030.

(28) Tans, P.; Keeling, R. *Trends in Atmospheric Carbon Dioxide*; NOAA/ESRL, www.esrl.noaa.gov/gmd/ccgg/trends/. Obtained December 9, 2011.
(29) Larsen, M. O.; Hellesen, B.; *Statistik 1*, 3rd ed.; Institute of Applied Chemistry, Technical University of Denmark, Lyngby, Denmark, 1998 (in Danish).
(30) Jensen, A. *Heating and devolatilization of coal particles*; Course note, Department of Chemical Engineering, Technical University of Denmark, Lyngby, Denmark, 1997.
(31) Agarwal, P. K.; Genetti, W. E.; Lee, Y. Y. *Chem. Eng. Sci.* **1986**, *41* (9), 2373−2383.
(32) Szekely, J.; Ewans, J. W.; Sohn, H. Y. *Gas-solid reactions*; New York: Academic Press, 1976; Vol. *51*.
(33) Agarwal, P. K.; Genetti, W. E.; Lee, Y. Y. *Fuel* **1984**, *63*, 1748−1752.
(34) Kim, S.-S.; Kim, J.; Park, Y.-H; Park, Y.-K. *Bioresour. Technol.* **2010**, *101*, 9797−9802.
(35) Kunii, D.; Levenspiel, O. *Fluidization Engineering*, 2nd ed.; Butterworths: Boston, MA, USA, 1991; ISBN: 0-409-90233-0.
(36) Leon, G.; Cruz-de-Leon, J.; Villasenor, L. *Holz als Roh- und Werkstoff* **2000**, *58*, 241−246.
(37) Sellassie, K. G.; Moo-Young, H. K.; Lioyd, T. B. *Int. J. Environ. Waste Manage.* **2007**, *1* (2/3), 179−191.
(38) Linjewile, T. M.; Hull, A. S.; Agarwal, P. K. *Chem. Eng. Sci.* **1993**, *48* (21), 3671−3675.
(39) Tscheng, S. H.; Watkinson, A. P. *Can. J. Chem. Eng.* **1979**, *57*, 433−443.
(40) Nielsen, A. R.; Aniol, R. W.; Larsen, M. B.; Glarborg, P.; Dam-Johansen, K. *Powder Technol.* **2011**, *210*, 273−280.
(41) Larsen, M. B. Alternative fuels in Cement Production. Ph.D. Thesis, Department of Chemical Engineering, Technical University of Denmark, Lyngby, Denmark, 2007; ISBN: 978-87-91435-49-8.
(42) Green, D. W.; Perry, R. H. *Perry's Chemical Engineers' Handbook*, 8th ed., McGraw-Hill: China, 2008; ISBN: 978-0-07-142294-9.
(43) Heydenrych, M. D. *Modelling of rotary kilns*. PhD Thesis, University of Twente, The Netherlands, 2001; ISBN: 90-36515440.
(44) Dias, R.; Teixeira, J. A.; Mota, M.; Yelshin, A. *Sep. Purif. Technol.* **2006**, *51*, 180−184.
(45) Johnsson, J. E.; Jensen, A. *Proc. Combust. Inst.* **2000**, *28*, 2353−2359.
(46) Arthur, J. R. *Trans. Faraday Soc.* **1951**, *47* (2), 164−178.
(47) Kastanaki, E.; Vamvuka, D. *Fuel* **2006**, *85*, 1186−1193.

Centre of Combustion and Harmful Emission Control
Department of Chemical and
Biochemical Engineering
Technical University of Denmark
Søltofts Plads, Building 229
DK-2800 Kgs. Lyngby
Denmark

Phone: +45 4525 2800
Fax: +45 4525 4588
Web: www.chec.kt.dtu.dk

ISBN : 978-87-92481-66-5